Regulation of Adrenocortical Morphogenesis and Function by WNT and FGF Signaling

A dissertation presented

by

Sining Leng

to

The Division of Medical Sciences

in partial fulfillment of the requirements

for the degree of

Doctor of Philosophy

in the subject of

Developmental and Regenerative Biology

Harvard University

Cambridge, Massachusetts

May 2019

© 2019 Sining Leng

All rights reserved.

Dissertation Advisor: Dr. David T. Breault Sining Leng

Regulation of Adrenocortical Morphogenesis and Function by WNT and FGF Signaling

Abstract

How morphology informs function has long been a topic of fascination in biology. In an adult organ, highly specialized cell types function together in microenvironments that are often drastically different depending on the anatomical location of the organ. However, little is known about how different morphological features can influence diverse cellular functions. The adrenal cortex is an ideal model to study this question. As part of the mammalian endocrine system, the adult cortex consists of concentric layers of tissue termed “zones”. Each zone produces distinct steroid hormones and adopts a unique morphology. The mechanisms governing the formation of these morphological features and their functional significance are unknown.

In this dissertation, we first examine the morphological features of the outer layer, zona glomerulosa (zG), and identify cellular and molecular mechanisms governing its formation. We show mature adrenal glomeruli consist of rosettes, a multicellular structure widely used in epithelial remodeling during development. Furthermore, rosette formation underlies a previously unknown process of postnatal glomerular morphogenesis. β-catenin, an integral component of the adherens junction and key transducer of canonical WNT signaling, is a potent regulator of glomerular morphology. β-catenin stabilization leads to increased FGFR2. Deletion of *Fgfr2* results in altered adherens junction stability and distribution, leading to decreased rosette frequency and disruption of glomerular morphology.

Next, we investigate the impact of WNT and FGF signaling modulation on zG physiological function. β-catenin stabilization causes zG hyperplasia due to a block of zonal

transdifferentiation, concurrent with increased aldosterone and elevated blood pressure. In contrast, *Fgfr2* deletion results in suppressed zG function, as evident by loss of *Cyp11b2* expression and increased plasma renin activity, a compensatory response to insufficient aldosterone output. Moreover, pharmacological inhibition of FGFR2 effectively lowers aldosterone production and zG proliferation, demonstrating the therapeutic potential of FGFR2 inhibition in treating hyperaldosteronism and adrenal hyperplasia.

Together, this dissertation provides fundamental insights into how the adrenal zG acquires its form. We show the WNT and FGF signaling pathways are important regulators of zG morphology and function. Our findings provide a conceptual framework for future studies on the link between zG tissue morphology and function.

Table of Contents

List of Figures

Acknowledgements

The morphogenesis of a developing scientist, I should speak from personal experience, requires many a permissive and instructive signal that would have to happen with impeccable spatial and temporal precision…

First and foremost, I would like to thank my mentor David Breault. Coming fresh out of a liberal arts college with barely enough research experience to get me here, and a different cultural background, it was hard for me to feel at home during the first year of graduate school. It was in David's lab where I first felt comfortable, confident, and respected for having simple (naïve) ideas. Together, we have navigated through an experience new to both of us. I appreciate his trust in me to take the lead in my own research and learning experience, even when it means spending a lot of time trying out different things. At the same time, he has kept such a close eye on my progress, that every small victory was celebrated and every failure shouldered together. Throughout the years, I have learned from David as much about how to be a scientist as about how to be a good person. His work ethics, honesty, kindness and fairness to everyone have set a high bar that I will always strive to meet. I believe it is these qualities of David that have attracted such a group of exemplary people in the lab, with whom I have shared six memorable years of my life. I also want to thank Diana Carlone, who has been my second mentor. From the moment when I joined the lab, she has always given me invaluable advice. Her tireless rigor will always remind me to do the best and most careful science I can. I want to thank Emanuele Pignatti, for it has been an absolute joy working together with him, even with all that head-busting discussions. He taught me hand by hand how to do experiments, and I learned from his perseverance, a quality that will carry me farther than I could imagine. Manasvi Shah, a sister to me, I would like to thank her for all the chats over coffee about work and life. Everyone in the Breault lab has taught me something, for that I'm very grateful.

I want to thank my husband Alessio Tovaglieri for his constant support and love. He is a true adventurer at heart. We went on so many beautiful trips together, deep into the snowy mountains, out in the open ocean, across the Yellowstone Hayden Valley, down and up the Grand Canyon… From all these trips, I learned the experience of Nature's beauty is always accompanied by a sense of fear, but fear brings one closer to one's true self. We also learned we need so little to be happy, and that we could always rely on each other in hardship.

My parents have not had it easy, with their only child half way around the earth, separated by 12 hours of time difference. I want to thank them for everything. No matter how far I've come, I can always rely on them for support. My dad loves to think and philosophize, and for that I could always count on him for a stimulating conversation. Since I was a teenager, my dad has always listened to everything that troubles me, and I thank him for the candid and trusting person I am now. My mom has been the proudest mom since I was born. She has shown me a truly unconditional love, and I could never repay her.

Chapter One:

Introduction

The adult adrenal cortex is a major site of steroid hormone production in mammals. It is composed of concentric zones of steroidogenic cells surrounding the chromaffin cells of the adrenal medulla (Gallo-Payet and Battista, 2014; Yates et al., 2013) (**Figure 1.1**). Each zone of the cortex produces distinct steroid hormones that affect a variety of physiological functions. The outer layer, the zona glomerulosa (zG) makes up about 15% of the cortex and produces aldosterone, a mineralocorticoid whose major function is to regulate intravascular volume through sodium retention and thereby controls blood pressure. Aldosterone excess in pathophysiological conditions such as primary aldosteronism can cause irreversible cardiovascular damage and ultimately lead to multi-system dysfunction (Galati et al., 2013; Magill, 2014). The inner layer, the zona fasciculata (zF), roughly eight times the size of the zG, synthesizes glucocorticoids, which have diverse effects on immunity, metabolism, development and behavior. In humans, some non-human primates (e.g., rhesus macaques, marmosets), ferrets and the spiny mouse, a third layer, the zona reticularis (zR) lies between the zF and the medulla and produces androgens (Pihlajoki et al., 2015). While traditional laboratory mice lack a true zR, a temporary zone, designated the X-zone, has been identified and is believed to be a remnant of the fetal adrenal cortex (Morohashi and Zubair, 2011).

Embryonic development of the adrenal gland is relatively well understood (Xing et al., 2015). At E9.0 in the mouse, a group of cells in the coelomic epithelium become committed to the adrenogonadal lineage by expressing Steroidogenic factor 1 (Sf1). These cells then delaminate into the underlying mesenchyme and form the adrenogonadal primordium (AGP). At E10.5, a subset of AGP cells marked by Sf1-Fetal Adrenal Enhancer (FAdE) enhancer activity separates out to form the fetal adrenal anlagen. At around E12.5, neural crest cells migrate into the fetal adrenal and become precursors of the medulla. The fetal cortex starts to regress at E14.5 as the definitive cortex emerges beneath the newly formed capsule. Lineage tracing studies have

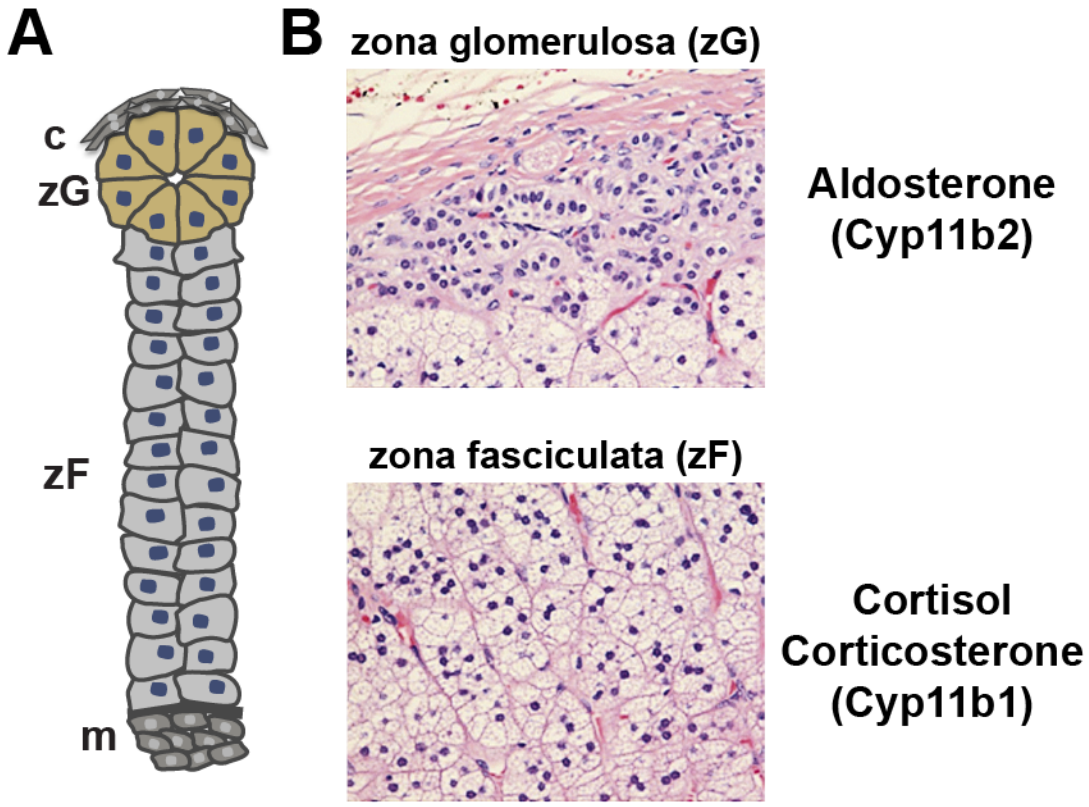

Figure 1.1. Functional and morphological zonation of the adult adrenal cortex.

A, schematic representing different layers of the adult cortex. The cortical epithelium consists of steroidogenic cells (blue nuclei) underlying a mesenchymal capsule (c). Zona glomerulosa (zG) cells (yellow) form compact clusters called glomeruli. Zona fasciculata (zF) cells (light grey) form parallel cords. The adrenal medulla (m) consists of chromaffin cells that are of neural crest origin. B, histological images of the zG and zF (hematoxylin and eosin staining). Cyp11b2 catalyzes the final steps of aldosterone synthesis in the zG. Cyp11b1 directs cortisol or corticosterone synthesis in the zF. Histological images are taken from McNicol, A. M. and Lack, E. E., 2015.

shown that the definitive cortex arises from the fetal cortex and later on gives rise to the adult cortex (Wood et al., 2013; Zubair et al., 2008).

Proper control of steroidogenic function in the adult adrenal cortex relies not only on appropriate endocrine signaling but also on the integrity of tissue structure and homeostasis (Gallo-Payet and Battista, 2014). Disruption of zonation and homeostasis has been implicated in many adrenal diseases such as primary aldosteronism, cortisol-producing adenomas, primary pigmented nodular adrenocortical disease (PPNAD), congenital adrenal hyper- and hypo-plasia and adrenocortical carcinoma (Walczak and Hammer, 2014). However, the cellular and molecular mechanisms that maintain normal tissue homeostasis in the adult cortex remain poorly understood. Here, we highlight the current knowledge of adult adrenocortical homeostasis and zonation, with an emphasis on 1) adrenal morphology and ultrastructure, 2) signaling pathways important for control of zonation, 3) evidence for adrenocortical stem cells and 4) transdifferentiation/direct conversion between differentiated cells.

Adrenal zonation: morphology and ultrastructure

The adrenal cortex is an epithelial tissue enveloped in a mesenchymal capsule. As part of an epithelial structure, adrenocortical cells express epithelial markers such as laminin I and cytokeratins, markers of the basement membrane such as type IV collagen and a diverse array of laminin-associated integrin subunits (i.e., alpha 3, beta 1) (Campbell et al., 2003; Otis et al., 2007; Virtanen et al., 2003; Miettinen et al., 1985). However, in contrast to classical epithelial tissues (e.g., as found in the intestine) adrenocortical cells do not express the epithelial cell marker E-cadherin, but instead express N-cadherin, generally thought to be a neuronal marker (Tsuchiya et al., 2006). Morphologically, the cortical zones demonstrate clear differences in their cellular structure and organization. For instance, cells in the zG are arranged in discrete cellular

clusters, referred to as glomeruli, which are surrounded by basement membrane proteins and a capillary network extending from the capsule (Otis et al., 2007). Cells in each glomerulus are densely packed, possess little cytoplasm and present with apposition of large membrane domains. Electron microscopic analysis reveals a limited number of lipid droplets and mitochondria with lamelliform cristae. In addition, rough endoplasmic reticulum is more abundant than the smooth endoplasmic reticulum (Black et al., 1979; Friend and Gilula, 1972; Nussdorfer, 1980). Notably, the structure of the zG is highly conserved among many species (Nussdorfer, 1980). Along with a morphological identity, zG cells possess a particular molecular signature and can be identified by the presence of patches of Cyp11b2 (a.k.a. Aldosterone Synthase, AS)-expressing cells (Walczak et al., 2014) and by the expression of Disabled homolog 2 (Dab2; Romero et al., 2007), Protein delta homolog 1 (Dlk1; Halder et al., 1998) and β-catenin (**Figure 1.2**), (as discussed below) (Eberhart and Argani, 2001; Walczak et al., 2014). Given the strong association between the region of β-catenin positivity and the morphologically identifiable zG, it is tempting to speculate that β-catenin may promote a transcriptional program that leads to the distinct zG morphology.

The cells in the zF, which produce glucocorticoids in response to the adrenocorticotropic hormone (ACTH), have strikingly different morphological and ultra-structural features. zF cells are organized in cord-like structures flanked by fenestrated blood vessels, which facilitate the rapid exchange of hormones between the circulation and steroidogenic cells. Cells in the zF are larger and less densely packed than those in the zG and possess a well-developed smooth endoplasmic reticulum, large gap junctions, many lipid droplets, and mitochondria characterized by tubule-vesicular cristae (Black et al., 1979; Nussdorfer, 1980). zF cells are commonly identified by the expression of Cyp11b1 (11-beta hydroxylase, 11β-OH; Gomez- Sanchez et al., 2014) and Akr1b7 (aldo-keto reductase family 1, member B7) (Aigueperse et al., 1999).

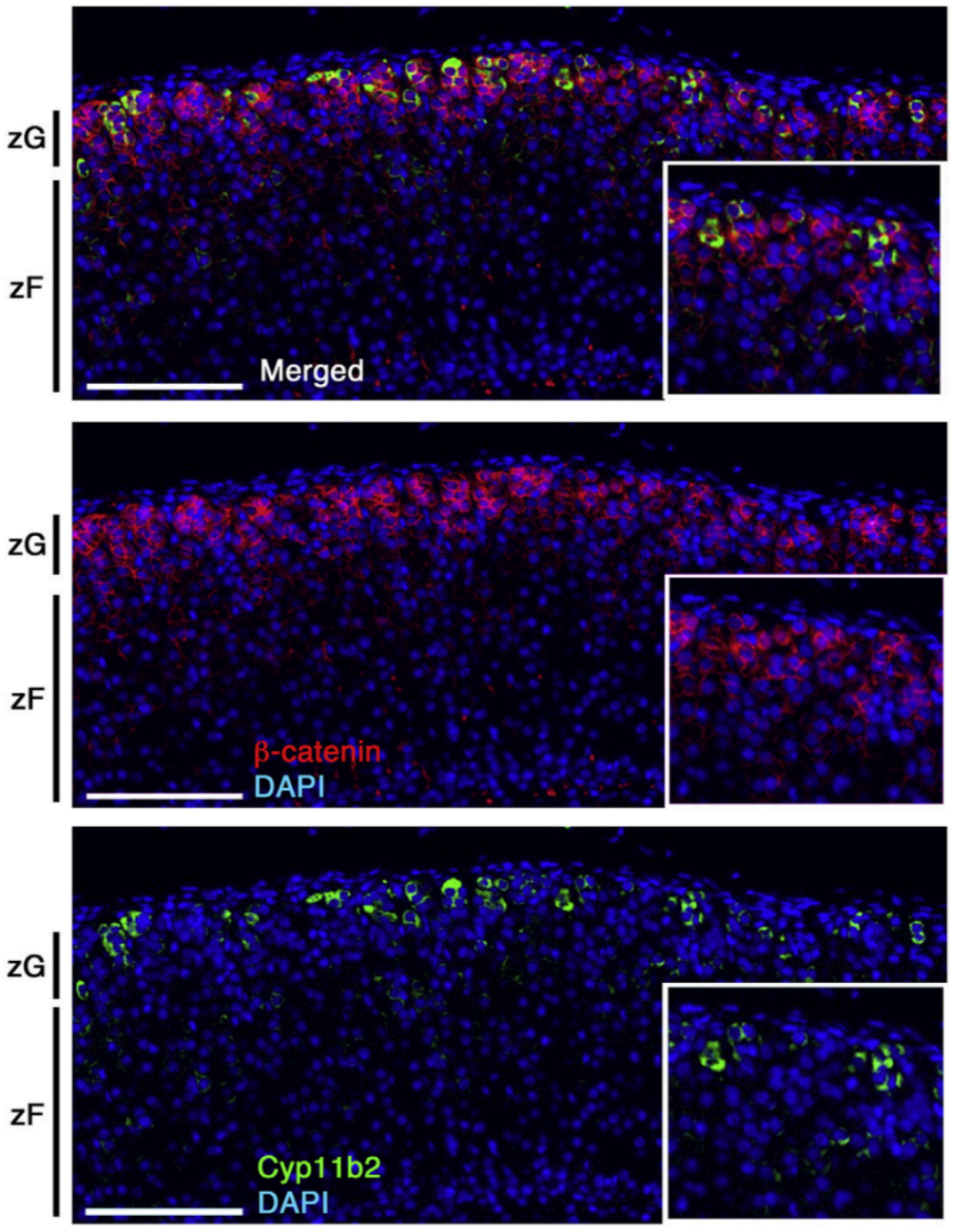

Figure 1.2. Molecular markers of the zona glomerulosa.

Immunofluorescence staining of a mouse adrenal cortex section. The expression pattern of Cyp11b2 is restricted to a few cells in the zG marked by β-catenin. Insets are magnified details of the larger image. Scale bars, 100μm.

The cells of the zR produce dehydroepiandrostenedione (DHEA) and the sulfated derivative DHEA-S during fetal life and upon adrenarche in humans, some non-human primates, ferrets and the spiny mouse (Pihlajoki et al., 2015). zR cells display similar characteristics to zF cells, though they tend to exhibit less lipid droplets, more lysosomes and lipofuscin pigment granules (Rhodin, 1971). The X-zone in mice represents a transient, fetal-derived region enriched in eosinophilic cells located between the zF and the cortical-medullary boundary (Morohashi and Zubair, 2011). The cells of the X-zone are smaller than zF cells, with varied degrees of cytoplasmic density and display diverse mitochondrial shapes endowed mainly with tubular cristae (Sato, 1968). The X-zone seems to be linked to catabolism of progesterone (Hershkovitz et al., 2007).

The existence of morphologically different zones in the adrenal cortex, without the presence of physical barriers between them, suggests the presence of molecular cues that tightly control the identity of each zone. In the following section, we will review data that implicate several signaling pathways in the regulation of zonation.

Signaling pathways and zonation

Over the past 15 years, significant advances have led to an increased understanding of how Angiotensin II (AngII), potassium ions (K^+) and ACTH, as well as their corresponding downstream signaling pathways, contribute to zonation. Important progress has also been made regarding the role of the canonical Wnt/β-catenin signaling pathway in maintaining proper zonation. In addition, several studies have shown that tight regulation of the ACTH/cyclic adenosine monophosphate (cAMP) and Wnt/β-catenin signaling pathways is required to preserve the morphological and functional boundaries between the neighboring zones of the cortex. The importance of these pathways in controlling normal adrenocortical homeostasis and

zonation is underscored by the consequences of somatic gain-of-function mutations, including those that give rise to aldosterone producing adenomas (APAs) (e.g., mutations in K^+ channels and components of the Wnt/β-catenin signaling pathway) and PPNAD (e.g., mutations in PRKAR1A, the gene encoding the cAMP-dependent protein kinase type I-alpha regulatory subunit) (Berthon et al., 2015; Boulkroun et al., 2015). The following sections highlight the role these various factors and pathways play in regulation of zonation during homeostasis and disease.

1. Regulation of zonation in the zG

The main stimuli responsible for modulating zG size are plasma angiotensin II (AngII) and K^+ levels (Gallo-Payet and Battista, 2014). AngII is an octa-peptide, derived from serial proteolytic cleavage of angiotensinogen and angiotensin I, which acutely regulates blood pressure through direct effects on vascular tone. As reviewed elsewhere, AngII also indirectly regulates blood pressure through its acute and chronic effects on the adrenal cortex, which include stimulating the synthesis of aldosterone through the transcriptional regulation of *Cyp11b2* and trophic effects on the zG (Bollag, 2014). Additional studies have shown that AngII, a low sodium diet or high potassium intake stimulates proliferation of zG cells and induces expansion of the zone (Deane et al., 1948; McEwan et al., 1999; Nishimoto et al., 2014; Shelton and Jones, 1971; McNeill, 2005). Conversely, zG size rapidly decreases upon sustained sodium loading (Shelton and Jones, 1971).

Most effects of AngII in the adrenal cortex are mediated by the Angiotensin II receptor type 1 (AT1R), a G-protein coupled receptor enriched in the zG. AT1R is responsible for the transactivation of several downstream mediators, including phospholipase C via calcium/calmodulin-dependent protein kinases (CaMKs) and diacylglycerol/protein kinase C (PKC) (Breault et al., 1996; Wang et al., 1997; Mehta and Griendling, 2007). The use of specific

AT1R blockers, such as losartan and candesartan, has confirmed a role for AT1R in aldosterone synthesis, zG cell proliferation and width (Davies et al., 2008; McEwan et al., 1999, 1996). The activity of AT1R is counter-balanced by the type-2 angiotensin receptor (AT2R), expressed throughout the cortex and enriched in the adrenal medulla, which promotes cell death and cell differentiation (Breault et al., 1998; Lu et al., 1995; reviewed in Steckelings et al., 2010).

The canonical Wnt/β-catenin signaling pathway has also been proposed to regulate zG proliferation and to be a main determinant of zG identity (Berthon et al., 2010; Drelon et al., 2015). β-catenin is the essential transducer of canonical Wnt signaling and its nuclear and cytoplasmic accumulation is a marker of an active signaling cascade (**Figure 1.3**) (Clevers and Nusse, 2017). The cytoplasmic amount of β-catenin is regulated by a destruction complex composed of the serine/threonine kinases casein kinase 1 (CK1), glycogen synthase kinase 3 (GSK3), adenomatous polyposis coli (APC), Axin, and Wilms' tumor gene on X chromosome (WTX). When Wnt ligands bind to the Frizzled and LRP5/6 receptors, Axin is recruited to the plasma membrane and relieves the destruction of β-catenin protein. β-catenin can then accumulate in the cytoplasm and translocate into the nucleus, where it acts as a transcriptional co-activator for members of the Tcf/Lef family of transcription factors.

Tcf/Lef transcription reporter activity as well as strong cytoplasmic and nuclear β-catenin staining have been used to establish that canonical Wnt/β-catenin signaling is active in the outer region of the adrenal cortex, beneath the capsule, overlapping with the morphologically distinct zG (**Figure 1.2**) (Berthon et al., 2010; Kim et al., 2008; Walczak et al., 2014). Exactly what triggers Wnt signaling activity in the zG is still not completely understood. Nineteen Wnt ligands exist, of which six have been identified in the mouse adrenal (Drelon et al., 2015). Of these, Wnt4 is specifically expressed in the zG region of the adult adrenal and is required for adrenal

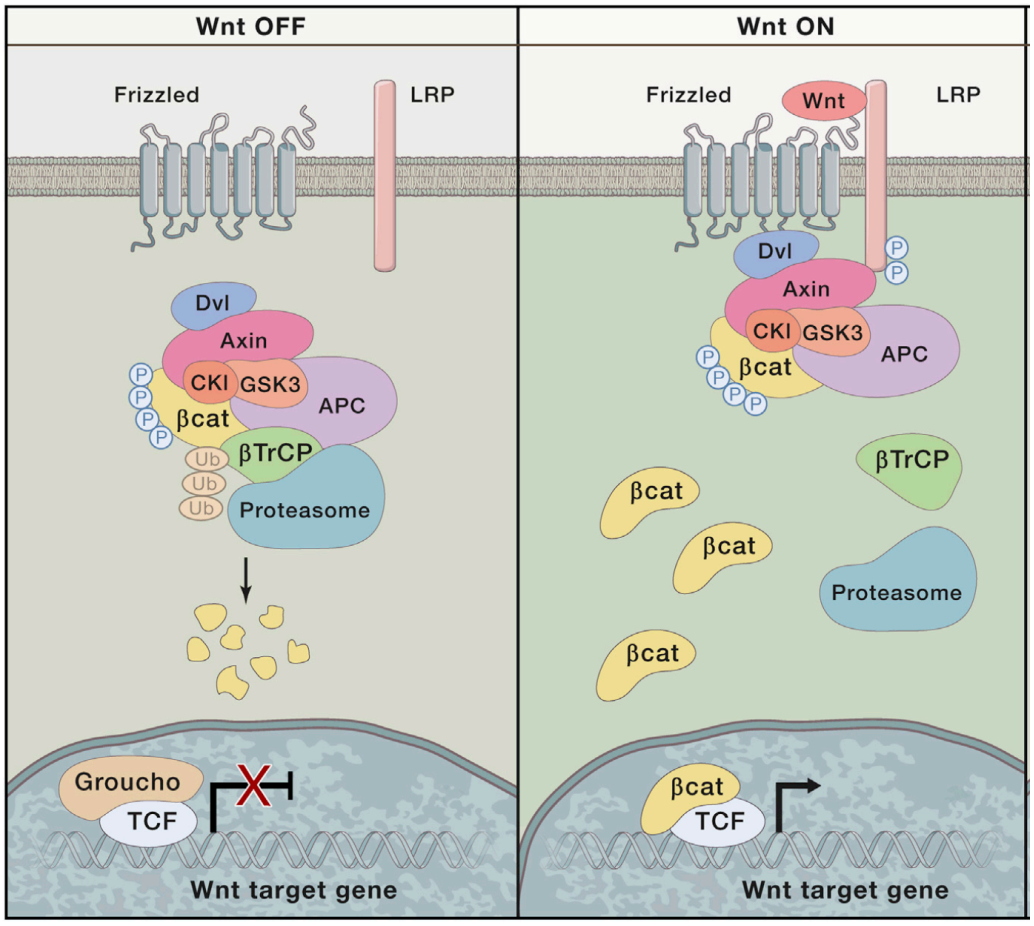

Figure 1.3. The WNT/β-catenin signaling pathway.

Schematic of the WNT/β-catenin signaling pathway components. Without Wnt ligand binding, the pathway is off. β-catenin is phosphorylated by the destruction complex and degraded by the proteasome. When Wnt ligands bind to the Frizzled and LRP receptors, the destruction complex is inhibited and β-catenin accumulates. β-catenin translocate into the nucleus and activate target gene transcription with TCF/Lef transcription factors. Adapted from Clevers and Nusse, 2017.

homeostasis (Heikkila et al., 2002). The expression patterns of the other ligands, including Wnt5a, Wnt5b, Wnt2b, Wnt9a, and Wnt11, have only been described in the fetal adrenal, where they are expressed in the capsular/subcapsular region. Recently, Rspo3 (encoding R-spondin 3) has been recognized as an essential Wnt ligand that signals from the capsule to the zG to activate canonical Wnt/β-catenin signaling and maintain zonation throughout life (Vidal et al., 2016).

Canonical Wnt/β-catenin signaling has also been linked to the steroidogenic activity of the zG. Human cell culture studies showed β-catenin directly binds to the AT1R enhancer to drive AT1R expression and indirectly activates CYP11B2 transcription via the transcriptional regulation of the orphan nuclear receptors NUR77 and NURR1 (Berthon et al., 2014). Additionally, in mice, constitutive activation of β-catenin or inactivation of APC leads to hyperaldosteronism (Berthon et al., 2010; Bhandaru et al., 2009), while deletion of either β-catenin or Wnt4 results in decreased *Cyp11b2* transcripts and lower aldosterone production (Heikkilä et al., 2002; Kim et al., 2008). Together, these data indicate that Wnt/β-catenin signaling plays an important role in regulating aldosterone production, perhaps through an interaction with AngII-dependent signaling. Interestingly, however, in mice, while the entire zG is Wnt-responsive, only a subset of zG cells express Cyp11b2 (**Figure 1.2**) (Berthon et al., 2010; Kim et al., 2008; Walczak et al., 2014), implying that Wnt/β-catenin signaling may be necessary but not sufficient for aldosterone production.

Given the well-documented contribution of Wnt/β-catenin signaling to the proliferative activity of several tissues (Masckauchán et al., 2005; Pei et al., 2012), this pathway may also play a role in the regulation of zG cell proliferation, thereby affecting the overall size of the zone. Indeed, recent studies have shown that loss of Rspo3 (leading to a decrease in Wnt/β-catenin signaling) results in decreased zG cell proliferation and overall adrenal size (Vidal et al., 2016), while

stabilization of β-catenin in the cortex stimulates cell proliferation (Berthon et al., 2010). Whether the response of zG cells to physiological cues, such as AngII and high K^+ levels, is mediated by Wnt/β-catenin signaling remains to be fully investigated. Therefore, it remains an interesting possibility that Wnt/β-catenin signaling may mediate the proliferative response of zG cells to physiological cues. It should be noted, however, that short-term treatment with AngII suppresses Wnt/β-catenin signaling (Berthon et al., 2014), suggesting the presence of a complex interplay (e.g., feedback loop) between endocrine and paracrine factors in the regulation of zG homeostasis and aldosterone production.

While inactivation of Wnt signaling impaired steroidogenesis and proliferation, stabilization of β-catenin or inactivation of the Wnt inhibitor Sfrp2 disrupted zonation leading to ectopic zG cells in the region normally occupied by zF cells (Berthon et al., 2010, 2014). While the cellular mechanism(s) underlying this effect are unknown, the presence of zG cells within the zF may either arise from (1) the failure of zG cells to transdifferentiate/directly convert into zF cells, or from (2) the reverse transdifferentiation (or de-differentiation) of zF cells into zG cells. The decreased amounts of Cyp11b1 and Akr1b7 transcripts in adrenals with stabilized β-catenin are consistent with both of these scenarios (Berthon et al., 2010). However, it has also been suggested that β-catenin can directly antagonize zF function. Activation of Wnt signaling in a mouse zF-like cell line, ATC7-L, causes reduced transcription of the zF-specific steroidogenic genes Cyp11b1 and Mc2r (Walczak et al., 2014). This results from β-catenin titrating Sf1 away from its target genes and sustaining the expression of the secreted factor coiled-coil domain containing 80 (Ccdc80), a putative zF inhibitor (Walczak et al., 2014). Altogether, these data imply that Wnt/β-catenin signaling can influence zonation by promoting the zG identity and antagonizing the zF identity.

Sustained activity of the Wnt/β-catenin signaling pathway is the most common alteration in APAs (about 70% of the tumors) (Berthon et al., 2014) and β-catenin activating mutations represent the second leading genetic mutation associated with this disease (about 5% of the tumors) (Åkerström et al., 2016). APAs carrying activating mutations in β-catenin exhibit a bimodal score for CYP11B2 expression, displaying either low or very high levels of the protein in the nodules (Åkerström et al., 2016). Since this study did not report clinical or genetic stratification associated with the different levels of CYP11B2 expression, variation may be explained by the β-catenin activating mutations arising from different cell populations or during different stages of the disease. Consistent with these hypotheses, β-catenin mutations can also be found in non-functioning adenomas and in carcinomas (Tissier et al., 2005), suggesting that the timing of the mutational event in the oncogenic process along with additional putative genetic hits may be critical in the outcome of the disease. Altogether, these data imply that canonical Wnt/β-catenin signaling plays a critical role in establishing and regulating zG steroidogenic activity and suppressing zF activity, both in homeostasis and disease.

2. Regulation of zonation in the zF

Steroidogenesis and cell proliferation in the zF are under the control of the ACTH/cAMP signaling pathway (Ruggiero and Lalli, 2016). This signaling cascade is initiated by ACTH, which acts on the melanocortin 2 G-protein coupled receptor (MC2R) and the MC2R accessory protein (MRAP) (Lefkowitz et al., 1970; Lehoux et al., 1998; Metherell et al., 2005). MC2R and MRAP expression are also regulated by the ACTH/cAMP pathway (Xing et al., 2010). The occupancy of the receptor triggers the release of the alpha subunit of the stimulatory G protein and the conversion of ATP into cAMP by adenylyl cyclase (Kim et al., 2005, 2007). These events ultimately result in the activation of the catalytic subunit of PKA and the subsequent phosphorylation of cytoplasmic and nuclear targets, which include the cAMP-responsive

element modulator (CREM) and the cAMP-responsive element binding protein (CREB) transcription factors (Peri et al., 2001).

A large amount of evidence suggests that the cAMP signaling pathway is primarily active in the zF. While several molecular components of the cAMP cascade are present in both the zF and the zG (Cote et al., 2001; Gorrigan et al., 2011), Cyp11b1, the enzyme that catalyzes the final step in the biosynthesis of cortisol and corticosterone, is a target of ACTH and selectively expressed in the zF (Freedman et al., 2013; Gomez-Sanchez et al., 2014). Additionally, the aldo-keto reductase Akr1b7, which is selectively expressed in the zF, is also a target of cAMP signaling (Aigueperse et al., 1999; Berthon et al., 2010; Sahut-Barnola et al., 2010). Together, these data suggest that the cAMP signaling pathway is primarily active in the zF.

In a physiological context, ACTH/cAMP signaling also controls the size of the zF without disrupting its functional and morphological boundaries with the zG or the X-zone. This is evident in humans, where mutations in genes encoding MC2R and MRAP are associated with glucocorticoid insufficiency, leading to adrenals with a hypoplastic zF but a morphologically intact zG and normal aldosterone production (Clark and Weber, 1998). Moreover, mice lacking T-box transcription factor (Tpit), encoding a transcription factor essential for the expression of the ACTH precursor proopiomelanocortin (POMC), develop severe adrenocortical hypoplasia mainly affecting the zF (Pulichino et al., 2003). Similarly, deletion of Pomc leads to overall reduced adrenal mass associated with impaired proliferative activity and hypoplasia of the zF (Karpac et al., 2005). Inactivation of the Mc2r gene also produces hypoplasia of the zF (Chida et al., 2007). In addition, this same effect is seen following suppression of the zF using dexamethasone (Freedman et al., 2013; Thomas et al., 2004). Overall, these results point to a role for physiological levels of ACTH/cAMP signaling in supporting adrenal mass and proliferation, with a primary effect on the zF.

On the other hand, dysregulated cAMP signaling in a pathological context, can also result in disruption of zonation. This emerges from studies on constitutive activation of cAMP signaling in the adrenal cortex, obtained with genetic deletion of the regulatory subunit 1a of PKA (Prkar1a). Adrenals with constitutive cAMP signaling present with large eosinophilic cells at the cortical-medullary boundary that express Cyp17, a mouse adrenal fetal marker, as well as markers of the zF and the X-zone (Akr1b7 and 20-alpha-hydroxylase, respectively) (Sahut-Barnola et al., 2010). These atypical cells were shown to expand in a centrifugal direction and to occupy most of the cortex in aged mice, thereby disrupting the concentric organization of the cortical zones. These data show that regulation of cAMP signaling is essential for the maintenance of proper structural and functional zonation, and suggest that disruption of this regulation may lead to destabilized zonal identity and altered cell differentiation.

Mechanisms underlying adrenocortical cell renewal in the adult

Classically, highly regenerative tissues maintain cellular homeostasis by utilizing an active stem/progenitor cell compartment, or by replication of pre-existing differentiated cells. In some tissues where mature cell types are post-mitotic, such as the gastrointestinal tract, the epidermis, and the hematopoietic system, tissue homeostasis relies heavily on the capacity of adult stem cells to self-renew and give rise to differentiated cell lineages (Barker et al., 2012; Blanpain and Fuchs, 2009; Oguro et al., 2013). In other tissues, however, such as the liver, normal homeostasis is largely achieved through direct replication of mature differentiated cells, whereas stem cell-like activities only emerge upon injury (Miyajima et al., 2014).

The adult adrenal cortex is a moderately proliferative tissue. Cells in the outer cortex including the zG and the outer zF exhibit a higher proliferation rate than the inner cortex, and cell death is

predominantly observed at the cortical-medullary boundary under physiological conditions (Kataoka et al., 1996; Mitani et al., 1999). Adrenocortical turnover is accompanied by the centripetal migration of cells from the outer to the inner cortex. A number of groups have attempted to measure the speed of centripetal migration in rodents using pulse-labeling techniques. Zajicek et al. reported that the time for a cell to traverse the entire cortex in rats is around 104 days (Zajicek et al., 1986). While Chang et al. estimated the speed of migration to be 13-20 μm/day in mice (Chang et al., 2013), which translates to 12-19 days to traverse the entire cortex (assuming an average cortical thickness of ~250 μm). However, label-retention studies used to measure the rate of tissue renewal in mice revealed that complete turnover took 60 days in the zG, and 120 days in the zF (Kataoka et al., 1996), much slower than would be inferred using the speed of migration. The discrepancy between these data may reflect an important feature of the adrenal, namely that not all cells participate in centripetal migration to the same degree. That is, some cells may migrate at a much lower speed or exhibit long-term tissue residence. Nonetheless, the speed of centripetal migration is a good proxy for overall tissue dynamics; while the prolonged turnover time of each zone may reflect the behavior of long-lived cortical cells.

1. Evidence for adrenocortical stem cells

While the full extent of the proliferative potential of differentiated zG and zF cells has not been thoroughly investigated, it has been proposed that the adult adrenal contain tissue-resident stem cells in the peripheral cortex capable of unlimited self-renewal and differentiation into steroidogenic cell types (Pihlajoki et al., 2015; Walczak and Hammer, 2014). This notion is supported by the observation that enucleated rat adrenal glands can fully regenerate from the remaining capsular and subcapsular cells (Greep and Deane, 1949), consistent with a remarkable degree of proliferative and differentiation potential, at least under extreme regenerative stress. During normal tissue maintenance, the constant centripetal migration of

cells implies that new cells are generated at the outer cortex, and have the potential to differentiate into the cells of the zG and zF. Collectively, these data point to a remarkable ability of the outer cortex to support long-term cortical renewal, assuming the turnover rate is constant. However, the degree to which ongoing cortical renewal is derived from adult stem cell activity versus proliferation of differentiated cortical cells remains to be elucidated.

The search for adult tissue stem cells is often aided by the presence of an easily identifiable niche with distinct anatomical and molecular features (Rezza et al., 2014). An increased understanding of the signaling network in the peripheral cortex has led to the identification of putative adrenal stem cell markers. One popular model contends that stem cells are located in the capsule as non-steroidogenic mesenchymal cells (Kim et al., 2009; Walczak and Hammer, 2014). The first direct evidence supporting this idea came from King et al., in 2009. Using genetic lineage tracing studies, the investigators effectively demonstrated capsular cells marked by Gli1 expression can give rise to all steroidogenic cell types in the adult cortex (King et al., 2009). Gli1 along with two other family members, Gli2 and Gli3, are transcription factors whose activities are controlled by the Hedgehog (Hh) paracrine signaling pathway. Hh signaling has well studied functions throughout vertebrate and invertebrate development and plays important roles in the maintenance and regeneration of numerous adult tissues (McMahon et al., 2003). Sonic hedgehog (Shh) is the only ligand expressed in the adrenal cortex, and its onset of expression at E11.5 together with other pathway components, such as the membrane receptors Patched1 (Ptch1) and Smoothened (Smo), suggest this pathway regulates adrenal organogenesis as well as adult homeostasis, potentially through regulating the activity of Gli1+ capsular stem cells (King et al., 2009). This hypothesis has been partly substantiated by three studies examining the effect of genetic ablation of Shh. Collectively, their data showed that loss of Shh expression from the subcapsular/zG region during embryonic development leads to decreased proliferation in the capsule and adrenal hypoplasia that persists into adulthood

(Ching and Vilain, 2009; Huang et al., 2010; King et al., 2009). Even though the role of Shh signaling in adult homeostasis has not been formally tested, the long-lasting effect of Shh ablation at fetal stages points to its important role in establishing and/or maintaining a key population of cells needed for continuous cortical renewal. Interestingly, while the Gli1+ cell lineage is long lasting in the adult cortex, its contribution to cortical renewal is relatively infrequent (King et al., 2009). This suggests that while Shh signaling is absolutely required for organogenesis, it may play a less crucial role once the adult cortex has formed. Cellular sources apart from the Gli1+ lineage must be in place to support continuous adult cortical renewal.

Another proposed marker of stem cell identity in the capsule is Wilms tumor suppressor gene 1 (Wt1). Wt1 is a transcription factor with many functions in tissue growth and homeostasis (Chau et al., 2011; Hohenstein and Hastie, 2006). It is known that formation of the AGP requires Wt1 partly through its role in regulating Sf1 expression (Val et al., 2007; Wilhelm and Englert, 2002). In 2013, Bandiera et al. demonstrated cortical cells can arise from Wt1-expressing cells in the adult capsule. However, lineage-marked cell patches are present at low frequency, suggesting relatively little contribution of Wt1+ capsular cells during adult tissue maintenance (Bandiera et al., 2013). Furthermore, it has been proposed that Tcf21/Pod1, a transcriptional modulator of Sf1 (Simon and Hammer, 2012), marks cells in the adrenal capsule that exhibit clonogenic activity during development. However, in the adult they seem to exclusively contribute to a mesenchymal lineage of non-endothelial stromal cells (Wood et al., 2013). Together, these lineage-tracing studies have identified mesenchymal cells in the adrenal capsule that can give rise to either steroidogenic cells or non-endothelial stromal cells in the cortex (**Figure 1.4A**). However, capsular contribution to cortical cell mass appears to be rather limited in the adult.

Given that the adult cortex maintains a steady rate of centripetal migration (at least during the time points examined), new cells need to be continuously generated to replenish displaced

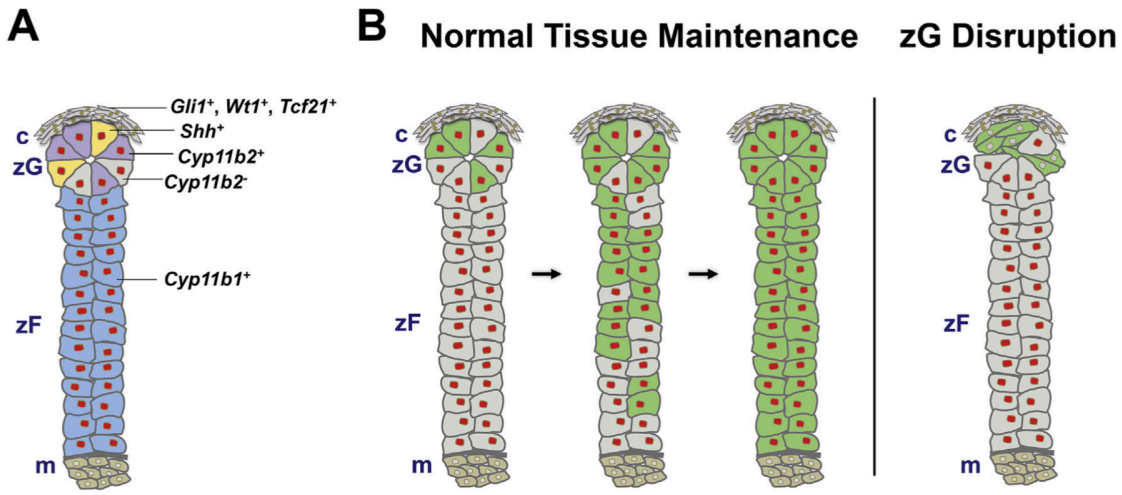

Figure 1.4. Cellular mechanisms underlying adrenocortical renewal in the adult.

A, Schematic showing location of proposed markers for clonogenic capsular cells (Gli1+, WT1+, Tcf21+; grey with brown nuclei), putative TA progenitors (Shh+; yellow), aldosterone-producing zG cells (Cyp11b2+; purple), non-aldosterone-producing zG cells (Cyp11b2-, can be identified with pan-zG markers such as At1r, β-catenin; grey with red nuclei), and zF cells (Cyp11b1+; blue). Red nuclei denote Sf1+ cells. B, Left panel, schematic showing progression of lineage marking in AS-Cre/+; R26R-mTmG mice during normal tissue maintenance. The Cyp11b2+ lineage gives rise to the entire cortex through transdifferentiation/ direct conversion and centripetal migration. Right panel, schematic showing disruption of the zG following Sf1 deletion in AS-Cre/+; Sf1 fl/fl; R26R-mTmG mice. In these mice Cyp11b2- cells give rise to a normal zF. Green cells denote lineage-marked Cyp11b2+ cells and their descendants and red nuclei denote Sf1+ cells. m, medulla.

cells. There is a clear discrepancy between the infrequent capsular contribution and the continuous need for new cortical cells, suggesting that other cell populations may function to maintain adult homeostasis. It has been proposed that Shh-expressing cells in the subcapsular/zG region serve as transit-amplifying (TA) progenitors to sustain cortical renewal (Laufer et al., 2012). The authors performed short-term lineage tracing to show that the Shh+ lineage can give rise to Cyp11b2+ and Cyp11b1+ cells during adult homeostasis, but it is unclear whether these cells do indeed sustain long-term cortical renewal (King et al., 2009). In addition, Shh-expressing cells are not more proliferative than other cells in the subcapsular region, which is inconsistent with their proposed identity as TA cells (Walczak et al., 2014). Thus, it remains to be demonstrated whether the adrenal cortex utilizes the classical stem cell-TA progenitor lineage hierarchy to maintain adult homeostasis and if not, what cellular mechanisms support the majority of adult cortical cell turnover.

2. Role of transdifferentiation/direct conversion

The centripetal migration model implies that mature aldosterone-producing zG cells have the ability to convert into zF cells as they cross the zonal boundary. Using a Cyp11b2 (AS)-Cre mouse model, Cyp11b2-expressing zG cells were permanently marked by GFP (Green Fluorescent Protein) expression and lineage-traced (Freedman et al., 2013). Remarkably, the entire zG and the majority of the zF became labeled within 3 months (**Figure 1.4B**), suggesting that all cortical cells are descendants from the Cyp11b2+ cell lineage during normal tissue maintenance. The extensive overlap between the GFP-marked population and the steroidogenic cortex has been further confirmed by co-staining with Sf1 and β-catenin as well as confocal 3D reconstructions (unpublished data). These data challenge the view that the adult adrenal cortex contains a strict lineage hierarchy of undifferentiated progenitors giving rise to mature cell types. It is also theoretically possible that mature cortical cells could dedifferentiate into immature progenitors, which could then give rise to mature zG and zF cells, however, there is no direct

evidence for such a phenomenon. Given the robust degree of GFP marking throughout the entire cortex in the AS-Cre model, it is unlikely that Cyp11b2+ lineage contribution to cortical renewal represents a minor event, such as mature cells dedifferentiating into progenitors. Hence, we propose that mature zG to zF transdifferentiation/direct conversion represents a major cellular mechanism of adult adrenocortical turnover during normal homeostasis. However, it remains unclear to what extent zG cells alone can sustain long-term cortical renewal, or to what degree zG cells rely on replenishment from the capsule. To address the self-renewing potential of mature zG cells, an inducible mouse model, such as AS-CreER, will greatly facilitate further investigation.

The idea that undifferentiated progenitors exist in the subcapsular cortex is partly based on the observation of heterogeneous Cyp11b2 expression in the zG region (**Figure 1.2**; Guasti et al., 2011; Walczak et al., 2014). Accordingly, Shh-expressing cells are thought to represent a unique non-Cyp11b2-expressing population in the zG, given the minimal overlap between the two markers (King et al., 2009; Walczak et al., 2014). However, many other markers such as At1r, Dab2, and β-catenin, identify the morphological zG as a homogeneous population (Berthon et al., 2010; Huang et al., 2013; Walczak et al., 2014). Given the wide range of aldosterone output in response to varying physiological demands, it is possible that at any given time only a subset of zG cells produce aldosterone. Total cortical labeling in the AS-Cre model, therefore, can be interpreted as a cumulative readout of all Cyp11b2-expressing cells, and their progeny, prior to the time of observation (**Figure 1.4B**). Interestingly, Shh expression has also been reported to respond to endocrine input. In the rat, levels of Shh transcript are markedly down-regulated upon low sodium diet and up-regulated when AngII signaling is blocked (Guasti et al., 2013), suggesting that Shh expression, in the opposite direction of Cyp11b2, is dynamically regulated by the physiological demand for aldosterone. Hence, it remains to be demonstrated whether Shh expression truly marks a unique population in the zG, or rather

represents a dynamic gene expression state that is complementary to the Cyp11b2-expressing state. In fact, the evidence supporting Shh-expressing cells as unique progenitors is based on the fact that the Shh+ lineage gives rise to Cyp11b2+ and Cyp11b1+ cells. However, as presented above, the Cyp11b2+ lineage behaves in the same way. Furthermore, because Cyp11b2+ cells can give rise to the zF, the ability of a cell to give rise to multiple cortical cell types can no longer be used as a "fail-safe" criteria to define bona fide, undifferentiated, stem/progenitor cells in the adrenal cortex, as mature zG cells can also give rise to other zonal cell types. The question of which cell population provides the major source of cortical replenishment remains to be further elucidated.

While during normal tissue maintenance all cortical cells descend from the Cyp11b2+ lineage, analysis of mice having undergone AS-Cre mediated Sf1 deletion revealed that the zF can also be derived from a separate (Cyp11b2-) cellular origin (Freedman et al., 2013) (**Figure 1.4B**). In this model, deletion of Sf1 using AS-Cre led to zG disruption (**Figure 1.4B**), which could no longer give rise to lineage-marked zF cells. Despite this, an entirely normal zF was still evident. Based on this observation, we previously proposed that an "alternative pathway" for zF formation might exist (Freedman et al., 2013), though we have yet to define such a mechanism. Upon further reflection, given the heterogeneous, and presumed dynamic, nature of Cyp11b2 expression in the zG it is also conceivable that under extreme conditions (where selective pressure to generate the zF is high), Cyp11b2-negative zG cells transit into the zF before Cyp11b2 can be expressed, thereby escaping Sf1-deletion. Whether or not putative progenitor/stem cells in the capsule are activated under these stressed conditions remains to be established. Testing this hypothesis would require combining models of zG-specific gene ablation and lineage-tracers that mark putative capsular stem cell populations.

Concluding remarks

Being a remarkably regenerative and multifunctional organ, the adult adrenal cortex presents a number of fascinating questions for developmental biologists as well as endocrine researchers. 1) How does it achieve such precise zonation of closely related yet notably different steroidogenic cells? 2) How is the control of zonation so sensitive and responsive to dynamic physiological demands? 3) What pathological conditions might disturb its regulation circuitry and give rise to clinically observed diseases? In the recent decade, researchers have begun to address these questions by applying knowledge of endocrine and paracrine signaling pathways as well as adult tissue stem cell biology. Two pathways have been identified that directly influence zonal identity, the canonical Wnt pathway for the zG, and cAMP signaling for the zF. Many insights have been gained regarding the connection between these pathway activities and steroidogenesis; however, it still remains largely unclear how zonation is established, maintained, and dynamically controlled. Wnt signaling modulators are being pursued as prime candidates for the dynamic control over zonation. It has also been proposed that cAMP signaling may directly or indirectly antagonize Wnt signaling activity (Drelon et al., 2015).

The notion that adrenocortical renewal relies on resident tissue stem cells is a long-standing hypothesis that has fueled a series of lineage-tracing studies in an attempt to identify such cells. Collectively, these studies have demonstrated that mesenchymal cells in the capsule are able to give rise to the steroidogenic lineage, yet the inductive signal remains unknown. In all cases identified so far, however, lineage contribution from the capsule is rather limited during adult homeostasis. Results from our lab have shown transdifferentiation/direct conversion of Cyp11b2+ zG cells to zF cells can account for turnover of the whole-cortex throughout adult life. Current data highlight an essential role of Sf1 in mediating transdifferentiation of zG cells, yet it still remains an open question what mechanisms govern the migration and conversion of cells

across the zG/zF boundary. Future studies on these topics will facilitate our understanding of zonation and the diseases that arise from its disruption.

Attributions

This chapter was originally published as:

Pignatti, E.*, Leng, S.*, Carlone, D. L., Breault, D. T. Regulation of Zonation and Homeostasis in the Adrenal Cortex. *Molecular and Cellular Endocrinology*. 2016 Sep; **441**(2017):146-155. S.L. was co-first author on this manuscript. E.P. and S.L. wrote the text with input from D.L.C. and D.T.B. It is modified to fit the style of the dissertation. Additional text and figures are included.

References

Aigueperse, C. *et al.* Cyclic AMP regulates expression of the gene coding for a mouse vas deferens protein related to the aldo-keto reductase superfamily in human and murine adrenocortical cells. *J. Endocrinol.* **160**, 147-154 (1999).

Åkerström, T. *et al*. Activating mutations in CTNNB1 in aldosterone producing adenomas. *Sci. Rep.* **6**, 19546 (2016).

Bandiera, R. *et al*. WT1 maintains adrenal-gonadal primordium identity and marks a population of AGP-like progenitors within the adrenal gland. *Dev. Cell* **27**, 5-18 (2013).

Barker, N. *et al*. Identifying the stem cell of the intestinal crypt: strategies and pitfalls. *Cell Stem Cell* **11**, 452-460 (2012).

Berthon, A. *et al*. WNT/β-catenin signaling is activated in aldosterone-producing adenomas and controls aldosterone production. *Hum. Mol. Genet.* **23**, 889-905 (2014).

Berthon, A. *et al*. Constitutive beta-catenin activation induces adrenal hyperplasia and promotes adrenal cancer development. *Hum. Mol. Genet.* **19**, 1561-1576 (2010).

Berthon, A. *et al*. PRKACA: the catalytic subunit of protein kinase A and adrenocortical tumors. *Front. Cell Dev. Biol.* **3**, 26 (2015).

Bhandaru, M. *et al.* Hyperaldosteronism, hypervolemia, and increased blood pressure in mice expressing defective APC. *Am. J. Physiol. Regul. Integr. Comp. Physiol.* **297**, R571-R575 (2009).

Black, V. H. *et al*. A correlated thin-section and freeze-fracture analysis of Guinea pig adrenocortical cells. *Am. J. Anat.* **156**, 453-503 (1979).

Blanpain, C. & Fuchs, E. Epidermal homeostasis: a balancing act of stem cells in the skin. *Nat. Rev. Mol. Cell Biol.* **10**, 207-217 (2009).

Bollag, W. B. Regulation of aldosterone synthesis and secretion. *Compr. Physiol.* **4**, 1017-1055. (2014).

Boulkroun, S. *et al.* Molecular and cellular mechanisms of aldosterone producing adenoma development. *Front. Endocrinol.* **6**, 95 (2015).

Breault, L. *et al.* The role of angiotensin II in human adrenal gland development. *Endocr. Res.* **24**, 953-954 (1998).

Breault, L. *et al.* Angiotensin II receptors in the human adrenal gland. *Endocr. Res.* **22**, 355-361 (1996).

Campbell, S. *et al.* Connection between integrins and cell activation in rat adrenal glomerulosa cells: a role for Arg-Gly-Asp peptide in the activation of the p42/p44(MAPK) pathway and intracellular calcium. *Endocrinology* **144**, 1486-1495 (2003).

Chang, S. P. *et al.* Cell proliferation, movement and differentiation during maintenance of the adult mouse adrenal cortex. *PLoS One* **8**, e81865 (2013).

Chau, Y. Y. *et al.* Acute multiple organ failure in adult mice deleted for the developmental regulator Wt1. *PLoS Genet.* **7**, e1002404 (2011).

Chida, D. *et al.* Melanocortin 2 receptor is required for adrenal gland development, steroidogenesis, and neonatal gluconeogenesis. *Proc. Natl. Acad. Sci.* **104**, 18205-18210 (2007).

Ching, S. & Vilain, E. Targeted disruption of Sonic Hedgehog in the mouse adrenal leads to adrenocortical hypoplasia. *Genesis* **47**, 628-637 (2009).

Clark, A. J. & Weber, A. Adrenocorticotropin insensitivity syndromes. *Endocr. Rev.* **19**, 828-843 (1998).

Clevers, H. & Nusse, R. Wnt/β-catenin signaling, disease, and emerging therapeutic modalities. *Cell* **169**, 985-999 (2017).

Cote, M. *et al.* Expression and regulation of adenylyl cyclase isoforms in the human adrenal gland. *J. Clin. Endocrinol. Metab.* **86**, 4495-4503 (2001).

Davies, L. A. *et al.* TASK channel deletion in mice causes primary hyperaldosteronism. *Proc. Natl. Acad. Sci.* **105**, 2203-2208 (2008).

Deane, H. W., Shaw, J. H. & Greep, R. O. The effect of altered sodium or potassium intake on the width and cytochemistry of the zona glomerulosa of the rat's adrenal cortex. *Endocrinology* **43**, 133-153 (1948).

Drelon, C. *et al.* Adrenal cortex tissue homeostasis and zonation: a WNT perspective. *Mol. Cell. Endocrinol*. **408**, 156-164 (2015).

Eberhart, C. G. & Argani, P. Wnt signaling in human development: beta-catenin nuclear translocation in fetal lung, kidney, placenta, capillaries, adrenal, and cartilage. *Pediatr. Dev. Pathol.* **4**, 351-7 (2001).

Freedman, B. D. *et al.* Adrenocortical zonation results from lineage conversion of differentiated zona glomerulosa cells. *Dev. Cell* **26**, 666-673 (2013).

Friend, D. S. & Gilula, N. B. A distinctive cell contact in the rat adrenal cortex. *J. Cell Biol.* **53**, 148-163 (1972).

Galati, S. J. *et al.* Primary aldosteronism: emerging trends. *Trends Endocrinol. Metab.* **24**, 421-430 (2013).

Gallo-Payet, N. & Battista, M. C. Steroidogenesis-adrenal cell signal transduction. *Compr Physiol.* **4**, 889-964 (2014).

Gomez-Sanchez, C. E. *et al*. Development of monoclonal antibodies against human CYP11B1 and CYP11B2. *Mol. Cell. Endocrinol.* **383**, 111-117 (2014).

Gorrigan, R. J. *et al.* Localization of the melanocortin-2-receptor and its accessory proteins in the developing and adult adrenal gland. *J. Mol. Endocrinol.* **46**, 227-232 (2011).

Greep, R. O. & Deane, H. W. Histological, cytochemical and physiological observations on the regeneration of the rat's adrenal gland following enucleation. *Endocrinology* **45**, 42-56 (1949).

Guasti, L. *et al*. Dlk1 up-regulates Gli1 expression in male rat adrenal capsule cells through the activation of β1 integrin and ERK1/2. *Endocrinology* **154**, 4675-4684 (2013).

Guasti, L. *et al.* Localization of Sonic hedgehog secreting and receiving cells in the developing and adult rat adrenal cortex. *Mol. Cell. Endocrinol.* **336**, 117-122 (2011).

Halder, S. K. *et al.* Cloning of a membrane-spanning protein with epidermal growth factor-like repeat motifs from adrenal glomerulosa cells. *Endocrinology* **139**, 3316-3328 (1998).

Heikkilä, M. *et al.* Wnt-4 deficiency alters mouse adrenal cortex function, reducing aldosterone production. *Endocrinology* **143**, 4358-4365 (2002).

Hershkovitz, L. *et al.* Adrenal 20alpha-hydroxysteroid dehydrogenase in the mouse catabolizes progesterone and 11-deoxycorticosterone and is restricted to the X-zone. *Endocrinology* **148**, 976-988 (2007).

Hohenstein, P. & Hastie, N. D. The many facets of the Wilms' tumour gene, WT1. *Hum. Mol. Genet.* **15**, R196-R201 (2006).

Huang, C. C. *et al.* Progenitor cell expansion and organ size of mouse adrenal is regulated by sonic hedgehog. *Endocrinology* **151**, 1119-1128 (2010).

Huang, Z. *et al.* Immunohistochemical detection of angiotensin II receptors in mouse cerebellum and adrenal gland using “in vivo cryotechnique”. *Histochem. Cell Biol.* **140**, 477-490 (2013).

Karpac, J. *et al.* Development, maintenance, and function of the adrenal gland in early postnatal proopiomelanocortin-null mutant mice. *Endocrinology* **146**, 2555-2562 (2005).

Kataoka, Y., Ikehara, Y. & Hattori, T. Cell proliferation and renewal of mouse adrenal cortex. *J. Anat.* **188** (Pt 2), 375-381 (1996).

Kim, A. C. *et al.* In search of adrenocortical stem and progenitor cells. *Endocr. Rev.* **30**, 241-263 (2009).

Kim, A. C. *et al.* Targeted disruption of beta-catenin in Sf1-expressing cells impairs development and maintenance of the adrenal cortex. *Development* **135**, 2593-2602 (2008).

Kim, C. *et al.* PKA-I holoenzyme structure reveals a mechanism for cAMP-dependent activation. *Cell* **130**, 1032-1043 (2007).

Kim, C., Xuong, N. H. & Taylor, S. S. Crystal structure of a complex between the catalytic and regulatory (RIalpha) subunits of PKA. *Science* **307**, 690-696 (2005).

King, P., Paul, A. & Laufer, E. Shh signaling regulates adrenocortical development and identifies progenitors of steroidogenic lineages. *Proc. Natl. Acad. Sci.* **106**, 21185-21190 (2009).

Laufer, E. *et al.* Sonic hedgehog signaling during adrenal development. *Mol. Cell. Endocrinol.* **351**, 19-27 (2012).

Lefkowitz, R. J. *et al.* ACTH receptors in the adrenal: specific binding of ACTH-125I and its relation to adenyl cyclase. *Proc. Natl. Acad. Sci.* **65**, 745-752 (1970).

Lehoux, J. G., Fleury, A. & Ducharme, L. The acute and chronic effects of adrenocorticotropin on the levels of messenger ribonucleic acid and protein of steroidogenic enzymes in rat adrenal in vivo. *Endocrinology* **139**, 3913-3922 (1998).

Lu, X. *et al.* Pharmacological characterization of angiotensin II AT(2) receptor subtype heterogeneity in the rat adrenal cortex and medulla. *Endocrine* **3**, 255-261 (1995).

Magill, S. B. Pathophysiology, diagnosis, and treatment of mineralocorticoid disorders. *Compr Physiol.* **4**,1083-119 (2014).

Masckauchán, T. N. *et al.* Wnt/beta-catenin signaling induces proliferation, survival and interleukin-8 in human endothelial cells. *Angiogenesis* **8**, 43-51 (2005).

McEwan, P. E., Lindop, G. B. & Kenyon, C. J. Control of cell proliferation in the rat adrenal gland in vivo by the renin-angiotensin system. *Am. J. Physiol.* **271**, E192-E198 (1996).

McEwan, P. E., Vinson, G. P. & Kenyon, C. J. Control of adrenal cell proliferation by AT1 receptors in response to angiotensin II and low-sodium diet. *Am. J. Physiol*. **276**, E303-E309 (1999).

McMahon, A. P., Ingham, P. W. & Tabin, C. J. Developmental roles and clinical significance of hedgehog signaling. *Curr. Top. Dev. Biol.* **53**, 1-114 (2003).

McNeill, H. Distribution of extracellular signal-regulated protein kinases 1 and 2 in the rat adrenal and their activation by angiotensin II. *Endocrinol.* **187**, 149-157 (2005).

McNicol, A. M., & Lack, E. E. The adrenal glands and tumors of extra-adrenal paraganglia. In M. Wick, V. LiVolsi, J. Pfeifer, E. Stelow, & P. Wakely, Jr (Eds.), *Silverberg's Principles and Practice of Surgical Pathology and Cytopathology* (pp. 2978-3040). Cambridge: Cambridge University Press.

Mehta, P. K. & Griendling, K. K. Angiotensin II cell signaling: physiological and pathological effects in the cardiovascular system. *Am. J. Physiol. Cell Physiol.* **292**, C82-C97 (2007).

Metherell, L. A. *et al.* Mutations in MRAP, encoding a new interacting partner of the ACTH receptor, cause familial glucocorticoid deficiency type 2. *Nat. Genet.* **37**, 166-170 (2005).

Miettinen, M., Lehto, V. P. & Virtanen, I. Immunofluorescence microscopic evaluation of the intermediate filament expression of the adrenal cortex and medulla and their tumors. *Am. J. Pathol.* **118**, 360-366 (1985).

Mitani, F. *et al.* Development of functional zonation in the rat adrenal cortex. *Endocrinology* **140**, 3342-3353 (1999).

Miyajima, A., Tanaka, M. & Itoh, T. Stem/progenitor cells in liver development, homeostasis, regeneration, and reprogramming. *Cell Stem Cell* **14**, 561-574 (2014).

Morohashi, K. & Zubair, M. The fetal and adult adrenal cortex. *Mol. Cell. Endocrinol.* **336**, 193-197 (2011).

Nishimoto, K. *et al*. Sodium deficiency regulates rat adrenal zona glomerulosa gene expression. *Endocrinology* **155**, 1363-1372 (2014).

Nussdorfer, G. G. Cytophysiology of the adrenal zona glomerulosa. *Int. Rev. Cytol.* **64**, 307-368 (1980).

Oguro, H., Ding, L. & Morrison, S. J. SLAM family markers resolve functionally distinct subpopulations of hematopoietic stem cells and multipotent progenitors. *Cell Stem Cell* **13**, 102-116 (2013).

Otis, M. *et al.* Expression of extracellular matrix proteins and integrins in rat adrenal gland: importance for ACTH-associated functions. *J. Endocrinol.* **193**, 331-347 (2007).

Pei, Y. WNT signaling increases proliferation and impairs differentiation of stem cells in the developing cerebellum. *Dev. Camb. Engl.* **139**, 1724-1733 (2012).

Peri, A. *et al.* Variable expression of the transcription factors cAMP response element-binding protein and inducible cAMP early repressor in the normal adrenal cortex and in adrenocortical adenomas and carcinomas. *J. Clin. Endocrinol. Metab.* **86**, 5443-5449 (2001).

Pihlajoki, M. *et al.* Adrenocortical zonation, renewal, and remodeling. *Front. Endocrinol.* **6**, 27 (2015).

Pulichino, A. M. *et al.* Human and mouse TPIT gene mutations cause early onset pituitary ACTH deficiency. *Genes Dev.* **17**, 711-716 (2003).

Rezza, A., Sennett, R. & Rendl, M. Adult stem cell niches: cellular and molecular components. *Curr Top Dev Biol.* **107**, 333-72 (2014).

Rhodin, J. A. The ultrastructure of the adrenal cortex of the rat under normal and experimental conditions. *J. Ultrastruct. Res.* **34**, 23-71 (1971).

Romero, D. G. *et al.* Disabled-2 is expressed in adrenal zona glomerulosa and is involved in aldosterone secretion. *Endocrinology* **148**, 2644-2652 (2007).

Ruggiero, C. & Lalli, E. Impact of ACTH signaling on transcriptional regulation of steroidogenic genes. *Front. Endocrinol.* **7**, 24 (2016).

Sahut-Barnola, I. *et al.* Cushing's syndrome and fetal features resurgence in adrenal cortex-specific Prkar1a knockout mice. *PLoS Genet.* **6**, e1000980 (2010).

Sato, T. The fine structure of the mouse adrenal X zone. *Z Zellforsch Mikrosk Anat.* **87**, 315-29 (1968).

Shelton, J. H. & Jones, A. L. The fine structure of the mouse adrenal cortex and the ultrastructural changes in the zona glomerulosa with low and high sodium diets. *Anat. Rec.* **170**, 147-181 (1971).

Simon, D. P. & Hammer, G. D. Adrenocortical stem and progenitor cells: implications for adrenocortical carcinoma. *Mol. Cell. Endocrinol.* **351**, 2-11 (2012).

Steckelings, U. M. *et al.* The past, present and future of angiotensin II type 2 receptor stimulation. *J. Renin Angiotensin Aldosterone Syst.* **11**, 67-73 (2010).

Thomas, M. *et al.* Dual hormonal regulation of endocrine tissue mass and vasculature by adrenocorticotropin in the adrenal cortex. *Endocrinology* **145**, 4320-4329 (2004).

Tissier, F. *et al.* Mutations of beta-catenin in adrenocortical tumors: activation of the Wnt signaling pathway is a frequent event in both benign and malignant adrenocortical tumors. *Cancer Res.* **65**, 7622-7627 (2005).

Tsuchiya, B. *et al.* Differential expression of N-cadherin and E-cadherin in normal human tissues. *Arch. Histol. Cytol.* **69**, 135-145 (2006).

Val, P., Martinez-Barbera, J. P. & Swain, A. Adrenal development is initiated by Cited2 and Wt1 through modulation of Sf-1 dosage. *Development* **134**, 2349-2358 (2007).

Vidal, V. *et al.* The adrenal capsule is a signaling center controlling cell renewal and zonation through Rspo3. *Genes Dev.* **30**, 1389-1394 (2016).

Virtanen, I. *et al.* Laminin isoforms in fetal and adult human adrenal cortex. *J. Clin. Endocrinol. Metab.* **88**, 4960-4966 (2003).

Walczak, E. M. & Hammer, G. D. Regulation of the adrenocortical stem cell niche: implications for disease. *Nat. Rev. Endocrinol.* **11**, 14-28 (2014).

Walczak, E. M. *et al.* Wnt signaling inhibits adrenal steroidogenesis by cell-autonomous and non-cell-autonomous mechanisms. *Mol. Endocrinol.* **28**, 1471-1486 (2014).

Wang, D. H. *et al.* Regulation of type 1 angiotensin II receptor in adrenal gland: role of alpha1-adrenoreceptor. *Hypertension* **30**, 345-350 (1997).

Wilhelm, D. & Englert, C. The Wilms tumor suppressor WT1 regulates early gonad development by activation of Sf1. *Genes Dev.* **16**, 1839-1851 (2002).

Wood, M. A. *et al.* Fetal adrenal capsular cells serve as progenitor cells for steroidogenic and stromal adrenocortical cell lineages in *M. musculus*. *Development* **140**, 4522-4532 (2013).

Xing, Y. *et al.* Development of adrenal cortex zonation. *Endocrinol. Metab. Clin. North. Am.* **44**, 243-274 (2015).

Xing, Y. *et al.* ACTH is a potent regulator of gene expression in human adrenal cells. *J. Mol. Endocrinol.* **45**, 59-68 (2010).

Yates, R. *et al.* Adrenocortical development, maintenance, and disease. *Curr. Top. Dev. Biol.* **106**, 239-312 (2013).

Zajicek, G., Ariel, I. & Arber, N. The streaming adrenal cortex: direct evidence of centripetal migration of adrenocytes by estimation of cell turnover rate. *J. Endocrinol.* **111**, 477-482 (1986).

Zubair, M., Parker, K. L., Morohashi, K. Developmental links between the fetal and adult zones of the adrenal cortex revealed by lineage tracing. *Mol. Cell. Biol.* **28**, 7030-7040 (2008).

Chapter Two:

β-Catenin and FGFR2 Regulate Rosette-Based Adrenocortical Morphogenesis

β-Catenin and FGFR2 Regulate Rosette-Based Adrenocortical Morphogenesis

Sining Leng[1,2,*], Emanuele Pignatti[1,3,*], Radhika S. Khetani[4], Simiao Xu[1,3], Miao Ji[1,3], Paula Q. Barrett[5], Diana L. Carlone[1,3,6], David T. Breault[1,3,6]

[1]*Division of Endocrinology, Boston Children's Hospital, Boston, MA 02115, USA*

[2]*Division of Medical Sciences, Harvard Medical School, Boston, MA 02115, USA*

[3]*Department of Pediatrics, Harvard Medical School, Boston, MA 02115, USA*

[4]*Department of Biostatistics, Harvard T.H. Chan School of Public Health, Boston, MA 02115, USA*

[5]*Departments of Pharmacology, University of Virginia, Charlottesville, VA 22947, USA*

[6]*Harvard Stem Cell Institute, Cambridge, MA 02138, USA*

**These authors contributed equally to this work.*

Attributions:

This chapter contains the manuscript titled "β-Catenin and FGFR2 Regulate Rosette-Based Adrenocortical Morphogenesis", submitted to Developmental Cell in April 2019. It is modified to fit the style of this dissertation. S. Leng was co-first author on this manuscript. S.L. and D.T.B. designed the project with additional contributions from E.P. and D.L.C.; S.L. (image acquisition and analysis), E.P. (gene expression), R.S.K. (RNA sequencing data analysis) and S.X. (Western Blot) did the research; M.J. contributed tools; and S.L., D.L.C. and D.T.B. wrote the manuscript.

Summary

Multicellular rosettes are widely used to mediate epithelial remodeling during embryonic development and organogenesis. However, their role in postnatal development and adult tissue homeostasis remains largely unknown. The endocrine epithelium of the adult adrenal cortex undergoes constant turnover and remodeling through transdifferentiation of the outer zona glomerulosa (zG) into the inner zona fasciculata (zF). While rosette-like structures have long been proposed to exist in the adult zG, which produces aldosterone, a potent regulator of blood pressure, exactly how these structures form and what role they play in zG function remains unclear. Here, using 3D confocal imaging and reconstruction, we demonstrate that mature zG cells organize into multicellular rosettes through adherens junction (AJ) constriction. Rosette formation underlies a previously unrecognized process of postnatal glomerular morphogenesis. Using genetic mouse models, quantitative morphometry and transcriptome analysis, we describe an essential role for β-catenin in regulating rosette dynamics and glomerular morphology. Furthermore, we show that β-catenin stabilization leads to increased FGFR2, which is required for rosette formation and AJ stability. Our results provide the basis for studying adrenal glomerular morphogenesis and the role of rosettes in on-going zG tissue maintenance and function.

Introduction

Tissue morphogenesis is critical for embryonic development and organ formation. Conserved morphogenetic processes, such as convergent extension, epithelial folding, branching, and invagination, are widely utilized to facilitate tissue remodeling during development across species (Walck-Shannon and Hardin, 2014). Multicellular rosettes have recently been recognized as a conserved mechanism to efficiently achieve complex cellular reorganization during such processes (Harding et al., 2014). Rosettes are defined as five or more cells joined together at a common point of contact (Blankenship et al., 2006). Rosette formation and resolution have been shown to facilitate two-dimensional tissue elongation (Blankenship et al., 2006; Chacon-Heszele et al., 2012; Lienkamp et al., 2012), as well as three-dimensional changes such as folding and branching during organogenesis (Lecaudey et al., 2008; Nishimura and Takeichi, 2008; Trichas et al., 2012; Villasenor et al., 2010). Despite the well-described role of rosettes in development, whether similar mechanisms are utilized to regulate tissue remodeling during postnatal development and in adult tissue homeostasis is largely unknown.

The dynamic properties of adherens junctions (AJ) play a crucial role in allowing for coordinated cell movement and shape changes during tissue morphogenesis (Guillot and Lecuit, 2013; Takeichi, 2014). AJ stability and dynamics can be regulated through cadherin expression and trafficking (Delva and Kowalczyk, 2009; Palacios et al., 2002), as well as by the mechanical tension generated by AJ-associated actin filaments (F-actin) and non-muscle myosin II molecular motors (Buckley et al., 2014; le Duc et al., 2010). AJ remodeling mediated by actomyosin contraction represents a common mechanism underlying rosette formation (Harding et al., 2014; Takeichi, 2014), while the mechanism(s) governing rosette resolution are less clear. On the other hand, the extracellular signals governing rosette formation are diverse, often involving the establishment of planar cell polarity and/or apical basal polarity, which in turn leads to polarized distribution of Rho GTPases and their effectors such as the myosin-activating

kinase ROCK (Blankenship et al., 2006; Ernst et al., 2012; Harding et al., 2014; Lienkamp et al., 2012; Nishimura et al., 2012; Simões et al., 2014). Whether similar AJ dynamics exist and participate in postnatal and adult tissue regulation remains unclear.

As a constantly self-renewing and highly regenerative organ, the adrenal cortex is an ideal system to study adult tissue dynamics (Pignatti et al., 2017; Walczak and Hammer, 2014). The adult cortex is organized into morphologically distinct concentric layers called “zones” that mature postnatally (Xing et al., 2015). The outer most layer, zona glomerulosa (zG), consists of small compact cell clusters that produce aldosterone, a potent mineralocorticoid regulating Na^+/K^+ balance and blood pressure (Bollag, 2014). Immediately adjacent to the zG is the zona fasciculata (zF), consisting of larger cortisol-producing cells arranged in parallel cords (Gallo-Payet and Battista, 2014). In addition to their unique morphologies, the zG and the zF also contain basement membranes that differ in laminin composition (Virtanen et al., 2003). During adult tissue turnover, zG cells migrate centripetally into the zF, undergoing transdifferentiation and a dramatic morphological remodeling (Freedman et al., 2013). Recent studies have begun to elucidate the signaling pathways essential for maintaining zonation (Pignatti et al., 2017). Wnt/β-catenin signaling is highly active in the zG, and its activity has been directly linked to zG identity and function (Drelon et al., 2014). On the other hand, the zF relies on high PKA/cAMP signaling activity, which in turn inhibits zG fate by down regulating Wnt/β-catenin activity (Drelon et al., 2016). In contrast, it is less clear what mechanism(s) give rise to the unique tissue structures of each zone and how remodeling occurs during transdifferentiation.

The compact cell clusters in the zG have been termed “glomerulus” or “rosette-like” due to their round morphological appearance. However, the exact nature of these structures and their functional significance in the adult adrenal have never been investigated. Given the well-described role of rosettes in mediating tissue morphogenesis, one appealing hypothesis is that

rosette formation and resolution underlie the establishment and remodeling of zone-specific tissue structures during homeostatic turnover. Furthermore, it was recently shown that zG cells residing within the same “rosette-like” cluster exhibit coordinated Ca^{2+} oscillation patterns, raising the possibility that rosettes may serve as functional units of aldosterone production (Guagliardo et al., in preparation, see Appendix III). These questions have not been formally addressed due to the lack of a detailed understanding of the adrenal glomerulus and the mechanisms governing its formation.

Here, we present the first detailed account of the adrenal glomerular morphology. Using 3D confocal imaging and reconstruction, we show that glomeruli in the adult zG are interconnected globular structures defined by a laminin β1-rich basement membrane. Within each glomerulus, zG cells organize into multicellular rosettes through AJ constriction. During the first few weeks after birth, rosette formation underlies a previously unknown process of glomerular morphogenesis. Using genetic loss- and gain-of-function mouse models, we find β-catenin is required for rosette formation and that constitutive β-catenin activation results in zG expansion, increased glomerular and rosette frequency. Furthermore, using RNA sequencing, we discover that transcripts enriched in β-catenin gain-of-function adrenals are involved in epithelial morphogenesis. Specifically, we show that *Fgfr2* acts downstream of β-catenin in regulating rosette formation through governing AJ dynamics and stability. Our results provide the first example of multicellular rosette, an intermediate developmental structure, present in an adult tissue. Our mechanistic findings suggest that similar principles governing embryonic morphogenesis can be utilized to facilitate dynamic tissue remodeling during postnatal development and adult homeostasis.

Results

Adrenal Glomeruli Consist of Multicellular Rosettes

To facilitate three-dimensional structural definition of the adrenal glomerulus, we stained near native 100 μm-thick adrenal slices for basement membrane (BM) components such as laminin and collagen. We found laminin subunit β1 (Lamb1) is highly enriched in the zG (**Figure 2.1A**), consistent with a previous report (Virtanen et al., 2003). From a 2D cross-section viewpoint, the glomeruli can be defined as distinct clusters of mature zG cells marked by Gq alpha subunit (Gαq) surrounded by the Lamb1+ BM (**Figure 2.1A**). Using 3D reconstructions, we found that glomeruli are globular structures tightly packed into the zG domain. We estimate that each glomerulus consists of 15 ± 5 mature zG cells. Interestingly, the glomeruli are interconnected through small openings on the BM, and glomeruli at the zonal boundary are "half-open" where zG cells are directly in contact with the zF. Type IV collagen (Col4a1) is also present in the zG BM and in addition, persists in the zF (**Figure S1.1A**). Like in other epithelial tissues, we found that the BM serves as a barrier between cortical cells and the surrounding vasculature (CD31+) and mesenchyme (Vimentin+) (**Figure S1.1B, C**).

To understand the cellular organization within each glomerulus, we co-stained adrenal slices for Lamb1 and adherens junction (AJ) proteins, including β-catenin and classical cadherins. We found that within each glomerulus, as outlined by Lamb1, zG cell membranes have strong β-catenin signal, which is weaker in the zF (**Figure 2.1B**). This membrane β-catenin signal is highly linear and continuous, typical of epithelial-type cell-cell adhesions, in contrast to the punctate appearance in the mesenchymal cells residing in the overlying capsule (**Figure 2.1B, middle**). Several type I and II classical cadherins are expressed in the adult adrenal gland (ENCODE, GEO accession number: GSM900188). We verified that N-cadherin (Cdh2) and K-cadherin (Cdh6) are both enriched in the zG (**Figure S1.2A**). However, E-cadherin (Cdh1) is not present in the adrenal cortex (**Figure S1.2B**). Using these AJ markers, we noticed that groups

Figure 2.1. Adrenal glomeruli consist of multicellular rosettes.

(A) Laminin β1 (Lamb1, green) marks a basement membrane surrounding distinct clusters of zG cells marked by Gαq (magenta), defining the outline of individual glomerulus. DAPI (blue), nuclei.

(B) Cells within glomeruli organize into rosettes. Confocal image showing immunostaining of Laminin β1 (green), β-catenin (red) and F-actin (gray) of an adult adrenal slice. Dotted circle highlights a rosette example. DAPI (blue), nuclei. Arrowhead, rosette center.

(C) Top, confocal z-stack images of the rosette encircled in (B), showing β-catenin (red), F-actin (gray) and nuclei (DAPI, blue). Z step size is 1μm. Arrows denote rosette center; arrowheads mark dispersed adherens junctions not in rosette center. Bottom, tracing of 12 cells participating in the rosette shown in top panel.

c, capsule, zG, zona glomerulosa, zF, zona fasciculata. All bars, 10μm.

Figure 2.1 (Continued)

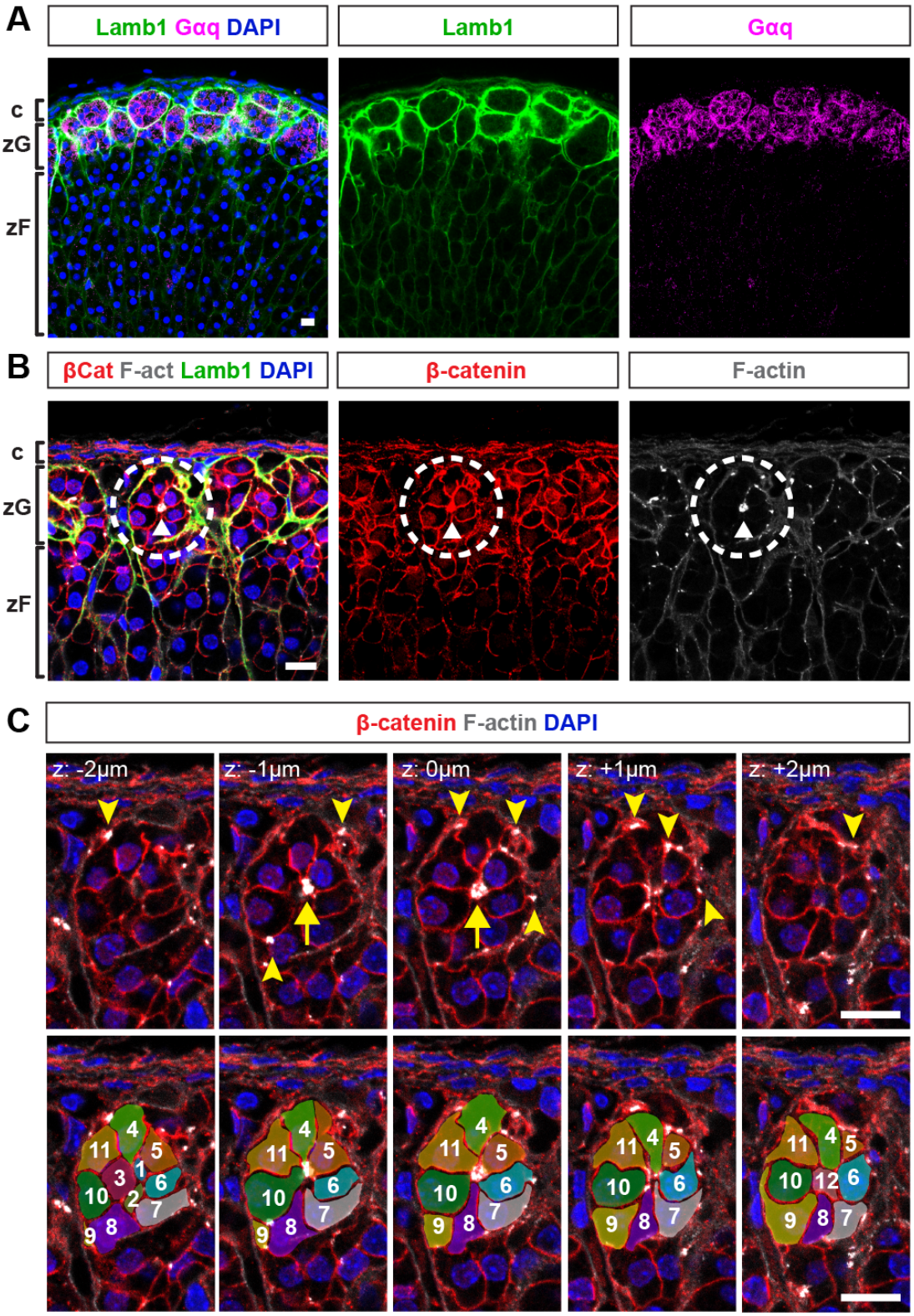

of zG cells within each glomerulus are connected at a common membrane center, forming multicellular rosettes (**Figure 2.1B, circle**). Since rosettes typically form through actomyosin-mediated AJ constriction, we examined the distribution of filamentous actin (F-actin) using Phalloidin staining (**Figure 2.1B**). We found that F-actin has a punctate appearance on zG cell membranes and these punctae appear as large aggregates at rosette centers (**Figure 2.1B, arrowhead**). To better understand rosette conformation, we performed confocal z-stack imaging and 3D reconstruction of the individual cells participating in a rosette. We found rosettes typically contain 10-15 cells that are connected at a single vertex located at the center of the structure (**Figure 2.1C**).

To confirm that rosette centers indeed contain constricted AJs, we co-stained F-actin with β-catenin, N-cadherin, and K-cadherin. We found that all AJ proteins colocalize with aggregated F-actin punctae at rosette centers (**Figure 2.2A, B**). In addition, small dispersed F-actin punctae also contain AJ proteins (**Figure 2.2A, B**), suggesting these may represent individual AJs that are not participating in constriction. To further confirm the identity of these junctions and to understand the ultrastructural details of rosettes, we performed electron microscopy. As previously reported (Black et al., 1979), adult zG cells are characterized by numerous mitochondria and few lipid droplets, in contrast to the lipid-rich zF cells (**Figure 2.2C, left**). We found that zG cells participate in rosettes via narrow membrane protrusions (**Figure 2.2C, middle**). Strikingly, stereotypical AJ structures with electron-dense actin filaments can be found in clusters, confirming AJ constriction (**Figure 2.2C, right**).

Together, these data demonstrate that adult zG cells form multicellular rosettes through actomyosin-mediate AJ constriction. To understand whether these structures are evolutionarily conserved, we performed staining of AJ proteins on thick sections of human adrenal and a Peruvian mouse strain, previously considered to not have a morphological zG (Shire, 1969).

Figure 2.2. Adherens junction components are enriched at rosette centers.

(A) Colocalization of N-cadherin (magenta) and F-actin (green) at rosette centers (arrows) and smaller F-actin punctae (arrowheads). DAPI (blue), nuclei. Bar, 10μm.

(B) Colocalization of K-cadherin (magenta) and F-actin (green) at rosette centers (arrows) and smaller F-actin punctae (arrowheads). DAPI (blue), nuclei. Bar, 10μm.

(C) Transmission electron micrographs showing adherens junctions in the zG. Left, dotted line marks a glomerulus. Red dots denote nuclei. Boxed area is shown in the middle panel where individual cells are colorized. Right, example of constricted adherens junctions (arrowheads). Bars, 5μm, 500nm, 200nm from left to right.

Figure 2.2 (continued)

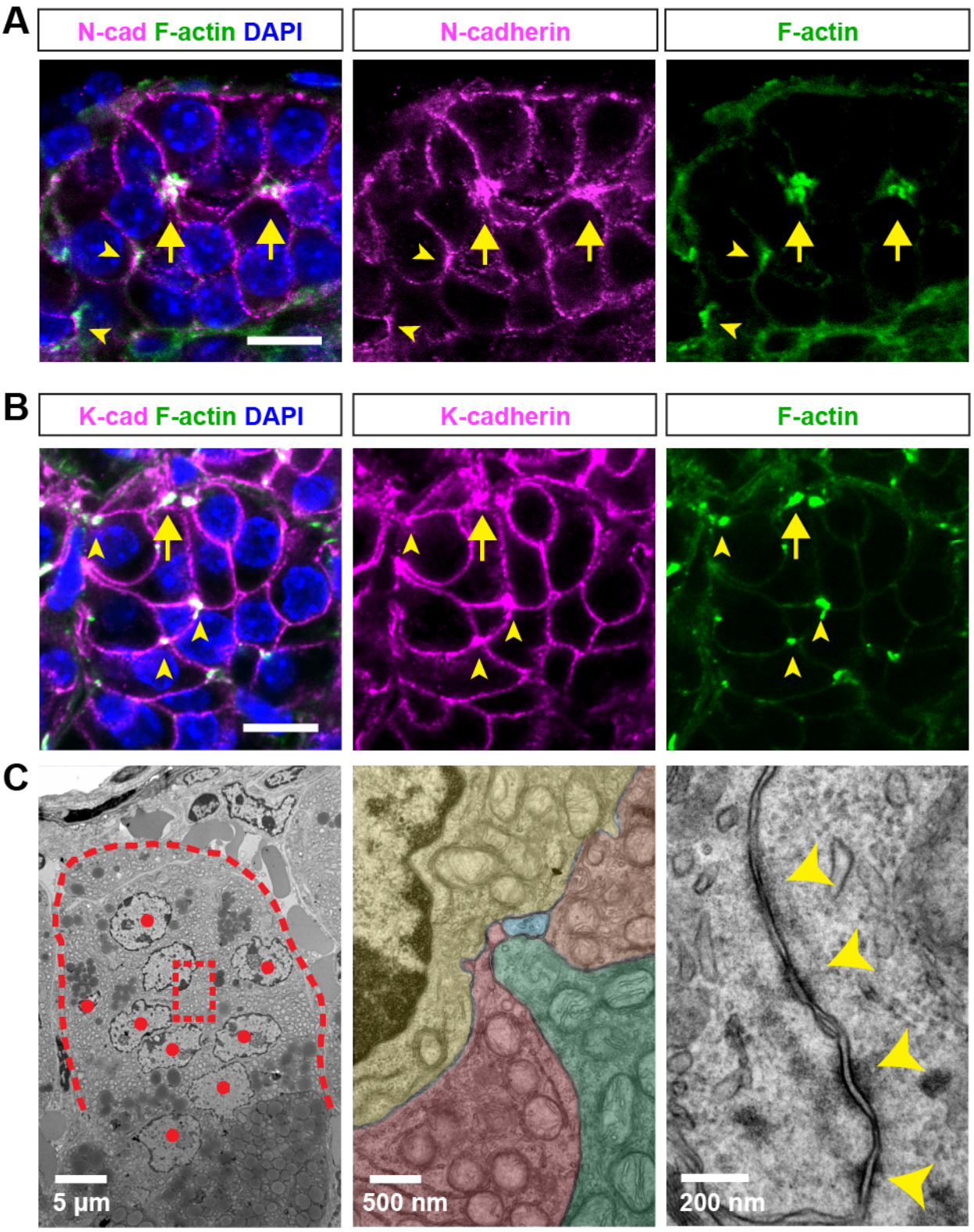

Interestingly, we found rosettes in both human and Peruvian mouse adrenals, highlighting a potentially conserved function for these structures (**Figure S1.2C, D**).

Rosette Formation Underlies Postnatal Glomeruli Morphogenesis

Since rosettes are known to mediate morphogenesis during development, we next investigated what role rosettes play in establishing zG morphology. To understand when and how glomeruli form in the zG, we examined zG morphology using the BM marker Lamb1 at postnatal days 0, 12, 3 weeks (P0, P12, 3wk) and compared them to the zG of 6-week-old adult mice. Interestingly, we found that mature glomeruli arise through a gradual morphogenetic process (**Figure 2.3A**). In neonatal adrenals (P0), the zG consists largely of flat sheet-like domains, which undergo invagination, folding and segmentation, leading to the formation of mature glomeruli with well-defined boundaries (**Figure 2.3A**). To quantify this process, we manually traced Lamb1 staining to identify individual developing glomeruli and conducted morphometric analyses (**Figure S1.3A**). Glomerular roundness, a shape descriptor indicating closeness to a perfect circle, significantly increases from P0 to adulthood (**Figure 2.3D**). Glomerular 2D cross-section area measurement revealed no difference among all stages (**Figure 2.3E**), suggesting increase in cell mass is not a main contributor to glomerular morphogenesis.

To understand whether rosette formation plays a role in glomerular morphogenesis, we examined F-actin distribution during the same time course (**Figure 2.3B**). At P0, F-actin appears as small punctae that are dispersed along cell-cell contacts. At P12, F-actin becomes enriched along the zG cell-cell contacts, forming lines. At 3wk, F-actin begins to form aggregates, which by 6 weeks of age form distinct clusters that mark mature rosette centers (**Figure 2.3B, C**). To confirm these findings, we measured the size and length of F-actin clusters at each stage using 3D volume reconstruction (**Figure S1.3B**). We found that F-actin clusters peak in length at P12 and become shorter in the adult, without any significant change in cluster

Figure 2.3. Rosette formation underlies postnatal glomeruli morphogenesis.

(A) Time course of postnatal glomeruli morphogenesis. Lamb1 (green) marks the basement membrane surrounding the developing glomeruli. Bars, 10 μm.

(B) F-actin (red) dynamics at indicated stages of glomerular morphogenesis. Bar, 10 μm.

(C) Schematic of F-actin dynamics during glomerular morphogenesis.

(D) Measurement of glomerular cross section roundness at indicated stages. Outlines of individual glomerulus were hand-traced based on Lamb1 staining. ANOVA, $p < 0.05$ followed by Dunn's multiple comparison test, P0 versus 6wk, $p < 0.0001$; P0 versus 3wk, $p < 0.05$; 3wk versus 6wk, $p < 0.0001$.

(E) Measurement of glomerular cross section area at indicated stages. ANOVA, $p > 0.05$.

(F) Measurement of F-actin cluster size at indicated stages using volume statistics in Imaris following 3D reconstruction. ANOVA, $p > 0.05$.

(G) Measurement of F-actin cluster length at indicated stages using volume statistics in Imaris following 3D reconstruction. ANOVA, $p < 0.05$; P12 versus 6wk Dunn's test, $p < 0.01$.

For each measurement, at least 3 animals from each stage were examined and at least 50 glomeruli or F-actin puncta examined per animal. A one-way ANOVA on ranks (Kruskal-Wallis test) was performed followed by Dunn's multiple comparison test for each pair.

Figure 2.3 (Continued)

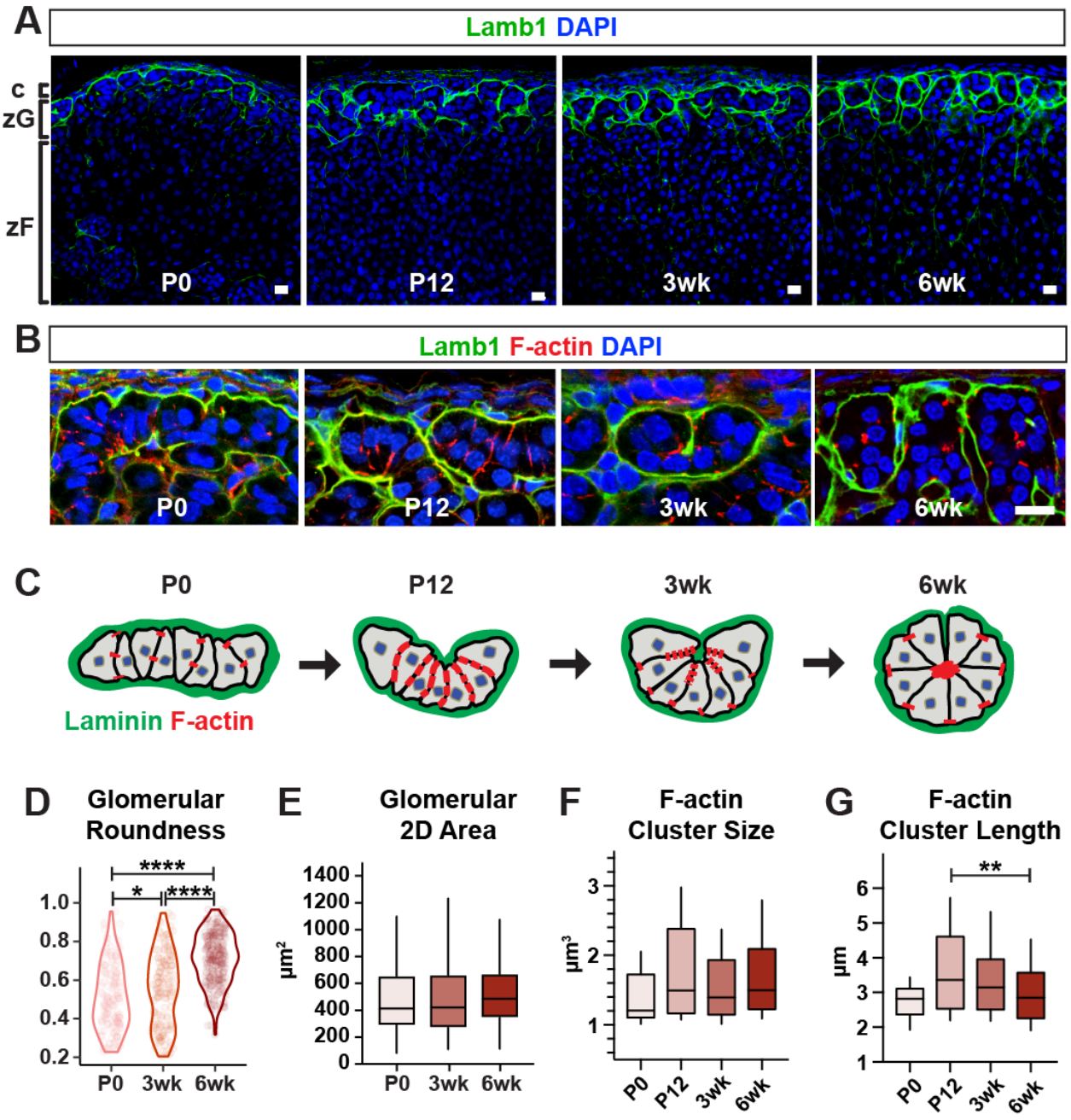

size (**Figure 2.3F, G**). Together, our data show that adult glomerular morphology matures postnatally, concurrent with rosette formation, suggesting rosette formation provides the morphogenetic force underlying zG maturation.

β-Catenin Regulates Rosette Structure and Glomerular Morphology

Since β-catenin is an integral AJ component, linking cadherin molecules to the actin cytoskeleton through binding α-catenin (Bek and Kemler, 2002; Meng and Takeichi, 2009), we next tested whether loss of β-catenin results in the inability of AJ to constrict, culminating in rosette disruption. For these studies, we generated mice with β-catenin conditional knockout in zG cells (*AS$^{Cre/+}$ :: Ctnnb1$^{fl/fl}$*, referred to as βCat-LOF). Since AS-Cre expression begins at birth and is continuously expressed in aldosterone-producing zG cells throughout adult life (Freedman et al., 2013), we analyzed adrenals at 10-13 weeks of age to evaluate the cumulative effect of β-catenin deletion. In both female and male βCat-LOF adrenals, we found that glomeruli are significantly smaller and less round (**Figure 2.4A, D, E**). However, overall size of zG is not significantly changed (**Figure 2.4B**). In addition, Phalloidin staining revealed absence of F-actin punctae and reduced rosette frequency in βCat-LOF adrenals (**Figure 2.4C, F**). Furthermore, we found that other AJ components, such as K-cadherin, are absent from β-catenin-deleted zG cell membranes (**Figure S1.4**). Together, these data suggest that β-catenin is required for intact rosette structure and glomerular morphology.

Wnt/β-catenin signaling is a potent regulator of zG identity (Drelon et al., 2014). We have shown that stabilizing β-catenin protein by genetically deleting exon 3 in zG cells leads to progressive zG expansion and a block in transdifferentiation into zF cells (*AS$^{Cre/+}$, Ctnnb1$^{fl(ex3)/+}$*; referred to as βCat-GOF) (Pignatti et al., in preparation, see Chapter 3). Here, we tested the impact of β-catenin stabilization on glomerular morphology and rosette frequency. We found that by 10 weeks of age, female βCat-GOF adrenals contain a markedly expanded zG containing a

Figure 2.4. β-catenin activity is required for glomerular morphogenesis.

(A) Lamb1 staining (green) shows disrupted glomerular morphology in β-catenin loss-of-function (LOF) adrenals compared to controls (Ctrl).

(B) Measurement of zG thickness. Two sample *t*-test, ns, not significant.

(C) F-actin staining (red) reveals loss of rosette structures in βCat LOF adrenals. Glomerular boundary is outlined by Lamb1 (green). DAPI (blue), nuclei. Boxed areas in left panels are shown in higher magnification on the right. Arrowheads point to rosette center.

(D) Measurement of glomerular roundness. Mann-Whitney non-parametric test, $p < 0.01$.

(E) Measurement of glomerular 2D area. Mann-Whitney non-parametric test, $p < 0.0001$.

(F) Rosette frequency per 40X z-stack (160x160x10 μm^3). Two sample *t*-test, $p < 0.001$.

For each measurement, at least 3 animals from each genotype were examined and at least 50 glomeruli examined per animal. Mann-Whitney non-parametric tests were applied in D and E. Unpaired *t*-tests were applied in B and F. All bars, 10 μm.

Figure 2.4 (Continued)

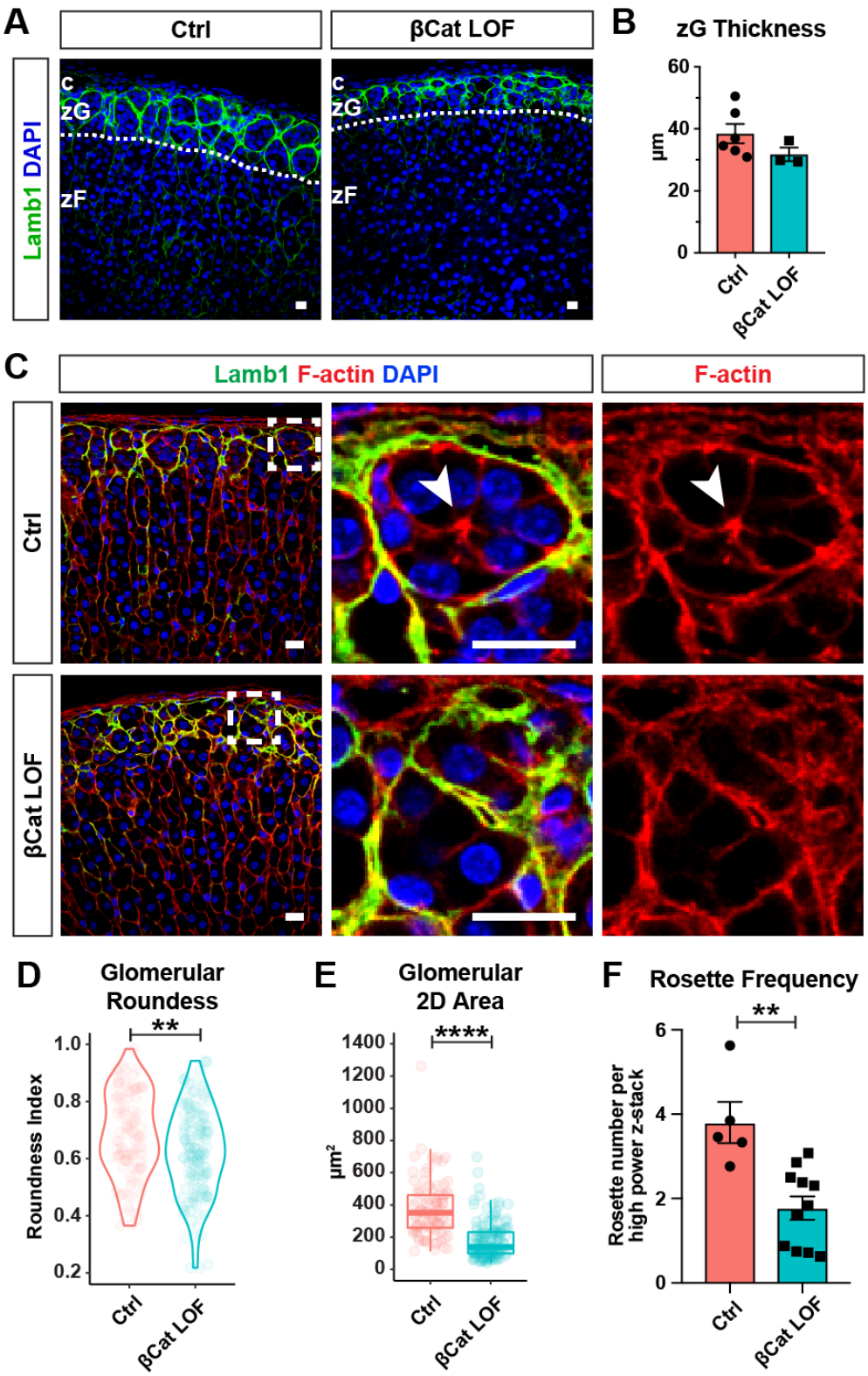

Lamb1+ BM (**Figure 2.5A, B**). This expanded zG contains glomeruli that are bigger and more elongated compared to female controls (**Figure 2.5D, E**). Analysis of rosette frequency also revealed a significant increase in βCat-GOF adrenals (**Figure 2.5F**). Similarly, in males, βCat-GOF resulted in significant zG expansion, albeit to a milder extent than females (**Figure S1.5A, B**). However, we found that the glomeruli in male βCat-GOF adrenals are similar in size and shape compared to controls (**Figure S1.5C, D**). In addition, male βCat-GOF adrenals have a more modest increase of rosette frequency compared to females (**Figure S1.5E**). This sexual dimorphism may reflect a difference in the rate of tissue turnover between male and female adrenal glands. Lastly, we found that zG-specific AJ components such as N-cadherin and K-cadherin are also present in the expanded zG tissue in βCat-GOF adrenals similarly in males and females (**Figure S1.5F, G**). In summary, these data show that the zG tissue accumulating in βCat-GOF adrenals, due to transdifferentiation block, maintains its classical glomerular morphology and rosette structures, suggesting β-catenin is a potent regulator of zG morphology.

Transcripts Enriched in βCat-GOF Adrenals Regulate Epithelial Morphogenesis

To investigate what mechanisms may act downstream of β-catenin to regulate zG morphology, we performed RNA sequencing on wild type and βCat-GOF adrenals. Differential expression analysis revealed 306 up-regulated and 219 down-regulated genes in βCat-GOF adrenals compared to controls (**Figure 2.6A**). To understand the functional significance of these changes, we performed enrichment analysis of Gene Ontology Biological Process terms using DAVID (v6.7). We found top-enriched terms are epithelial morphogenesis, Wnt signaling pathway, regulation of cell adhesion, and adherens junction assembly (**Figure 2.6B**), suggesting a gene expression program is involved in regulating zG morphology. Among the up-regulated Wnt signaling pathway genes are well-established β-catenin targets, such as *Axin2*, *Lef1*, *Notum*, *Nkd1*, *Apcdd1*, confirming the expansion of the β-catenin activity domain (**Figure S1.6B, C**). Interestingly, several non-canonical Wnt pathway members are also up-regulated,

Figure 2.5. β-catenin stabilization results in glomerular expansion.

(A) Lamb1 staining (green) shows expanded glomerular morphology in β-catenin gain-of-function (GOF) adrenals of female mice.

(B) Measurement of zG thickness. Two sample *t*-test, $p < 0.01$.

(C) F-actin staining (red) reveals presence of rosette structures in expanded glomeruli of βCat GOF adrenals in females. Glomerular boundary is outlined by Lamb1 (green). DAPI (blue), nuclei. Boxed areas shown in higher magnification on the right.

(D) Measurement of glomerular roundness. Mann-Whitney non-parametric test, $p < 0.001$.

(E) Measurement of glomerular 2D area. Mann-Whitney non-parametric test, $p < 0.0001$.

(F) Rosette frequency per 40X z-stack (160x160x10 μm^3). Two sample *t*-test, $p < 0.001$.

For each measurement, at least 3 animals from each genotype were examined and at least 50 glomeruli examined per animal. Mann-Whitney non-parametric tests were applied in D and E. Unpaired t-tests were applied in B and F. All bars, 10 μm.

Figure 2.5 (Continued)

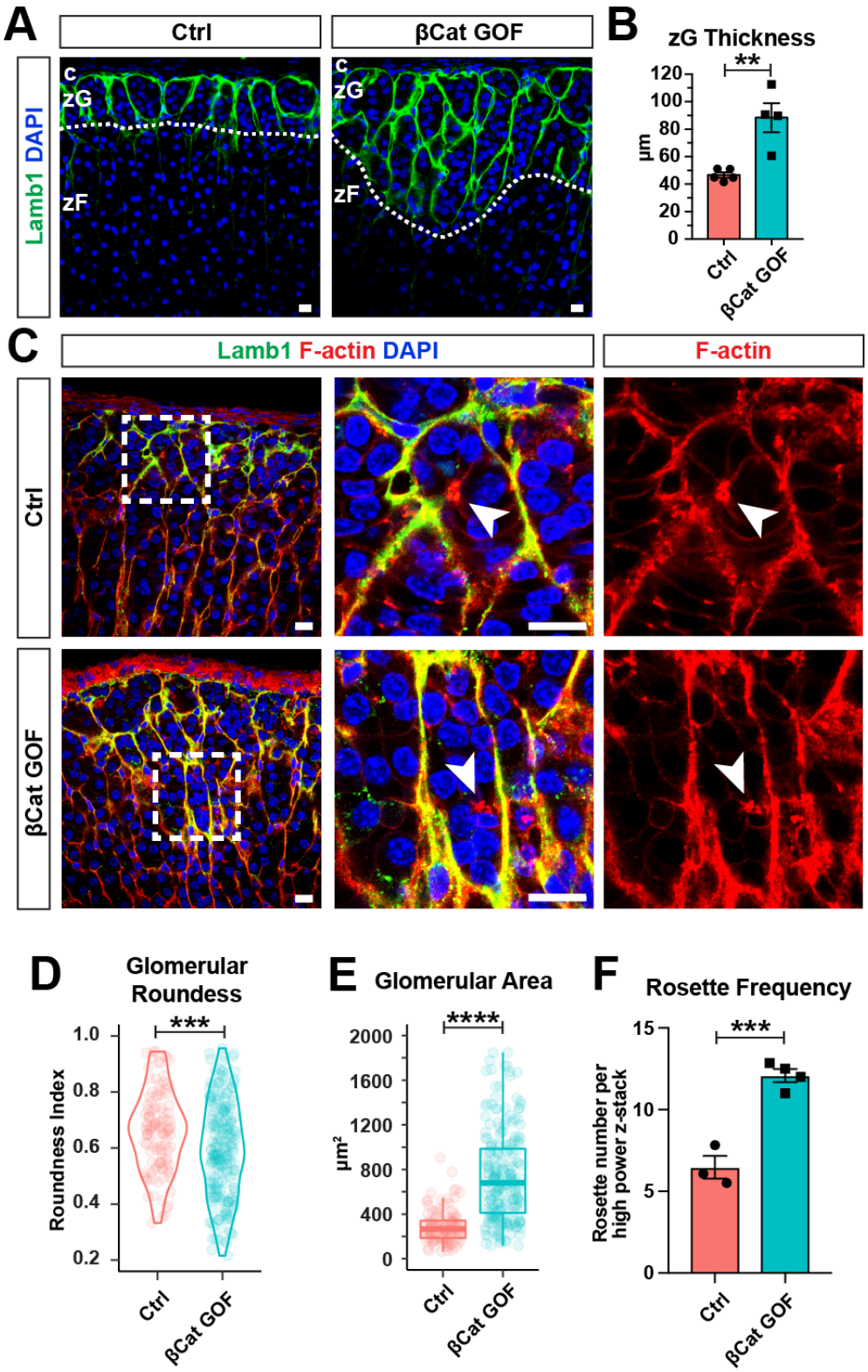

including *Nfatc4*, *Daam2*, *Ror2*, and *Dact1*, suggesting a potential role in the regulation of rosette dynamics and glomerular morphology. Among the up-regulated Wnt signaling pathway genes are well-established β-catenin targets, such as *Axin2*, *Lef1*, *Notum*, *Nkd1*, *Apcdd1*, confirming the expansion of the β-catenin activity domain (**Figures S1.6B and S1.6C**). Interestingly, several non-canonical Wnt pathway members are also up-regulated, including *Nfatc4*, *Daam2*, *Ror2*, and *Dact1*, suggesting a potential role in the regulation of rosette dynamics and glomerular morphology.

Among the genes representing the GO term epithelial morphogenesis, we found known regulators of rosette formation, including *Fgfr2* and *Shroom3* (**Figures S1.6A**). In the developing lateral line primordium of the zebrafish *Danio rerio*, Fgf signaling plays an important role in rosette formation by inducing *Shroom3* expression (Ernst et al., 2012). Shroom3 is an actin-binding protein that recruits ROCK to cell junctions where ROCK triggers AJ constriction by myosin phosphorylation (Mohan et al., 2012; Nishimura and Takeichi, 2008). We found increased FGFR2 protein in total adrenal protein extract from βCat-GOF mice (**Figure 2.6C, D**). Since whole gland RNA extract was used in the RNAseq experiment, we examined the localization of *Fgfr2* and *Shroom3* transcripts in adrenal cortex using single-molecule *in situ* hybridization (RNAscope). We found that both transcripts are expressed by the epithelial compartment (**Figure 2.6E, left**). *Fgfr2* is slightly more enriched in the zG than in the zF, whereas *Shroom3* expression is highly specific to the zG. Furthermore, we found that the expression domains of both genes are expanded in βCat-GOF adrenals, correlating with the morphological expansion of the zG (**Figure 2.6E, right**). Together, our data reveal numerous transcriptional changes that correlate with a morphologically expanded zG driven by constitutive β-catenin activity. Many of these genes have well-established roles in regulating epithelial morphogenesis, cell adhesion and junctional dynamics, suggesting they may be potentially involved in regulating zG rosette formation and glomeruli morphology.

Figure 2.6. Transcripts enriched in βCat-GOF adrenals regulate epithelial morphogenesis

(A) Heatmap of differentially expressed genes between control and βCat GOF adrenals based on RPKM values. Fold change > 1.4, adjusted $p < 0.05$, basemean expression > 100 were used as cutoff criteria. Dendrograms show hierarchical clustering of samples (top) and genes (left).

(B) Enrichment of Gene Ontology terms (Biological Processes) upregulated in βCat GOF adrenals.

(C) Western blot showing upregulation of FGFR2 in control and βCat GOF adrenals.

(D) Normalized intensity of (C). Two sample *t*-test, $p < 0.01$. N = 5, 5.

(E) Single-molecule *in situ* hybridization (RNAscope) of *Fgfr2* and *Shroom3* in control and βCat GOF adrenals. Blue, hematoxylin counterstain. Bars, 10 μm.

Figure 2.6 (Continued)

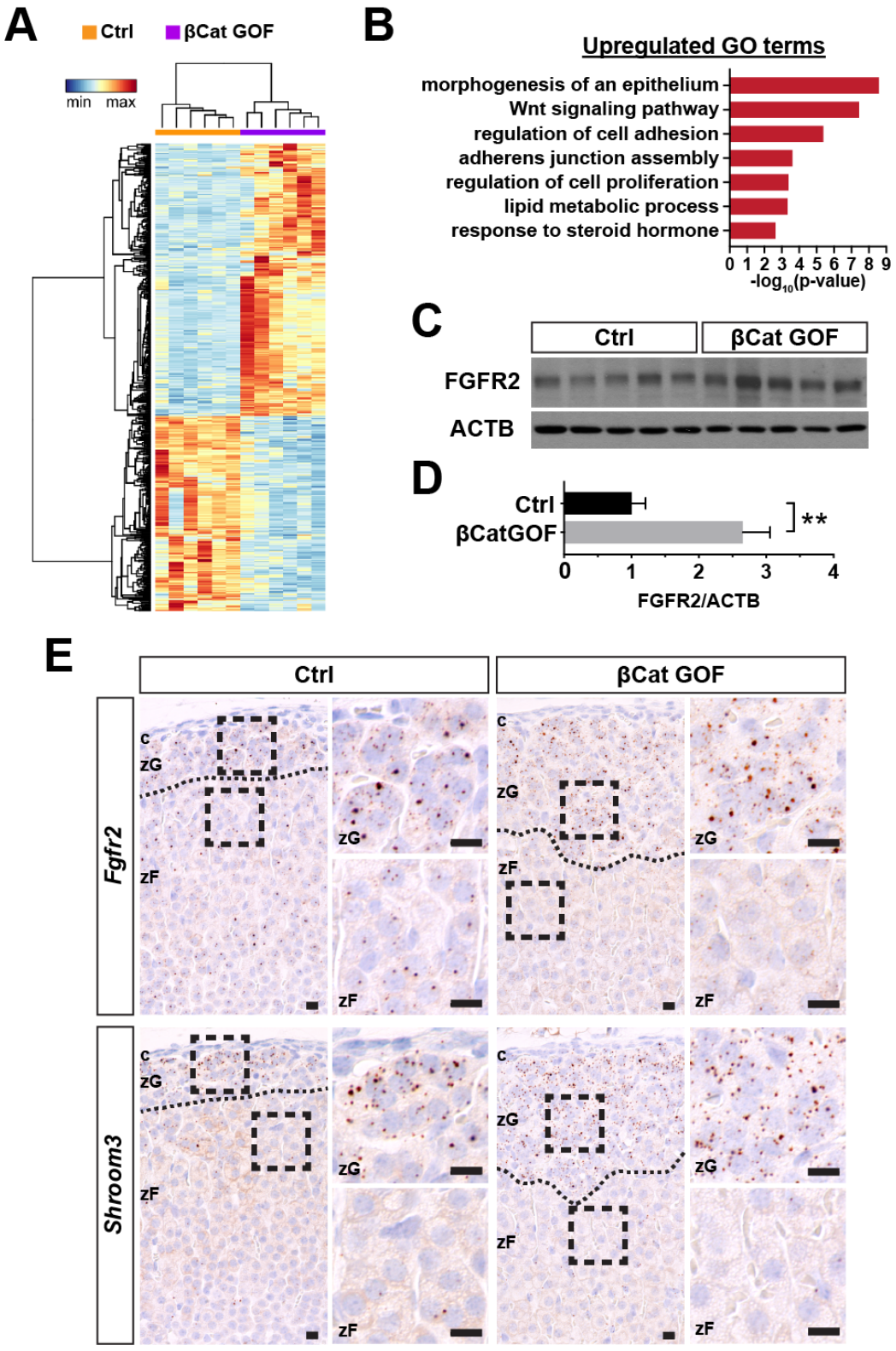

FGFR2 is Required for Rosette Formation and AJ Stability

Given FGF signaling and its downstream target *Shroom3* are important regulators of rosette formation during development in zebrafish and that *Fgfr2* and *Shroom3* expression levels are both increased in βCat-GOF adrenals, we next investigated whether *Fgfr2* has a role in zG rosette formation. To this end, we generated zG-specific *Fgfr2* conditional knockout mice (*AS*$^{Cre/+}$*, Fgfr2*$^{fl/fl}$; referred to as Fgfr2-LOF). Analysis of adult male and female mice revealed a severely disrupted zG morphology, but no significant change in zG thickness (**Figure 2.7A, B**). Morphometric analyses revealed that glomeruli in Fgfr2-LOF adrenals have smaller cross-sectional area (**Figure 2.7E**), but no significant change in glomerular roundness (**Figure 2.7D**). In addition, Phalloidin staining revealed that F-actin punctae are present but fail to aggregate into rosette centers; instead they appear small and dispersed (**Figure 2.7C**), suggesting defective AJ constriction. Consistent with this, rosette frequency is markedly decreased in Fgfr2-LOF adrenals (**Figure 2.7F**). *Shroom3* transcript level is significantly decreased (**Figure S1.7B**), consistent with its role in mediating AJ constriction downstream of FGF signaling. Furthermore, we noticed that β-catenin signal is lost from the membrane of zG cells in Fgfr2-LOF adrenals, suggesting disrupted AJs in these cells (**Figure S1.7A**). In addition, both *Cdh2* and *Cdh6* transcripts are reduced in Fgfr2-LOF adrenals (**Figure S1.7C, D**), further supporting perturbation of AJ integrity. Since β-catenin localization is altered, we next examined whether *Fgfr2* loss affects canonical Wnt activity. Immunostaining of Lef1, an established β-catenin transcriptional target, revealed strong nuclear signal in both control and Fgfr2-LOF zG (**Figure S1.7E**), suggesting canonical Wnt activity is not changed after *Fgfr2* deletion. Consistent with this, qRT-PCR analysis of *Axin2* using whole gland RNA extract revealed no significant difference (**Figure S1.7F**). Together, our data demonstrate that *Fgfr2* is required for zG rosette formation through regulating AJ integrity and dynamics, without affecting canonical Wnt activity.

Figure 2.7. Fgfr2 is required for glomerular morphogenesis.

(A) Lamb1 staining (green) shows disrupted glomerular morphology in Fgfr2 loss-of-function (LOF) adrenals compared to controls (Ctrl).

(B) Measurement of zG thickness. Two sample *t*-test, ns, not significant.

(C) F-actin staining (red) reveals loss of rosette structures in the glomeruli of Fgfr2 LOF adrenals. Glomerular boundary is outlined by Lamb1 (green). DAPI marks nuclei (blue). Boxed areas are shown in higher magnification on the right. Arrowheads point to rosette centers.

(D) Measurement of glomerular roundness. Mann-Whitney non-parametric test, ns, not significant.

(E) Measurement of glomerular 2D area. Mann-Whitney non-parametric test, $p < 0.0001$.

(F) Rosette frequency per 40X z-stack (160x160x10 μm^3). Two sample *t*-test, $p < 0.0001$.

For each measurement, at least 3 animals from each genotype were examined and at least 50 glomeruli examined per animal. Mann-Whitney non-parametric tests were applied in D and E. Unpaired *t*-tests were applied in B and F. All bars, 10 μm.

Figure 2.7 (Continued)

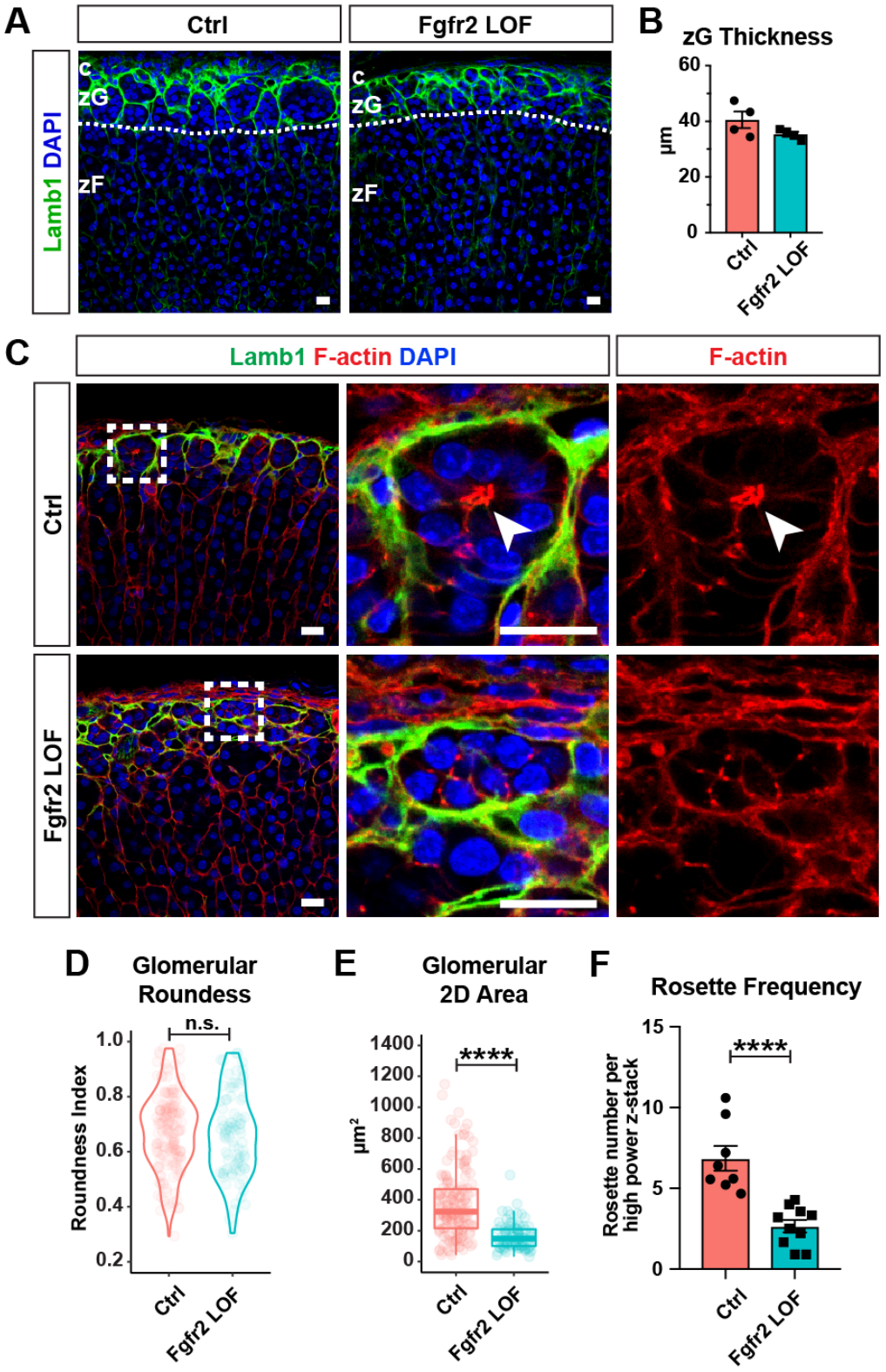

Discussion

Multicellular rosettes represent a widely utilized developmental phenomenon. First described in the developing Drosophila embryo, rosettes were described as a key morphogenetic step during germ band extension (Blankenship et al., 2006). Polarizing signals orchestrate the redistribution of adherens junction and actomyosin along the extending body axis (Simões et al., 2010). Subsequent actomyosin contraction at the boundary of neighboring cells bring them together at an intersecting membrane vertex, forming the classical rosette shape. The relaxation of this contraction leads to neighbor exchange and tissue elongation. Since then, this type of rosette has been shown to function in many systems including the vertebrate kidney, where the developing tubule utilizes a planar-cell-polarity (PCP)-based rosette mechanism to achieve elongation (Lienkamp et al., 2012). In both examples, rosette geometry is relatively simple. Cells participating in a rosette share a common center along the entire lateral side, much like a "pinwheel". Rosettes have also been shown to adopt a more complicated three-dimensional geometry. For example, during neuromast assembly in the zebrafish lateral line primordium, rosettes form by apical constriction in a group of neighboring cells (Lecaudey et al., 2008). The resulting structure resembles a "garlic bulb" shape where rosette membership is only apparent at one point of contact. In this case, rosettes tend to not fully resolve but continue to differentiate into mature organ. This type of rosette is also exemplified by the developing pancreas during exocrine duct branching (Villasenor et al., 2010).

Here, we describe the first example of bona fide rosette structures present in an adult organ. We find that in the mature adrenal glomeruli, 10-15 cells share a common membrane center where their adherens junctions are densely constricted. The geometry of these rosettes is rather complicated. Enwrapped in a basement membrane, glomerular cells have a clear basal domain where AJ components are absent. However, zG cells have highly irregular shapes and no clear apical domain can be geometrically defined. In fact, proteins that are traditionally considered to

mark the apical membrane, such as Par3, aPKC, ZO-1, are absent from the zG (data not shown). We propose that zG rosettes represent a variation of rosettes formed via apical constriction. During postnatal glomerular morphogenesis, rosettes form through highly dynamic AJ rearrangement. Through this process, nascent zG cells are brought together from a flat epithelial sheet into a compact, interconnected network of globular structures. The significance of such morphogenesis remains to be elucidated. One possibility is that segmentation of groups of cells into distinct glomerulus effectively increases the surface area of the basement membrane, and hence increased exposure to the vasculature. As part of the renin-angiotensin endocrine system, the adrenal zG is a crucial hormonal regulator of Na^+/K^+ balance and blood pressure. Hence, there is a constant need for zG cells to monitor the level of circulating Angiotensin II (AngII) and interstitial K^+ concentration and rapidly respond to such stimuli. Having an extensive epithelial-vascular interface will likely enhance the sensitivity of zG cells and the efficiency of aldosterone release. Another possible function of the glomerular morphology is based on the idea of zG cell cooperativity. In physiological conditions, zG cells have a negative resting membrane potential that can be rapidly depolarized by increase in extracellular K^+ and/or AngII (Spät and Hunyady, 2004). Subsequent opening of voltage-gated Ca^{2+} channels leads to a rapid increase of intracellular Ca^{2+} concentration and activation of the aldosterone synthetic pathway (Guagliardo et al., 2012). A recent report using the fluorescent Ca^{2+} sensor GCamP6 in cultured adrenal slices revealed a high degree of cooperativity between cells residing within the same “rosette-like” cluster (Guagliardo et al., in preparation, see Appendix III). What causes such cooperativity remains unknown, since gap junctions are not found in the zG (Bell and Murray, 2016; Davis et al., 2002). It will be of interest to examine the Ca^{2+} oscillation pattern and aldosterone production in the zG of various mutants with rosette defects. However, many aspects of rosette formation and glomerular morphogenesis remain unclear, such as what mechanism specifies the location of adherens junctions, what signal

triggers the onset of rosette formation, and to what extend cell-matrix interaction and vascular signals contribute to this process.

β-catenin has dual functions in the zG as an integral structural molecule of adherens junctions and as an effector of canonical Wnt signaling in the cytoplasm and nucleus (Nelson and Nusse, 2004). Our genetic β-catenin loss- and gain-of-function models cannot distinguish between these distinct functions. In the LOF model, β-catenin signal is absent from the cell membrane, suggesting this compartment of β-catenin has been successfully removed. This resulted in the loss of F-actin signal, consistent with the role of β-catenin as a linker protein between α-catenin and the actin cytoskeleton. In fact, we found that other AJ components, such as K-cadherin, were also absent, suggesting a complete disruption of AJs in these cells. This is consistent with the fact that AJ stability is heavily dependent on the mechano-tension provided by actomyosin (Arnold et al., 2017). In addition, rosette frequency markedly decreases in these mice, consistent with our hypothesis that the rosette structure requires AJ constriction. However, we cannot rule out the possibility that the loss of nuclear β-catenin activity also contributes to this phenotype. To definitively separate these possibilities, α-catenin, K-cadherin, and/or N-cadherin, are logical targets for future studies. On the other hand, in the β-catenin GOF model, where we observed a progressive expansion of the zG, rosette frequency increases, as glomeruli accumulate. These data suggest that β-catenin is not merely necessary but a strong driver of zG morphogenesis. However, the extent to which the direct participation of β-catenin in AJs is sufficient or downstream targets of β-catenin activity are needed to induce zG morphogenesis remain open questions.

Canonical Wnt signaling is widely involved in the development and morphogenesis of embryonic tissues (Steinhart and Angers, 2018). It activates a broad transcriptional program that regulates numerous aspects of organogenesis, ranging from proliferation to cell fate specification

(Cadigan and Waterman, 2012). It can also regulate morphogenesis by inducing paracrine factors that directly affect cell migration, adhesion, and polarity, such as the FGF signaling pathway (Mariani et al., 2017; Volckaert and De Langhe, 2015). There are many examples in development where Wnt/β-catenin signaling induces the expression of FGF ligands and/or receptors, and in turn FGF signaling can inhibit or potentiate the level of canonical Wnt signaling. In the current study, we have identified numerous enriched transcripts in βCat-GOF adrenals by RNAseq. These transcripts may or may not be direct transcriptional targets of β-catenin, but nonetheless they provide interesting hypotheses regarding the role of β-catenin in zG morphogenesis. One of these genes is *Fgfr2*. Our single molecule *in situ* hybridization data show that the expression domain of *Fgfr2* overlaps with the area of Wnt activation, namely the zG in wild type and expanded zG in βCat-GOF adrenals. This is consistent with previous reports showing *Fgfr2* expression pattern in the fetal adrenal is localized to the outer cortex, where Wnt/β-catenin signaling is active (Guasti et al., 2013; Häfner et al., 2015; Kim et al., 2008). On the other hand, our RNAseq data revealed no change in the expression of FGF ligands (data not shown). During neuromast assembly in the lateral line primordium of zebrafish, Fgf signaling plays an essential role in rosette formation by triggering Shroom3-mediated apical constriction (Ernst et al., 2012). Our data suggest that in the adrenal cortex *Shroom3* transcript level is modulated by FGFR2. Upon *Fgfr2* deletion, zG rosette frequency markedly decreases due to failed AJ constriction. In addition, expression of N- and K-cadherin is also reduced, suggesting FGFR2 may have a general role in regulating cell adhesion in the zG. We find that *Fgfr2* deletion has no effect on canonical Wnt activity, placing the FGF pathway downstream of Wnt/β-catenin in this context. Formal proof of this hypothesis will require deletion of *Fgfr2* in βCat-GOF mice. In addition to FGF signaling, the non-canonical Wnt/PCP pathway also plays a prominent role in tissue morphogenesis during development (Humphries and Mlodzik, 2018). It will be interesting to investigate what role non-canonical Wnt signaling might play in zG rosette dynamics.

Our data show that rosettes are present in the adult zG across species, suggesting a potentially conserved role in on-going adult tissue maintenance and function. Since the adrenal cortex constantly self-renews throughout life, it is highly likely that existing rosettes resolve as cells transit from zG to zF and new rosettes form to replace their loss. This remains to be formally demonstrated, however, potentially using inducible lineage-tracing in adult animals. Our work provides a conceptual framework for future studies to tackle these intriguing questions

Materials and Methods

Mice

All animal procedures were approved by Boston Children's Hospital's Institutional Animal Care and Use Committee. Mouse strains used in this study were: AS^{Cre} ($Cyp11b2^{tm1.1(cre)Brlt}$, Freedman et al., 2013), $Ctnnb1^{flox}$ ($Ctnnb1^{tm2Kem}$, Brault et al., 2001), $Ctnnb1^{fl(ex3)}$ ($Ctnnb1^{tm1Mmt}$, Harada et al., 1999), $Fgfr2^{flox}$ ($Fgfr2^{tm1Dor}$, Yu et al., 2003). To generate bigenic $AS^{Cre/+}$ :: $Ctnnb1^{fl/fl}$ mice (referred to as βCat-LOF), $AS^{Cre/+}$ mice were bred with $Ctnnb1^{fl/fl}$ mice. To generate bigenic $AS^{Cre/+}$ :: $Ctnnb1^{fl(ex3)/+}$ mice (referred to as βCat-GOF), $AS^{Cre/+}$ mice were bred with $Ctnnb1^{fl(ex3)/+}$ mice. To generate bigenic $AS^{Cre/+}$ :: $Fgfr2^{fl/fl}$ mice (referred to as Fgfr2-LOF), $AS^{Cre/+}$mice were bred with $Fgfr2^{fl/fl}$ mice. All animals were maintained on a mixed sv129-C57Bl/6 genetic background, with *ad lib* food and water, under a 12-hour light / 12-hour dark cycle. PCR was used for genotyping. Littermates were used whenever possible and both male and female animals were studied.

Tissue Preparation

After dissection, adrenals were trimmed of surrounding fat tissue and rinsed in PBS. For immunofluorescence, adrenals were cut into halves with a surgical blade and fixed in 4% PFA at

4ºC overnight. For RNAscope *in situ* hybridization, intact adrenals were fixed in 4% PFA at room temperature overnight.

Floating Section Immunofluorescence

After fixation, adrenals were embedded in 4% low-melting-temperature SeaPlaque Agarose (Lonza, 50100) and sectioned at thickness of 100 μm with a vibratome. Individual slices were separated by free floating in PBS. Slices were washed with 0.1% Tween-20 in PBS for 10 min for three times, and blocked in 5% Normal Goat Serum, 1% Bovine Serum Albumin, 0.1% Tween-20 in PBS for 1 hour at RT with gentle rocking. Slices were incubated with primary antibodies diluted in blocking solution at 4ºC overnight. After three 20 min washes with 0.1% Tween-20 in PBS, slices were incubated with secondary antibodies diluted in 0.1% Tween-20 in PBS for 2 hr at RT. For F-actin staining, Alexa Fluor 647-conjugated Phalloidin (Invitrogen, A22287) was added to the secondary antibody mix for the last 30 min at final concentration of 1:100. For nuclear staining, DAPI (4′,6-diamidino-2-phenylindole) was added to secondary antibody mix for the last 5 min at final concentration of 1:500-1:1000. Slices were then washed with 0.1% Tween-20 in PBS for 20 min for three times, processed for tissue clearing or directly mounted on Superfrost Plus slides (Fisher Scientific, 12-550-15) with ProLong Gold Antifade Mountant (Thermo Fisher Scientific, P36930). Primary antibodies used for this application include: Rat anti-Laminin β1 (Santa Cruz, sc-33709), Rabbit anti-Gαq (Abcam, ab75825), Rabbit anti-β-catenin (Abcam, ab16051), Rabbit anti-Col4a1 (Novus Biologicals, NB120-6586), Rat anti-CD31 (BD Bioscience, 557355), Rabbit anti-Vimentin (Abcam, ab92547),, Rabbit anti-N-cadherin (Novus Biologicals, NBP2-38856), Rabbit anti-K-cadherin (Abcam, ab133632), Rat anti-E-cadherin (Abcam, ab11512). The following secondary antibodies were used: Alexa Fluor 647/594/488-conjugated goat anti-rabbit IgG, Alexa Fluor 647/594-conjugated goat anti-rat IgG (Invitrogen). Images of 100 μm-thick sections were acquired using an upright Zeiss LSM710 or LSM700 confocal microscope with either a 10X/0.3 EC Plan-Neofluar, a 40X/1.4 oil Plan-

Apochromat or a 63X/1.4 oil Plan-Apochromat objective and adjusted for brightness and contrast in ImageJ.

Tissue Clearing

After immunostaining, floating 100 µm-thick slices were dehydrated by an ethanol gradient and washed in 100% ethanol twice for 5 min. In a 10-well glass staining dish (Electron Microscopy Sciences, 71564), slices were washed with 50% ethanol in BABB solution (benzyl alcohol : benzyl benzoate (Sigma-Aldrich) in 1:2 ratio (v/v)) for 5 min at RT. Slices were then incubated in fresh BABB solution for 10 min at RT and mounted on Superfrost Plus slides (Fisher Scientific, 12-550-15) with BABB. Cover glass (0.16 to 0.19 mm in thickness) were applied and sealed with silicone grease (Dow Corning, 1597418).

Paraffin Section Immunofluorescence

After fixation, adrenals were dehydrated in ethanol, xylene and embedded in paraffin blocks. Paraffin sections were cut at 5 µm thickness. Sections were rinsed in xylene, an ethanol gradient and then PBS. Antigen retrieval was performed in Tris-EDTA pH 9.0 (for Lef1) or 10 mM Sodium Citrate pH 6.0 (all others). Sections were blocked in 5% Normal Goat Serum, 0.1% Tween-20 in PBS for 1 hour at RT. Primary antibodies were diluted 1:200 in 5% NGS in PBS and incubated on sections at 4ºC overnight. Slides were washed three times for 5 min in 0.1% Tween-20 in PBS. Secondary antibodies were diluted in 1:200 in PBS and incubated on sections at RT for 1-2 hours. For nuclear staining, DAPI (4′,6-diamidino-2-phenylindole) was added to secondary antibody mixture at a final concentration of 1:1000. After three 5-min washes with 0.1% Tween-20 in PBS, slides were mounted with ProLong Gold Antifade Mountant (Thermo Fisher Scientific, P36930). Primary antibodies used for this application include: Mouse anti-β-catenin (BD Biosciences, 610153), Rabbit anti-K-cadherin (Abcam, ab133632), Chicken anti-GFP (Aves Labs, GF-1020), Rabbit anti-Lef1 (Abcam, ab137872). The

following secondary antibodies were used: Alexa Fluor 647-conjugated goat anti-rabbit IgG, Alexa Fluor 647-conjugated goat anti-mouse IgG, Alexa Fluor 488-conjugated goat anti-chicken IgG (Invitrogen). Images were acquired using a Nikon upright Eclipse 90i microscope with a 20X/0.75 Plan-Apochromat objective and adjusted for brightness and contrast in ImageJ.

Human and Peruvian Mouse Adrenal Samples

Human adrenal sample was a gift from Dr. Felix Beuschlein. Peruvian mouse adrenal sample was a gift from Dr. Celso Gomez-Sances. In both cases, paraffin blocks were cut into 10-14 μm-thick sections to obtain maximum spatial information of zG morphology.

Image Analysis

Quantifications of glomerular roundness, glomerular 2D area and Lamb1-positive zG thickness were performed on confocal images of 100 μm-thick sections stained with Lamb1 in ImageJ. Outlines of individual glomerulus were hand-traced following Lamb1 signal. Gaps in Lamb1 signal at glomerular junctions were closed if smaller than 5 μm. Gaps in Lamb1 signal at zG/zF boundary were closed based on the morphological boundary of zG. Glomerular roundness measurements were obtained using the built-in shape descriptor function of ImageJ, where roundness is calculated as $4 \times \text{Area} / \pi \times (\text{Major Axis})^2$. Glomerular 2D area measurements were calculated as μm^2. Lamb1-positive zG thickness measurements were obtained by drawing a transverse line across the Lamb1-positive region. Quantifications of rosette frequency, F-actin cluster size and length were performed on confocal Z-stack images of Phalloidin-stained 100 μm-thick sections. For each Z-stack, analysis was confined to a pre-defined 160 x 160 x 10 μm^3 cortical area justified to the capsule. Rosette centers were identified by satisfaction of two criteria: a greater-than-5-cell contact point and the presence of F-actin aggregate at the contact point. Rosette frequency was reported as the number of rosette centers per 160 x 160 x 10 μm^3 stack. Measurements of F-actin cluster size and length were obtained from volume renderings

of Z-stacks of Phalloidin-stained sections in Imaris (Bitplane, v7.6.4). Automatic thresholding with background subtraction (local contrast) was applied to each Z-stack for 3D rendering. F-actin cluster size was expressed in μm^3. F-actin cluster length was calculated as the maximal axial length of the object-oriented minimum Bounding Box statistical variable. For 3D reconstruction of a rosette, outlines of individual cells were hand-traced based on β-catenin staining signal and volume-rendered in Imaris (Bitplane, v7.6.4).

RNA Isolation and RNA Sequencing

Total RNA was isolated from whole adrenals trimmed of adherent fat and homogenized in TRI Reagent (Sigma) using a Direct-zol RNA miniprep kit (Zymo Research), following the manufacturer's protocol. RNA quality was evaluated using an Agilent 2100 Bioanalyzer (Agilent Technologies, Santa Clara, CA), and only samples with RIN > 7.0 were used for RNA sequencing (RNA-seq). Library preparation and sequencing were performed as previously described (Engeland et al., 2018). Data from all samples were processed using an RNA-seq pipeline implemented in the bcbio-nextgen project (bcbio-nextgen,0.9.1a-b73c090). The following steps were performed by the bcbio pipeline. Adapter sequences were trimmed from reads using cutadapt (version 1.13), the trimmed reads were aligned to the mm10 genome using STAR (version 2.4.1d) (Dobin et al., 2013), and gene expression (uniquely mapping reads) was quantified using featureCounts (version 1.4.4) (Liao et al., 2014). To determine which genes were differentially expressed between the control and mutant mice, the count matrix generated by featureCounts was used as input to DESeq2 (version 1.6.3) (Love et al., 2014). To identify differentially expressed genes, the following cutoffs were applied: fold change > 1.4, q-value < 0.05, basemean expression > 100 RPKM. Up-regulated gene list was submitted to DAVID (v6.7) for functional annotation enrichment analysis.

Gene Expression Analysis

Total RNA was isolated from whole adrenals as described above, using a Direct-zol microprep kit (Zymo Research). 500 ng of RNA was reverse-transcribed into cDNA using the High-Capacity cDNA Reverse Transcription Kit (Applied Biosystems, 4368814). Gene expression analysis was performed by quantitative Real Time PCR (qRT-PCR) using a QuantStudio 6 Flex thermocycler (Applied Biosystems). The following Taqman gene expression assays (Applied Biosystems) were used: *Axin2* (Mm00443610_m1), *Cdh2* (Mm01162497_m1), *Cdh6* (Mm01310024_m1), *Lef1* (Mm00550265_m1), *Shroom3* (Mm00497207_m1), *Ppib* (Mm00478295_m1), *Sulf1* (Mm00552283_m1), *Nkd1* (Mm00471902_m1), *Nfatc4* (Mm00452375_m1), *Shh* (Mm00436528_m1), *Sema5a* (Mm00436500_m1), *Daam2* (Mm01273811_m1), *Ajuba* (Mm00495049_m1), *Dact1* (Mm00458117_m1), *Wnt4* (Mm01194003_m1), *Dab2* (Mm01307290_m1), *Gli3* (Mm00492337_m1), *Tcf7* (Mm00493445_m1), *Fzd5* (Mm00445623_s1), *Lama5* (Mm01222029_m1), *Prickle1* (Mm01297035_m1). *Ppib* transcripts were used as the endogenous control and data were expressed using the 2^{-ddCt} method.

Single-Molecule RNA *in situ* Hybridization

After fixation, adrenals were embedded in paraffin blocks and sectioned at 5 μm thickness. Single-molecule RNA in situ hybridization was performed using a RNAscope 2.5 HD Brown Reagent Kit (Advanced Cell Diagnostics, 322300), following manufacturer's protocol. Target retrieval was performed for 7 min (Basham et al., 2019). Slides were counter-stained with 30% Gill's Hematoxylin (Fisher Scientific, 23-245654) and mounted with Cytoseal XYL (Fisher Scientific, 22-050-262). The following probes were used: *Fgfr2* (ACD, 454951), *Shroom3* (472221), positive control *Ppib* (ACD, 313911), negative control *dapB* (ACD, 310043).

Transmission Electron Microscopy

Adrenals were fixed in 2.5% glutaraldehyde, 1.25% paraformaldehyde, and 0.03% picric acid in 0.1 M sodium cacodylate buffer (pH 7.4) for 2 hours at RT, washed in 0.1M cacodylate buffer and post-fixed with 1% Osmiumtetroxide (OsO_4) / 1.5% Potassiumferrocyanide ($KFeCN_6$) for 1 hour. Samples were washed in water twice, in 50mM Maleate buffer pH 5.15 (MB) once, and incubated in 1% uranyl acetate in MB for 1hr followed by 1 wash in MB, 2 washes in water and subsequent dehydration in an ethanol gradient (10min each; 50%, 70%, 90%, 2x10min 100%). Samples were then put in propyleneoxide for 1 hr and infiltrated overnight in a 1:1 mixture of propyleneoxide and TAAB Epon (TAAB Laboratories Equipment, Aldermaston, England). On the following day, samples were embedded in TAAB Epon and polymerized at 60 ºC for 48 hrs. Ultrathin sections (about 80nm) were cut on a Reichert Ultracut-S microtome, picked up on to copper grids stained with lead citrate and examined in a JEOL 1200EX Transmission electron microscope or a TecnaiG² Spirit BioTWIN and images were recorded with an AMT 2k CCD camera.

Western Blotting

Adrenal lysates were prepared by homogenizing in lysis buffer (50 mM Tris pH 7.5, 150 mM NaCl, 1 mM EDTA, 1% NP40, 0.5% sodium deoxycholate, 1.0% SDS, 2 mM NaF, 2 mM sodium orthovanadate, and supplemented with protease and phosphatase inhibitors), sonicating and centrifuging at 13,000 g for 10 minutes. Lysates were subjected to SDS-PAGE and transferred onto a PVDF membrane (Thermo Scientific). After blocking, blots were incubated overnight with primary antibodies (1:1000 to 5000 dilution). Secondary antibody conjugated with horseradish peroxidase and chemiluminescent ECL substrate (Bio-Rad, 1705060) were used to develop blots. Antibodies used for this application are: Rabbit anti-FGFR2 clone D4L2V (Cell Signaling Technology, 23328), Rabbit anti-β-Actin clone 13E5 (Cell Signaling Technology, 4970), HRP-linked goat anti-rabbit IgG (Cell Signaling Technology, 7074)

Quantification and Statistical Analysis

All statistical analyses and graphs were generated in R (v3.3.2) or Prism 7 (GraphPad Software). Non-parametric tests were applied to glomerular morphometric data, including Mann-Whitney *U* test and Kruskal-Wallis one-way ANOVA on ranks with Dunn's multiple comparison correction. Unpaired two-tailed *t*-tests were used to analyze rosette frequency, zG thickness, and qRT-PCR data, using the Holm-Sidak method for multiple comparison correction. $P < 0.05$ was considered statistically significant. For all box and whisker plots, box boundaries are the 25th and 75th percentiles, and the whiskers are the 5th and 95th percentiles. For all bar plots, error bars represent SEM. Exact values of n are reported in each figure legend.

References

Arnold, T.R., Stephenson, R.E., and Miller, A.L. (2017). Rho GTPases and actomyosin: Partners in regulating epithelial cell-cell junction structure and function. Exp. Cell Res. 358, 20–30.

Basham, K.J., Rodriguez, S., Turcu, A.F., Lerario, A.M., Logan, C.Y., Rysztak, M.R., Gomez-Sanchez, C.E., Breault, D.T., Koo, B.-K., Clevers, H., et al. (2019). A ZNRF3-dependent Wnt/β-catenin signaling gradient is required for adrenal homeostasis. Genes Dev. 33, 209–220.

Bek, S., and Kemler, R. (2002). Protein kinase CKII regulates the interaction of beta-catenin with alpha-catenin and its protein stability. J. Cell Sci. 115, 4743–4753.

Bell, C.L., and Murray, S.A. (2016). Adrenocortical Gap Junctions and Their Functions. Front. Endocrinol. 7, 82.

Black, V.H., Robbins, D., McNamara, N., and Huima, T. (1979). A correlated thin-section and freeze-fracture analysis of guinea pig adrenocortical cells. Am. J. Anat. 156, 453–503.

Blankenship, J.T., Backovic, S.T., Sanny, J.S.P., Weitz, O., and Zallen, J.A. (2006). Multicellular Rosette Formation Links Planar Cell Polarity to Tissue Morphogenesis. Dev. Cell 11, 459–470.

Bollag, W.B. (2014). Regulation of aldosterone synthesis and secretion. Compr. Physiol. 4, 1017–1055.

Brault, V., Moore, R., Kutsch, S., Ishibashi, M., Rowitch, D.H., McMahon, A.P., Sommer, L., Boussadia, O., and Kemler, R. (2001). Inactivation of the beta-catenin gene by Wnt1-Cre-mediated deletion results in dramatic brain malformation and failure of craniofacial development. Dev. Camb. Engl. 128, 1253–1264.

Buckley, C.D., Tan, J., Anderson, K.L., Hanein, D., Volkmann, N., Weis, W.I., Nelson, W.J., and Dunn, A.R. (2014). Cell adhesion. The minimal cadherin-catenin complex binds to actin filaments under force. Science 346, 1254211.

Cadigan, K.M., and Waterman, M.L. (2012). TCF/LEFs and Wnt signaling in the nucleus. Cold Spring Harb. Perspect. Biol. 4.

Chacon-Heszele, M.F., Ren, D., Reynolds, A.B., Chi, F., and Chen, P. (2012). Regulation of cochlear convergent extension by the vertebrate planar cell polarity pathway is dependent on p120-catenin. Development 139, 968–978.

Davis, K.T., Prentice, N., Gay, V.L., and Murray, S.A. (2002). Gap junction proteins and cell-cell communication in the three functional zones of the adrenal gland. J. Endocrinol. 173, 13–21.

Delva, E., and Kowalczyk, A.P. (2009). Regulation of cadherin trafficking. Traffic Cph. Den. 10, 259–267.

Dobin, A., Davis, C.A., Schlesinger, F., Drenkow, J., Zaleski, C., Jha, S., Batut, P., Chaisson, M., and Gingeras, T.R. (2013). STAR: ultrafast universal RNA-seq aligner. Bioinforma. Oxf. Engl. 29, 15–21.

Drelon, C., Berthon, A., Mathieu, M., Martinez, A., and Val, P. (2014). Adrenal cortex tissue homeostasis and zonation: A WNT perspective. Mol. Cell. Endocrinol.

Drelon, C., Berthon, A., Sahut-Barnola, I., Mathieu, M., Dumontet, T., Rodriguez, S., Batisse-Lignier, M., Tabbal, H., Tauveron, I., Lefrançois-Martinez, A.-M., et al. (2016). PKA inhibits WNT signalling in adrenal cortex zonation and prevents malignant tumour development. Nat. Commun. 7, 12751.

le Duc, Q., Shi, Q., Blonk, I., Sonnenberg, A., Wang, N., Leckband, D., and de Rooij, J. (2010). Vinculin potentiates E-cadherin mechanosensing and is recruited to actin-anchored sites within adherens junctions in a myosin II-dependent manner. J. Cell Biol. 189, 1107–1115.

Engeland, W.C., Massman, L., Mishra, S., Yoder, J.M., Leng, S., Pignatti, E., Piper, M.E., Carlone, D.L., Breault, D.T., and Kofuji, P. (2018). The Adrenal Clock Prevents Aberrant Light-Induced Alterations in Circadian Glucocorticoid Rhythms. Endocrinology 159, 3950–3964.

Ernst, S., Liu, K., Agarwala, S., Moratscheck, N., Avci, M.E., Nogare, D.D., Chitnis, A.B., Ronneberger, O., and Lecaudey, V. (2012). Shroom3 is required downstream of FGF signalling to mediate proneuromast assembly in zebrafish. Development 139, 4571–4581.

Freedman, B.D., Kempna, P.B., Carlone, D.L., Shah, M.S., Guagliardo, N.A., Barrett, P.Q., Gomez-Sanchez, C.E., Majzoub, J.A., and Breault, D.T. (2013). Adrenocortical Zonation Results from Lineage Conversion of Differentiated Zona Glomerulosa Cells. Dev. Cell 26, 666–673.

Gallo-Payet, N., and Battista, M.-C. (2014). Steroidogenesis-Adrenal Cell Signal Transduction. In Comprehensive Physiology, R. Terjung, ed. (Hoboken, NJ, USA: John Wiley & Sons, Inc.), pp. 889–964.

Guagliardo, N.A., Yao, J., Hu, C., and Barrett, P.Q. (2012). Minireview: aldosterone biosynthesis: electrically gated for our protection. Endocrinology 153, 3579–3586.

Guasti, L., Candy Sze, W.C., McKay, T., Grose, R., and King, P.J. (2013). FGF signalling through Fgfr2 isoform IIIb regulates adrenal cortex development. Mol. Cell. Endocrinol. 371, 182–188.

Guillot, C., and Lecuit, T. (2013). Mechanics of epithelial tissue homeostasis and morphogenesis. Science 340, 1185–1189.

Häfner, R., Bohnenpoll, T., Rudat, C., Schultheiss, T.M., and Kispert, A. (2015). Fgfr2 is required for the expansion of the early adrenocortical primordium. Mol. Cell. Endocrinol. 413, 168–177.

Harada, N., Tamai, Y., Ishikawa, T., Sauer, B., Takaku, K., Oshima, M., and Taketo, M.M. (1999). Intestinal polyposis in mice with a dominant stable mutation of the beta-catenin gene. EMBO J. 18, 5931–5942.

Harding, M.J., McGraw, H.F., and Nechiporuk, A. (2014). The roles and regulation of multicellular rosette structures during morphogenesis. Development 141, 2549–2558.

Humphries, A.C., and Mlodzik, M. (2018). From instruction to output: Wnt/PCP signaling in development and cancer. Curr. Opin. Cell Biol. 51, 110–116.

Kim, A.C., Reuter, A.L., Zubair, M., Else, T., Serecky, K., Bingham, N.C., Lavery, G.G., Parker, K.L., and Hammer, G.D. (2008). Targeted disruption of beta-catenin in Sf1-expressing cells impairs development and maintenance of the adrenal cortex. Dev. Camb. Engl. 135, 2593–2602.

Lecaudey, V., Cakan-Akdogan, G., Norton, W.H.J., and Gilmour, D. (2008). Dynamic Fgf signaling couples morphogenesis and migration in the zebrafish lateral line primordium. Development 135, 2695–2705.

Liao, Y., Smyth, G.K., and Shi, W. (2014). featureCounts: an efficient general purpose program for assigning sequence reads to genomic features. Bioinforma. Oxf. Engl. 30, 923–930.

Lienkamp, S.S., Liu, K., Karner, C.M., Carroll, T.J., Ronneberger, O., Wallingford, J.B., and Walz, G. (2012). Vertebrate kidney tubules elongate using a planar cell polarity–dependent, rosette-based mechanism of convergent extension. Nat. Genet. 44, 1382–1387.

Love, M.I., Huber, W., and Anders, S. (2014). Moderated estimation of fold change and dispersion for RNA-seq data with DESeq2. Genome Biol. 15, 550.

Mariani, F.V., Fernandez-Teran, M., and Ros, M.A. (2017). Ectoderm-mesoderm crosstalk in the embryonic limb: The role of fibroblast growth factor signaling. Dev. Dyn. Off. Publ. Am. Assoc. Anat. 246, 208–216.

Meng, W., and Takeichi, M. (2009). Adherens junction: molecular architecture and regulation. Cold Spring Harb. Perspect. Biol. 1, a002899.

Mohan, S., Rizaldy, R., Das, D., Bauer, R.J., Heroux, A., Trakselis, M.A., Hildebrand, J.D., and VanDemark, A.P. (2012). Structure of Shroom domain 2 reveals a three-segmented coiled-coil required for dimerization, Rock binding, and apical constriction. Mol. Biol. Cell 23, 2131–2142.

Muzumdar, M.D., Tasic, B., Miyamichi, K., Li, L., and Luo, L. (2007). A global double-fluorescent Cre reporter mouse. Genes. N. Y. N 2000 45, 593–605.

Nelson, W.J., and Nusse, R. (2004). Convergence of Wnt, beta-catenin, and cadherin pathways. Science 303, 1483–1487.

Nishimura, T., and Takeichi, M. (2008). Shroom3-mediated recruitment of Rho kinases to the apical cell junctions regulates epithelial and neuroepithelial planar remodeling. Development 135, 1493–1502.

Nishimura, T., Honda, H., and Takeichi, M. (2012). Planar Cell Polarity Links Axes of Spatial Dynamics in Neural-Tube Closure. Cell 149, 1084–1097.

Palacios, F., Schweitzer, J.K., Boshans, R.L., and D'Souza-Schorey, C. (2002). ARF6-GTP recruits Nm23-H1 to facilitate dynamin-mediated endocytosis during adherens junctions disassembly. Nat. Cell Biol. 4, 929–936.

Pignatti, E., Leng, S., Carlone, D.L., and Breault, D.T. (2017). Regulation of zonation and homeostasis in the adrenal cortex. Mol. Cell. Endocrinol. 441, 146–155.

Shire, J.G. (1969). A strain difference in the adrenal zona glomerulosa determined by one gene-locus. Endocrinology 85, 415–422.

Simões, S. de M., Blankenship, J.T., Weitz, O., Farrell, D.L., Tamada, M., Fernandez-Gonzalez, R., and Zallen, J.A. (2010). Rho-kinase directs Bazooka/Par-3 planar polarity during Drosophila axis elongation. Dev. Cell 19, 377–388.

Simões, S. de M., Mainieri, A., and Zallen, J.A. (2014). Rho GTPase and Shroom direct planar polarized actomyosin contractility during convergent extension. J. Cell Biol. 204, 575–589.

Spät, A., and Hunyady, L. (2004). Control of aldosterone secretion: a model for convergence in cellular signaling pathways. Physiol. Rev. 84, 489–539.

Steinhart, Z., and Angers, S. (2018). Wnt signaling in development and tissue homeostasis. Dev. Camb. Engl. 145.

Takeichi, M. (2014). Dynamic contacts: rearranging adherens junctions to drive epithelial remodelling. Nat. Rev. Mol. Cell Biol. 15, 397–410.

Trichas, G., Smith, A.M., White, N., Wilkins, V., Watanabe, T., Moore, A., Joyce, B., Sugnaseelan, J., Rodriguez, T.A., Kay, D., et al. (2012). Multi-Cellular Rosettes in the Mouse Visceral Endoderm Facilitate the Ordered Migration of Anterior Visceral Endoderm Cells. PLoS Biol. 10, e1001256.

Villasenor, A., Chong, D.C., Henkemeyer, M., and Cleaver, O. (2010). Epithelial dynamics of pancreatic branching morphogenesis. Development 137, 4295–4305.

Virtanen, I., Korhonen, M., Petäjäniemi, N., Karhunen, T., Thornell, L.-E., Sorokin, L.M., and Konttinen, Y.T. (2003). Laminin isoforms in fetal and adult human adrenal cortex. J. Clin. Endocrinol. Metab. 88, 4960–4966.

Volckaert, T., and De Langhe, S.P. (2015). Wnt and FGF mediated epithelial-mesenchymal crosstalk during lung development. Dev. Dyn. Off. Publ. Am. Assoc. Anat. 244, 342–366.

Walck-Shannon, E., and Hardin, J. (2014). Cell intercalation from top to bottom. Nat. Rev. Mol. Cell Biol. 15, 34–48.

Walczak, E.M., and Hammer, G.D. (2014). Regulation of the adrenocortical stem cell niche: implications for disease. Nat. Rev. Endocrinol. 11, 14–28.

Xing, Y., Lerario, A.M., Rainey, W., and Hammer, G.D. (2015). Development of Adrenal Cortex Zonation. Endocrinol. Metab. Clin. North Am. *44*, 243–274.

Yu, K., Xu, J., Liu, Z., Sosic, D., Shao, J., Olson, E.N., Towler, D.A., and Ornitz, D.M. (2003). Conditional inactivation of FGF receptor 2 reveals an essential role for FGF signaling in the regulation of osteoblast function and bone growth. Dev. Camb. Engl. *130*, 3063–3074.

Chapter Three:

β-Catenin Blocks Zonal Transdifferentiation and Causes Hyperaldosteronism

β-Catenin Blocks Zonal Transdifferentiation and Causes Hyperaldosteronism

Emanuele Pignatti[1,2,*], Sining Leng[1,3,*], Nick A. Guagliardo[4], Manasvi S. Shah[1,2], Qingen Ke[5], Peter M. Kang[5], Paula Q. Barrett[4], Diana L. Carlone[1,2,6], David T. Breault[1,2,6]

[1]*Division of Endocrinology, Boston Children's Hospital, Boston, MA 02115, USA*

[2]*Department of Pediatrics, Harvard Medical School, Boston, MA 02115, USA*

[3]*Division of Medical Sciences, Harvard Medical School, Boston, MA 02115, USA*

[4]*Department of Pharmacology, University of Virginia, Charlottesville, VA, 22947, USA*

[5]*Cardiovascular Division, Beth Israel Deaconess Medical Center, Boston, MA 02215, USA.*

[6]*Harvard Stem Cell Institute, Cambridge, MA 02138, USA*

**These authors contributed equally to this work.*

Attributions:

This chapter contains the manuscript titled “β-Catenin blocks zonal transdifferentiation and causes hyperaldosteronism”. It has been modified to fit the style of this dissertation. S.L. is co-first author. E.P., S.L. and D.T.B. designed the experiments with additional input from D.L.C. E.P. (all experiments unless otherwise stated), S.L. (data analysis and interpretation), M.S.S. (quantitative analysis), Q.K. and P.K. (blood pressure) did the research. N.A.G. and P.Q.B. provided valuable intellectual input on hormone analysis. E.P., D.L.C. and D.T.B. prepared the figures and wrote the manuscript.

Summary

Constitutive activation of canonical Wnt/β-catenin signaling has been linked to hyperplasia in a range of tissues, including the adrenal cortex, although the cellular mechanisms responsible for this effect remain poorly understood. To investigate the consequence of somatic β-catenin gain-of-function (GOF) mutations within zona glomerulosa (zG) cells, we generated mice with zG-specific stabilization of β-catenin (βcat-GOF). As expected, βcat-GOF caused a progressive hyperplastic expansion of the zG, concurrent with increased aldosterone biosynthesis and elevated blood pressure. βcat-GOF also led to an unanticipated retention of normal feedback regulation of the renin-angiotensin system (RAAS), consistent with an early stage of primary aldosteronism (PA). Surprisingly, hyperplasic expansion of the zG was not driven by an increase in cell proliferation nor a decrease in cell death, but rather was the result of a block in zonal transdifferentiation. Nevertheless, chronic activation of RAAS in βcat-GOF mice, using genetic, pharmacological and dietary models, produced a striking increase in zG proliferation and consequent adrenomegaly. Together, these data provide a new understanding of context-dependent mechanisms controlling zonal transdifferentiation and zG hyperplasia that have important therapeutic implications for PA patients with somatic β-catenin GOF mutations.

Introduction

The canonical WNT/β-catenin signaling pathway is a critical regulator of adrenal development and homeostasis (1), and has been linked to both adrenal hyperplasia and tumorigenesis (2). WNT/β-catenin signaling is active within the zona glomerulosa (zG) region, where aldosterone-producing cells reside and is required for aldosterone production (3). Moreover, constitutive activation of β-catenin within adrenocortical cells leads to hyperplasia and excess production of aldosterone from zG cells, resulting in primary aldosteronism (PA) (4). PA is the most common form of secondary hypertension affecting ~10% of all hypertensive patients and ~20% of

patients with resistant hypertension (5, 6). In addition to the adverse cardiovascular outcomes associated with hypertension, PA is an independent risk factor for stroke, myocardial infarction, atrial fibrillation, cardiac failure and renal failure (7, 8). Despite its high prevalence and associated morbidity and mortality, an integrated understanding of the molecular mechanisms leading to PA is lacking.

PA is most commonly caused by unilateral aldosterone-producing adenomas (APA) or bilateral idiopathic adrenal hyperplasia (IAH) (9). Recently, exome sequencing studies have identified recurrent somatic mutations in genes including *KCNJ5*, *ATP1A1*, *ATP2B3*, and *CACNA1D* in over 50% of APAs, but not in IAH (10). These mutations have been functionally linked to zG cell depolarization and aldosterone hypersecretion (6), but evidence from animal models and *in vitro* studies suggest that they alone are insufficient to drive zG hyperplasia (11, 12). It is conceivable that alterations in key signaling pathways, normally required for adrenal development and/or homeostasis, may mediate the cellular hyperplasia that underlies PA. Consistent with this, analysis of APAs has revealed that the majority (~70%) demonstrate activation of WNT/β-catenin signaling (13), implicating this pathway in the initiation and/or progression of the hyperplastic response. Despite these recent advances, a significant need exists for model systems to elucidate the cellular mechanisms responsible for adrenal hyperplasia.

To investigate the impact of somatic β-catenin gain-of-function (GOF) mutations within zG cells, we generated mice with zG-specific stabilization of β-catenin (βcat-GOF). Our data revealed that βcat-GOF led to a progressive hyperplastic expansion of the zG with a corresponding increase in aldosterone and blood pressure. However, stabilization of β-catenin did not affect the normal feedback regulation of the renin-angiotensin system (RAAS), consistent with an early stage of PA. Remarkably, the hyperplasic expansion of the zG was caused by a block in zonal transdifferentiation rather than by changes in cell proliferation or cell death. We also found that

chronic activation of RAAS in βcat-GOF mice, using genetic, pharmacological and dietary models, led to a marked increase in zG proliferation and subsequent adrenomegaly. Together, these data provide new insight into context-dependent mechanisms that control zonal transdifferentiation and zG hyperplasia and have important therapeutic implications for patients with somatic β-catenin GOF mutations that arise in the zG.

Results

Stabilization of β-catenin in zG cells results in expansion of the zG.

To investigate the cellular mechanisms by which activation of canonical Wnt/β-catenin signaling leads to adrenal hyperplasia, we compared mice with zG-specific stabilization of β-catenin (βcat-GOF) (**Figure 3.1A**) to βcat-WT control mice. In βcat-GOF mice, conditional deletion of exon 3 of the *Ctnnb1* gene, which encodes β-catenin, following Cre-mediated recombination results in stabilization of β-catenin (and constitutive activation of β-catenin) specifically within zG cells. Increased expression of *Axin2* and *Lef1*, well-established targets of β-catenin, confirmed activation of this pathway in βcat-GOF adrenals (**Figure 3.1B**).

To begin to understand the impact of βcat-GOF on adrenal homeostasis over time, we analyzed the β-catenin expression domain in young adult, adult and aged mice. As expected, β-catenin expression in βcat-WT adrenals was largely restricted to the zG at all ages (**Figure 3.1C**), consistent with a previous report (14). In contrast, βcat-GOF adrenals showed a progressive expansion of β-catenin expressing cells displacing the underlying zona Fasciculata (zF) region (**Figures 3.1C, S2.1A**). Male and female mice displayed a similar pattern (**Figure S2.1B**). Thus, unless otherwise stated, the following studies were performed with female mice.

To determine whether the expanded region of β-catenin-expressing cells retain their zG identity, we performed co-immunostaining for β-catenin and Dab2, an established zG marker (15).

Figure 3.1. Stabilization of β-catenin results in zG expansion.

(A) Schematic representation of the alleles comprising βcat-GOF (βGOF) mice. Cre recombinase is expressed under the control of the Aldosterone Synthase (AS) promoter and drives excision of the third exon of Ctnnb1, encoding β-catenin leading to stabilization in AS-expressing zG cells. βcat-WT (βWT) control mice have two copies of the wildtype Ctnnb1 allele. (B) Real-Time quantitative PCR (RT-qPCR) for Axin2 (n = 5-8 mice) and Lef1, (n = 7 mice). (C) Representative adrenal sections stained for β-catenin (β-cat, red), (n = 5-10 mice). (D) Representative adrenal sections co-stained for β-catenin (β-cat, red) and Dab2 (green), (n = 3-4 mice). (E) Representative adrenal sections co-stained for β-catenin (β-cat, red) and Gαq (green), (n = 7-9 mice). (F) Representative adrenal sections co-stained for β-catenin (β-cat, red) and Akr1b7 (green), (n = 3 mice). (G) Analysis of cellular density using quantification of DAPI-stained nuclei normalized per unit area, (n = 5-6 mice). All sections were counter-stained with nuclear DAPI (blue) and were from adult mice unless otherwise stated. The dotted lines define the border between β-catenin-positive and - negative regions. c, capsule. zG, zona Glomerulosa. zF, zona Fasciculata. Scale bars: 50 μm. For panel (B), statistical analysis was performed using an unpaired Student's t-test or Mann-Whitney test. For panel (G), statistical analysis was performed using a two-way ANOVA test in conjunction with a Tukey's range test. ns, not significant. **P < 0.01; ****P < 0.0001.

Figure 3.1 (continued)

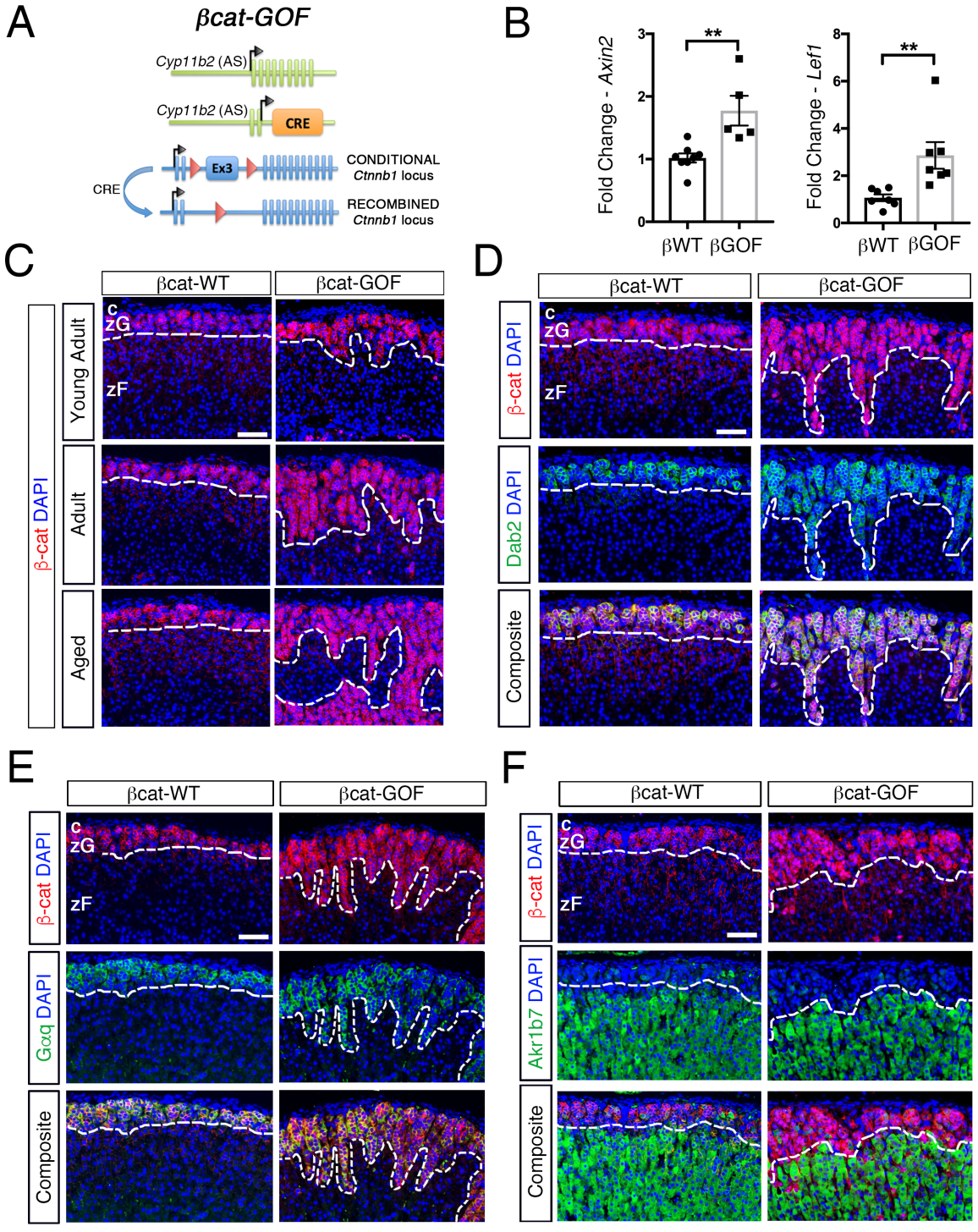

Similar to βcat-WT adrenals, Dab2 expression co-localized with β-catenin in βcat-GOF adrenals, (**Figure 3.1D**), indicating that cells within the expanded β-catenin-positive region maintained a zG-like identity. In addition, we performed immunostaining for Gαq, the alpha subunit of the heterotrimeric G protein activated by Angiotensin II (AngII). Analysis of βcat-WT adrenals showed that Gαq specifically marks zG cells within the cortex and co-localizes with both β-catenin and Dab2 (**Figure S2.1C**). Consistent with their expression of Dab2, β-catenin-expressing cells in βcat-GOF adrenals also co-stained for Gαq (**Figures 3.1E, S2.1C**), confirming their zG identity. To further rule out that these cells exhibit zF-like features, we examined the expression pattern of Aldose reductase-related protein 1 (Akr1b7), a zF marker (16), which revealed mutually exclusive expression of β-catenin and Akr1b7 in both βcat-WT and βcat-GOF adrenals (**Figure 3.1F**). Finally, we performed histomorphometric analysis of βcat-WT and βcat-GOF adrenals by assessing the number of DAPI-positive nuclei per unit area (mm^2) for each region. The analysis revealed that the cellular density of the expanded zG region in the βcat-GOF adrenal was indistinguishable from βcat-WT (**Figure 3.1G**), indicating that the greater zG area in βcat-GOF mice is the result of hyperplasia and not hypertrophy. Together, these data show that stabilization of β-catenin within zG cells leads to a progressive hyperplastic expansion of the zG.

Stabilization of β-catenin leads to early stage PA.

Since high levels of β-catenin are nearly exclusively expressed in the zG (14), the site of aldosterone production, and activation of Wnt/β-catenin signaling is indicated in up to 70% of patients with PA (13), we assessed whether aldosterone levels were elevated in βcat-GOF mice. Compared with age-matched βcat-WT controls, βcat-GOF mice showed higher plasma aldosterone levels (**Figure 3.2A, S2.2A**). Because overproduction of aldosterone is associated with increased blood pressure, we next assessed systolic, diastolic, and mean arterial blood pressure, which were all elevated in adult and aged βcat-GOF mice, compared with age-

Figure 3.2. β-catenin GOF mice develop hyperaldosteronism and high blood pressure. (A) Quantification of plasma aldosterone levels in adult (*n* = 13-19) and aged (*n* = 9) mice. (B) Systolic blood pressure (BP) in adult (*n* = 8) and aged (*n* = 4) mice. (C) Paired plasma aldosterone levels from mice fed normal salt (NS) followed by high-salt (HS) chow, (*n* = 9-11 mice). (D) RT-qPCR for *Cyp11b2*, encoding AS, from adult (*n* = 7-9) and aged (*n* = 6- 9) whole adrenals. (E) Representative adrenal sections co-stained for β-catenin (β-cat, red) and Aldosterone Synthase (AS, green), (*n* = 5-9 mice). (F) Quantification of AS-positive cells in equatorial sections from adult (*n* = 5-7) and aged (*n* = 4-7) mice, normalized by cortical area. c, capsule. zG, zona Glomerulosa. zF, zona Fasciculata. Scale bars: 50 μm. Statistical analysis was performed using an unpaired Student's *t*-test or Mann-Whitney test for all panels, but panel (C). For panel (C), statistical analysis was performed using a two-way ANOVA test in conjunction with a Tukey's range test. *ns,* not significant. **P* < 0.05; ***P* < 0.01; ****P* < 0.001; *****P* < 0.0001.

Figure 3.2 (continued)

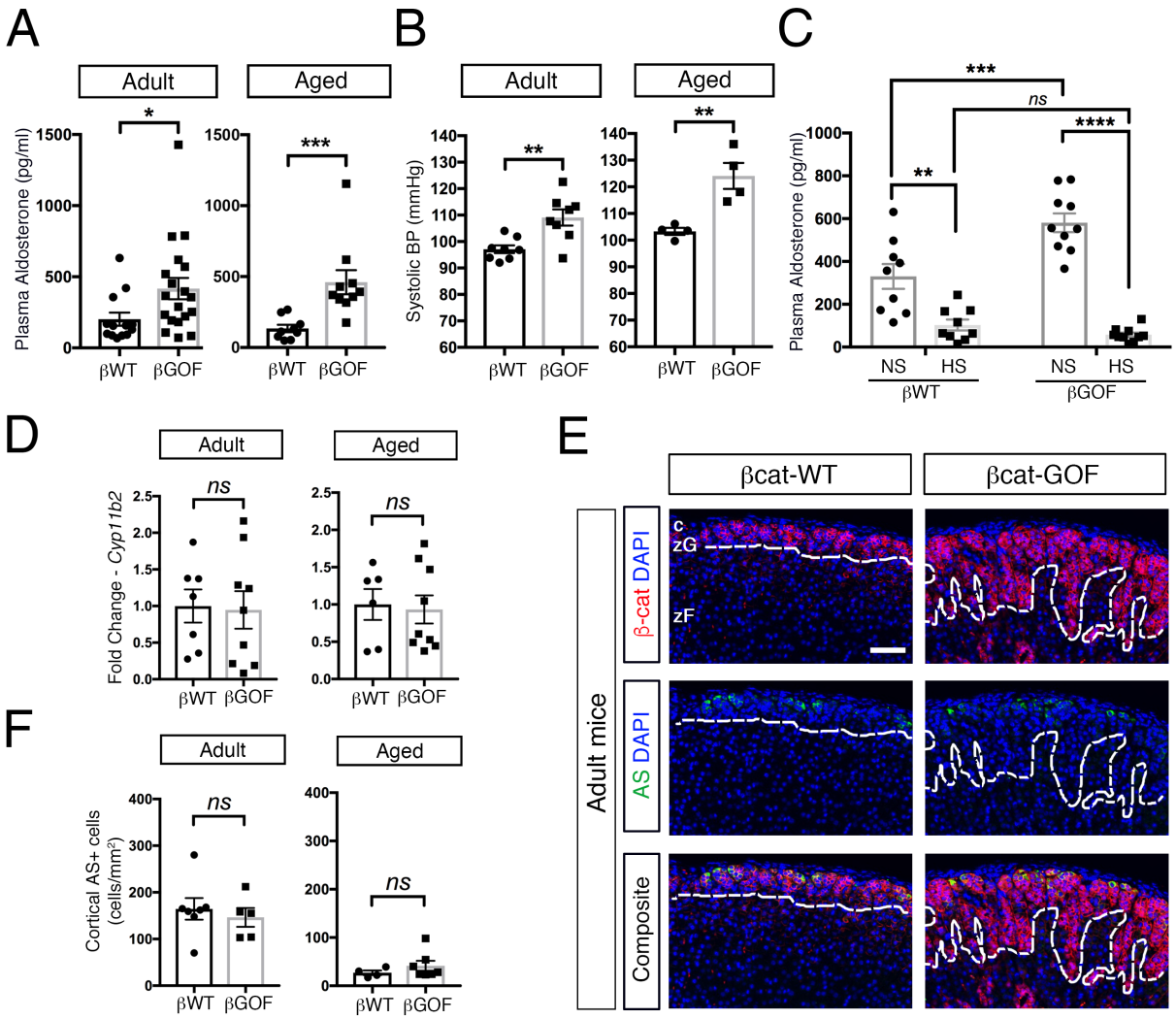

matched βcat-WT controls (**Figures 3.2B, S2.2B, C**). As predicted from the literature (4, 13), these data indicate that β-catenin stabilization in the zG is sufficient to increase plasma aldosterone levels, and elevate blood pressure, indicating that βcat-GOF mice serve as a model of PA.

PA represents a spectrum of disorders in which impaired feedback results in a variable degree of aldosterone autonomy and thus an inability to respond to volume expansion (17). To assess whether the increase in aldosterone in βcat-GOF mice is the result of autonomous production from zG cells, βcat-WT and βcat-GOF mice were subjected to a high-salt (HS) diet for a period of 5 days, which is sufficient to suppress aldosterone production. Analysis of plasma aldosterone levels on HS diet, compared to levels obtained on a normal-salt diet, revealed aldosterone suppression in both groups and a normalization of aldosterone production between genotypes (**Figure 3.2C**). These results indicate that the higher level of aldosterone in βcat-GOF mice does not arise from autonomous aldosterone production and that aldosterone-producing cells in these mice maintain normal feedback regulation, consistent with an early stage of PA.

Stabilization of β-catenin is not associated with increased *Cyp11b2* expression.

Because βcat-GOF mice demonstrate expansion of the zG, we next asked whether the increase in aldosterone levels in these mice was due to enhanced *Cyp11b2* (encoding AS) expression. Surprisingly, quantitative RT-PCR of whole adrenals showed no difference in the overall level of *Cyp11b2* (**Figure 3.2D**). We next assessed the distribution and number of AS-positive cells in adult and aged adrenals by immunostaining. Results from this study revealed that isolated patches of AS-positive cells in the subcapsular region of the zG, as previously described (3, 18), were present in both βcat-WT and βcat-GOF adrenals (**Figures 3.2E, S2.2D**). Quantitation of these patches showed that the overall number of AS-positive cells was unchanged between

βcat-WT and βcat-GOF (**Figure 3.2F**), in both adult and aged mice, consistent with the gene expression analysis (**Figure 3.2D**). Together, these data suggest that the elevated plasma aldosterone level in βcat-GOF mice does not result from an increase in AS-expressing cells.

Stabilization of β-catenin in zG cells blocks zG-to-zF cell transdifferentiation.

To understand the cellular mechanisms underlying zG expansion in βcat-GOF mice, we first tested the hypothesis that the expansion resulted from increased proliferation following stabilization of β-catenin, a known oncogene. To address this, the proliferation index of zG cells in βcat-WT and βcat-GOF adrenals was determined by scoring the number of Ki67-positive cells per zG area, as defined by the β-catenin expression domain. The total number of Ki67-positive cells in the βcat-GOF adrenals showed a modest increase with age (**Figure S2.3A**), consistent with the gradual expansion of the zG area (**Figure 3.1**). However, when the total number of Ki67-positive cells was normalized by the zG area (**Figure S2.1A**), we observed a significant overall decrease in the fraction of proliferating zG cells (zG proliferation index, **Figure 3.3A**). This result indicates that an increase in cell division is not responsible for the expansion of β-catenin-expressing cells in βcat-GOF mice. Since an increase in cell survival could also explain the increase in zG cells, we next assessed the impact of βcat-GOF on apoptosis by staining for activated caspase-3 or TUNEL in βcat-WT and βcat-GOF adrenals. Despite an overall low level of apoptosis, no differences were observed between groups (**Figure S2.3 B-E**).

We next asked whether the expanded zG region in βcat-GOF adrenals results from an alteration in zG-to-zF transdifferentiation. We have previously shown that zG cells undergo conversion to zF cells through a process of transdifferentiation (19). To address this with βcat-GOF adrenals, we performed functional lineage-tracing experiments using the mTmG reporter allele (**Figure 3.3B**). As expected, in βcat-WT adrenals GFP marked both zG cells (defined by Dab2 or Gαq co-expression) and zF cells (defined by Akr1b7 co-expression or the absence of Dab2 or Gαq

Figure 3.3. Stabilization of β-catenin blocks zG-to-zF cell transdifferentiation.

(A) Left: Representative adrenal sections co-stained for β-catenin (β-cat, red) and Ki67 (green). Right: Quantification of the Ki67-positive cells normalized for the β-catenin-positive zG domain (zG proliferation index), (*n* = 5-9 mice). (B) Schematic representation of the alleles comprising βcat-GOF::mTmG mice. βcat-WT::mTmG control mice have two copies of the wildtype *Ctnnb1* allele. (C) Representative adrenal sections co-stained for Dab2 (red) and GFP (green), (*n* = 9 mice). (D) Representative adrenal sections co-stained for Gαq (red) and GFP (green), (*n* = 9 mice). (E) Representative adrenal sections co-stained Akr1b7 (red) and GFP (green), (*n* = 3 mice). (F) Representative adrenal sections co-stained for β-catenin (β-cat, red) and GFP (green), (*n* = 5 mice). All sections were counter- stained with nuclear DAPI (blue) and were from adult mice. The dotted lines define the border between positive and negative regions for β-catenin, Dab2, Gaq or Akr1b7, as indicated. c, capsule. zG, zona Glomerulosa. zF, zona Fasciculata. Scale bars: 50 μm. Statistical analysis was performed using an unpaired Student's *t*-test or Mann- Whitney test. *ns,* not significant; **P* < 0.05; ****P* < 0.001.

Figure 3.3 (continued)

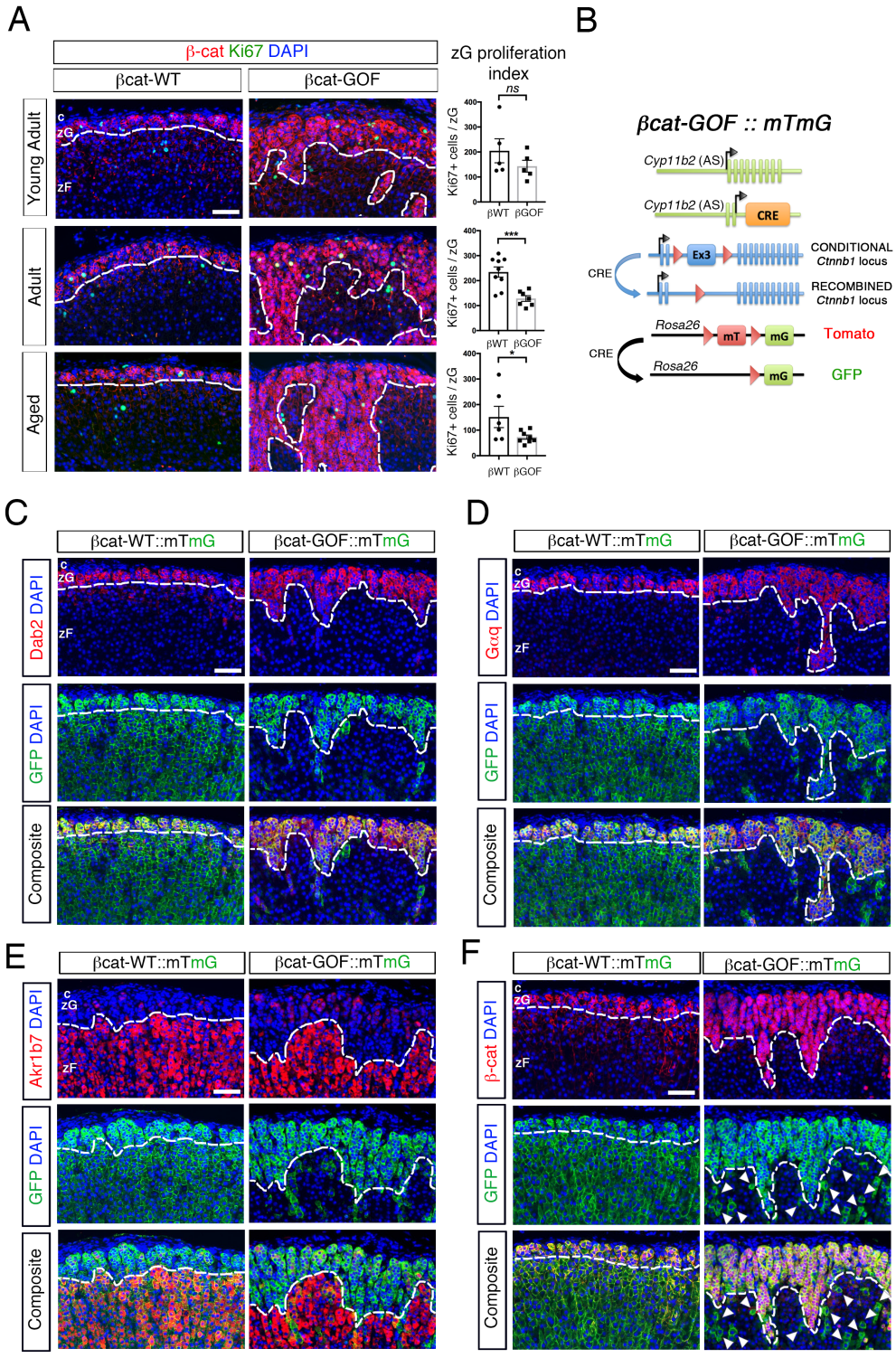

co-expression) that have undergone transdifferentiation (**Figure 3.3C-E**). In contrast, in βcat-GOF adrenals GFP expression was largely confined to zG cells, whereas nearly all zF cells failed to express GFP (**Figure 3.3C-E**). In fact, the few GFP-positive cells which had undergone transdifferentiation into zF cells no longer expressed β-catenin, establishing that these cells had escaped recombination of the *Ctnnb1*$^{flox(ex3)}$ allele (**Figure 3.3F, arrowheads**). Together, these data indicate that stabilization of β-catenin within zG cells blocks zG-to-zF transdifferentiation, a previously unrecognized mechanism, leading to a progressive expansion of the zG, at least under baseline physiological conditions.

Chronic RAAS activation in βcat-GOF mice leads to accelerated zG hyperplasia.

PA, when coupled with intravascular volume expansion, is classically associated with feedback suppression of RAAS. In this setting, reduced levels of AngII, a trophic factor for the zG, may serve to restrict cellular proliferation and slow disease progression. To determine if an enhanced trophic drive in βcat-GOF mice would accelerate disease progression, we chronically activated RAAS using genetic, pharmacological and dietary models. To genetically activate RAAS, we employed *AS*$^{Cre/Cre}$ mice (AS(KO)), a model of CYP11B2(AS) deficiency that results in a ~3 fold increase in plasma renin activity (19). By combining this model with the βcat-GOF model we generated *AS*$^{Cre/Cre}$ :: *Ctnnb*$^{flox(ex3)}$ (AS(KO)-βcat-GOF) mice (**Figure 3.4A, B**). Gross analysis of adrenals from adult and aged AS(KO)-βcat-GOF mice revealed a progressive increase (30- to 320-fold) in adrenal weight, compared with adrenals from AS(KO), βcat-GOF and βcat-WT mice (**Figure S2.4A, B**). Next, we performed immunostaining for Gαq to define the initial impact on the zG of combined βcat-GOF and chronic RAAS activation. While the zG was notably expanded in AS(KO) mice compared with βcat-WT controls, in AS(KO)-βcat-GOF adrenals the zG occupied nearly the entire cortex (**Figure 3.4C, D**). Analysis of proliferation revealed a significant increase in Ki67-positive cells in the β-catenin-positive domain of AS(KO) and

Figure 3.4. Genetic activation of RAAS leads to marked adrenal hyperplasia.

(A) Schematic representation of the alleles comprising AS(KO) and AS(KO)-βcat-GOF mice. The presence of two AS-Cre alleles results in aldosterone deficiency. (B) Left: Schematic representation of RAAS under physiological conditions. Right: Activation of RAAS in AS(KO) mice. (C) Representative adrenal sections stained for Gαq (green), (*n* = 5-6 mice). (D) Quantification of Gαq-positive area from (C) normalized for cortical area, (*n* = 5-6 mice). (E) Representative adrenal sections co- stained for β-catenin (β-cat, red) and Ki67 (green), (*n* = 5-6 mice). Arrowheads mark co-positive cells. (F) Quantification of the Ki67-positive cells from (E) normalized for the β-catenin-positive domain (zG proliferation index), (*n* = 5-6 mice). All sections were counter-stained with nuclear DAPI (blue) and were obtained from young adult mice. The dotted lines define the border between β-catenin/Gαq-positive and -negative regions. zG, zona Glomerulosa. zF, zona Fasciculata. MR, mineralocorticoid receptors. Aldo, aldosterone. AngII, Angiotensin II. Scale bars: 50 μm. Statistical analysis was performed using a one-way ANOVA test in conjunction with a Tukey's range test. **P* < 0.05; ***P* < 0.01; ****P* < 0.001; *****P* < 0.0001.

Figure 3.4 (continued)

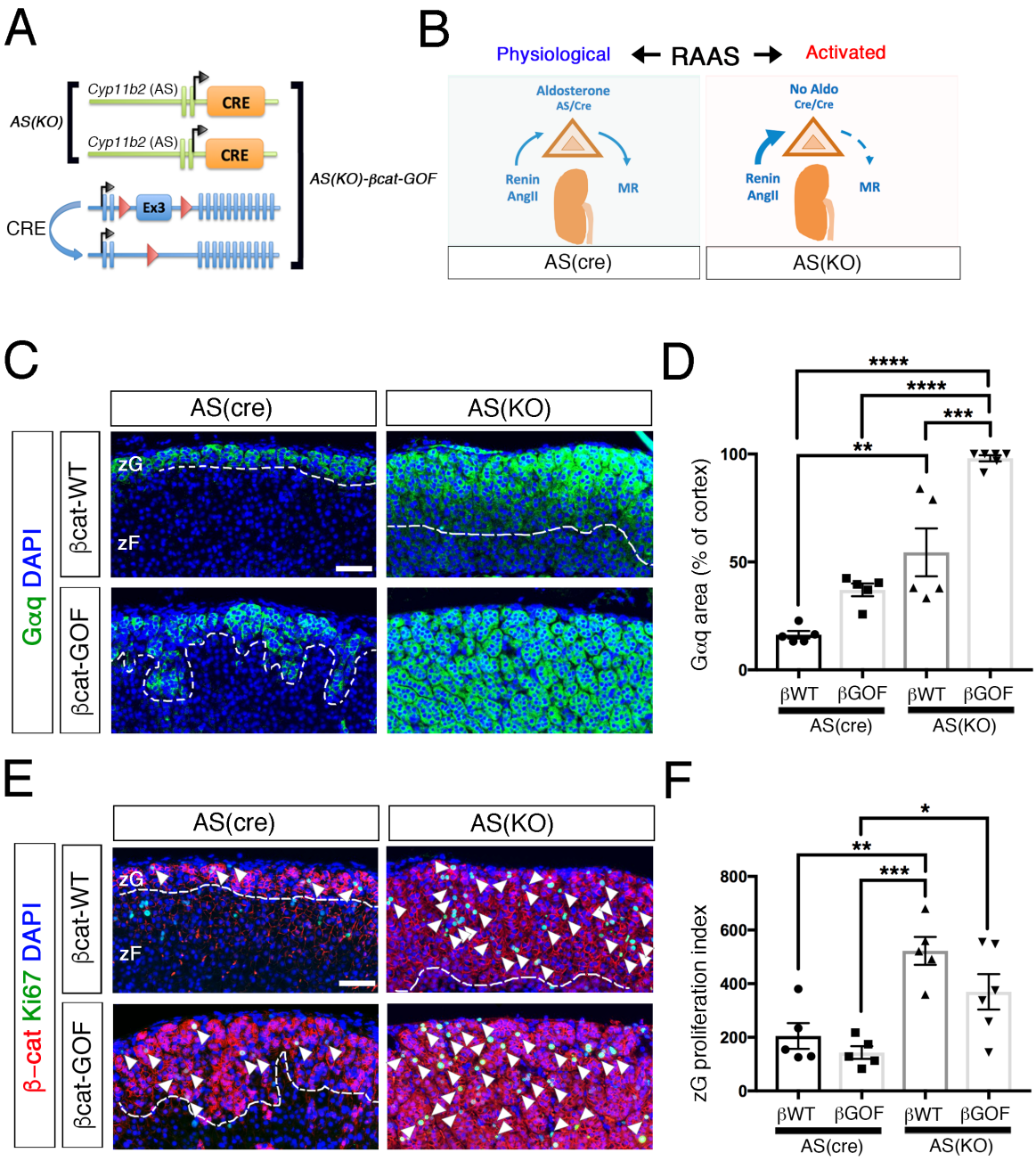

AS(KO)-βcat-GOF adrenals, compared with βcat-WT and βcat-GOF (**Figures 3.4E, F, S2.4C, D**). Next, we assessed the impact of chronic RAAS activation on zonal transdifferentiation using lineage-tracing analysis. Consistent with our prior findings (**Figure 3.2C-F**), zG-to-zF transdifferentiation was also blocked in AS(KO)-βcat-GOF adrenals (**Figure 3.4E**). Thus, the combination of increased proliferation resulting from enhanced trophic drive and a block in zonal transdifferentiation causes the dramatic increase in zG and adrenal size in AS(KO)-βcat-GOF adrenals.

To further validate the impact of combining chronic RAAS activation and βcat-GOF on the zG, we activated RAAS using either spironolactone (a mineralocorticoid receptor antagonist) or a low-salt diet (**Figure 3.5A**), two therapies commonly prescribed for patients with PA. βcat-WT and βcat-GOF mice were treated with spironolactone or low-salt diet for 50 days (**Figure 3.5B**). Immunostaining for Gαq revealed that treatment with either spironolactone or low-salt diet led to a marked expansion of the zG in βcat-GOF mice compared to non-treated βcat-GOF control mice (**Figure 3.5C, D**). No change was observed in βcat-WT adrenals irrespective of treatment. In addition, while both treatments increased the total number of AS-positive cells within the zG, surprisingly no differences were detected in the number of AS-positive cells between βcat-WT and βcat-GOF mice (**Figure S2.5A, B**). We next assessed the effect of spironolactone or low-salt diet on the zG proliferation index in βcat-WT and βcat-GOF mice. Both treatments significantly increased the proliferation index in βcat-GOF adrenals (**Figures 3.5E, F, S2.5C, D**). Moreover, treatment with either spironolactone or low-salt diet led to a modest, but significant, increase in adrenal weight in βcat-GOF mice compared with βcat-WT mice (**Figure S2.5E**). Taken together, these data establish that chronic RAAS activation, in the setting of βcat-GOF, leads to accelerated zG expansion, increased proliferation and an increase in adrenal weight.

Figure 3.5. Pharmacological and dietary activation of RAAS accelerates zG expansion in βcat-GOF adrenals.

(A) Schematic representation of RAAS following treatment with spironolactone or low-salt diet and (B) the experimental protocol. (C) Representative adrenal sections were stained for Gαq (green), (*n* = 7-9 mice). (D) Quantification of Gαq-positive area from (C) normalized for cortical area, (*n* = 7-9 mice). (E) Representative adrenal sections co- stained for β-catenin (β-cat, red) and Ki67 (green), arrowheads mark co-positive cells, (*n* = 7-9 mice). (F) Quantification of the Ki67-positive cells from (E) normalized for the β-catenin-positive domain (zG proliferation index), (*n* = 7-9 mice). All sections were counter-stained with nuclear DAPI (blue) and were from adult mice. The dotted lines define the border between β-catenin/Gαq-positive and -negative regions. zG, zona Glomerulosa. zF, zona Fasciculata. Scale bars: 50 μm. Statistical analysis between genotypes was performed using an unpaired Student's *t*-test or Mann-Whitney test. Statistical analysis between treatment groups was performed using a one-way ANOVA test in conjunction with a Tukey's range test. *ns*, not significant. **P* < 0.05; ****P* < 0.001; *****P* < 0.0001.

Figure 3.5 (continued)

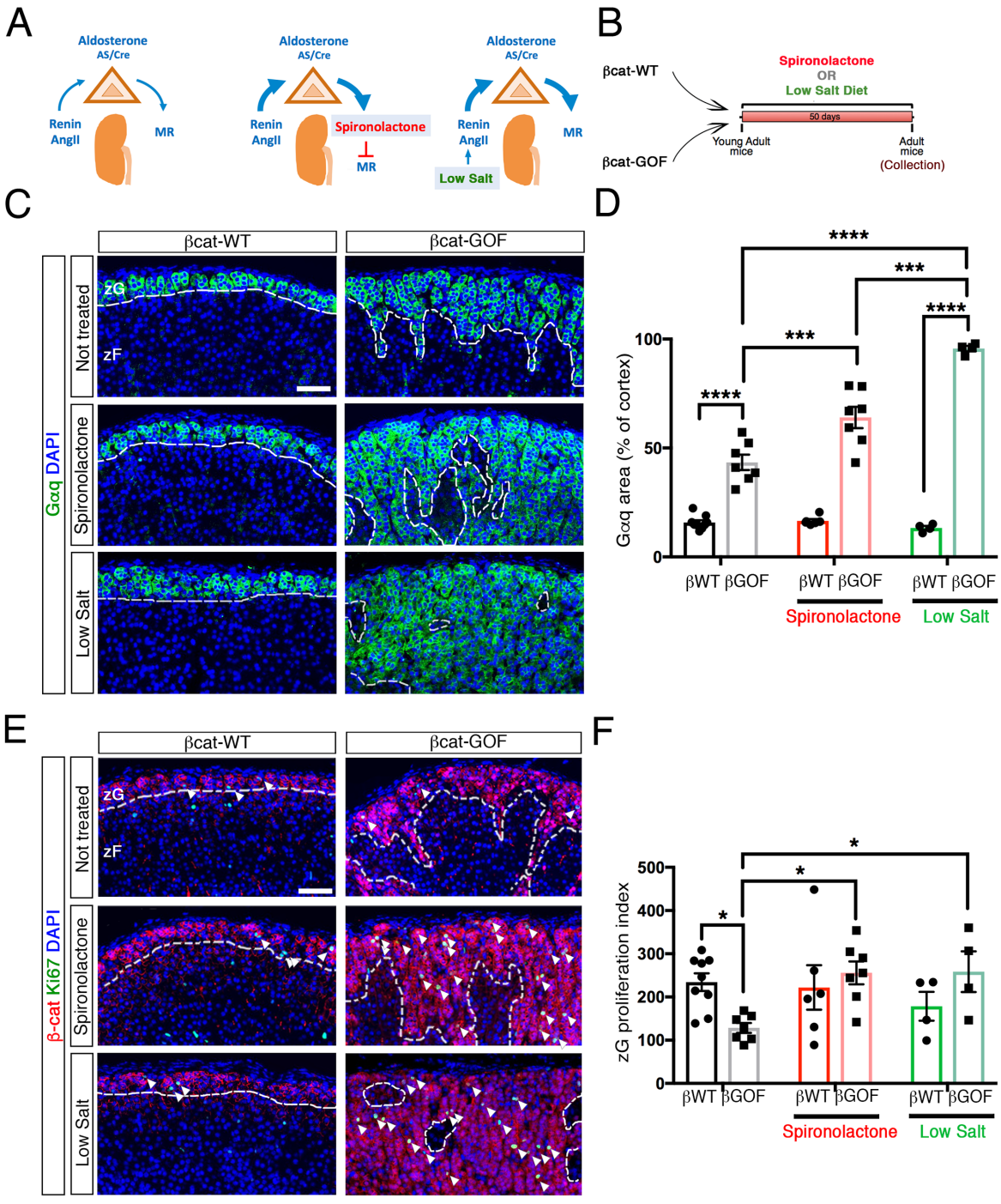

Discussion

PA is the most common form of secondary hypertension, which results in increased cardiovascular risk, morbidity and mortality in affected individuals. Recent advances indicate that PA exists across a continuum of disease severity, ranging from mild to severe, suggesting current estimates of disease prevalence may underrepresent the true disease burden (6, 17). While recent advances have led to the identification of recurrent somatic mutations causing APAs (10), the molecular mechanisms that give rise to bilateral IAH remain elusive. Moreover, the cellular mechanisms that underlie the initiation and progression of adrenocortical lesions that over-produce aldosterone remain poorly understood. Activation of WNT/β-catenin signaling has been linked to PA and is found in the majority of APAs, but how this pathway contributes to the pathophysiology of PA and interacts with known somatic mutations remains largely unknown. Activation of WNT/β-catenin signaling has been previously shown to promote cellular proliferation and/or prevent apoptosis in a variety of cell types (20). However, we find that stabilization of β-catenin within zG cells did not lead to an increase in proliferation nor a decrease in apoptosis but rather led to impaired adrenal lineage development by blocking zG-to-zF transdifferentiation. Our results are consistent with previous studies implicating WNT/β-catenin signaling as a master regulator of zG identity (21, 22) and further indicate that inhibition of this pathway is required for transdifferentiation. Therefore, our findings add *failure to undergo transdifferentiation* to the list of pathophysiological mechanisms that can impair normal tissue homeostasis in the presence of excess WNT/β-catenin activity (**Figure S2.5F**).

Stabilization of β-catenin has previously been implicated in the oncogenic transformation of a wide range of organs, including the adrenal cortex (20, 23–25). Thus, the observation that stabilization of β-catenin within zG cells leads to a decrease in zG cell proliferation raises the possibility of either adrenal-specific regulation and/or the need for additional gain- or loss-of-function events. The zG, like other endocrine tissues, is regulated by a feedback loop that

includes AngII, an essential trophic factor that controls both hormone production as well as cellular proliferation. To assess the impact of chronically activating RAAS, we employed a genetic model of aldosterone deficiency, treatment with spironolactone or a low salt diet. We found that chronic RAAS activation leads to an increase in cellular proliferation and adrenal mass specifically in βcat-GOF mice, but not in βcat-WT mice. Taken together, these data suggest that chronic RAAS activation may contribute to gain-of-function events with potentially important clinical implications in the setting of βcat-GOF. Delineation of the impact of RAAS activation will require careful retrospective analysis in patients discovered to have underlying βcat-GOF mutations at the time of resection or prospective analysis in cohorts with germ-line mutations that lead to activation of the WNT/β-catenin pathway.

While β-catenin stabilization in zG cells leads to an increase in aldosterone production in adult and aged mice, the mechanism(s) underlying this increase remain unclear. Results from our study indicate that there is no correlation between the level of plasma aldosterone and either the level of *Cyp11b2* gene expression or the number of AS-positive cells in βcat-GOF mice. This observation suggests that additional factors, independent of the Wnt/β-catenin pathway, regulate the expression of *Cyp11b2* and AS and is consistent with the observation that AS-positive cells exhibit a patchy distribution in the zG in both βcat-WT and βcat-GOF mice (**Figures 3.2E, S2.2C** and (3, 18)). Our results also imply that βcat-GOF results in an increase in aldosterone secretion on a per-cell basis, possibly due to enhanced steroidogenesis and/or sensitivity to AngII. The precise mechanism(s), however, that link WNT/β-catenin pathway to aldosterone secretion and/or steroidogenesis remain to be determined.

It is increasingly recognized that PA encompasses a wide spectrum of disorders ranging from mild to overt disease (17, 26). On the mild end, patients can present with normotension or mild hypertension with low or normal renin and potassium levels, while on the overt end, patients

present with resistant hypertension, suppression of renin levels and hypokalemia (17). With the recognition of preclinical forms, the overall prevalence of PA has increased significantly (5, 9). Understanding the earliest stages of PA offers the hope of developing earlier detection and treatment strategies. Our data reveal that βcat-GOF mice exhibit mildly increased aldosterone levels and blood pressure early in life. Despite this, stabilization of β-catenin in zG cells did not lead to autonomous aldosterone production since these mice maintained normal feedback regulation in response to HS diet. Thus, these findings indicate that βcat-GOF mice represent a mild, preclinical, renin-dependent model of PA, that can be used to study the earliest stages of the disease. This study contributes essential new insight into the role of the WNT/β-catenin pathway in adrenocortical transdifferentiation and in the pathogenesis of PA and provides a new model to identify novel targeted therapeutic strategies for the treatment of this condition.

Methods

Animals

Generation of the aldosterone synthase (AS)-Cre strain (Cyp11b2$^{tm1.1(cre)Brlt}$) was previously described (19). To generate bigenic *Cyp11b2*$^{tm1.1(cre)Brlt/+}$ :: *Ctnnb1*$^{flox(ex3)/+}$ mice (referred to as βcat-GOF or βGOF), the *Cyp11b2*$^{tm1.1(cre)Brlt}$ strain was crossed with the *Ctnnb1*$^{flox(ex3)/+}$ strain (27). To generate trigenic *Cyp11b2*$^{tm1.1(cre)Brlt/+}$ :: *Ctnnb1*$^{flox(ex3)/+}$ :: *Gt(ROSA)26Sor*$^{tm4(ACTB-tdTomato,-EGFP)Luo/J}$ mice (referred to as βcat-GOF::mTmG), the βcat-GOF mice were crossed with the *Gt(ROSA)26Sor*$^{tm4(ACTB-tdTomato,-EGFP)Luo/J}$ (mTmG) Cre-reporter line (28). AS deficiency was achieved by breeding the AS-Cre allele to homozygosity (AS(KO) mice), as previously described (19). AS(KO)-βcat-GOF mice were bred by intercrossing AS(KO) mice with *Ctnnb1*$^{flox(ex3)/+}$ mice. All mice were maintained on a mixed sv129-C57Bl/6 genetic background, with free access to food and water, unless otherwise specified, under a 12-hour light/12-hour dark cycle. To control for genetic background, whenever possible, experiments were performed

using littermate control mice (βcat-WT or βWT) that did not carry the Ctnnb1$^{flox(ex3)/+}$ allele and were positive or negative for the *Cyp11b2*$^{tm1.1(cre)Brlt}$ and the *Gt(ROSA)26Sor*$^{tm4(ACTB-tdTomato,-EGFP)Luo/J}$ allele. Studies were conducted on age-matched cohorts of mice that were 'young adult' (10 weeks of age), 'adult' (15-to-21 weeks of age) or 'aged' (38-to-53 weeks of age).

Mouse Experiments

All animal procedures were approved by the Boston Children's Hospital IACUC (protocol number 16-08-3240R). Mice were fed high-salt (8% NaCl), normal-salt (0.575% NaCl) or low-salt (0.175% NaCl) chow (ScottPharma Solutions) for 5 or 50 days, as indicated. Mice were allowed free access to water. Spironolactone treatment was performed by adding 83 mg/L of spironolactone (Aldactone, Pfizer Inc.) to the water for 50 days. Blood pressure was recorded in mice via carotid catheterization under isoflurane-mediated anesthesia, as previously described (29).

Hormonal Analysis

Plasma was collected by retro-orbital blood collection with heparinized capillary tubes. Plasma aldosterone levels were measured using a competitive radioimmunoassay according to the manufacturer's protocol (Tecan).

Gene Expression Analysis

RNA was purified from whole adrenals cleaned of adherent fat and homogenized in TRI®Reagent (Sigma) using the Direct-zol^{TM} RNA kit (Zymo Research), following the manufacturer's protocol. Further processing of total RNA involved treatment with DNAse (Promega) and reverse transcription into cDNA using the High-Capacity cDNA Reverse Transcription Kit (Life Technologies). Gene expression analysis was performed by Real Time quantitative PCR (RTqPCR) using a QuantStudio 6 Flex thermocycler (Life Technologies). We

used the following Taqman primers from Life Technologies: *Axin2* (Mm00443610_m1), *Lef1* (Mm00550265_m1), *Cyp11b2* (Mm01204955_g1), *Actb* (Mm026119580_g1). *Actb* transcripts, encoding β-actin, were used as the internal control and data were expressed using the 2^{-ddCt} method.

Tissue Preparation, Immunofluorescence, Microscopy and Quantification

Mouse adrenals were cleared of adherent fat, weighed, fixed in 4% paraformaldehyde for 1 to 3 hours at 4°C, dehydrated in ethanol, xylene and embedded in paraffin blocks. Five µm-thick sections were processed for immunostaining by stepwise rehydration and permeabilization with 50 mM Tween-20 in PBS. Antigen retrieval was performed in 10 mM Sodium Citrate pH 6.0. Immunostaining was done using the following primary antibodies: anti-β-catenin (mouse monoclonal, BD Biosciences, cat. 610153; and rabbit polyclonal, Abcam, ab16051), anti-GFP (chicken polyclonal, Aves Labs, GF-1020), anti-activated Caspase 3 (rabbit monoclonal, BD Biosciences, 559565), anti-Dab2 (mouse monoclonal, BD Biosciences, 610464), anti-Akr1b7 (rabbit polyclonal, kindly provided by Dr. Pierre Val (4, 16)), anti-Gαq (rabbit polyclonal, Abcam, ab75825), anti-AS (rabbit polyclonal, kindly provided by Dr. Celso E. Gomez-Sanchez (19)), anti-Ki67 (rabbit monoclonal, Thermo Scientific, RM-9106). TUNEL staining was performed using the Click-iT™ Plus TUNEL Assay (Invitrogen), according to manufacturer's instructions. All primary antibodies were used at a 1:200 dilution. We used the following secondary antibodies for indirect staining: donkey anti-rabbit conjugated with Alexa Fluor® 647, goat anti-mouse Alexa Fluor® 594 and goat anti-chicken Alexa Fluor® 488 (Molecular Probes). Sections were counter-stained with DAPI (4′,6-diamidino-2-phenylindole) and mounted in Prolong Gold Mount Solution (Thermo Fisher Scientific). Images were captured with a Nikon upright Eclipse 90i microscope. For every image, three Z-stacks were collected and deconvoluted to obtain the best resolution using the LIS-Elements Nikon software. Background autofluorescence was acquired from an empty green or red channel to allow subsequent subtraction of

autofluorescence (e.g., from red blood cells and lipofuscin) from the other channels using the Image Calculator tool in Fiji software. Quantification of AS-, Ki67-, TUNEL- and activated Caspase 3-positive cells or Gαq and β-catenin-positive areas was performed using one complete equatorial section per mouse adrenal. Absolute cell numbers were normalized by zone-specific area (mm^2), as indicated. Quantification of nuclear density was performed on representative regions of interest from equatorial sections by counting DAPI-positive nuclei per zone-specific area (mm^2).

Statistics

Two-tailed Student's *t*-Test or Mann-Whitney test were used for comparisons between groups of two and One-Way or Two-Way ANOVA and Tukey post-hoc analysis were used for comparisons between groups of three or more. Data are presented as Mean±SEM. Prism 7 software (GraphPad) was used for statistical analysis.

References

1. Drelon C, Berthon A, Mathieu M, Martinez A, Val P. Adrenal cortex tissue homeostasis and zonation: A WNT perspective. *Mol. Cell. Endocrinol.* [published online ahead of print: December 24, 2014]; doi:10.1016/j.mce.2014.12.014

2. Aragao-Santiago L et al. Mouse Models of Primary Aldosteronism: From Physiology to Pathophysiology. *Endocrinology* 2017;158(12):4129–4138.

3. Pignatti E, Leng S, Carlone DL, Breault DT. Regulation of zonation and homeostasis in the adrenal cortex. *Mol. Cell. Endocrinol.* 2017;441:146–155.

4. Berthon A et al. Constitutive beta-catenin activation induces adrenal hyperplasia and promotes adrenal cancer development. *Hum. Mol. Genet.* 2010;19(8):1561–1576.

5. Monticone S et al. Prevalence and Clinical Manifestations of Primary Aldosteronism Encountered in Primary Care Practice. *J. Am. Coll. Cardiol.* 2017;69(14):1811–1820.

6. Zennaro M-C, Boulkroun S, Fernandes-Rosa F. Genetic Causes of Functional Adrenocortical Adenomas. *Endocr. Rev.* 2017;38(6):516–537.

7. Rossi GP et al. Vascular remodeling and duration of hypertension predict outcome of adrenalectomy in primary aldosteronism patients. *Hypertension* 2008;51(5):1366–1371.

8. Milliez P et al. Evidence for an increased rate of cardiovascular events in patients with primary aldosteronism. *J. Am. Coll. Cardiol.* 2005;45(8):1243–1248.

9. Funder JW et al. The Management of Primary Aldosteronism: Case Detection, Diagnosis, and Treatment: An Endocrine Society Clinical Practice Guideline. *J. Clin. Endocrinol. Metab.* 2016;101(5):1889–1916.

10. Perez-Rivas LG, Williams TA, Reincke M. Inherited Forms of Primary Hyperaldosteronism: New Genes, New Phenotypes and Proposition of A New Classification. *Exp. Clin. Endocrinol. Diabetes Off. J. Ger. Soc. Endocrinol. Ger. Diabetes Assoc.* [published online ahead of print: September 10, 2018]; doi:10.1055/a-0713-0629

11. Boulkroun S, Fernandes-Rosa FL, Zennaro M-C. Molecular and Cellular Mechanisms of Aldosterone Producing Adenoma Development. *Front. Endocrinol.* 2015;6:95.

12. Lalli E, Barhanin J, Zennaro M-C, Warth R. Local Control of Aldosterone Production and Primary Aldosteronism. *Trends Endocrinol. Metab. TEM* 2016;27(3):123–131.

13. Berthon A et al. WNT/β-catenin signalling is activated in aldosterone-producing adenomas and controls aldosterone production. *Hum. Mol. Genet.* 2014;23(4):889–905.

14. Basham KJ et al. ZNRF3 Regulates the Strength of Wnt/β-catenin Signaling to Mediate Adrenal Homeostasis. *Genes Dev.* In press;

15. Romero DG et al. Disabled-2 is expressed in adrenal zona glomerulosa and is involved in aldosterone secretion. *Endocrinology* 2007;148(6):2644–2652.

16. Aigueperse C, Martinez A, Lefrançois-Martinez AM, Veyssière G, Jean CI. Cyclic AMP regulates expression of the gene coding for a mouse vas deferens protein related to the aldo-

keto reductase superfamily in human and murine adrenocortical cells. *J. Endocrinol.* 1999;160(1):147–154.

17. Vaidya A, Mulatero P, Baudrand R, Adler GK. The Expanding Spectrum of Primary Aldosteronism: Implications for Diagnosis, Pathogenesis, and Treatment. *Endocr. Rev.* [published online ahead of print: August 15, 2018]; doi:10.1210/er.2018-00139

18. Walczak EM et al. Wnt signaling inhibits adrenal steroidogenesis by cell-autonomous and non-cell-autonomous mechanisms. *Mol. Endocrinol. Baltim. Md* 2014;28(9):1471–1486.

19. Freedman BD et al. Adrenocortical Zonation Results from Lineage Conversion of Differentiated Zona Glomerulosa Cells. *Dev. Cell* 2013;26(6):666–673.

20. Nusse R, Clevers H. Wnt/β-Catenin Signaling, Disease, and Emerging Therapeutic Modalities. *Cell* 2017;169(6):985–999.

21. Drelon C et al. PKA inhibits WNT signalling in adrenal cortex zonation and prevents malignant tumour development. *Nat. Commun.* 2016;7:12751.

22. Vidal V et al. The adrenal capsule is a signaling center controlling cell renewal and zonation through Rspo3. *Genes Dev.* 2016;30(12):1389–1394.

23. Tissier F et al. Mutations of beta-catenin in adrenocortical tumors: activation of the Wnt signaling pathway is a frequent event in both benign and malignant adrenocortical tumors. *Cancer Res.* 2005;65(17):7622–7627.

24. Assié G et al. Integrated genomic characterization of adrenocortical carcinoma. *Nat. Genet.* 2014;46(6):607–612.

25. Zheng S et al. Comprehensive Pan-Genomic Characterization of Adrenocortical Carcinoma. *Cancer Cell* 2016;29(5):723–736.

26. Guagliardo NA et al. Adrenal Tissue-Specific Deletion of TASK Channels Causes Aldosterone-Driven Angiotensin II-Independent Hypertension. *Hypertens. Dallas Tex 1979* 2019;73(2):407–414.

27. Harada N et al. Intestinal polyposis in mice with a dominant stable mutation of the beta-catenin gene. *EMBO J.* 1999;18(21):5931–5942.

28. Muzumdar MD, Tasic B, Miyamichi K, Li L, Luo L. A global double-fluorescent Cre reporter mouse. *Genes. N. Y. N 2000* 2007;45(9):593–605.

29. Resch JM et al. Aldosterone-Sensing Neurons in the NTS Exhibit State-Dependent Pacemaker Activity and Drive Sodium Appetite via Synergy with Angiotensin II Signaling. *Neuron* 2017;96(1):190-206.e7.

Chapter Four:

Effects of FGFR2 Inhibition on zG Homeostasis and Function

Effects of FGFR2 Inhibition on zG Homeostasis and Function

Sining Leng[1,2], Nick A. Guagliardo[4], Dulanjalee Kariyawasam[1,3], Emanuele Pignatti[1,3], Paula Q. Barrett[4], Diana L. Carlone[1,3,5], David T. Breault[1,2,3,5]

[1]*Division of Endocrinology, Boston Children's Hospital, Boston, MA 02115, USA*

[2]*Division of Medical Sciences, Harvard Medical School, Boston, MA 02115, USA*

[3]*Department of Pediatrics, Harvard Medical School, Boston, MA 02115, USA*

[4]*Department of Pharmacology, University of Virginia, Charlottesville, VA, 22947, USA*

[5]*Harvard Stem Cell Institute, Cambridge, MA 02138, USA*

Attributions:

S.L. and D.T.B. conceived the project. S.L. (all experiments unless otherwise specified), N.A.G. (metabolic cage, urine analysis), D.K. (βCat GOF, Fgfr2 cKO double mutant analysis), E.P. (RIA assays) did the research; S.L. produced text and figures with input from P.Q.B, D.L.C., D.T.B.

Summary

Hyperaldosteronism is a detrimental disease affecting 10% of all hypertension patients and 20% of resistant hypertension. To improve the diagnosis and treatment of this condition, further understanding of the mechanisms regulating zG homeostasis and function is warranted. FGF signaling plays an important role in fetal adrenal development, but its function in the adult adrenal is unknown. Previously, we identified *Fgfr2* as a potent regulator of zG tissue morphology and its expression is induced in a mouse model of hyperaldosteronism. Here we examine the effects of FGFR2 inhibition on zG tissue homeostasis and physiological function. We find that FGFR2 is essential for zG cell proliferation and normal cortical tissue turnover. *Fgfr2* deletion results in loss of *Cyp11b2* and *Dab2* expression, suggesting loss of zG cell identity and function. Plasma aldosterone level is maintained by an increased renin activity in these mice, suggesting a compensated hypoaldosteronism. Furthermore, we show that small molecule FGFR inhibitors recapitulate these findings, offering the potential of a new therapeutic strategy for hyperaldosteronism.

Introduction

Aldosterone is a potent mineralocorticoid produced by the adrenal zona glomerulosa (zG)[1]. It activates the mineralocorticoid receptor, a ubiquitously expressed nuclear receptor controlling a variety of transcriptional and non-genomic outcomes[2]. The most well understood action of aldosterone is in the kidney, where it promotes Na^+ reabsorption and K^+ excretion by the renal epithelial cells of the distal tubule and collecting duct, thereby controlling intravascular volume and blood pressure[3]. Recently, the effects of aldosterone, independent of hypertension, on cardiovascular remodeling and renal damage have been increasingly appreciated, raising the urgency in prompt diagnosis and treatment of hyperaldosteronism[4,5]. Aldosterone production in the zG is tightly regulated by various endocrine signals, the two prominent secretagogues

including Angiotensin II (AngII) and extracellular potassium[6,7]. Under baseline conditions, the zG cell membrane maintains a negative resting potential. Ligand binding to the G-protein coupled angiotensin receptor as well as a rise in extracellular K^+ concentration trigger zG cell membrane depolarization and Ca^{2+} influx. Subsequent signaling events involving calcium/calmodulin-dependent protein kinases I/II (CaMKs) and various PKC isoforms can acutely boost aldosterone biosynthesis and chronically increase the expression of key enzymes such as *StAR* and *Cyp11b2*. To date, many somatic mutations have been identified in genes encoding ion channels that govern zG cell electrophysiology and Ca^{2+} influx as the culprit behind aldosterone-producing adenomas (APA)[8]. However, the cause of many cases of APAs and bilateral adrenal hyperplasia (BAH) remains unclear[9]. Therefore, further understanding of zG homeostasis and function is needed to develop novel therapeutic strategies to treat these conditions.

The WNT/β-catenin signaling pathway is a well-known regulator of adrenal zG homeostasis[10], and is activated in ~70% of APAs[11]. Recently, we generated a mouse model with β-catenin gain-of-function (βCat GOF) in the adult zG, which develops zG hyperplasia, hyperaldosteronism, and high blood pressure (see chapter 3). Using RNA sequencing, we identified numerous transcripts potentially acting downstream of β-catenin in regulating zG homeostasis and function. Using genetic loss of function model, we have described a prominent role of *Fgfr2* in establishing zG morphology (see chapter 2). The Fibroblast Growth Factor (FGF) signaling pathway regulates a wide variety of cellular processes during embryonic development and in adult tissues, such as proliferation, survival, and differentiation[12]. Four distinct FGF receptors (FGFR1-4) have been described and can activate diverse intracellular signaling cascades[12]. In the developing adrenal cortex, *Fgfr2* promotes the expansion of the adrenal primordium[13]. Consistent with this, genetic studies have shown that deletion of *Fgfr2* during development results in severe adrenal hypoplasia[13–15]. Interestingly, *Fgfr2* is predominantly expressed in the subcapsular region where WNT/β-catenin signaling is active[14],

suggesting a potential interaction between these two pathways. Despite its important function in regulating adrenal development and morphogenesis, the function of FGFR2 in adult adrenal homeostasis and function remains unknown.

Results

To understand the impact of *Fgfr2* deletion on adrenocortical tissue homeostasis, we used the zG-specific *Fgfr2* conditional knockout mouse strain combined with a lineage tracing reporter allele (*ASCre/+; Fgfr2 fl/fl; R26R-mTmG*, referred to as Fgfr2 cKO). It was previously shown that during adrenocortical turnover, AS-expressing zG cells migrate centripetally and transdifferentiate into zF cells[16] (**Figure 4.1B**). Consistent with this, we found that descendants of the AS+ lineage (marked by GFP) occupy most of the zG and the zF by 6 weeks of age, and populate the entire cortex by 20 weeks of age (**Figure 4.1A**). In Fgfr2 cKO adrenals, this process is significantly delayed. At 6 weeks of age, GFP+ cells only occupy a small proportion of the zG and have minor contribution to the zF (**Figure 4.1A**). At 20 weeks of age, more GFP+ cells are present in both zG and zF, but at a lower percentage than controls (**Figure 4.1A, C**). Next, we examined whether *Fgfr2* deletion has an impact on proliferation. We found the amount of Ki67 and GFP co-positive cells in the zG is significantly lower in Fgfr2 cKO adrenals than in controls (**Figure 4.2**), suggesting *Fgfr2* is required for zG cell proliferation. We observed no increase of apoptosis in Fgfr2 cKO adrenals, suggesting cell death is not affected by loss of *Fgfr2* (data not shown). Together, these data show that *Fgfr2* is required for tissue homeostatic maintenance in the adult adrenal cortex.

Next, we examined the impact of *Fgfr2* deletion on zG physiology. Measurement of plasma aldosterone levels in control and Fgfr2 cKO animals revealed no significant difference under baseline or sodium restricted conditions (**Figure 4.3A**). However, plasma renin activity, a

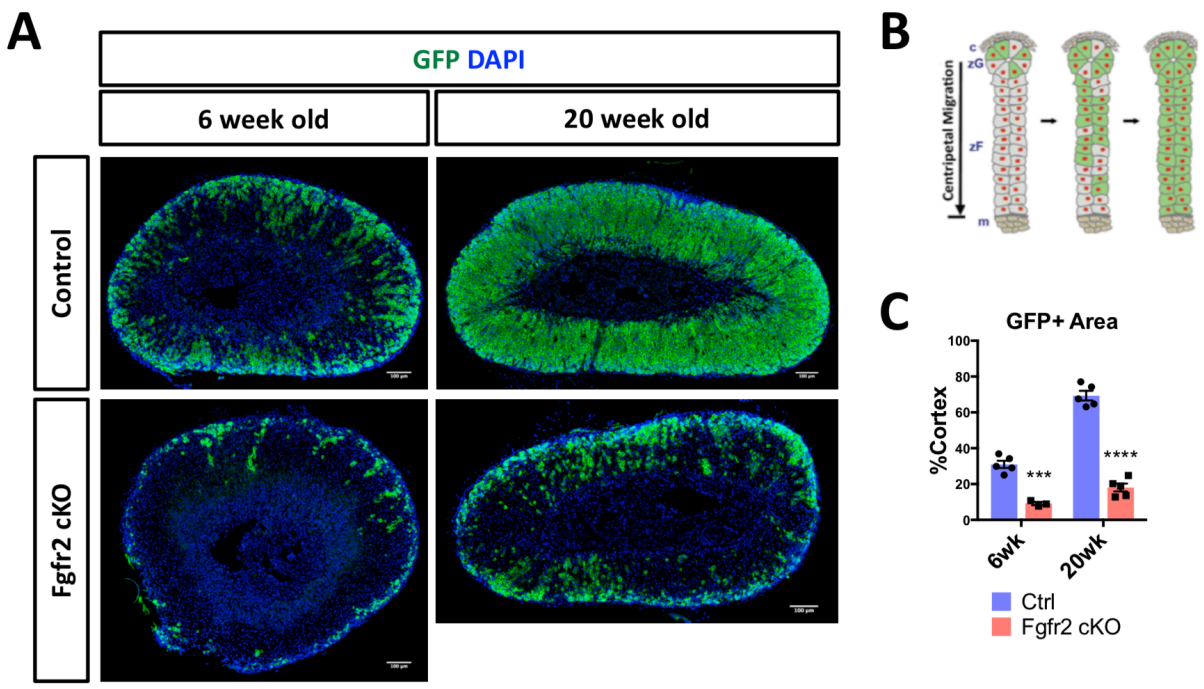

Figure 4.1. Lineage tracing shows reduced cortical turnover in Fgfr2 cKO adrenals.

A, GFP (green) immunostaining of control (ASCre/+; mTmG) and Fgfr2cKO (ASCre/+; mTmG; Fgfr2 fl/fl) adrenals from female mice at indicated ages. DAPI (blue), nuclei. Bars, 100μm. B, schematic representing cellular dynamics of adrenocortical tissue turnover. Green denotes descendants of the ASCre-lineage. C, quantification of data shown in A. Two sample *t*-test between ctrl and Fgfr2cKO groups, ***, $p < 0.001$, ****, $p < 0.0001$.

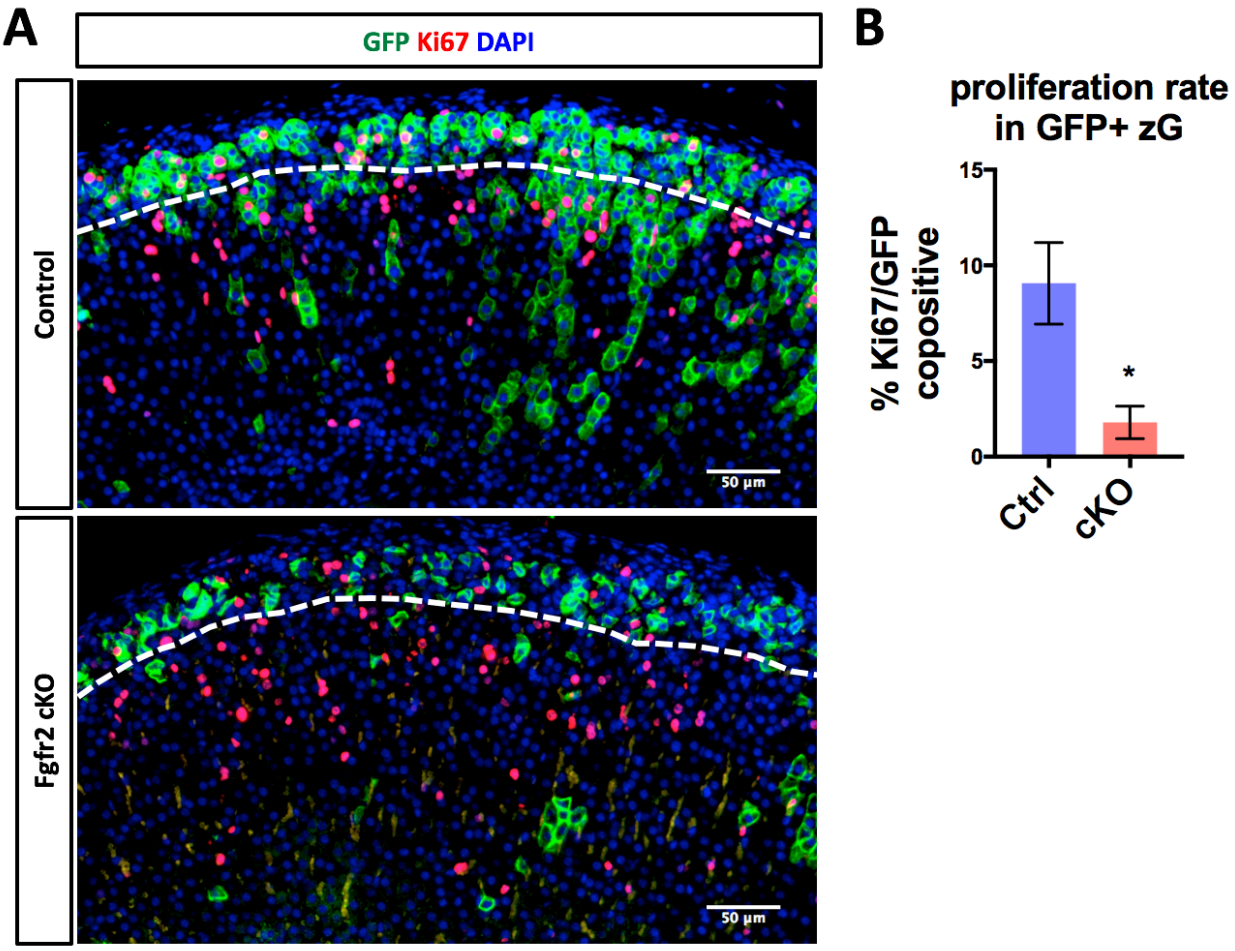

Figure 4.2. Fgfr2 deletion impairs zG proliferation.

A, Co-immunostaining of GFP (green) and Ki67 (red) in control (ASCre/+; mTmG) and Fgfr2cKO (ASCre/+; mTmG; Fgfr2fl/fl) adrenals from 6-week-old female mice. Bars, 50μm. B, quantification of data shown in A. Two sample *t*-test, *, $p < 0.05$. N = 3, 3. Error bars, mean ± SEM.

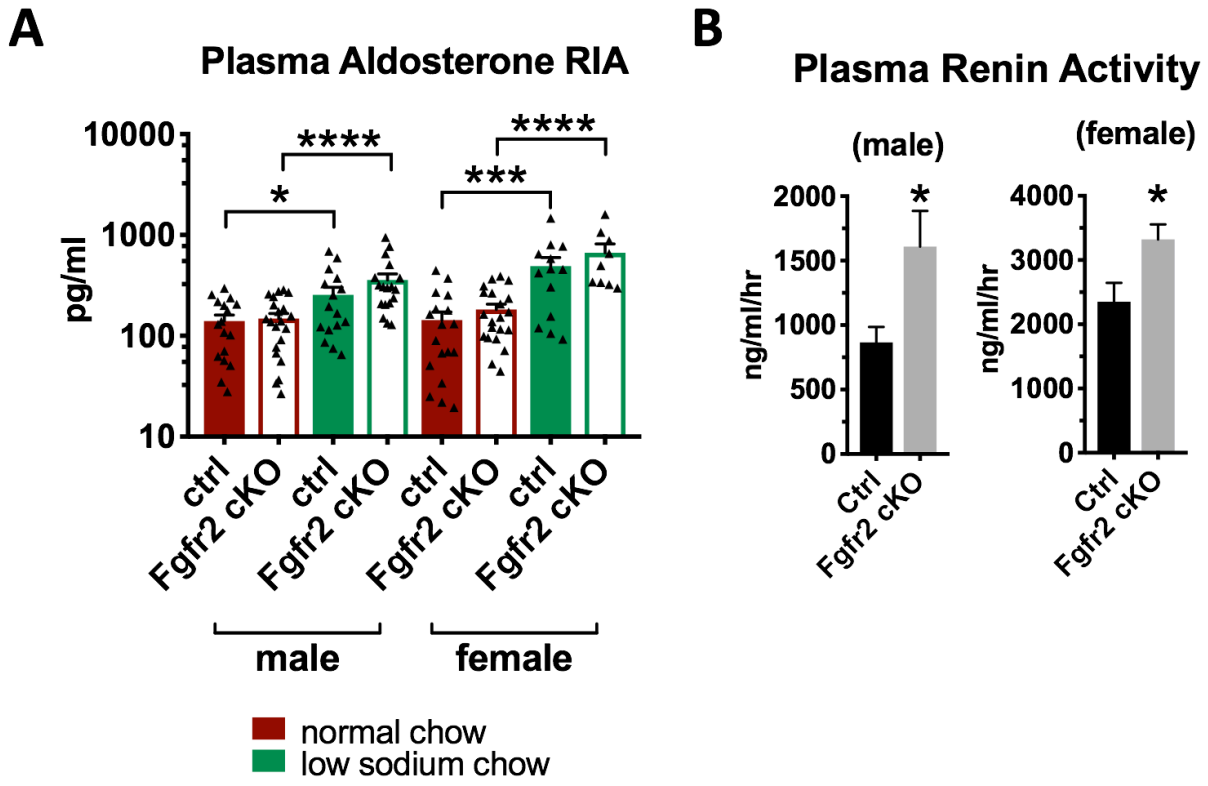

Figure 4.3. Fgfr2 cKO animals have compensated hypoaldosteronism.

A, Plasma aldosterone levels of 20-week-old male and female mice on normal chow diet (red bars) or low sodium (LS) chow diet (green bars). Two sample *t*-test, *, $p < 0.05$, ***, $p < 0.001$, ****, $p < 0.0001$. B, Plasma renin activity levels of male and female mice on normal chow diet. Two sample *t*-test, *, $p < 0.05$. N = 10 for each group. Error bars, mean ± SEM.

classic criterion used to assess zG function, is elevated in Fgfr2 cKO animals, suggesting enhanced endocrine feedback stimulation (**Figure 4.3B**). Interestingly, we found that Cyp11b2, the enzyme catalyzing the last two reactions of aldosterone synthesis, is absent from GFP+ cells in Fgfr2 cKO adrenals (**Figure 4.4A**), suggesting that these cells may have lost the ability to produce aldosterone. This phenotype is more pronounced when mice have undergone stimulation with dietary sodium restriction or potassium loading (**Figure 4.4B, C**). Under these conditions, almost 100% of zG cells are Cyp11b2+ in control mice. In contrast, Cyp11b2 is absent from GFP+ cells in Fgfr2 cKO animals. Disabled homolog 2 (Dab2) is another marker of the zG and has been shown to be involved in aldosterone production[21]. We found that similarly, Dab2 is absent from GFP+ zG cells in Fgfr2 cKO adrenals under baseline or stimulated conditions (**Figure 4.5**). We further confirmed these changes by RNAscope *in situ* hybridization (**Figure 4.6A**) and qRT-PCR (**Figure 4.6B**). Together, these data show that *Fgfr2* deletion has a profound impact on the ability of zG cells to produce aldosterone under baseline or stimulated conditions.

To further confirm the inability of zG cells to respond to physiological stimulus in Fgfr2 cKO mice, we utilized a model of severe aldosterone deficiency. Homozygous ASCre/Cre animals lack both functional copies of *Cyp11b2* and therefore are unable to produce aldosterone[16]. As a result, the renin-angiotensin system is maximally stimulated as evident by very high level of plasma renin activity and Angiotensin II (AngII) levels, which leads to marked increase of zG proliferation and zG size. Using this model, we assessed the impact of *Fgfr2* deletion on zG response to high AngII stimulation. In ASCre/Cre mice, we observed an expected increase of zG size and proliferation (**Figure 4.7**). However, *Fgfr2* deletion blocked this effect, further supporting the conclusion that Fgfr2 is required for zG cells to respond to endocrine stimuli.

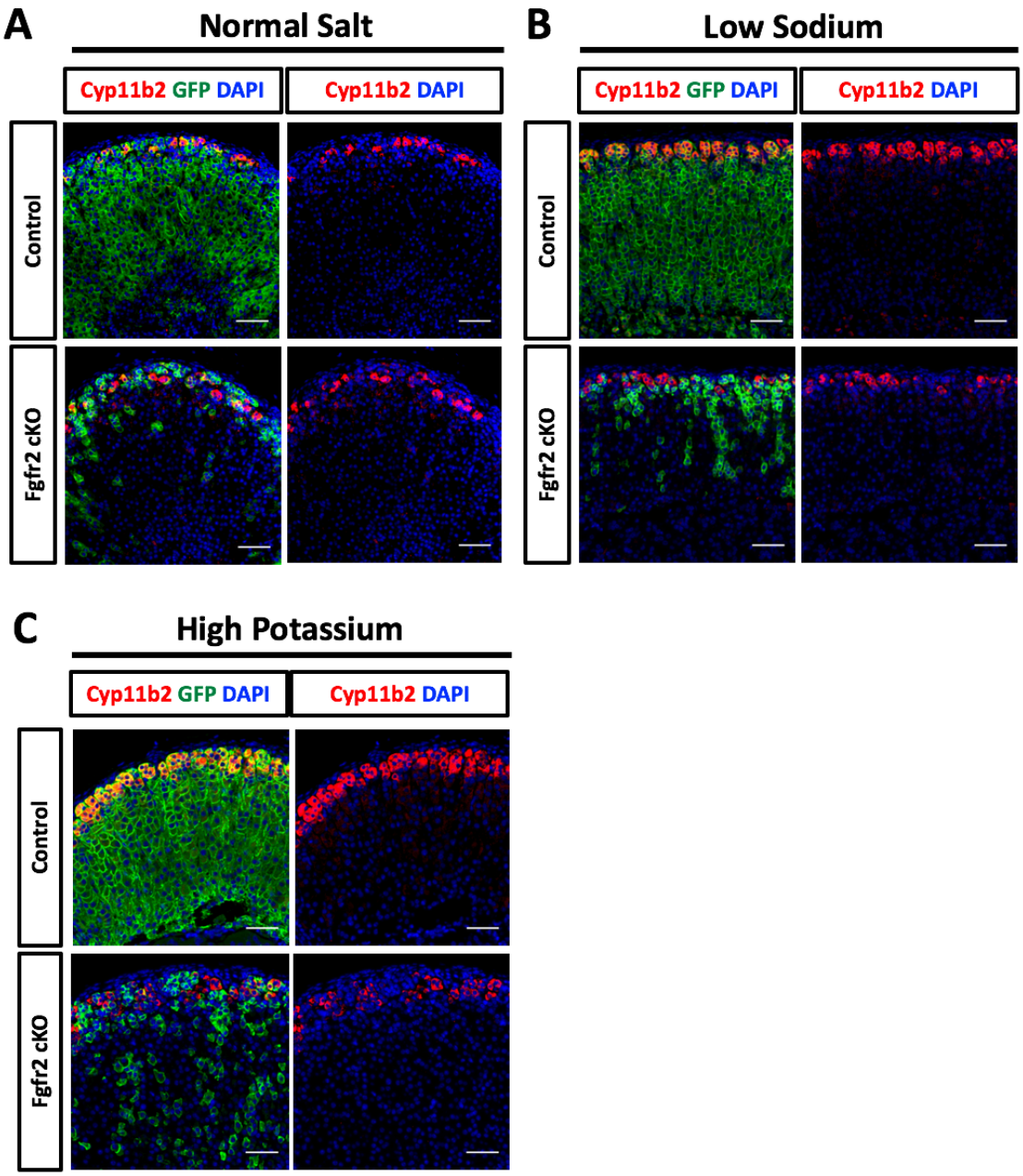

Figure 4.4. Loss of Cyp11b2 in Fgfr2 cKO adrenals.

Representative pictures of GFP (green) and Cyp11b2 (red) co-immunostaining of control (ASCre/+; mTmG) and Fgfr2cKO (ASCre/+; mTmG; Fgfr2fl/fl) adrenals from adult female mice on A, normal salt, B, low sodium, and C, high potassium diet. Bars, 50μm.

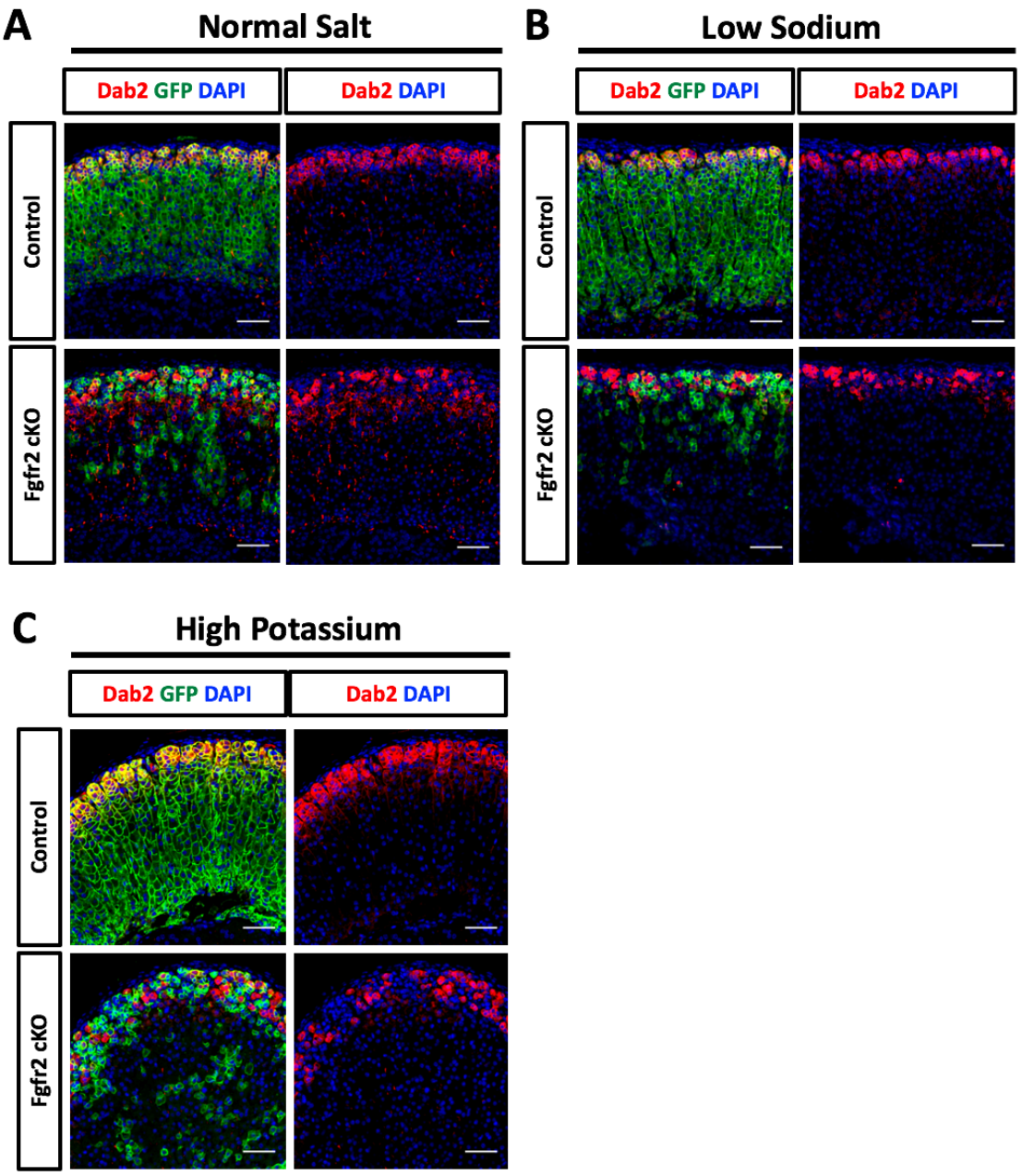

Figure 4.5. Loss of Dab2 in Fgfr2 cKO adrenals.

Representative pictures of GFP (green) and Dab2 (red) co-immunostaining of control (ASCre/+; mTmG) and Fgfr2cKO (ASCre/+; mTmG; Fgfr2fl/fl) adrenals from adult female mice on A, normal salt, B, low sodium, and C, high potassium diet. Bars, 50μm.

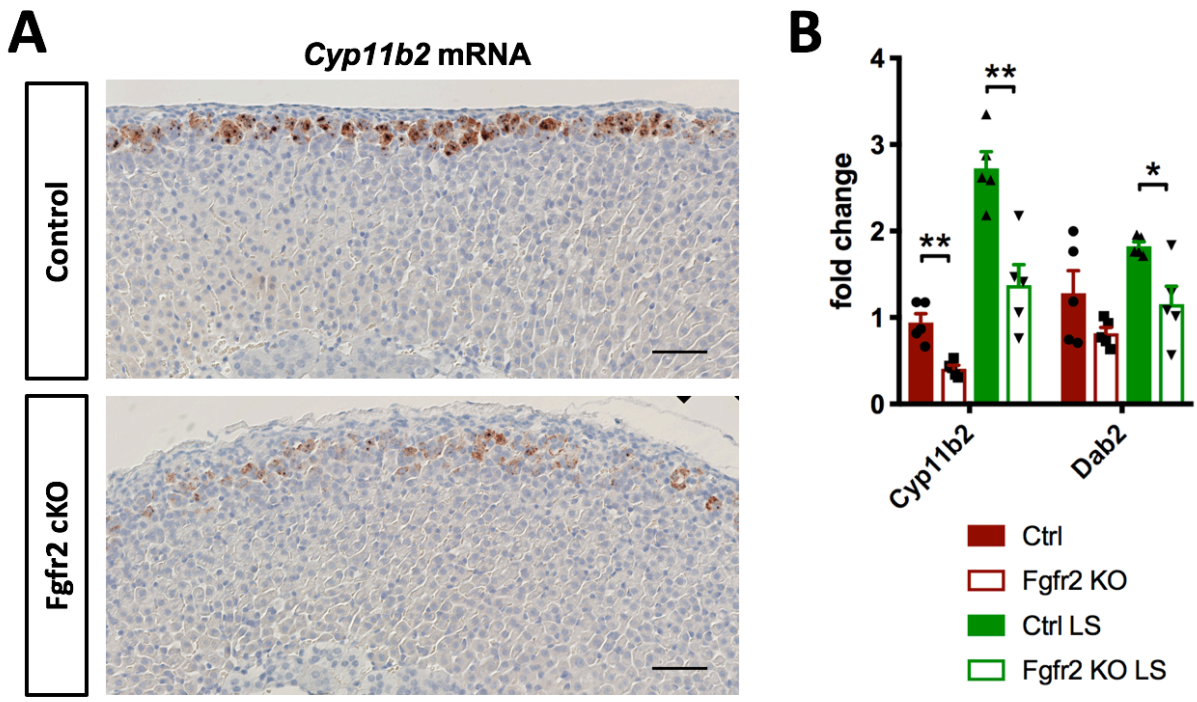

Figure 4.6. Fgfr2 deletion results in lower Cyp11b2 and Dab2 transcript levels.

A, representative bright field images of *in situ* hybridization (RNAscope) of *Cyp11b2* (brown) on adrenals of adult male mice. Nuclei are stained with hematoxylin. Bars, 50μm. B, qRT-PCR of *Cyp11b2* and *Dab2* using whole adrenal RNA extract from adult male mice on normal chow diet (red bars) or low sodium (LS) chow diet (green bars). Two sample *t*-test, *, $p < 0.05$, **, $p < 0.01$. Error bars, mean ± SEM.

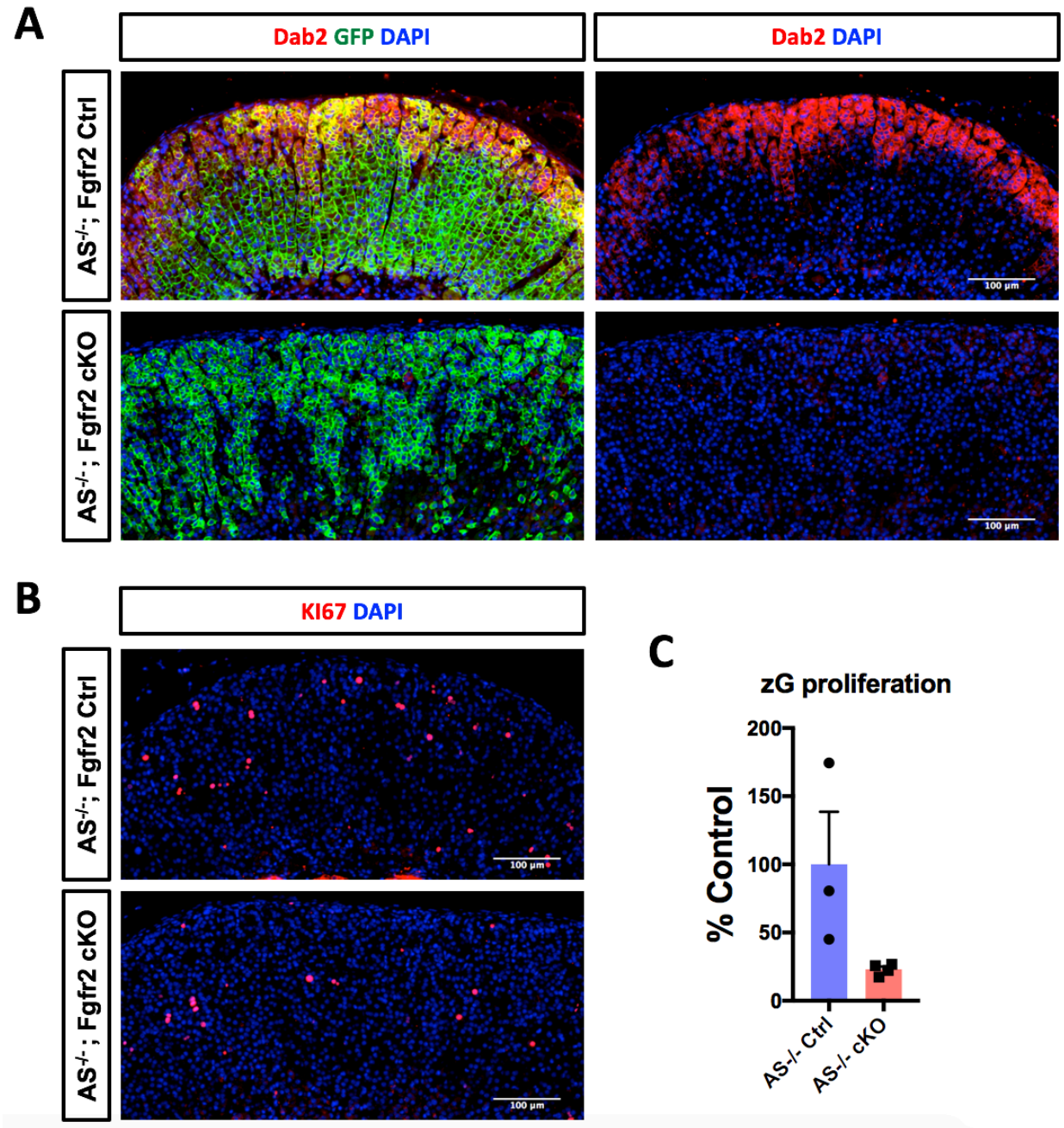

Figure 4.7. zG response to high RAAS stimulation is impaired by Fgfr2 deletion.

A, Representative image of GFP (green) and Dab2 (red) co-immunostaining of ASKO control (ASCre/Cre; mTmG) and ASKO-Fgfr2cKO (ASCre/Cre; mTmG; Fgfr2fl/fl) adrenals. B, Ki67 staining of ASKO control and ASKO-Fgfr2cKO adrenals. C, quantification of data shown in B. Bars, 100µm. Error bars, mean ± SEM.

To examine the impact of *Fgfr2* deletion on zF function, we performed immunostaining of Cyp11b1, the enzyme catalyzing the terminal step of corticosterone synthesis in mice. GFP+ cell in the zF of Fgfr2 cKO adrenals maintain normal Cyp11b1 level (**Figure 4.8**). Moreover, Cyp11b1 remains excluded from the outer cortex, suggesting zonation pattern is not disturbed.

Since FGFR2 is a well-characterized target for anti-neoplastic therapies, several small molecule inhibitors have been developed to antagonize its activity[17]. We chose two molecules, AZD4547 and BGJ398, both of which are second generation tyrosine kinase inhibitors with high specificity to FGFR1/2/3 and minimal off-target effects on VEGFR[18,19]. To test the impact of these compounds on zG function, we first treated adult mice with 10mg/kg/day drug or vehicle by oral gavage for 12 days. There was a significant reduction in zG proliferation in mice treated with either compound (**Figure 4.9A-D**). To assess zG function, we conducted metabolic cage studies with adult mice fed with 30mg/kg/day of either compound. Daily measurements of urinary aldosterone levels showed a significant and sustained reduction when mice were treated with AZD4547 (**Figure 4.9E**). Moreover, a similar course of BGJ398 treatment at 30mg/kg/day significantly reduced *Cyclin D1* and *Cyp11b2* expression, suggesting decreased proliferation and aldosterone production capacity (**Figure 4.9F**).

Lastly, we tested whether *Fgfr2* deletion can block the progression of zG hyperplasia driven by β-catenin gain-of-function (GOF) mutation. Previously, we have shown that constitutive activation of WNT/β-catenin signaling in the zG (βCat GOF) blocks transdifferentiation and leads to adrenal hyperplasia (see chapter 3). Furthermore, βCat GOF mice have significantly higher plasma aldosterone level and elevated blood pressure (see chapter 3). To test whether FGFR2 acts downstream of β-catenin to mediate these phenotypes, we bred Fgfr2 cKO mice with βCat GOF mice, generating βCat GOF; Fgfr2 cKO double mutant mice (ASCre/+; β-catenin fl(ex3)/+; Fgfr2 fl/fl; R26R-mTmG). Initial analysis of adult animals revealed that *Fgfr2* deletion

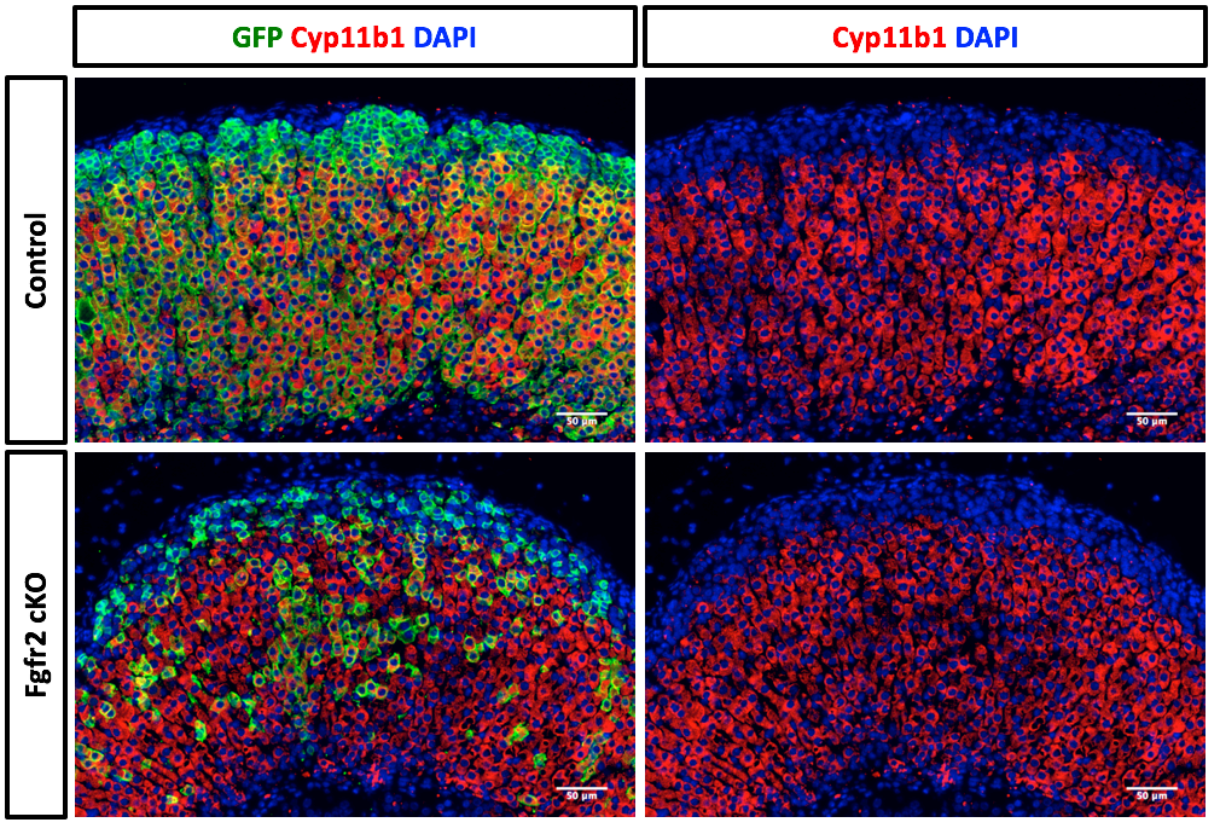

Figure 4.8. Fgfr2 is not required for zF identity.

Representative images of GFP (green) and Cyp11b1 (red) co-immunostaining of control (ASCre/+; mTmG) and Fgfr2cKO (ASCre/+; mTmG; Fgfr2fl/fl) adrenals from adult mice. Bars, 50μm.

Figure 4.9. FGFR inhibitors impairs zG proliferation and aldosterone production.

A-D, zG proliferation is reduced in mice treated with 10mg/kg/day AZD4547 or BGJ398 for 12 days by oral gavage. A, C, representative images of β-catenin (green) and Ki67 (red) co-immunostaining. Bars, 50μm. B, D, quantification of data shown in A and C. Two sample *t*-test, *, $p < 0.05$, ***, $p < 0.001$. E, urinary aldosterone levels of adult mice treated with 30mg/kg/day p. o. AZD4547. Treatment started on day 4. N = 6 each group. Two-way ANOVA analysis, ##, $p < 0.01$, followed by Bonferroni's multiple comparison correction test, *, $p < 0.05$. F, qRT-PCR analysis of *Cyp11b2* and *Cyclin D1* transcript levels in adrenals from mice treated with 30mg/kg/day p. o. BGJ398 for 7 days. Two sample *t*-test, *, $p < 0.05$. Error bars, mean ± SEM.

Figure 4.9 (continued)

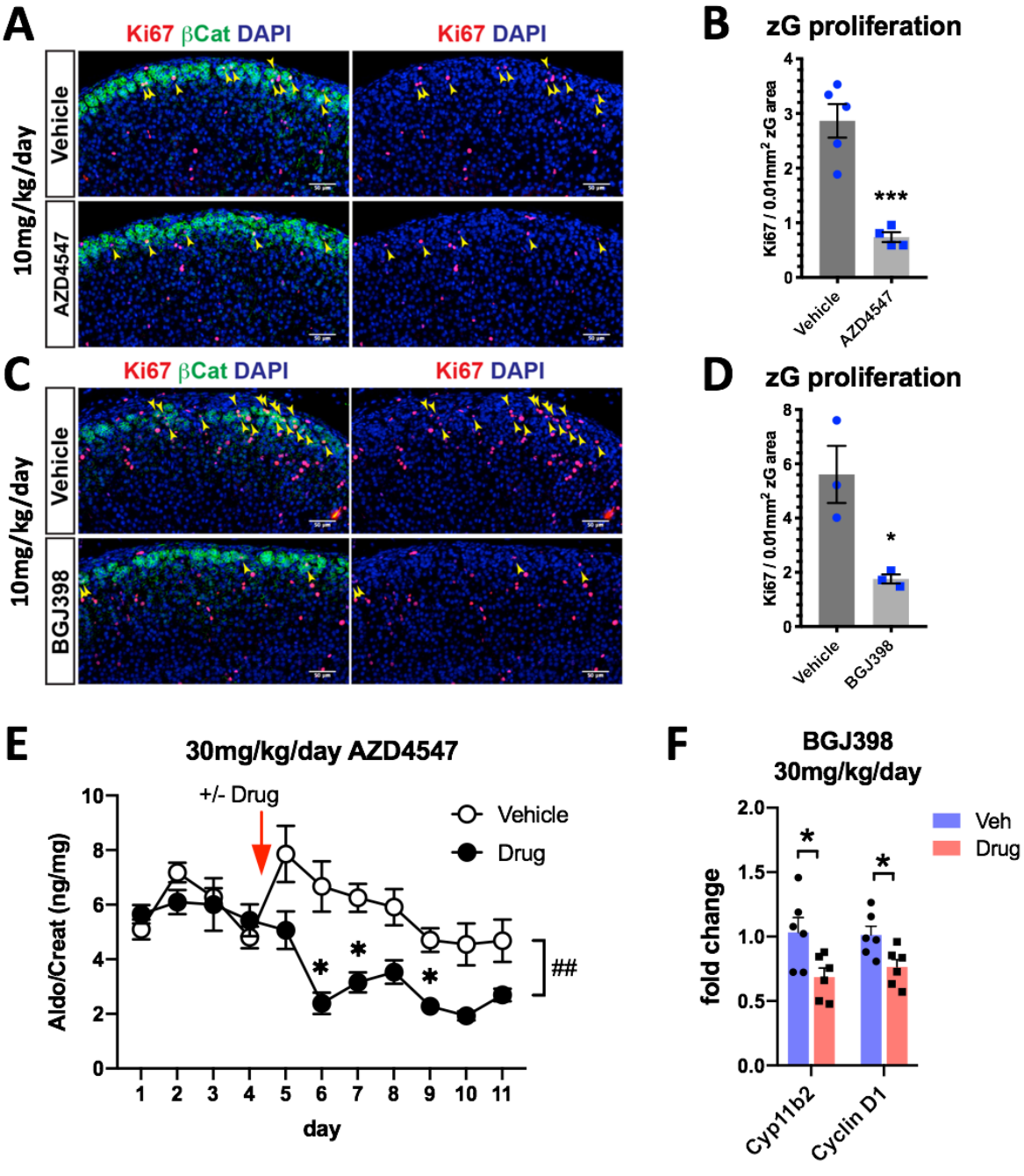

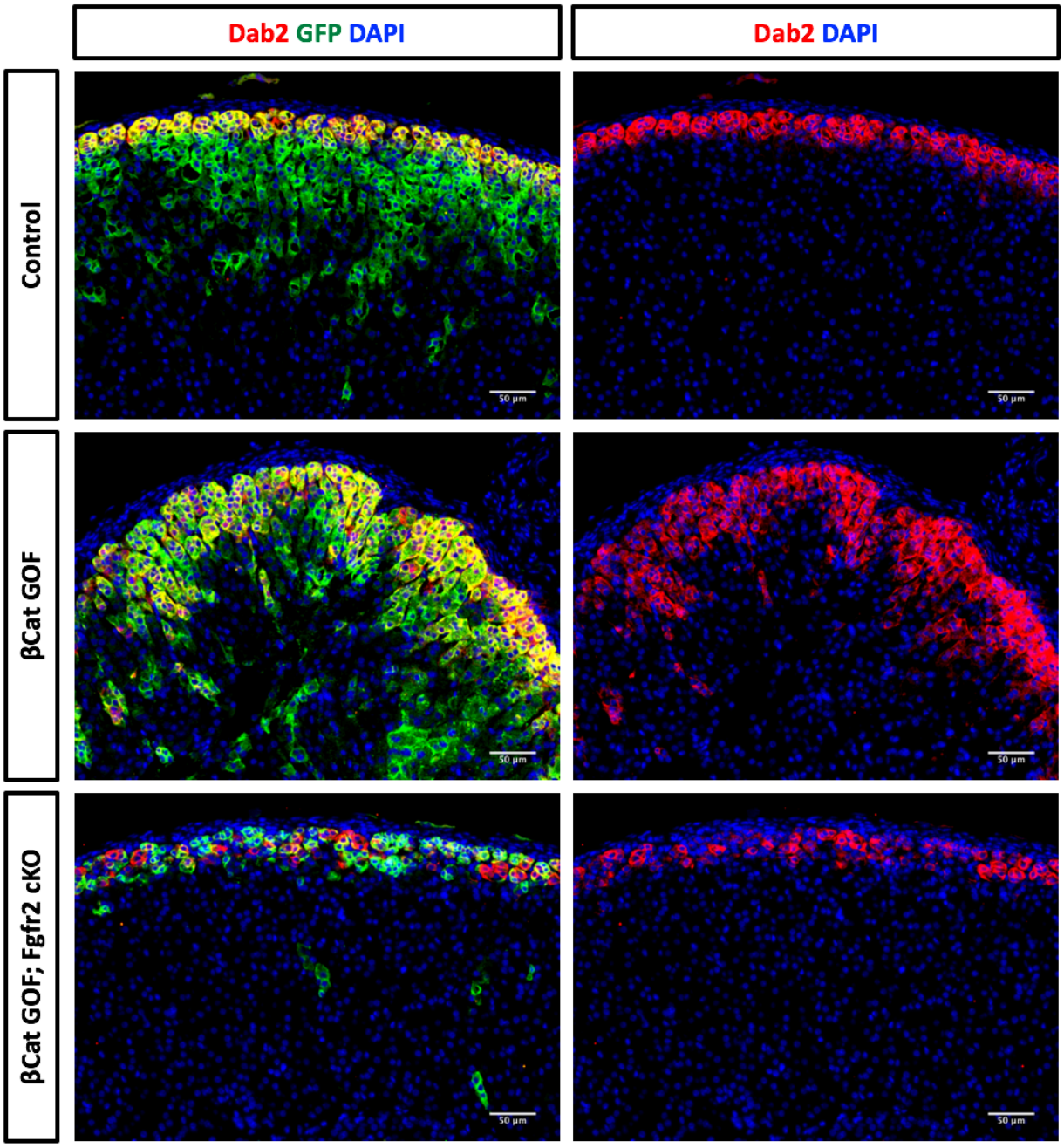

Figure 4.10. Fgfr2 deletion prevents zG hyperplasia driven by β-catenin gain-of-function. Representative images of GFP (green) and Dab2 (red) co-immunostaining of control (ASCre/+; mTmG), βCat GOF (ASCre/+; mTmG; β-catenin fl(ex3)/+), and βCat GOF; Fgfr2 cKO (ASCre/+; mTmG; β-catenin fl(ex3)/+; Fgfr2 fl/fl) adrenals from adult mice. Bars, 50μm.

prevents zG hyperplasia progression driven by constitutive β-catenin activity (**Figure 4.10**). Furthermore, GFP+ zG cells in double mutant adrenals do not express Dab2, suggesting FGFR2 acts downstream of β-catenin in maintaining zG identity.

Discussion

The data presented here show that FGFR2 inhibition has a profound impact on zG tissue homeostasis and function. Lineage tracing experiments revealed that *Fgfr2* is required for zG cells to participate in cortical turnover. This is at least partially due to decrease in proliferation. *AS-Cre* expression is active in a subset of zG cells at any given time, depending on the physiological demand of aldosterone. A decrease in proliferation will give *Fgfr2*-deleted cells a selection disadvantage compared to other wild type zG cells. Hence, we see a significant proportion of the zG remain GFP-negative. Another possible reason for decreased zG lineage contribution is that *AS-Cre* expression itself is down-regulated. As we have shown, *Fgfr2* deletion causes a reduction in *Cyp11b2* expression, suggesting that *AS-Cre* locus expression could be similarly affected. However, we found that Cyp11b2 protein is still present in wild type zG cells in Fgfr2 cKO adrenals, suggesting the reduction of *Cyp11b2* transcript level is mainly contributed by *Fgfr2*-deleted cells. Hence, by a similar logic, it is unlikely that *AS-Cre* expression is affected in wild type zG cells in Fgfr2 cKO adrenals. However, one cannot rule out a non-cell autonomous effect of *Fgfr2* deletion on *Cyp11b2* or *AS-Cre* expression.

Our data show that FGFR2 is required for the expression of two important markers of zG cell identity and function, *Cyp11b2* and *Dab2*. Expression of *Cyp11b2* is under the dynamic control of endocrine signals including Angiotensin II and extracellular potassium[6,7]. Both signals can trigger zG cell depolarization and Ca^{2+} influx, leading to the activation of CaMKs and transcription factors such as Nurr1 and CREB, which in turn activate *Cyp11b2* transcription. Our

data show that Fgfr2-deleted zG cells fail to express *Cyp11b2* in response to either high AngII or K^+, suggesting a common link between the two pathways is disrupted in these cells. Therefore, it will be interesting to determine whether *Fgfr2* deletion results in any Ca^{2+} signaling defect. Dab2 is an adapter protein for cargo selection in clathrin-mediated endocytosis[20]. It was identified as a zG-specific marker and its expression is regulated by AngII[21]. Overexpression of *Dab2* in adrenocortical cell line can boost basal and AngII-stimulated aldosterone production[21]. However, the precise function of Dab2 in the zG is currently unknown. Our data suggest that *Fgfr2* is required for *Dab2* expression in the zG. However, this could also be a secondary effect due to loss of responsiveness to AngII signaling. Expression of both *Cyp11b2* and *Dab2* are maintained in wild type zG cells in Fgfr2 cKO adrenals. This is likely the reason why plasma aldosterone levels are normal in these mice. However, elevated renin activity suggests that the zG function is maintained at the expense of increased feedback activity. The precise mechanism(s) by which FGFR2 regulates zG function remain to be determined. Unbiased approaches such as transcriptome and metabolome profiling will likely be needed to gain further insights in the future.

Receptor tyrosine kinases are popular drug targets in oncology, and their alterations are also frequently involved in other types of disorders in metabolism, immunology, and cardiovascular health[22]. Mutations and amplifications of FGFRs are prevalent in numerous cancer types[17]. We have selected two small molecules currently in Phase I/II clinical trials for anti-neoplastic therapy. AZD4547 and BGJ398 are both second generation FGFR inhibitors with minimal off-target effects[18,19]. Our data suggest that both compounds are effective at inhibiting aldosterone production at previously published doses. These data are consistent with results from the genetic knockout studies, and furthermore, suggest that FGFR inhibition could be an effective strategy to lower aldosterone production. Given the adverse effects of aldosterone on cardiovascular health, hyperaldosteronism is a dangerous condition that affects nearly 10% of

the hypertensive population[4]. The pathophysiology of HA often involves dysregulated activation of Ca^{2+} signaling and/or hyperplasia in the zG[8]. Given the effects of FGFR2 inhibition on zG physiological function and proliferation, it will be of great interest to understand the downstream mechanism(s) and to test whether these small molecules can be effective at treating HA. In our βCat GOF mouse model, *Fgfr2* deletion effectively blocks the progression of zG hyperplasia, suggesting *Fgfr2* is epistatic to *β-catenin* in this process. It remains to be determined whether aldosterone production and blood pressure can be normalized in these mice, and more importantly, whether treatment of βCat GOF mice with FGFR inhibitors can alleviate these symptoms.

Methods

Animal Experiments

All animal procedures were approved by Boston Children's Hospital's and University of Virginia's Institutional Animal Care and Use Committee. Mouse strains used in this study were: C57BL/6J (Jackson Laboratory), ASCre (Cyp11b2tm1.1(cre)Brlt[16]), Ctnnb1fl(ex3) (Ctnnb1tm1Mmt[23]), Fgfr2flox (Fgfr2tm1Dor[24]), and R26R-mTmG (Gt(ROSA)26Sortm4(ACTB-tdTomato,-EGFP)Luo[25]). All animals were maintained on a mixed sv129-C57Bl/6 genetic background, with *ad lib* food and water, under a 12-hour light / 12-hour dark cycle. PCR was used for genotyping. Littermates were used whenever possible and both male and female animals were studied. When indicated, mice were fed normal-chow (0.32% Na+), low-salt (0.05% Na+) chow, or high-potassium (4% K+) chow (ScottPharma Solutions) for 7 days.

Tissue Preparation

After dissection, adrenals were trimmed of surrounding fat tissue and rinsed in PBS. For immunofluorescence, adrenals were cut into halves with a surgical blade and fixed in 4% PFA at

4ºC for 1 hour. For RNAscope in situ hybridization, intact adrenals were fixed in 4% PFA at room temperature overnight.

Paraffin Section Immunofluorescence

After fixation, adrenals were dehydrated in ethanol, xylene and embedded in paraffin blocks. Paraffin sections were cut at 5 μm thickness. Sections were rinsed in xylene, an ethanol gradient and then PBS. Antigen retrieval was performed in Tris-EDTA pH 9.0 (for Cyp11b1 and Cyp11b2) or 10 mM Sodium Citrate pH 6.0 (all others). Sections were blocked in 5% Normal Goat Serum, 0.1% Tween-20 in PBS for 1 hour at RT. Primary antibodies were diluted 1:200 in 5% NGS in PBS and incubated on sections at 4ºC overnight. Slides were washed three times for 5 min in 0.1% Tween-20 in PBS. Secondary antibodies were diluted in 1:200 in PBS and incubated on sections at RT for 1-2 hours. For nuclear staining, DAPI (4',6-diamidino-2-phenylindole) was added to secondary antibody mixture at a final concentration of 1:1000. After three 5-min washes with 0.1% Tween-20 in PBS, slides were mounted with ProLong Gold Antifade Mountant (Thermo Fisher Scientific, P36930). Primary antibodies used for this chapter include: Mouse anti-β-catenin (BD Biosciences, 610153), Chicken anti-GFP (Aves Labs, GF-1020), Mouse anti-Dab2 (BD Biosciences, 610464), Rabbit anti-Cyp11b2 and Cyp11b1-555 (kindly provided by Dr. Celso E. Gomez-Sanchez), Rabbit anti-Ki67 (Cell Signaling Technology, 9129). The following secondary antibodies were used: Alexa Fluor 647-conjugated goat anti-rabbit IgG, Alexa Fluor 647-conjugated goat anti-mouse IgG, Alexa Fluor 488-conjugated goat anti-chicken IgG (Invitrogen). Images were acquired using a Nikon upright Eclipse 90i microscope and adjusted for brightness and contrast in ImageJ.

RNA Isolation and Gene Expression Analysis

Total RNA was isolated from whole adrenals trimmed of adherent fat and homogenized in TRI Reagent (Sigma) using a Direct-zol RNA microprep kit (Zymo Research), following the

manufacturer's protocol. 500 ng of RNA was reverse-transcribed into cDNA using the High-Capacity cDNA Reverse Transcription Kit (Applied Biosystems, 4368814). Gene expression analysis was performed by quantitative Real Time PCR (qRT-PCR) using a QuantStudio 6 Flex thermocycler (Applied Biosystems). The following Taqman gene expression assays (Applied Biosystems) were used: *Cyp11b2* (Mm01204955_g1), *Actb* (Mm026119580_g1), *Dab2* (Mm01307290_m1).

Single-Molecule RNA in situ Hybridization

After fixation, adrenals were embedded in paraffin blocks and sectioned at 5 μm thickness. Single-molecule RNA in situ hybridization was performed using a RNAscope 2.5 HD Brown Reagent Kit (Advanced Cell Diagnostics, 322300), following manufacturer's protocol. Target retrieval was performed for 7 min[26]. Slides were counter-stained with 30% Gill's Hematoxylin (Fisher Scientific, 23-245654) and mounted with Cytoseal XYL (Fisher Scientific, 22-050-262). The following probes were used: *Cyp11b2* (ACD, 505851), positive control *Ppib* (ACD, 313911), negative control *dapB* (ACD, 310043).

Metabolic Cage Experiments

Adult male mice ~80 days old (C57BL/6J) were housed in a temperature and humidity controlled environment on a 12:12 light:dark cycle. Metabolic cage experiments were conducted as described previously[27]. Mice were individually housed in metabolic cages designed for urine collection, with *ad libitum* access to water and standard rodent chow. In addition, mice were given a ~100mg pellet of peanut butter (Jif creamy peanut butter, Kroger) on their drinking spout daily; by the second day, all the mice consumed the peanut butter within 2 minutes. After a habituation period of 4 days, urine was sampled every twenty-four hours for 11 days: 4 days of baseline measurements and 7 days of drug/vehicle. During the last 7 days, mice received either

a plain peanut butter pellet, or a peanut butter pellet containing AZD4547 or BGJ398 30mg/kg/day. Peanut butter/drug suspension was formulated as previously described[28].

Urine and Plasma Hormone Analysis

Urinary aldosterone was measured using an aldosterone I125 radioimmunoassay (Tecan, Morrisville, NC), and standardized to urinary creatinine (Jaffe' colorimetric assay, Cayman Chemicals, Ann Arbor, MI) to account for differences in GFR and urine volume. Plasma was collected by retro-orbital blood collection with hematocrit tubes. Plasma aldosterone levels were determined using an aldosterone I125 radioimmunoassay (Tecan, Morrisville, NC, MG13051). Plasma renin activity was determined using a competitive radioimmunoassay for Ang I (Tecan, Morrisville, NC, 30120823) as previously described[27].

References

1. Bollag, W. B. Regulation of aldosterone synthesis and secretion. *Compr. Physiol.* **4**, 1017–1055 (2014).

2. Hawkins, U. A., Gomez-Sanchez, E. P., Gomez-Sanchez, C. M. & Gomez-Sanchez, C. E. The ubiquitous mineralocorticoid receptor: clinical implications. *Curr. Hypertens. Rep.* **14**, 573–580 (2012).

3. Viengchareun, S. *et al.* The mineralocorticoid receptor: insights into its molecular and (patho)physiological biology. *Nucl. Recept. Signal.* **5**, e012 (2007).

4. Brown, N. J. This is not Dr. Conn's aldosterone anymore. *Trans. Am. Clin. Climatol. Assoc.* **122**, 229–243 (2011).

5. Catena, C., Colussi, G. & Sechi, L. A. Treatment of Primary Aldosteronism and Organ Protection. *Int. J. Endocrinol.* **2015**, 597247 (2015).

6. Spät, A. & Hunyady, L. Control of aldosterone secretion: a model for convergence in cellular signaling pathways. *Physiol. Rev.* **84**, 489–539 (2004).

7. Hattangady, N. G., Olala, L. O., Bollag, W. B. & Rainey, W. E. Acute and chronic regulation of aldosterone production. *Mol. Cell. Endocrinol.* **350**, 151–162 (2012).

8. Fernandes-Rosa, F. L. *et al.* Different Somatic Mutations in Multinodular Adrenals With Aldosterone-Producing Adenoma. *Hypertension* **66**, 1014–1022 (2015).

9. Zennaro, M.-C., Boulkroun, S. & Fernandes-Rosa, F. An update on novel mechanisms of primary aldosteronism. *J. Endocrinol.* **224**, R63–R77 (2015).

10. Drelon, C., Berthon, A., Mathieu, M., Martinez, A. & Val, P. Adrenal cortex tissue homeostasis and zonation: A WNT perspective. *Mol. Cell. Endocrinol.* (2014). doi:10.1016/j.mce.2014.12.014

11. Berthon, A. *et al.* WNT/β-catenin signalling is activated in aldosterone-producing adenomas and controls aldosterone production. *Hum. Mol. Genet.* **23**, 889–905 (2014).

12. Ornitz, D. M. & Itoh, N. The Fibroblast Growth Factor signaling pathway. *Wiley Interdiscip. Rev. Dev. Biol.* **4**, 215–266 (2015).

13. Häfner, R., Bohnenpoll, T., Rudat, C., Schultheiss, T. M. & Kispert, A. Fgfr2 is required for the expansion of the early adrenocortical primordium. *Mol. Cell. Endocrinol.* **413**, 168–177 (2015).

14. Guasti, L., Candy Sze, W. C., McKay, T., Grose, R. & King, P. J. FGF signalling through Fgfr2 isoform IIIb regulates adrenal cortex development. *Mol. Cell. Endocrinol.* **371**, 182–188 (2013).

15. Kim, Y. *et al.* Fibroblast growth factor receptor 2 regulates proliferation and Sertoli differentiation during male sex determination. *Proc. Natl. Acad. Sci. U. S. A.* **104**, 16558–16563 (2007).

16. Freedman, B. D. *et al.* Adrenocortical Zonation Results from Lineage Conversion of Differentiated Zona Glomerulosa Cells. *Dev. Cell* **26**, 666–673 (2013).

17. Chae, Y. K. *et al.* Inhibition of the fibroblast growth factor receptor (FGFR) pathway: the current landscape and barriers to clinical application. *Oncotarget* **8**, 16052–16074 (2017).

18. Gavine, P. R. *et al.* AZD4547: an orally bioavailable, potent, and selective inhibitor of the fibroblast growth factor receptor tyrosine kinase family. *Cancer Res.* **72**, 2045–2056 (2012).

19. Guagnano, V. *et al.* Discovery of 3-(2,6-dichloro-3,5-dimethoxy-phenyl)-1-{6-[4-(4-ethyl-piperazin-1-yl)-phenylamino]-pyrimidin-4-yl}-1-methyl-urea (NVP-BGJ398), a potent and selective inhibitor of the fibroblast growth factor receptor family of receptor tyrosine kinase. *J. Med. Chem.* **54**, 7066–7083 (2011).

20. Tao, W., Moore, R., Smith, E. R. & Xu, X.-X. Endocytosis and Physiology: Insights from Disabled-2 Deficient Mice. *Front. Cell Dev. Biol.* **4**, 129 (2016).

21. Romero, D. G. *et al.* Disabled-2 is expressed in adrenal zona glomerulosa and is involved in aldosterone secretion. *Endocrinology* **148**, 2644–2652 (2007).

22. Ferguson, F. M. & Gray, N. S. Kinase inhibitors: the road ahead. *Nat. Rev. Drug Discov.* **17**, 353–377 (2018).

23. Harada, N. *et al.* Intestinal polyposis in mice with a dominant stable mutation of the beta-catenin gene. *EMBO J.* **18**, 5931–5942 (1999).

24. Yu, K. *et al.* Conditional inactivation of FGF receptor 2 reveals an essential role for FGF signaling in the regulation of osteoblast function and bone growth. *Dev. Camb. Engl.* **130**, 3063–3074 (2003).

25. Muzumdar, M. D., Tasic, B., Miyamichi, K., Li, L. & Luo, L. A global double-fluorescent Cre reporter mouse. *Genes. N. Y. N 2000* **45**, 593–605 (2007).

26. Basham, K. J. *et al.* A ZNRF3-dependent Wnt/β-catenin signaling gradient is required for adrenal homeostasis. *Genes Dev.* **33**, 209–220 (2019).

27. Davies, L. A. *et al.* TASK channel deletion in mice causes primary hyperaldosteronism. *Proc. Natl. Acad. Sci.* **105**, 2203–2208 (2008).

28. Gonzales, C. *et al.* Alternative method of oral administration by peanut butter pellet formulation results in target engagement of BACE1 and attenuation of gavage-induced stress responses in mice. *Pharmacol. Biochem. Behav.* **126**, 28–35 (2014).

Chapter Five:

Conclusion and Future Direction

The adrenal gland is a remarkable system to study the complex cellular dynamics of an adult organ. Organized into concentric layers, the adult cortex consists of diverse cell types that are distinguished by unique signaling mechanisms, ultrastructure details, and morphological features. Despite this diversity, mature cortical cells represent several stages of differentiation from a common cellular lineage. Lineage tracing experiments have demonstrated cells from the zG migrate centripetally and transdifferentiate into zF cells[1]. This type of transdifferentiation has not been reported in other adult organs under physiological conditions, but is thought to exist during injury and regeneration or can be artificially induced by expression of lineage-specifying transcription factors[2–4]. Several classic paracrine and autocrine signaling pathways are involved in maintaining the self-renewal and differentiation of the adult adrenal cortex, such as the WNT/β-catenin and Shh signaling pathways[5,6]. A growing body of genetic studies has contributed to a basic understanding of how these pathways regulate adrenocortical zonation and maintenance. WNT/β-catenin signaling activity specifies the identity of the zG layer, possibly by directly or indirectly inducing a zG-specific gene expression program[7,8]. WNT/β-catenin is also required for long-term cortical renewal, yet the mechanism behind this is unclear[9]. One model contends that WNT signaling regulates Shh expression in the zG, which signals to Gli1-expressing cells in the mesenchymal capsule, a putative niche for adrenal stem cells[10]. However, this theory awaits formal experimental proof. FGF signaling plays an important role during fetal adrenal development[11]. However, its role in the adult cortex and interplay with WNT and Shh pathways have not been thoroughly investigated.

Steroid hormones produced by the adrenal cortex have significant impact on human health. Aldosterone produced by the zG has potent effects on electrolyte balance and blood pressure[12]. Glucocorticoids produced by the zF regulate glucose homeostasis and immune system activity[13]. Over or under production of these hormones are the cause of significant morbidity and mortality in diseases. One example is hyperaldosteronism, a condition estimated to be the

cause of 10% hypertension cases and 20% resistant hypertension[14]. Excess aldosterone is also associated with higher risks of stroke, myocardial infarction, atrial fibrillation, cardiac failure and renal failure[15]. Better understanding of the mechanisms controlling adrenocortical tissue homeostasis and function is essential to gain insights into disease pathogenesis and develop novel therapies. This dissertation investigates the role of WNT and FGF signaling, two pathways widely involved in development and adult tissue homeostasis, in the regulation of adrenocortical morphogenesis and function.

Mechanisms of adrenocortical morphogenesis

The unique morphological features of the zG and zF have long been recognized. Yet their functional significance has remained elusive. In Chapter Two, we provide an account for the cellular and molecular details of zG morphology, providing a foundation for further studies of their regulation. Using 3D imaging and reconstruction, we show the zG consists of glomeruli enwrapped in a basement membrane with unique molecular composition. Within each glomerulus, zG cells are organized into rosettes by constricting a set of adherens junctions at a common contact point. By following F-actin dynamic, we show that zG cells initially have small dispersed AJs, which during the first 10 days after birth become enriched along the entire cell-cell contact. Subsequently these AJ-rich contacts shrink, allowing rosettes to form. Concurrently, the flat sheet-like domains in the nascent zG undergo invagination and folding, gradually giving rise to the compact round glomeruli in the adult zG. Our data do not prove causality between rosette formation and zG morphogenesis. In fact, it remains theoretically possible that both events happen concurrently under the influence of common signals. To formally prove causation, one could use chemical inhibitors of actomyosin activity, such as blebbistatin[16], to disrupt rosette formation and follow glomerular morphogenesis. However, there are several foreseeable technical challenges. First, rosette formation and glomerular

morphogenesis take place during 3-5 weeks of postnatal life. It will be difficult to completely disrupt actomyosin activity *in vivo* for such an extensive period, which may also cause toxic effects in the animal. Alternatively, *ex vivo* setups may allow for ease of manipulation, but the timeline of rosette formation will need to be reexamined. Furthermore, since the methodology for long-term adrenal slice culture has not been established, it may prove to be technically challenging. In recent years, organotypic culture systems have become a powerful tool to model adult organ dynamics *in vitro*. Adrenal organoids will be an invaluable tool to study mechanisms of morphogenesis in the future.

Using the AS-Cre mouse model, we have begun to dissect the genetic mechanisms of postnatal zG morphogenesis. AS-Cre activity begins at birth[1], allowing us to bypass crucial stages of fetal adrenal development and evaluate the effects of genetic mutants on rosette formation and zG morphogenesis postnatally. However, the caveat of these models is that AS-Cre doesn't hit every single zG cells at once. Instead, this locus is regulated by endocrine signals that reflect the animal's demand on aldosterone. In wild type mice, AS-Cre lineage covers most zG by 6 weeks of age (**Figure 4.1**), but it is much less efficient in mutants where proliferation is affected. Therefore, we studied the phenotypes of β-catenin LOF and Fgfr2 LOF mice at >10 weeks of age, by which time we can readout the cumulative effect of AS-Cre activity. Despite this caveat, we saw a dramatic reduction of rosette frequency and disruption of glomerular morphology in β-catenin LOF and Fgfr2 LOF adrenals, and conversely increase of rosette frequency and glomeruli in β-catenin GOF adrenals. Moreover, our data suggest these two genes regulate zG morphology in different ways. β-catenin is an integral component of the adherens junction, and its deletion leads to an expected loss of AJs and subsequent loss of rosettes. β-catenin may also directly or indirectly regulate transcripts that are potentially important mediators of rosette formation. On the other hand, loss of *Fgfr2* results in small dispersed F-actin punctae, reminiscent of the AJs in nascent zG. This effect is possibly mediated by Shroom3, which is

required for positioning ROCK to junctional complex to activate actomyosin in many morphogenetic contexts[17–19]. Notably, glomeruli in β-catenin and Fgfr2 LOF mice do not fully resemble zG structures in P0 animals, as one would expect if rosette formation were blocked in these mutants. It is possibly due to inefficient AS-Cre targeting during zG morphogenesis, as discussed earlier. Wild type zG cells in these LOF models will likely progress normally, driving a partially normal morphogenesis. One could try to circumvent this issue by using the ASCre/Cre model of aldosterone deficiency, where Cre activity is markedly enhanced. It will also be interesting to investigate whether rosette formation is accelerated in this model to understand the role of endocrine signals in zG morphogenesis.

We have shown that rosette formation initially occurs to facilitate postnatal morphogenesis. However, it is unclear whether new rosettes continue to form throughout adult life. This question pertains the mechanism by which zG renews itself. Do zG cells maintain long-term self-renewal by largely replicating themselves? Or rather, do putative stem cells in the capsule give rise to new zG? In either case, newborn zG cells must either form new rosettes or integrate into existing rosettes. It is likely that similar AJ-based mechanisms are involved. Live imaging of adrenal slice cultures and following cellular dynamics in the adult will provide further insights. Alternatively, one could perform pulse-chase labeling experiments using the ASCreER model (see Appendix IV) to elucidate adult zG turnover dynamics.

Another outstanding question is the mechanism of rosette resolution when zG cells undergo centripetal migration and transdifferentiation. zF mainly consists of single columns of cells. How do zG cells exit a rosette and reorganize into a single column? One possible mechanism is through cell intercalation. This will require AJs to disaggregate from rosette center and cells to be guided to establish a circumferential contact with the basement membrane. A recent study in the developing intestine shows midgut tube elongation utilizes a process of filopodial pathfinding

and cell intercalation mediated by Wnt5a/Ror2 signaling[20]. Interestingly, Wnt5a is the second most abundant Wnt ligand in the adrenal cortex. We have localized its expression to a few layers of zF cells immediately adjacent to the zG. Furthermore, we found that Ror2 is expressed predominantly in the zG. These intriguing data suggest that Wnt5a ligand originating from the zF may serve as a signal guiding zG cell intercalation. It will be interesting to study the effects of *Ror2* and *Wnt5a* deletion on rosette resolution.

Regulation of zG function by WNT and FGF signaling

In Chapters Three and Four, we investigate the impact of WNT and FGF signaling modulation on zG physiological function. Using the β-catenin GOF model, we show that stabilized β-catenin, mimicking constitutive activation of WNT signaling, causes a progressive zG tissue expansion by blocking transdifferentiation into zF. Combined with the morphological data shown in Chapter Two, our findings further strengthen the popular model that WNT/β-catenin dictates zG identity, implying that WNT/β-catenin activity needs to be downregulated for transdifferentiation to occur during normal homeostatic turnover. However, the mechanisms behind this downregulation remain to be determined. Recent studies focusing on the ACTH/cAMP/PKA pathway in the zF show that PKA signaling inhibits β-catenin activation[21], suggesting upregulation of PKA activity may be crucial in allowing for transdifferentiation to occur. Interestingly, our RNAseq data show that several cAMP/PKA inhibitors, including *Pde2a*, a cyclic nucleotide phosphodiesterase, are upregulated in β-catenin GOF adrenals (data not shown), implying β-catenin activity may cause PKA inhibition. How does a cell make the switch under this “tug of war” of WNT and PKA antagonism? What role might rosette resolution play in mediating the migration of cells across this “war zone”? These are intriguing questions that will require extensive future studies.

We find β-catenin GOF mice exhibit high plasma aldosterone levels and elevated blood pressure, consistent with a previous report using a less specific Cre model[7]. However, in contrast to this previous study, the reason for hyperaldosteronism in our mice is mysterious, since there is no increase in the number of Cyp11b2-expressing cells or transcript level. Furthermore, aldosterone production in these mice can be suppressed by high salt diet, suggesting intact endocrine regulation. A remaining possibility is that zG cells in these mice are more sensitive to AngII and/or K^+. Our data on RAAS activation in βCat GOF mice show that the tropic effect of AngII is enhanced in the β-catenin GOF context, suggesting a functional cooperativity between AngII and β-catenin. However, the underlying molecular mechanism remains to be determined.

Our preliminary analyses of Fgfr2 LOF mice suggest that FGF signaling has a major role in regulating zG identity and function. Immunohistological and transcript analyses reveal that *Fgfr2* deletion causes zG cells to lose their functional markers Cyp11b2 and Dab2. However, we observed no change in the localization of Gαq (data not shown), another pan-zG marker. Hence the effect of *Fgfr2* deletion is likely the loss of responsiveness to AngII and K^+, rather than a general de-differentiation phenomenon. FGF signaling can activate several downstream pathways, such as the RAS-MAPK, PI3K-AKT, PLCγ, and STAT signaling pathways[22]. It will be important to determine which of these possible pathways are activated downstream of FGFR2 signaling in the zG. In addition, we are currently investigating the downstream targets of FGFR2 by profiling the transcriptome of Fgfr2 LOF and control adrenals.

Based on our findings in the genetic Fgfr2 LOF model, we have explored the possibility of using FGFR inhibitors to target zG function. Strikingly, both inhibitors we tested exhibit pronounced effects on zG proliferation and function in terms of aldosterone levels and *Cyp11b2* expression. We will further pursue the usage of these drugs in treating hyperaldosteronism, first by testing

their efficacy in normalizing aldosterone level and blood pressure in βCat GOF mice. If proven useful, these drugs could potentially become a novel therapeutic option for the treatment of hyperaldosteronism.

Lastly, I would like to return to the question posed at the beginning of this dissertation, namely, what have we learned from the study of zG morphology about its function? Using a descriptive approach, we have begun to understand the composition of adrenal glomeruli. By detailing the cellular and molecular dynamics during their formation, we uncover a link between multicellular rosette formation and glomerular morphogenesis. Based on this model, we describe two important regulators of glomerular morphology, β-catenin and Fgfr2. We show that modulating these two pathways also have profound impacts on zG function. However, our current data cannot determine whether these changes in zG function are due to altered morphology. Recently, our work in collaboration with Dr. Paula Barrett provide the first evidence of cooperativity in Ca2+ oscillation among zG cells of the same rosette (see Appendix III). It will be very interesting to examine whether our rosette mutants have altered Ca2+ activity pattern. We hope that our studies have laid the foundation to better dissect the relationship between zG morphology and function in future studies.

References:

1. Freedman, B. D. *et al.* Adrenocortical Zonation Results from Lineage Conversion of Differentiated Zona Glomerulosa Cells. *Dev. Cell* **26**, 666–673 (2013).

2. Yao, E. *et al.* Notch Signaling Controls Transdifferentiation of Pulmonary Neuroendocrine Cells in Response to Lung Injury. *Stem Cells Dayt. Ohio* **36**, 377–391 (2018).

3. Schaub, J. R. *et al.* De novo formation of the biliary system by TGFβ-mediated hepatocyte transdifferentiation. *Nature* **557**, 247–251 (2018).

4. Zhou, Q., Brown, J., Kanarek, A., Rajagopal, J. & Melton, D. A. In vivo reprogramming of adult pancreatic exocrine cells to beta-cells. *Nature* **455**, 627–632 (2008).

5. Drelon, C., Berthon, A., Mathieu, M., Martinez, A. & Val, P. Adrenal cortex tissue homeostasis and zonation: A WNT perspective. *Mol. Cell. Endocrinol.* (2014).

6. Laufer, E., Kesper, D., Vortkamp, A. & King, P. Sonic hedgehog signaling during adrenal development. *Mol. Cell. Endocrinol.* **351**, 19–27 (2012).

7. Berthon, A. *et al.* Constitutive beta-catenin activation induces adrenal hyperplasia and promotes adrenal cancer development. *Hum. Mol. Genet.* **19**, 1561–1576 (2010).

8. Vidal, V. *et al.* The adrenal capsule is a signaling center controlling cell renewal and zonation through *Rspo3*. *Genes Dev.* **30**, 1389–1394 (2016).

9. Kim, A. C. *et al.* Targeted disruption of beta-catenin in Sf1-expressing cells impairs development and maintenance of the adrenal cortex. *Dev. Camb. Engl.* **135**, 2593–2602 (2008).

10. Walczak, E. M. & Hammer, G. D. Regulation of the adrenocortical stem cell niche: implications for disease. *Nat. Rev. Endocrinol.* **11**, 14–28 (2014).

11. Guasti, L., Candy Sze, W. C., McKay, T., Grose, R. & King, P. J. FGF signalling through Fgfr2 isoform IIIb regulates adrenal cortex development. *Mol. Cell. Endocrinol.* **371**, 182–188 (2013).

12. Bollag, W. B. Regulation of Aldosterone Synthesis and Secretion. in *Comprehensive Physiology* (ed. Terjung, R.) 1017–1055 (John Wiley & Sons, Inc., 2014).

13. Gallo-Payet, N. & Battista, M.-C. Steroidogenesis-Adrenal Cell Signal Transduction. in *Comprehensive Physiology* (ed. Terjung, R.) 889–964 (John Wiley & Sons, Inc., 2014).

14. Brown, N. J. This is not Dr. Conn's aldosterone anymore. *Trans. Am. Clin. Climatol. Assoc.* **122**, 229–243 (2011).

15. Fernandes-Rosa, F. L. *et al.* Different Somatic Mutations in Multinodular Adrenals With Aldosterone-Producing Adenoma. *Hypertension* **66**, 1014–1022 (2015).

16. Lienkamp, S. S. *et al.* Vertebrate kidney tubules elongate using a planar cell polarity–dependent, rosette-based mechanism of convergent extension. *Nat. Genet.* **44**, 1382–1387 (2012).

17. Nishimura, T. & Takeichi, M. Shroom3-mediated recruitment of Rho kinases to the apical cell junctions regulates epithelial and neuroepithelial planar remodeling. *Development* **135**, 1493–1502 (2008).

18. Mohan, S. *et al.* Structure of Shroom domain 2 reveals a three-segmented coiled-coil required for dimerization, Rock binding, and apical constriction. *Mol. Biol. Cell* **23**, 2131–2142 (2012).

19. Ernst, S. *et al.* Shroom3 is required downstream of FGF signalling to mediate proneuromast assembly in zebrafish. *Development* **139**, 4571–4581 (2012).

20. Wang, S., Cebrian, C., Schnell, S. & Gumucio, D. L. Radial WNT5A-Guided Post-mitotic Filopodial Pathfinding Is Critical for Midgut Tube Elongation. *Dev. Cell* **46**, 173–188.e3 (2018).

21. Drelon, C. *et al.* PKA inhibits WNT signalling in adrenal cortex zonation and prevents malignant tumour development. *Nat. Commun.* **7**, 12751 (2016).

22. Ornitz, D. M. & Itoh, N. The Fibroblast Growth Factor signaling pathway. *Wiley Interdiscip. Rev. Dev. Biol.* **4**, 215–266 (2015).

Appendix I:

Supplemental Figures for Chapter Two

Figure S1.1. A basement membrane separates the glomeruli from adjacent stromal compartments. (A) Type IV collagen (Col4a1, magenta) is present in the basement membrane in both zG and zF. Laminin β1 (Lamb1, green) is enriched in the zG. (B) vascular compartment (CD31, magenta) surrounding each glomerulus (Gαq, green) and zF cords. (C) mesenchymal compartment (Vimentin, magenta) consists of capsular cells and cells between the glomeruli. DAPI (blue), nuclei. c, capsule, zG, zona glomerulosa, zF, zona fasciculata. All bars, 10μm.

Figure S1.1 (continued)

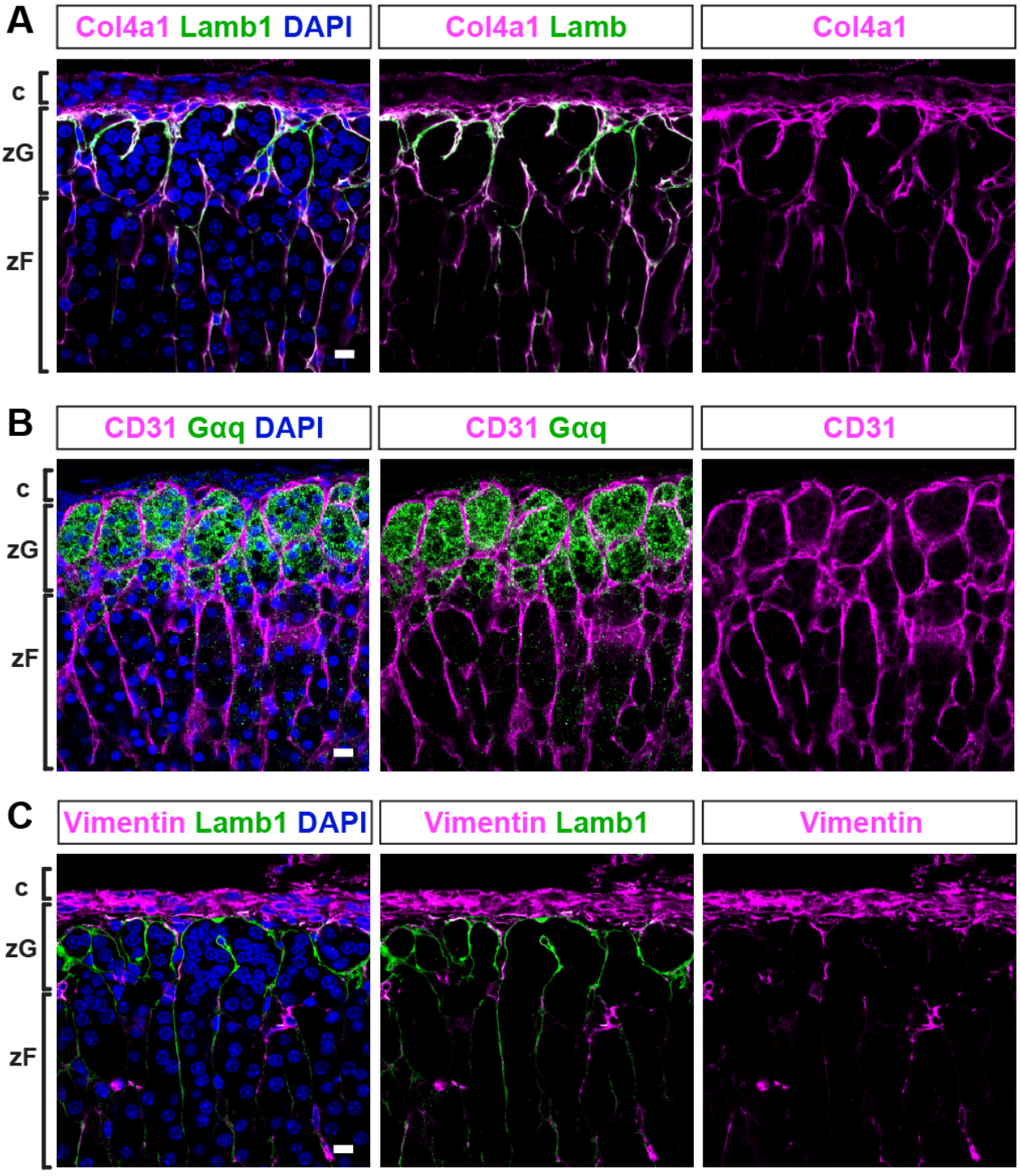

Figure S1.2. Adherens junction components are enriched at rosette centers. (A) N-cadherin and K-cadherin are predominantly expressed in the zG. Dotted lines denote zG and zF boundary. c, capsule. (B) E-cadherin is not present in the adrenal cortex. A mouse small intestine tissue section was used as positive control for E-cadherin staining. Intestinal crypts are highlighted by a dotted line. (C) β-catenin staining of a human adrenal section shows rosette structures. Boxed area is shown on the right. (D) K-cadherin staining of a Peruvian mouse adrenal section showing a rosette. Boxed area is shown on the right. Arrows point to rosette centers. All bars, 10μm.

Figure S1.2 (continued)

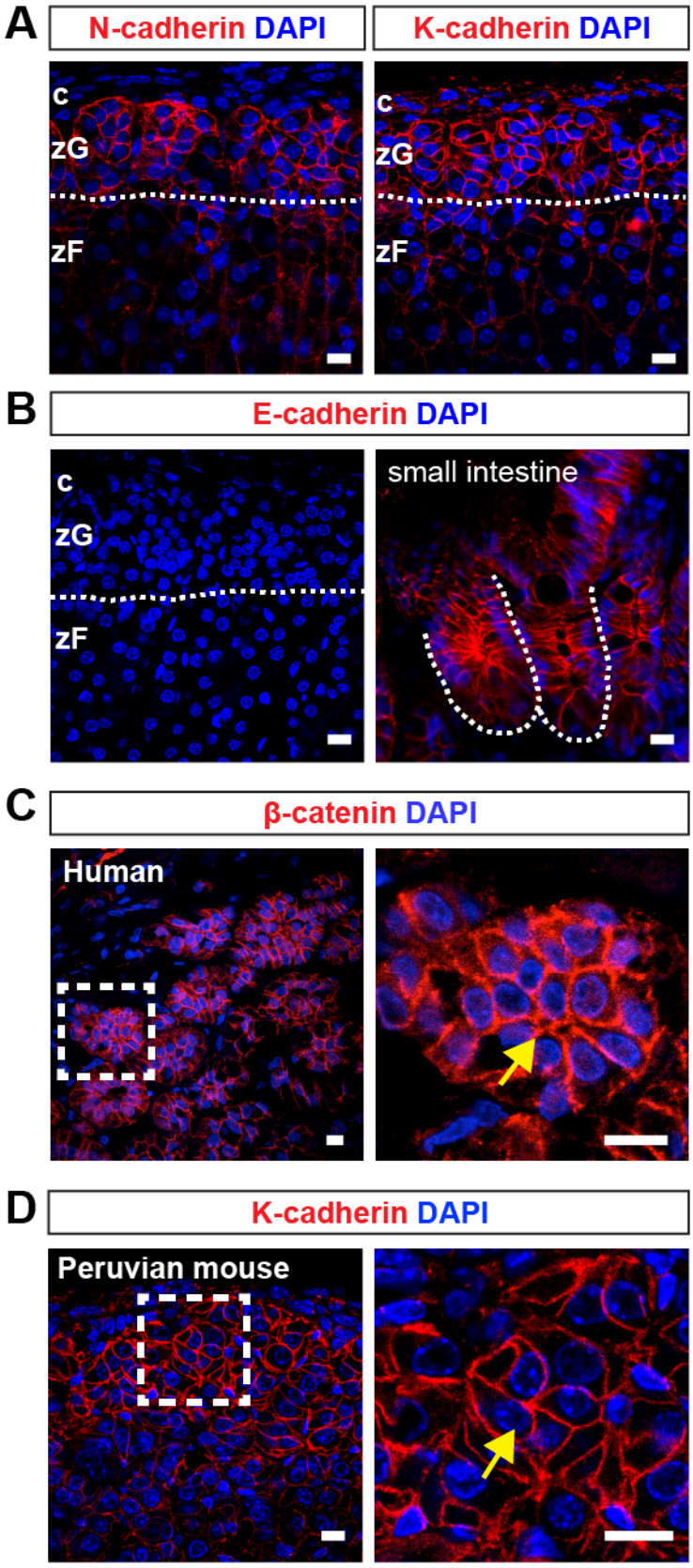

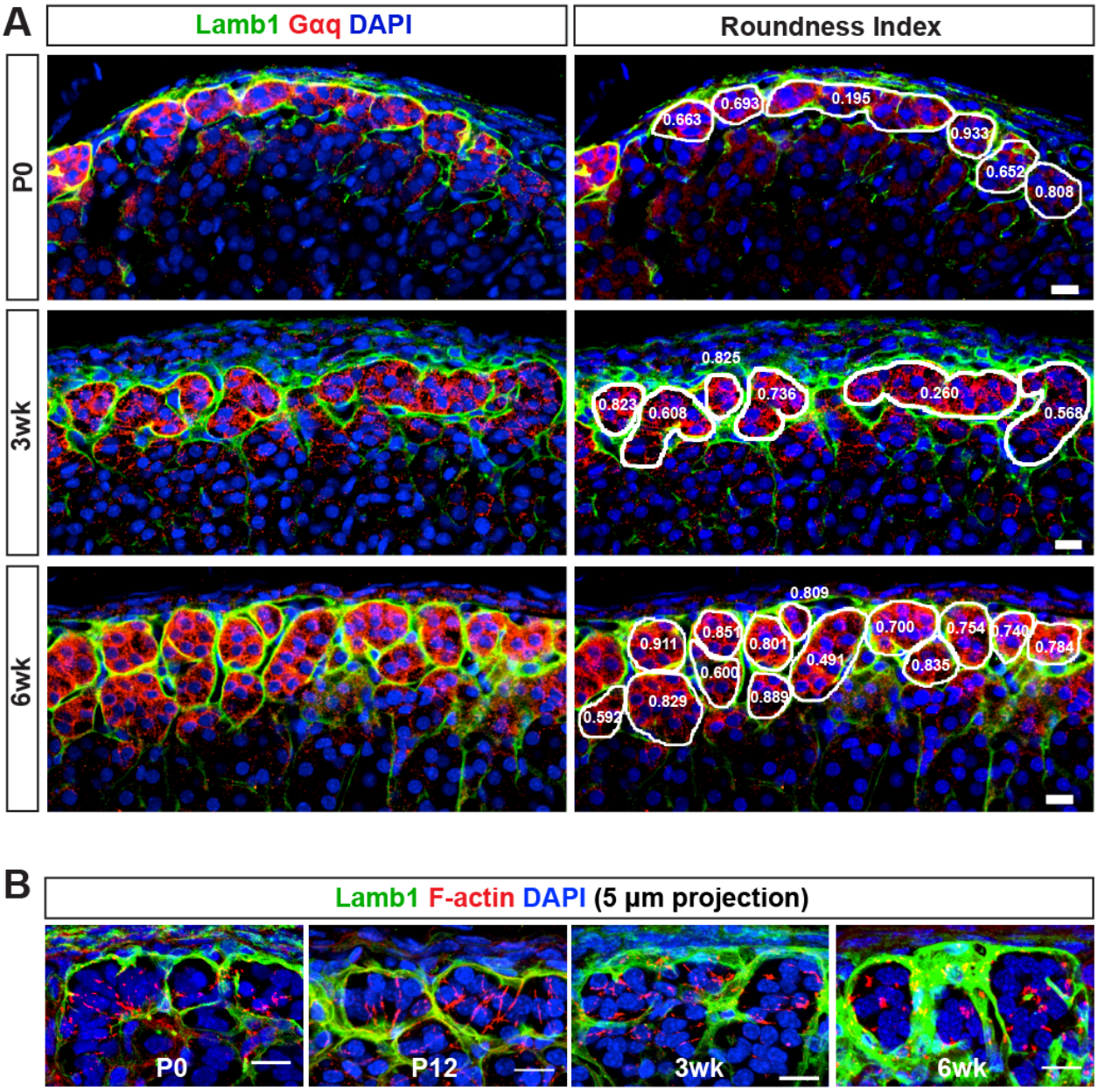

Figure S1.3. Rosette formation underlies glomerular morphogenesis. (A) Left, Lamb1 and Gαq staining shows progression of morphogenesis at indicated stages. Right, examples of hand-traced glomerular outlines and corresponding roundness index. (B) Top, F-actin (red) and Lamb1 (green) staining shown as maximum intensity projections of 5µm confocal Z-stacks. All bars, 10µm.

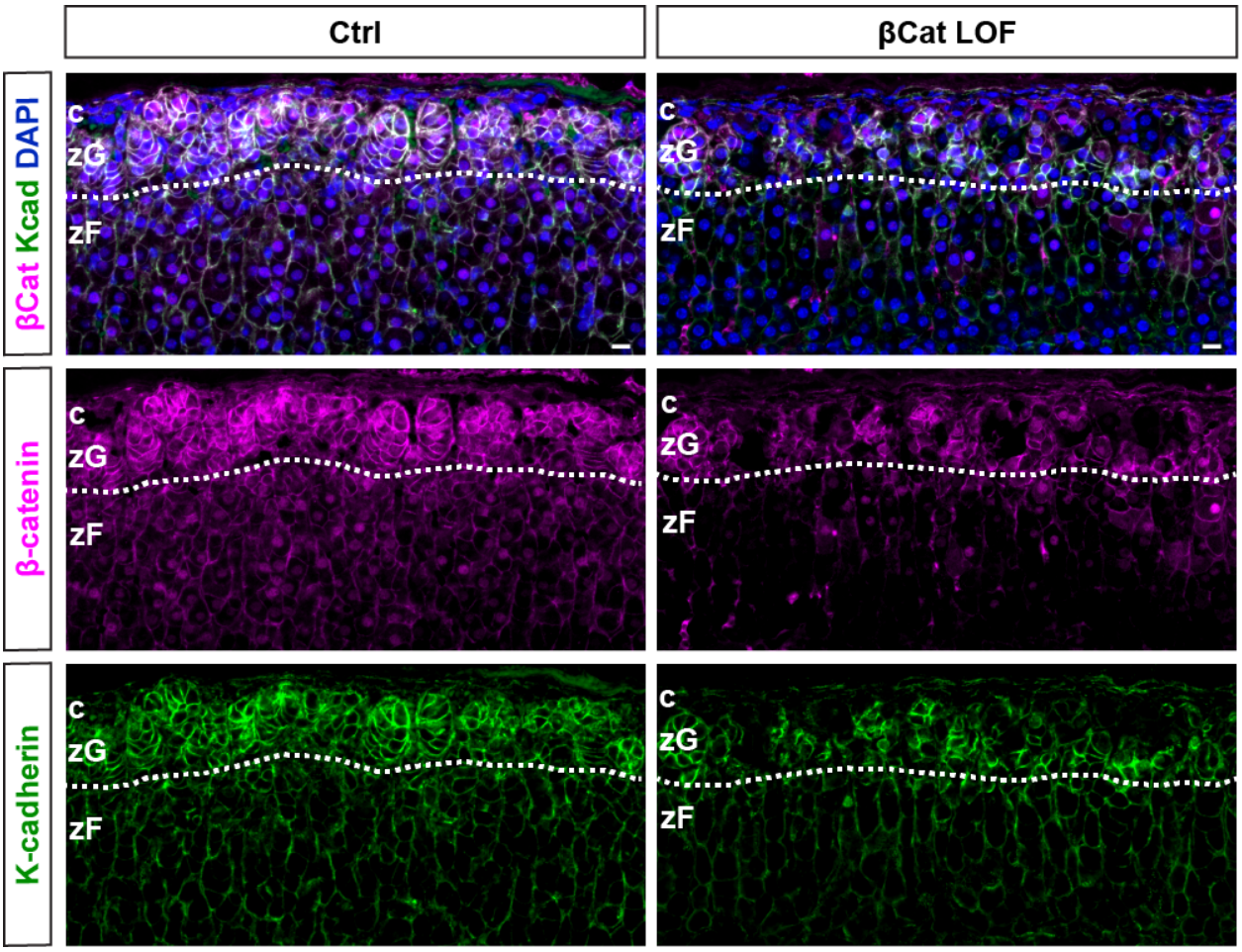

Figure S1.4. β-catenin LOF results in loss of K-cadherin. β-catenin (magenta) and K-cadherin (green) immunostaining in control and βCat LOF adrenals. DAPI (blue), nuclei. Dotted lines denote zG and zF boundary. c, capsule. Bars, 10μm.

Figure S1.5. β-catenin stabilization results in increased rosette frequency in males. (A) Lamb1 staining (green) shows expanded glomerular morphology in male β-catenin gain-of-function (GOF) adrenals. (B) Measurement of zG thickness in males. Two sample *t*-test, $p<0.01$. (C) Measurement of glomerular cross section roundness in males. Mann-Whitney non-parametric test, ns, not significant. (D) Measurement of glomerular cross section area in males. Mann-Whitney non-parametric test, ns, not significant. (E) Quantification of rosette frequency per 40X z-stack (160x160x10 μm^3) in males. Two sample *t*-test, $*p<0.05$. (F-G) K-cadherin (F) and N-cadherin (G) expression domains are expanded in βCat GOF adrenals in both males and females. All bars, 10μm.

Figure S1.5 (continued)

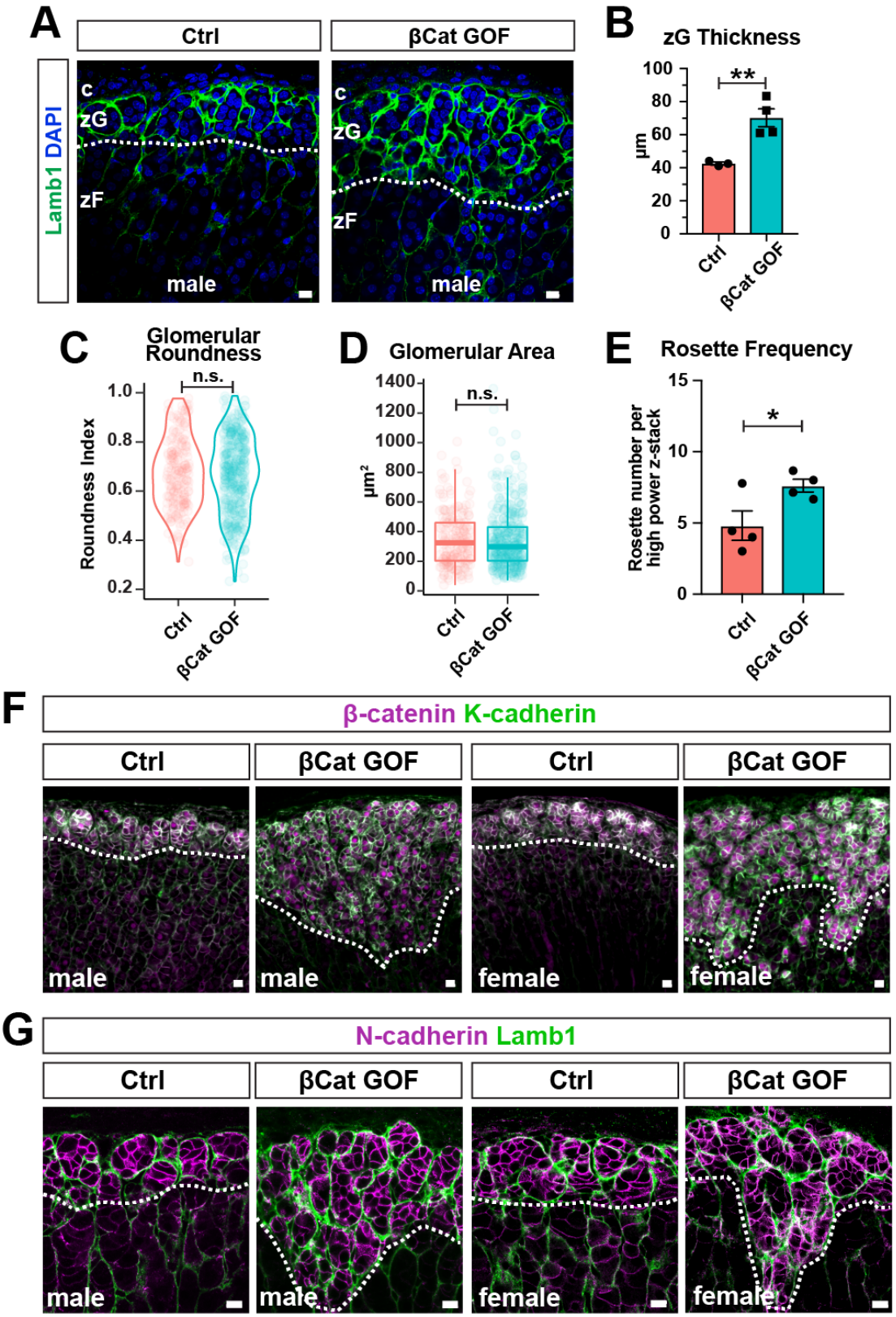

Figure S1.6. Genes associated with epithelial morphogenesis and Wnt signaling pathway. (A) Heatmap of genes representing the GO term “epithelial morphogenesis”. (B) Heatmap of genes representing the GO term “Wnt signaling pathway”. (C) qRT-PCR validation of selected genes. Two sample *t*-test followed by Bonferroni’s multiple comparison correction, *$p < 0.05$, **$p < 0.01$.

Figure S1.6 (continued)

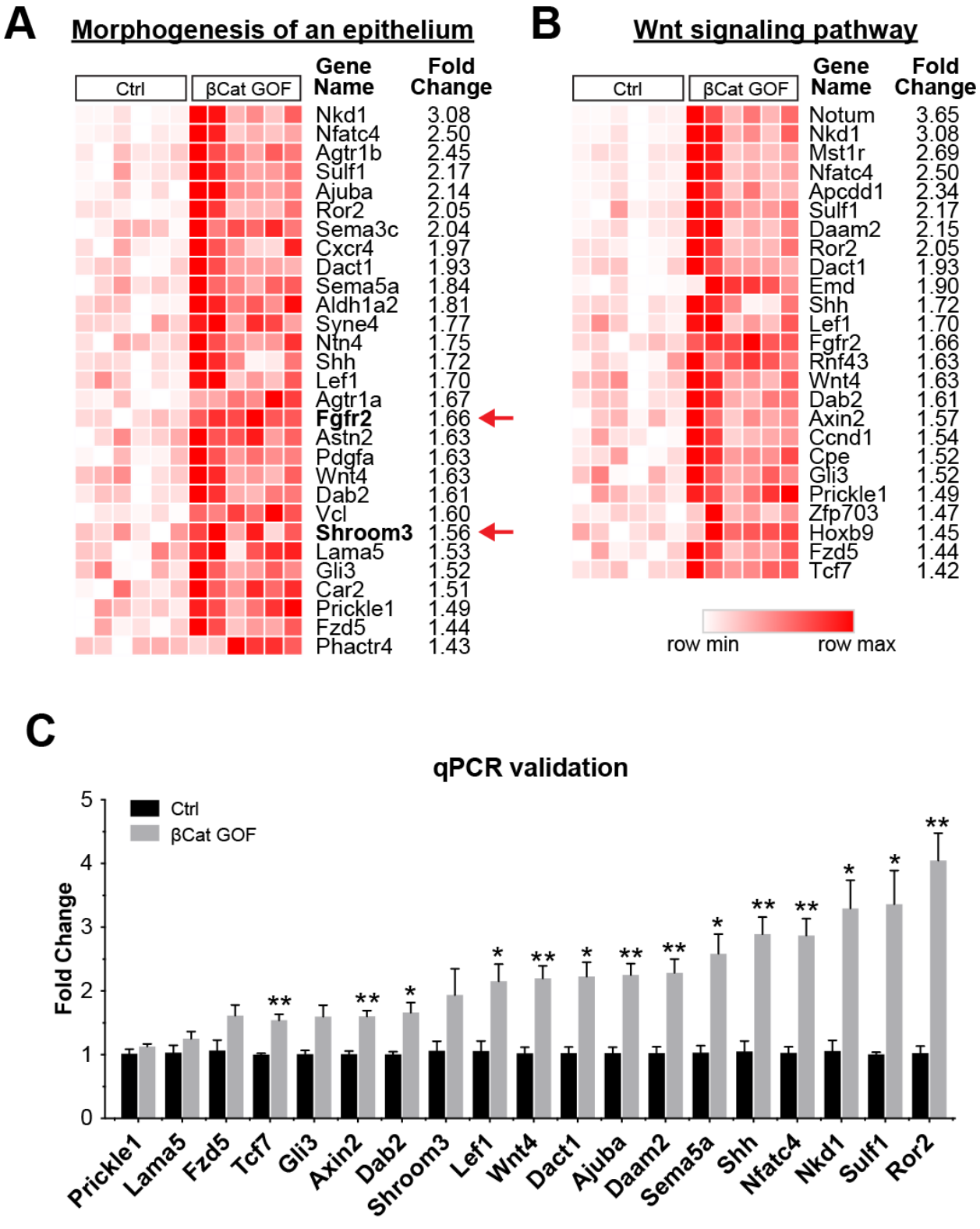

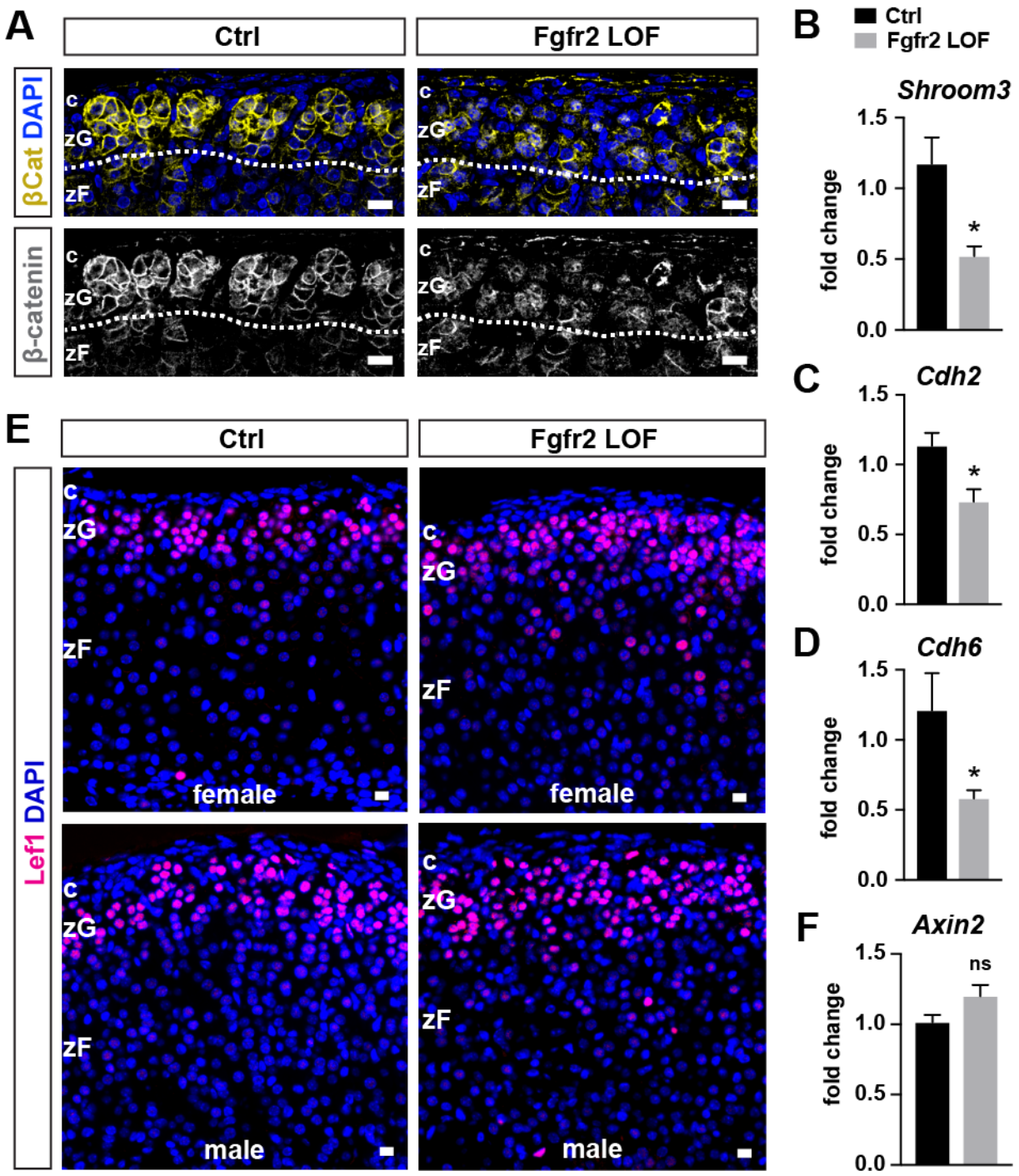

Figure S1.7. Fgfr2 is required for AJ stability and does not affect canonical Wnt signaling.

(A) Membrane β-catenin staining is lost from zG cells in Fgfr2 LOF adrenals. (B-D, F) qRT-PCR analysis of *Shroom3, Cdh2*, *Cdh6, Axin2* from whole gland RNA extract. Two sample *t*-test, ns, not significant, *p<0.05. (E) Lef1 staining reveals no change. All bars, 10μm.

Appendix II:

Supplemental Figures for Chapter Three

Figure S2.1. Stabilization of β-catenin in zG cells results in zG expansion. (A) Quantification of the β-catenin-positive region, normalized by cortical area, (*n* = 5-9 mice). (B) Representative cortical sections from female (*n* = 15) and male (*n* = 3) mice stained for β-catenin (β-cat, red). (C) Representative cortical sections co-stained for Gαq (green) and β-catenin (red) (left panels) or Dab2 (red), (right panels, *n* = 3 mice). DAPI (blue), nuclei. Dotted lines define the border between positive and negative regions for β-catenin or Dab2, as indicated. c, capsule. zG, zona Glomerulosa. zF, zona Fasciculata. Scale bars: 50 μm. Statistical analysis was performed using an unpaired Student's *t*-test or Mann-Whitney test. ***$P < 0.001$; ****$P < 0.0001$.

Figure S2.1 (continued)

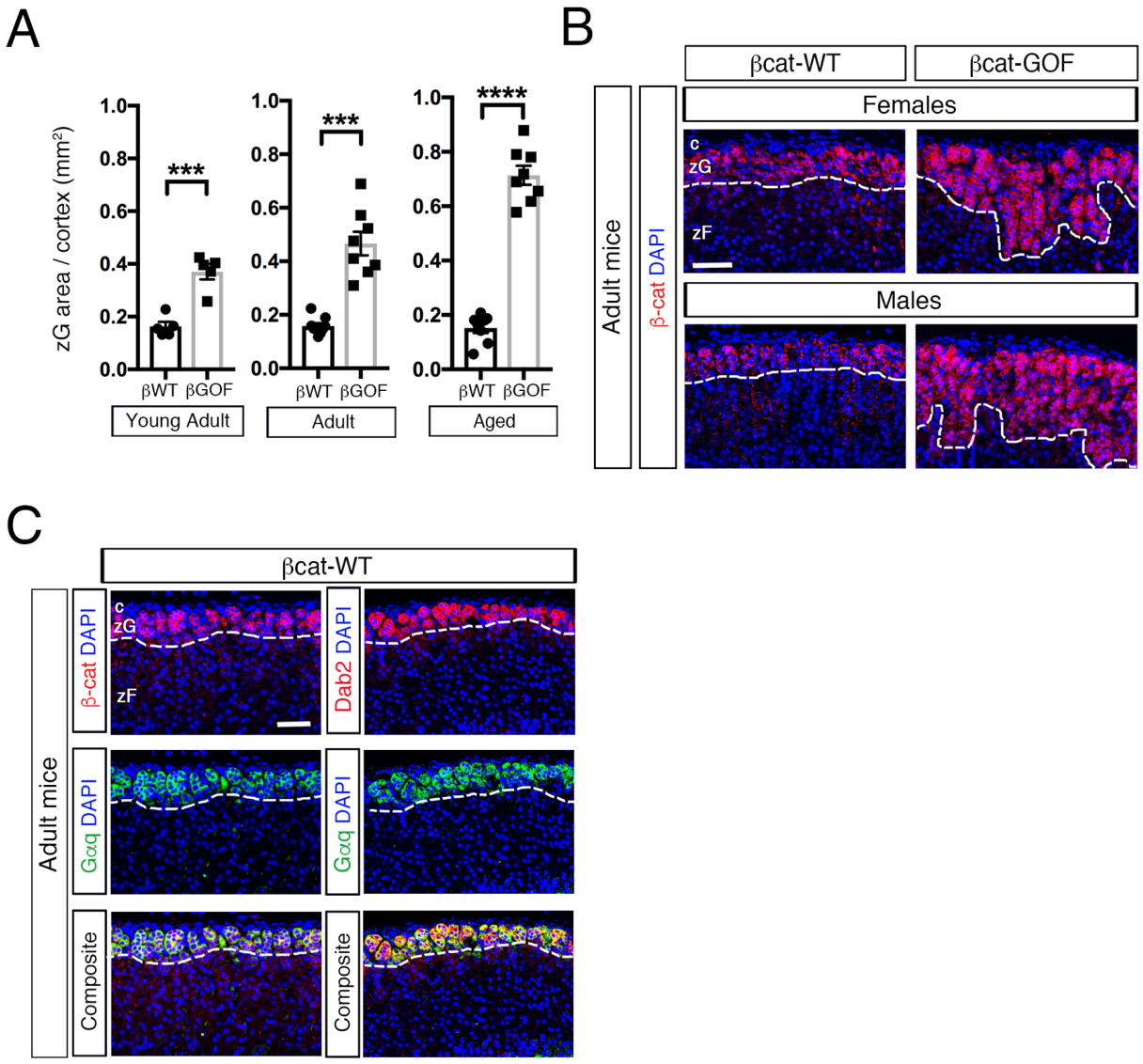

Figure S2.2. Blood pressure and Localization of AS+ cells in βcat-GOF mice. (A) Quantification of plasma aldosterone levels in 5-week-old (*n* = 5) and 10-week-old (young adult, *n* = 5-6) mice. (B and C) Diastolic and mean arterial blood pressure (BP) measured by carotid catheterization in anesthetized adult and aged mice (*n* = 4-8). (D) Representative adrenal sections were co-stained for AS (green) and β-catenin (β-cat, red) from aged mice (*n* = 4- 8). All sections are counter-stained with nuclear DAPI (blue). Statistical analysis was performed using an unpaired Student's *t*-test or Mann-Whitney test. *$P < 0.05$; **$P < 0.01$.

Figure S2.2 (continued)

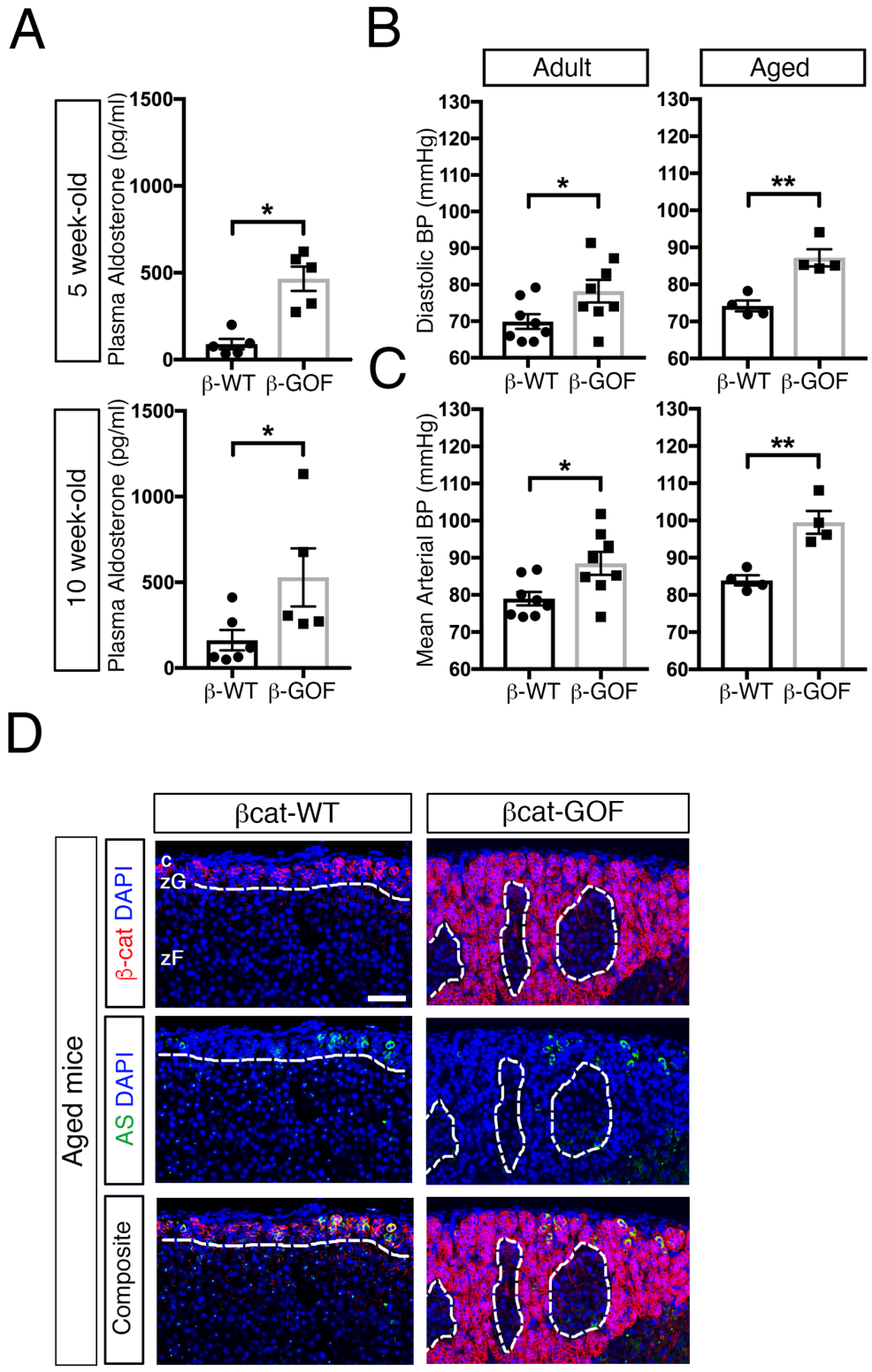

Figure S2.3. Analysis of cellular proliferation and apoptosis following β-catenin stabilization. (A) Quantification of the total Ki67-positive cells per cortical area, (*n* = 5-9 mice). (B) Representative adrenal sections were stained for activated Caspase 3-positive (green), (*n* = 4 mice). (C) Quantification of activated Caspase 3-positive cells from (C) per cortical area, (*n* = 4 mice). (D) Representative adrenal sections were stained for TUNEL (green), (*n* = 3 mice). (E) Quantification of TUNEL-positive cells from (E) per cortical area, (*n* = 4 mice). All sections are counter-stained with nuclear DAPI (blue) Scale bar: 200 μm. Scale bar in magnified insets: 50 μm. *ns,* not significant. Statistical analysis was performed using an unpaired Student's *t*-test or Mann-Whitney test. **P* < 0.05; ***P* < 0.01.

Figure S2.3 (continued)

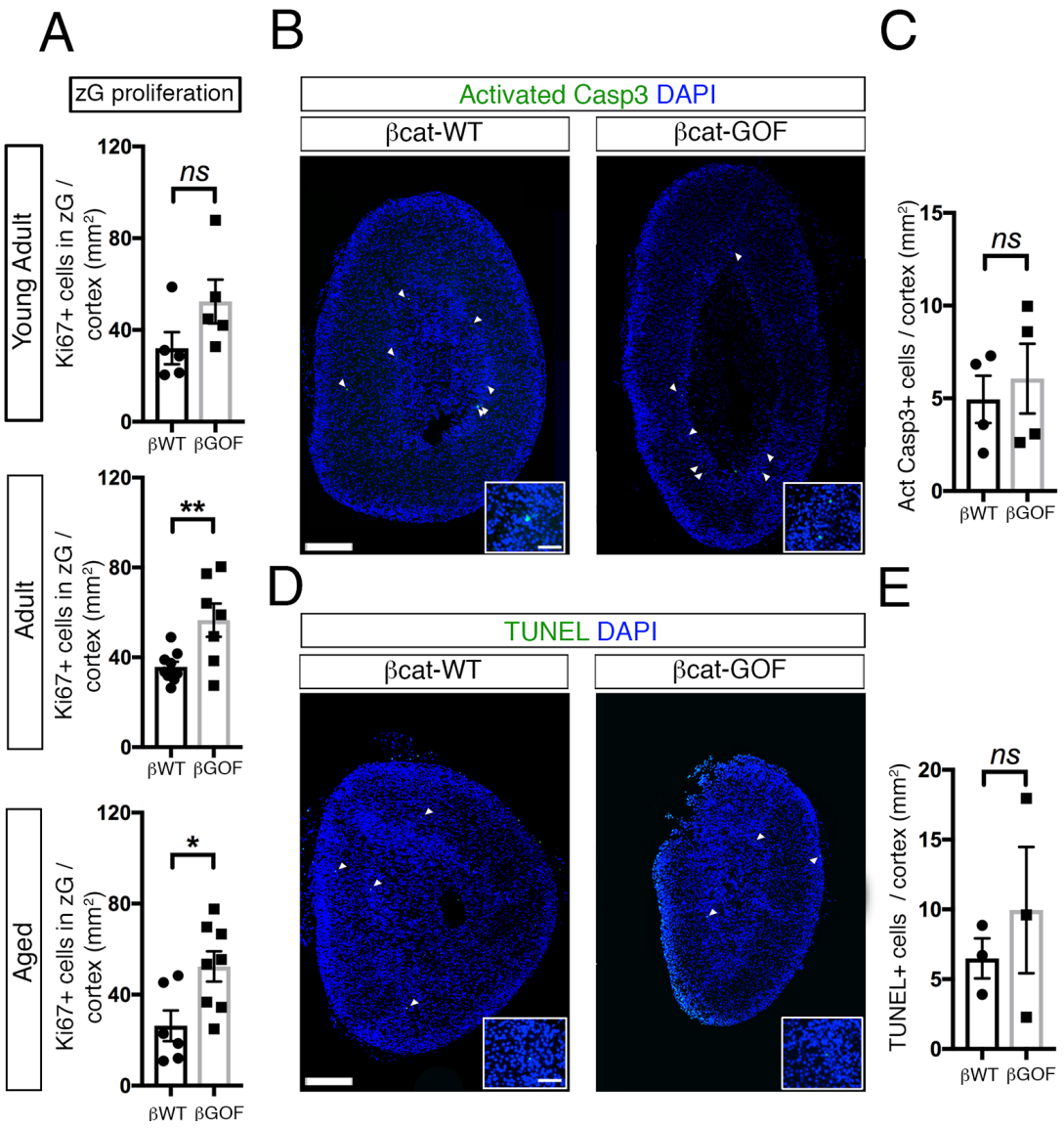

Figure S2.4. Genetic activation of the RAAS results in accelerated zG expansion. (A and B) Representative gross images and weight of adrenal glands from adult and aged mice (*n* = 6-17). (C) Red channel from Figure 3.4E stained for β- catenin. (D) Green channels from Figure 3.4E stained for Ki67, arrowheads mark positive cells. (E) Representative adrenal sections were co-stained for Dab2 (red) and GFP (green) in young adult mice (*n* = 3). All sections were counter-stained with nuclear DAPI (blue). The dotted lines define the border between positive and negative regions for β-catenin or Dab2, as indicated. zG, zona Glomerulosa. zF, zona Fasciculata. Scale bars: 50 μm, unless indicated in the figure. Statistical analysis was performed using a one-way ANOVA test in conjunction with a Tukey's range test. $^{**}P < 0.01$; $^{***}P < 0.001$; $^{****}P < 0.0001$.

Figure S2.4 (continued)

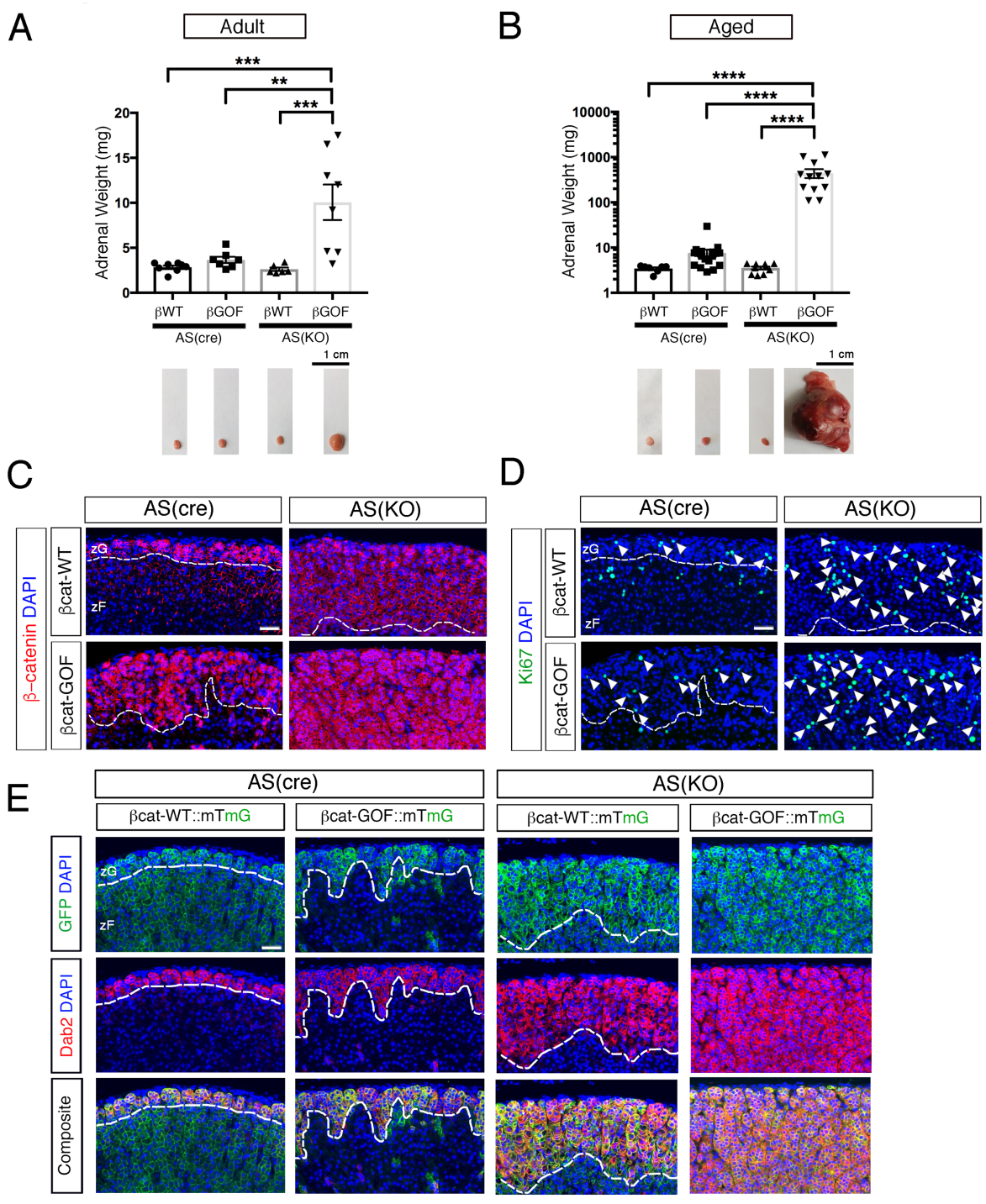

Figure S2.5. Spironolactone and low-salt diet activate RAAS and increase zG proliferation in βcat-GOF mice. (A) Representative adrenal sections co-stained for AS (green) and β-catenin (β-cat, red) from animals treated with spironolactone or low-salt, compared to non-treated animals, (*n* = 5-9). (B) Quantification of the total AS-positive cells per cortical area, (*n* = 5-9 mice). C) Red channel from Figure 3.5E stained for β-catenin. (D) Green channels from Figure 3.5E stained for Ki67, arrowheads mark positive cells. (E) Adrenal gland weights from adult mice following treatments as indicated, (*n* = 6-7 mice). (F) Schematic representation of the effect of RAAS activation following spironolactone or low-salt diet in a β-catenin GOF setting. Light blue circles represent zG cells. Red circles represent zF cells. Blue nuclei indicate proliferating cells, representative of Ki67-positive cells shown in (D) and Figure 3.5E. Arrows indicate the ongoing process of zG-to-zF cell transdifferentiation, which allows zG cells to migrate into the zF. Transdifferentiation is blocked in βcat-GOF adrenals, as indicated by the "T" symbol. zG proliferation index (total number of Ki67-positive cells normalized by zG area) is decreased in zG of βcat-GOF compared to controls, and increased in βcat-GOF exposed to activated RAAS. All sections were counter-stained with nuclear DAPI (blue). The dotted lines define the border between β-catenin-positive and negative regions. zG, zona Glomerulosa. zF, zona Fasciculata. Scale bars: 50 μm. Statistical analysis between genotypes was performed using an unpaired Student's *t*-test or Mann-Whitney test (significance displayed with asterisks or *ns*). Statistical analysis between treatment groups was performed using a one-way ANOVA in conjunction with a Tukey's range test (significance displayed with hash symbols). *ns*, not significant. **P* < 0.055; ##*P* < 0.01; ####*P* < 0.0001.

Figure S2.5 (continued)

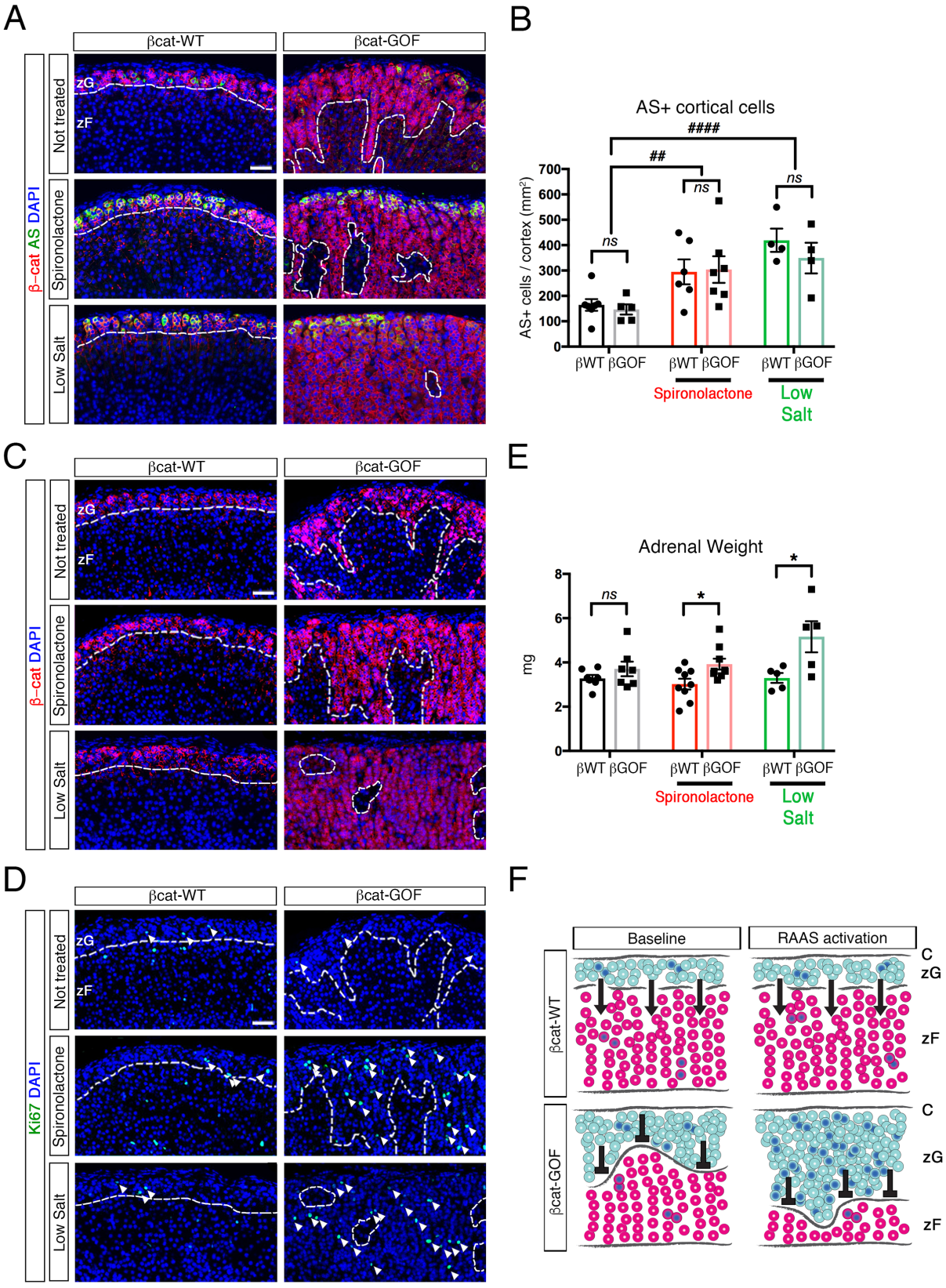

Appendix III:

Coordinated Calcium Burst Firing of zG Cell Ensembles within the Aldosterone Producing Adrenal Rosette

Coordinated Calcium Burst Firing of zG Cell Ensembles within the Aldosterone Producing Adrenal Rosette

Nick A. Guagliardo[1], Peter M. Klein[1,3], Christina A. Gancayco[2], Adam Lu[1,3], Sining Leng[4], Rany M. Markem[1], David T. Breault[4], Paula Q. Barrett[1] and Mark P. Beenhakker[1,3]

Departments of [1]Pharmacology and [2]Medicine-Research Computing, University of Virginia, Charlottesville, VA, USA. [3]Neuroscience Graduate Program, University of Virginia, Charlottesville, VA, USA [4]Division of Endocrinology, Boston Children's Hospital, Boston, MA, USA and Harvard Stem Cell Institute, Cambridge, MA, USA.

Attributions

This appendix contains the manuscript titled "Coordinated Calcium Burst Firing of zG Cell Ensembles within the Aldosterone Producing Adrenal Rosette", submitted to Journal of Clinical Investigation in April, 2019. Experiments were conceived and designed by NAG, PMK, PQB, MPB, and DTB. DTB provided $AS^{Cre/+}$ mice. Calcium imaging experiments were conducted by NAG, PMK and RRM, immunohistochemistry by SL. NAG, CAG, AL, PMK, MPB, PQB contributed to the analysis of data and interpretation of results. MPB, PQB, NAG wrote the manuscript, with editing contributions from all authors.

Abstract

Within the adrenal gland, the aldosterone-producing zona glomerulosa (zG) cells arrange in distinct clusters, termed rosettes, that provide a structural framework for adrenal cortex plasticity. Whether this organization serves a functional role in signaling remains unexplored. To determine if structure informs function, we generated mice with zG-specific expression of GCaMP3 and imaged zG cells within their native rosette structure. Angiotensin II (Ang II) evoked periodic Ca_v3-dependent calcium oscillations (spikes) and bouts of spikes (bursts). Ang II dose-dependently increased the number of active cells and the number of bursts/active cell but the number of spikes per burst and burst duration remained dose-invariant. Thus, Ang II regulated zG cellular activity by controlling burst occurrence. We evaluated a role for the rosette in burst signaling by altering cell-cell connections. Perturbation of N-cadherin interactions shortened only the duration of Ang II-evoked bursts, suggesting that rosette architecture supports activity prolongation. The significance of the rosette to zG cell calcium activity was underscored further by the temporal correlation of Ang II-evoked spikes within a rosette. Together, these data define the calcium burst as the fundamental unit of zG layer activity evoked by Ang II, and highlight a new role for the rosette in zG-layer calcium signaling.

Introduction

The aldosterone-producing zona glomerulosa (zG)-layer of the adrenal gland is in a constant state of self-renewal (1). Capsular mesenchymal stem cells continuously enter the layer and zG-lineage (1, 2). Fully differentiated zG cells exit the zG-layer, transdifferentiating into bona-fide corticosterone-producing zona fasciculata cells (3). Low sodium and high potassium diets drive zG-layer expansion whereas high sodium and low potassium diets permit its reciprocal contraction (4, 5). Therefore, it is not surprising that the zG-layer anatomically organizes its cell

collectives into rosettes, a higher order structure and common intermediate in organogenesis (6).

Rosette formation is driven by cytoskeleton rearrangement (7). Although the cues responsible for such rearrangements remain ill-defined, the actin-myosin network within these multicellular structures remains highly dynamic. This plasticity provides architectural stability while accommodating layer remodeling and centripetal cellular migration (7, 8). In contrast to rosettes facilitating embryonic tissue development that are rapidly resolved, rosettes facilitating tissue homeostasis are more persistent (6). In the adrenal gland, the structure of the zG layer develops postnatally and the architectural unit of the layer, the rosette, is maintained throughout adulthood (9). Whether the rosette structure of the zG-layer plays a role beyond tissue remodeling and homeostasis remains unexplored.

Based on the behavior of isolated zG cells and the absence of gap junctions in the zG-layer (10, 11), the conventional view has emphasized the quiescence and autonomy of zG cells (11). Numerous electrophysiological studies of zG cells isolated from human, bovine and rodent glands have shown that zG cells maintain a steady hyperpolarized membrane voltage that can be baseline shifted by hormones such as Angiotensin II (Ang II), or drugs such as potassium channel blockers (12). In agreement with this reported behavior, isolated zG cells respond to Ang II by producing a large, transient rise in intracellular calcium that is followed by a small, sustained increase in most isolated cell studies (12). By contrast, some studies report a second, less common phenotype in which a small percentage of cells display brief oscillatory changes in intracellular calcium following application of low doses of Ang II (12-15).

We recently demonstrated by patch-clamp electrophysiology that within the layer, zG cells are excitable and display large rhythmic changes in membrane voltage that are slow in periodicity (seconds) and require Cav3.2 channel activity (16). Our studies confirmed and extended previous findings in which sharp electrode voltage recordings demonstrated zG cell excitability in feline adrenal slices (17). Motivated by these key findings and the premise that multicellular assemblies often do not simply reflect the additive behavior of single cells, we studied the ensemble signaling behavior of individual zG cells within the community structure of the rosette. We measured intracellular calcium, the critical signal that drives the production of aldosterone, in adrenal tissue slices expressing the genetically encoded calcium reporter, GCaMP3. We find that Ang II, the major regulator of aldosterone production from the zG-layer, elicits a stereotypic zG cell oscillatory calcium response that is concentration dependent. However, this dependence does not manifest as a simple change in oscillation frequency as is primarily observed with intrinsic electrical oscillators. Instead, we show that while zG oscillation frequency is fixed across Ang II concentrations, oscillatory events are organized into sustained bouts of activity, the occurrence of which changes with concentration. Finally, we provide evidence for the hypothesis that the adrenal rosette, a dynamic multi-cellular arrangement of zG cells, can promote coordinated bouts of activity among its constituent cells.

Results

Ang II Generates Periodic Intracellular Calcium Signals in zG cells

We used a transgenic approach to study the regulation of intracellular calcium in zG cells that are retained within their native rosette structure. Mice in which Cre recombinase was targeted to the Cyp11b2 (AS, aldosterone synthase) genomic locus (3) were crossed with floxed GCaMP3 mice to generate a mouse line ($AS^{Cre/+}$::$ROSA26^{floxGCaMP3/HZE}$, zG-GCaMP3) in which GCaMP3 was targeted to zG cells. We used wide-field imaging to capture calcium-dependent fluorescent

Figure S3.1. Ang II-elicited Ca^{2+} signaling in zG cells expressing GCaMP3. (A) Photomicrograph (63x magnification) of adrenal slice from a zG-GCaMP3 expressing mouse before Ang II stimulation. Individual cells within rosettes can be distinguished by their dark nucleus, surrounded by cytosolic GCaMP3; exemplar rosette highlighted by dashed circle. Scale bar: 20μm. (B) Representative trace of fluorescence intensity (top) imaged in a zG cell before and after stimulation with 3nM Ang II (red line, 90 seconds after start of record) and corresponding raster plot (middle) of Ca^{2+} spikes captured at 20 Hz for 10 mins. (bottom) Spectrogram of oscillation frequency after Fourier transformation. A magnification of the region indicated by dashed red rectangle is provided on the far right. (C) Raster plot of Ca_{2+} spikes (left) and corresponding spectrogram of oscillation frequencies (right) from all cells measured in a single adrenal slice. Red line indicates when 3nM Ang II was added to the bath solution. Scale bar: 60s. **(D)** Frequency distribution of inter-calcium spike intervals (0.1 min bins) elicited by 3nM Ang II is normally distributed (mean±SEM [Hz]: 0.519±0.006, *n* = 24,052).

Figure S3.1 (continued)

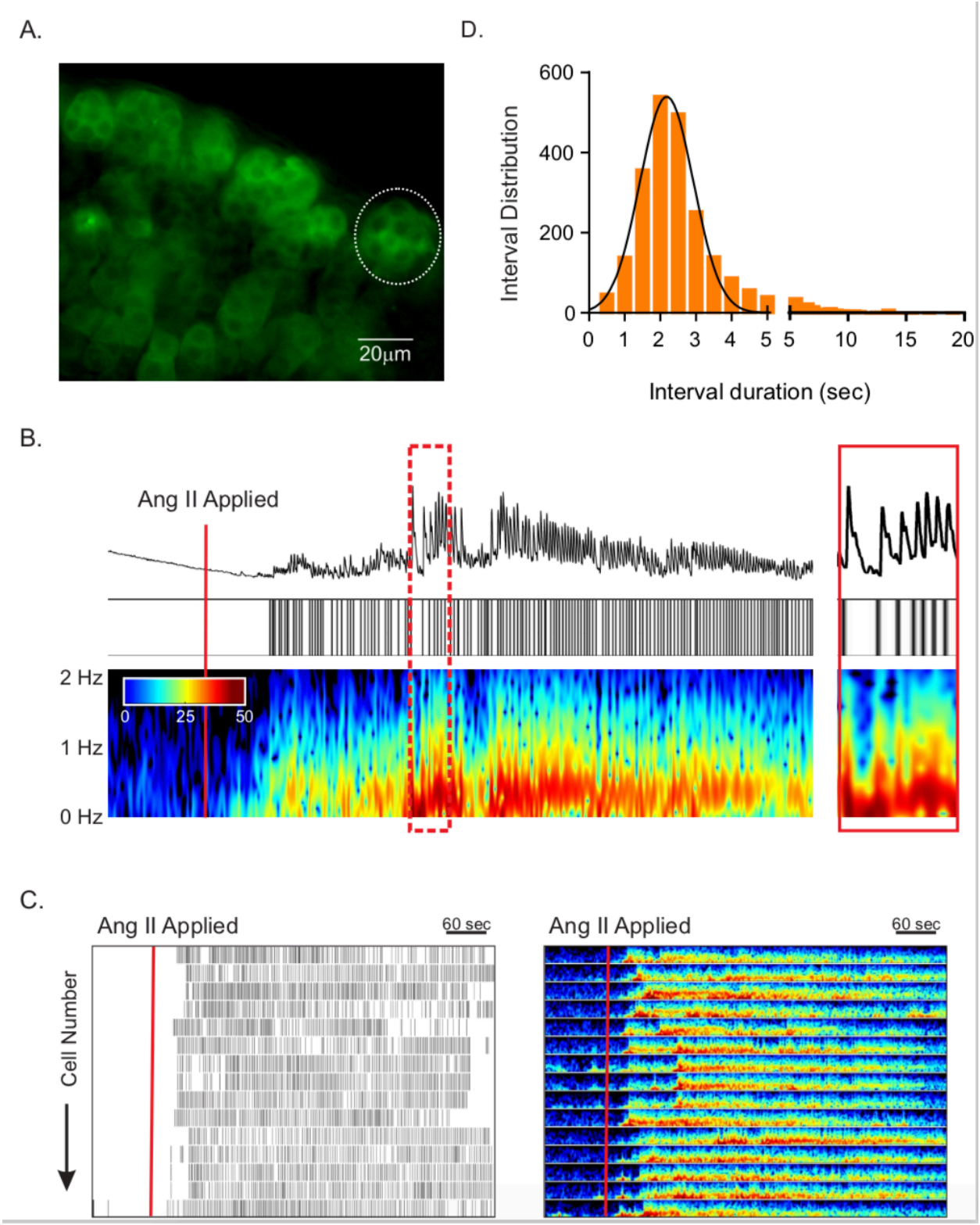

signals in the zG-layer of adrenal slices acutely prepared from zG-GCaMP3 mice. An example of such a slice is shown in **Figure S3.1A** in which the dark nuclei and the bright cytosolic fluorescence enhances the visualization of each cell and the rosette structure of the zG layer. Because Ang II is the major regulator of zG cell activity, we recorded the calcium activity of individual zG cells before and during stimulation with Ang II.

We observed few calcium signals among zG cells during basal, unstimulated conditions. However, exposure to 3nM Ang II produced robust, periodic calcium oscillations in all recorded zG cells (**Figure S3.1B, C**; see Supplemental Video 1). Within an exemplar zG cell, oscillations began within 90 seconds and reached a steady oscillatory state within 5 minutes of Ang II exposure during which time the cell generated prominent ~0.5Hz calcium oscillations (**Figure S3.1B**). The peak of each visible oscillatory calcium signal within a slice was detected (see Methods) and is presented in raster plot format in which each row displays the activity of a single cell and each mark the timing of an individual oscillatory event, referred to here as *calcium spikes* (**Figure S3.1C, left panel**). Applying this analysis to all recorded zG cells within the slice demonstrated unambiguously that the response to 3nM Ang II is highly stereotyped (**Figure S3.1C, right panel**); all cells oscillated within a narrow frequency bandwidth. In agreement with this 0.5Hz dominant oscillation frequency reported by Fourier transformation of the raw signals, the distribution of inter-calcium spike intervals among all recorded zG cells within the adrenal slice was normally distributed with a mean value of 2.2 seconds (**Figure S3.1D**).

We next sought to characterize the aggregate Ang II-evoked activity of zG cells within a slice. As is evident in the composite raster showing the activity of four representative cells from each hormone concentration, overall activity increased with dose (**Figure S3.2A**). To further quantify

Figure S3.2. Ca^{2+} spikes elicited by Ang II are dose dependent and require $Ca_V3.2$ channel activity. (A) Representative raster plot of Ca^{2+} spikes after application of 50pM, 300pM, 3nM, or 1μM Ang II. (B) Mean events/cell dose dependently increases with Ang II (50pM: *n* = 5 slices, 94 cells; 300pM: *n* = 6 slices, 247 cells; 3nM: *n* = 8 slices, 165 cells; 1uM: *n* = 4 slices, 90 cells); 2-way ANOVA: P<0.0001 indicating an overall effect of time and dose. (C) Raster of representative cells and (D) mean events/cell with application of the $Ca_V3.2$ channel antagonist TTA-P2 (10μM). TTA-P2 (applied at 4.5 min) inhibits Ca^{2+} spikes elicited by 3nM Ang II (applied at 1.5 min). TTA-P2: *n* = 4, 96 cells; No TTA-P2: *n* = 4, 90 cells; 2-way ANOVA: P<0.0001 for overall effect of time and drug. (E) 20μM CPA did not inhibit Ca^{2+} spikes, indicating intracellular Ca^{2+} stores are not required for Ca^{2+} oscillations. CPA: *n* = 5 slices, 89 cells; No CPA: *n* = 5 slices, 106 cells; 2-way ANOVA: P=0.94 for CPA effect. (F) Fraction of total cells that responded to 1μM Ang II; mean±SEM: 50pM: 0.19±0.03, *n* = 7 slices; 300pM: 0.44±0.01, *n* = 7 slices, 3nM: 0.89±0.02, *n* = 8. One-way ANOVA, P < 0.001; Tukey's multiple comparisons test: 50pM vs 300pM: P < 0.001, 50pM vs 3nM: P < 0.001, 300pM vs 3nM: P < 0.001. (B, D-F) Mean data from each mouse were represented as a single point in calculating N/experimental condition.

Figure S3.2 (continued)

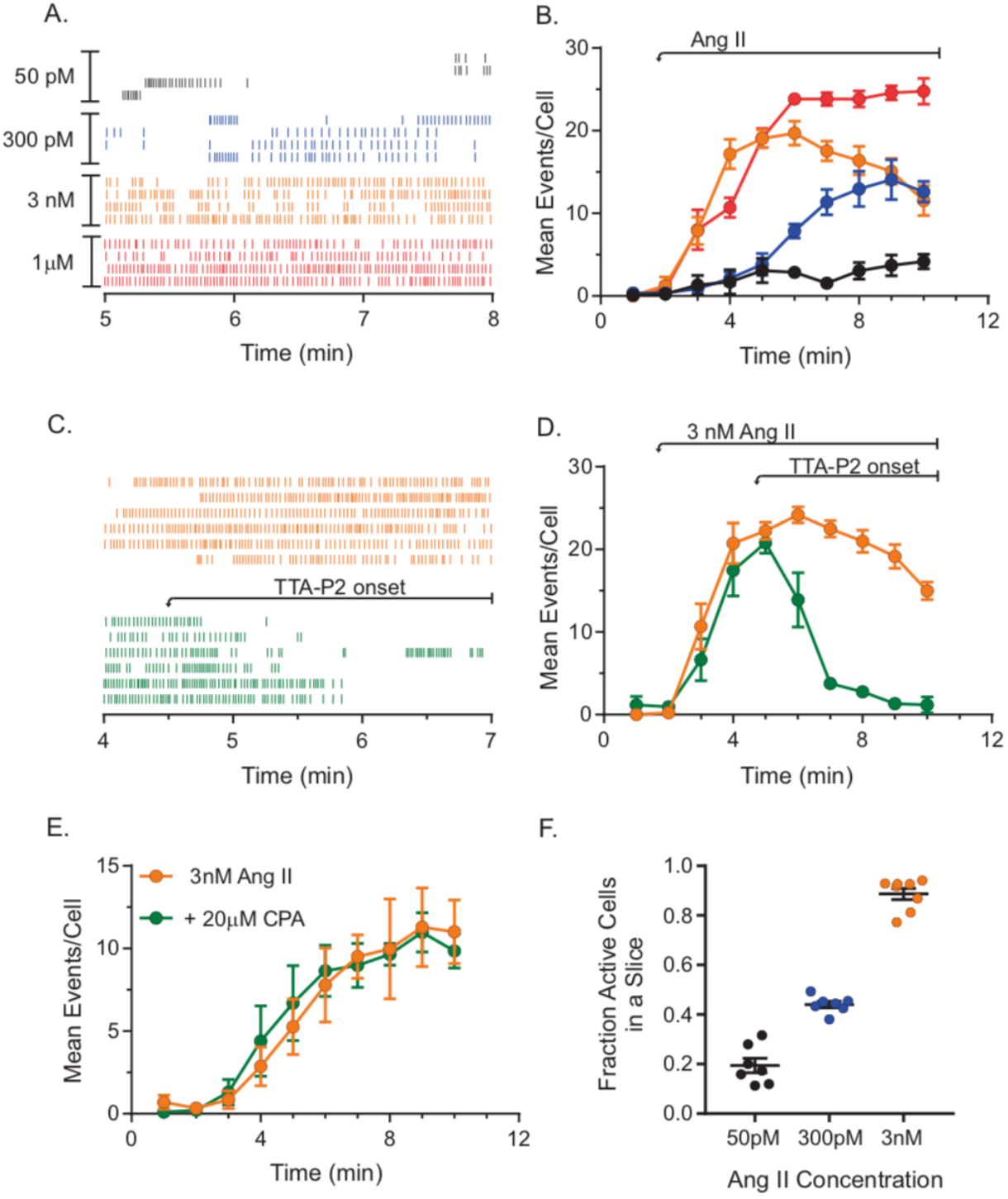

activity, we determined the mean number of spikes per minute of each recorded zG cell within a slice and then averaged across slices from different animals (**Figure S3.2B**). Both a dose- and time-dependence was observed; zG cell calcium spikes became more numerous with increasing concentrations of Ang II and were evoked with a shorter latency (**Figure S3.2A, B**). Consistent with electrophysiological recordings of zG cells (16), Ang II-evoked calcium oscillations were dependent on Cav3 calcium channels, as such activity was abolished by the pan Cav3 family antagonist, TTA-P2 (18) (**Figure S3.2C, D**). By contrast, preincubation with cyclopiazonic acid (CPA), an inhibitor of SERCA ATPase (19), did not reduce the subsequent number of evoked zG calcium oscillations, indicating that the generation of calcium spikes was not dependent on endoplasmic reticular calcium stores (**Figure S3.2E**). Together, these data suggest that in the rosette, Ang II evokes graded oscillatory calcium responses that are in strong agreement with previously described voltage oscillations (16).

Upon closer inspection of calcium spike raster plots, we observed that at lower Ang II concentrations zG cells are still capable of producing robust bouts of oscillatory calcium activity (**Figure S3.2A**). However, at these lower concentrations, not only did oscillatory bouts occur infrequently within individual zG cells, but fewer zG cells were active within a slice (**Figure S3.2F**). To quantify the number of active zG cells across concentrations, we recorded the activity of each slice at a single, submaximal dose of Ang II and then in response to a maximal dose of 1μM. We determine fractional activation by normalizing the number of active zG cells observed at each experimental concentration (i.e. 50pM, 300pM and 3nM) to the number of active zG cells at 1μM, with active cells defined as those producing a minimum of three calcium spikes. We observed that Ang II dose-dependently increased the number of active zG cells (**Figure S3.2F**); 50pM Ang II evoked calcium oscillations in ~20% of zG cells, whereas 3nM Ang

II elicited oscillations in nearly all Ang II-reactive zG cells. Together these data indicate that Ang II dose dependently increases the number of active cells as well as their activity.

Burst Structure of zG Cell Calcium Oscillations

As noted above, we observed that at all tested doses Ang II evoked bouts of oscillatory activity. To determine whether a macroscopic structure underlies the dose-dependent increase in Ang II evoked-activity (**Figure S3.2B**), we established objective criteria to identify cohesive bouts of activity, referred to here as *bursts*.

To identify zG bursts, we first binned calcium spike intervals calculated from raster activity plots from all zG cells stimulated at each dose of Ang II (e.g. 300pM: **Figure S3.3A**). As we observed previously for an individual adrenal slice stimulated with 3nM Ang II (**Figure S3.1D**), the resultant interspike interval histogram across all 300pM Ang II-treated slices revealed a prominent peak at 2 seconds (c.f. **Figures S3.1D and S3.3A**). However, we also observed a smaller, secondary population of spike intervals greater than 5 seconds that reflected the duration of inactivity between two successive bursts. Indeed, the entire distribution of spike intervals was well-fitted by the sum of a Gaussian function (centered around the prominent peak of the histogram) plus an exponential function that captures the decay associated with the longer, inter-burst spike intervals. This model fitting assumes that inter-spike intervals within a burst are normally distributed, whereas burst occurrence follows a Poisson process with an exponential inter-burst interval distribution. The intersection of the Gaussian and exponential functions determined the threshold value that was used to separate (a) *intra-burst* calcium spike intervals within a single, cohesive burst of activity, from (b) *inter-burst* calcium spike intervals associated with two successive bursts (**Figure S3.3B**). Strikingly, applying this thresholding strategy to zG cell activity on a per-concentration basis revealed that intra-burst calcium spike

Figure S3.3. Ang II dose-dependently increases the number of bursts per cell.

(A) Histogram of binned Ca^{2+} spike intervals across all cells stimulated with 3nM Ang II and fitted to a Gaussian function (orange dotted line) and exponential function (orange solid line). The intersection of these two functions (blue arrow) represents the threshold for discriminating between intra-burst spikes and inter-burst spikes. (B) Example of trace data from a zG cell stimulated with 300pM Ang II and the subsequent spike/burst assignment. Ca^{2+} spikes (red dots) are grouped with a burst (black lines) if the distance (time) from the previous spike is less than the calculated threshold. To qualify as a burst, the spike train must contain a minimum of three consecutive sub-threshold events. (C-G) zG cells stimulated with one of four Ang II doses: 50pM (black, *n* = 5, 59 cells), 300pM (blue, *n* = 6, 217 cells), 3nM (orange, *n* = 7, 163 cells) or 1μM (red, *n* = 4, 95 cells). (C) Top. Mean spike interval per cell in a slice (black, 50pM; blue, 300pM; orange, 3nM; red, 1μM). No significant differences among groups were found (Kruskal-Wallis, P=0.2071). Bottom. Fractional distribution of intra-burst Ca^{2+} spike intervals was not dependent on Ang II dose, however (D, E) number of bursts per cell is concentration dependent (D: median value [25%-75%]: 50pM: 2 (1-3); 300pM: 4 (3-6); 3nM: 8 (6-11); 1μM: 11 (9-15) E: means±SEM [bursts/cell]: 50pM: 2.17±0.36, 300pM: 4.41±0.41, 3nM: 8.44±0.54, 1μM: 11.44±0.55) Kruskal-Wallis test: P = 0.0002; Dunn's multiple comparison test: 50pM vs 3nM (P = 0.008); 50pM vs 1μM (P = 0.004); 300pM vs 1μM (P = 0.03); non-linear curve fit: R^2 = 0.91, EC_{50} = 808.9pM. (F, G) Inter-burst intervals also show dose dependence as seen in a fractional distribution histogram (F) and plot of mean interburst interval (G, means±SEM [seconds]: 50pM: 41.2±9.9; 300pM: 34.9±3.2, 3nM: 20.1±3.3, 1μM: 14.9±0.3); Kruskal-Wallis test, P = 0.005; Dunn's multiple comparison test: 50pM vs 1μM (P = 0.027) and 300pM vs 1μM (P = 0.023), non-linear curve fit: R^2 = 0.46, IC_{50} = 876.49pM. (E,G) Mean data from each mouse were represented as a single point in calculating N/experimental condition.

Figure S3.3 (continued)

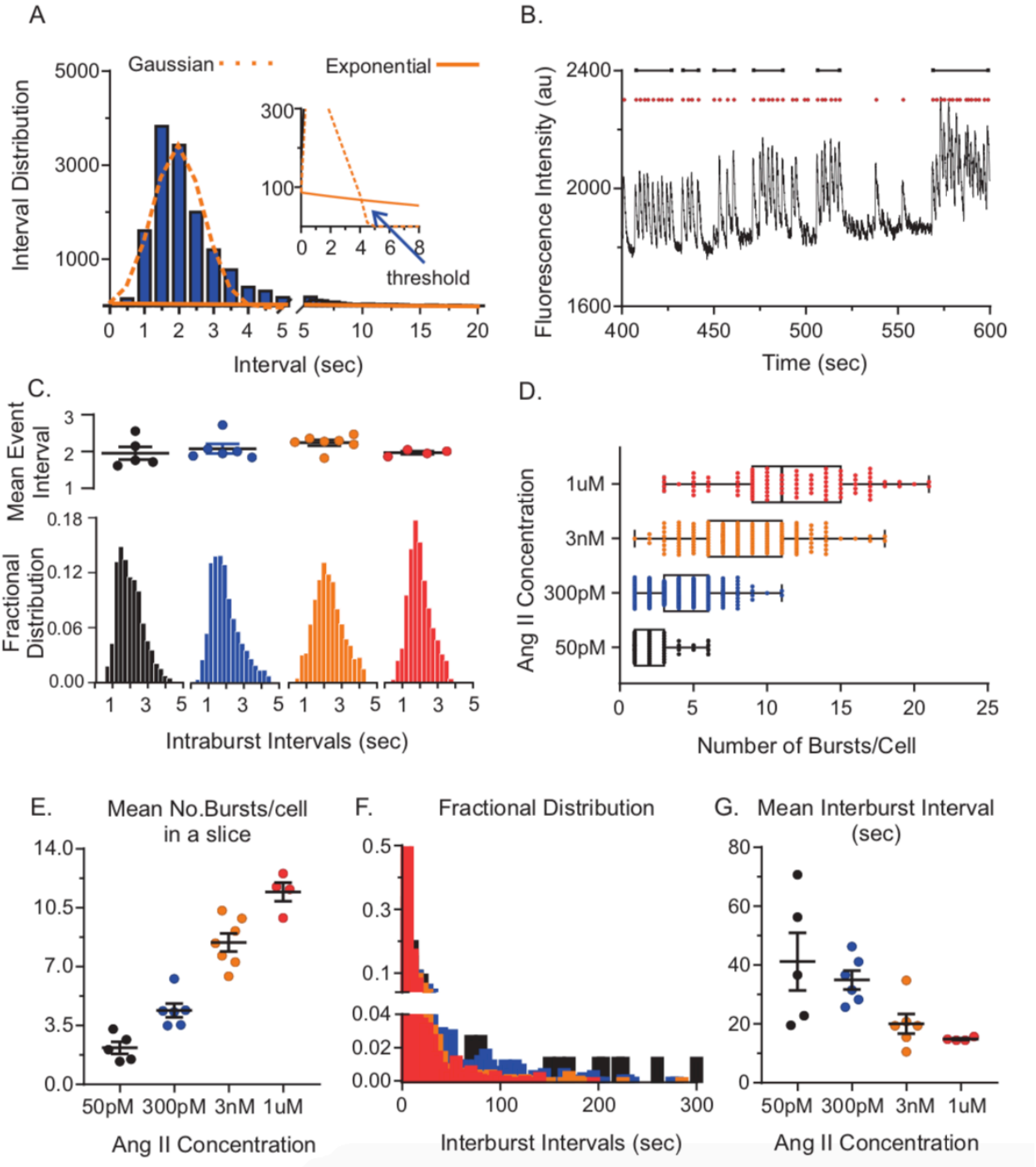

intervals of zG cells do not depend on Ang II concentration (**Figure S3.3C, bottom**). To compare the distribution of spike intervals across doses, we calculated the mean spike interval per cell in a slice and found these values to be equivalent (**Figure S3.3C, top**). To evaluate the robustness of this unanticipated result, alternative thresholding approaches were applied (20) (**Figure S3.7**), yielding similar threshold values and comparable conclusions about burst structure.

Although the intervals of zG cell calcium spikes within a burst were similar across four orders of Ang II concentration, the number of evoked bursts per zG cell was concentration-dependent. Thus, 50pM Ang II evoked 1-3 bursts (25-75% values) within most active zG cells during a 8.5-minute recording period, whereas 1μM Ang II evoked 9-15 bursts (25-75% values) within most active zG cells during a comparable period (**Figure S3.3D**). When the number of bursts produced by all zG cells within a slice was averaged, a clear dose-dependency emerged (**Figure S3.3E**). Correspondingly, the interval between bursts (i.e. inter-burst interval) was also Ang II concentration-dependent, with longer inter-burst intervals occurring at lower doses (**Figure S3.3F, G**). Thus, in aggregate, our data indicate that the primary dose-dependent action of Ang II was to increase burst occurrence.

We next evaluated the properties of individual zG cell calcium bursts across the various Ang II concentrations. To our surprise, we discovered that several features of zG cell bursts are also dose invariant. Neither the duration of individual zG bursts (**Figure S3.4A, B**), nor the number of zG calcium spikes per burst (**Figure S3.4C, D**), varied with Ang II concentration. However, consistent with the observation that inter-burst intervals are brief during high agonist concentrations, the latency to periodic calcium activity among zG cells evoked by Ang II was shortest with 3nM and 1μM Ang II, relative to 50pM and 300pM Ang II (**Figure S3.4E**). It is

Figure S3.4. Burst analysis of Ang II-elicited Ca^{2+} spikes.

(A-D) Burst duration and number of spikes/burst are consistent across Ang II concentrations. A, box plot of individual cells, median value (25-75%): 50pM: 14.6 (8.2-14.6); 300pM: 13.9 (7.3-29.3); 3nM: 13.9 (7.3-30.8); 1μM: 11.2 (6.3-26.0); B, means±SEM [seconds]: 50pM: 26.3±2.2; 300pM: 26.3±2.2; 3nM: 29.4±2.7; 1μM: 23.6±2.1; Kruskal-Wallis test: P = 0.4783; C, box plot of individual cells, median value (25-75%): 50pM: 6 (4-14), 300pM: 6 (4-14), 3nM: 7 (4-14.5), 1μM: 9 (5-16); D, means±SEM; Kruskal-Wallis test: P = 0.65). (E) However, both the time it took for a cell to respond to Ang II (time to first burst, means±SEM (seconds): 50pM: 291±44; 300pM: 252±11;3nM: 79±9; 1μM: 81±21; Kruskal-Wallis test: P = 0.002, Dunn's multiple comparison test: 50pM vs 3nM: P = 0.006; 50pM vs 1μM P = 0.0398; non-linear curve fit: $R^2 = 0.77$, $IC_{50} =$ 366.1pM) and fraction of nonburst events (F,G) decreased with Ang II dose (F, box plot of individual cells, median value (25-75%): 50pM: 0.14 (.04-0.41), *n* = 74; 300pM: 0.10 (0.04-0.20), *n* = 250; 3nM: 0.11 (0.57-0.14), *n* = 151; 1μM: 0.07 (0.04-0.14) *n* = 95; G, means±SEM: 50pM: 0.32±0.05; 300pM: 0.19±0.03; 3nM: 0.13±0.02; 1μM: 0.12±0.01; Kruskal-Wallis test, P = 0.008, Dunn's multiple comparison test: 50pM vs 3nM, non-linear curve fit: $R^2 = 0.77$, $IC_{50} = 366.1$pM). . Unless otherwise noted, for Ang II concentrations: 50pM (black): *n* = 5, 135 cells; 300pM (blue): *n* = 6, 1017 cells; 3nM (orange): *n* = 7, 1398 cells; 1uM (red): *n* = 4, 1098 cells. (B, D, E,G) Mean data from each mouse were represented as a single point in calculating N/experimental condition.

Figure S3.4 (continued)

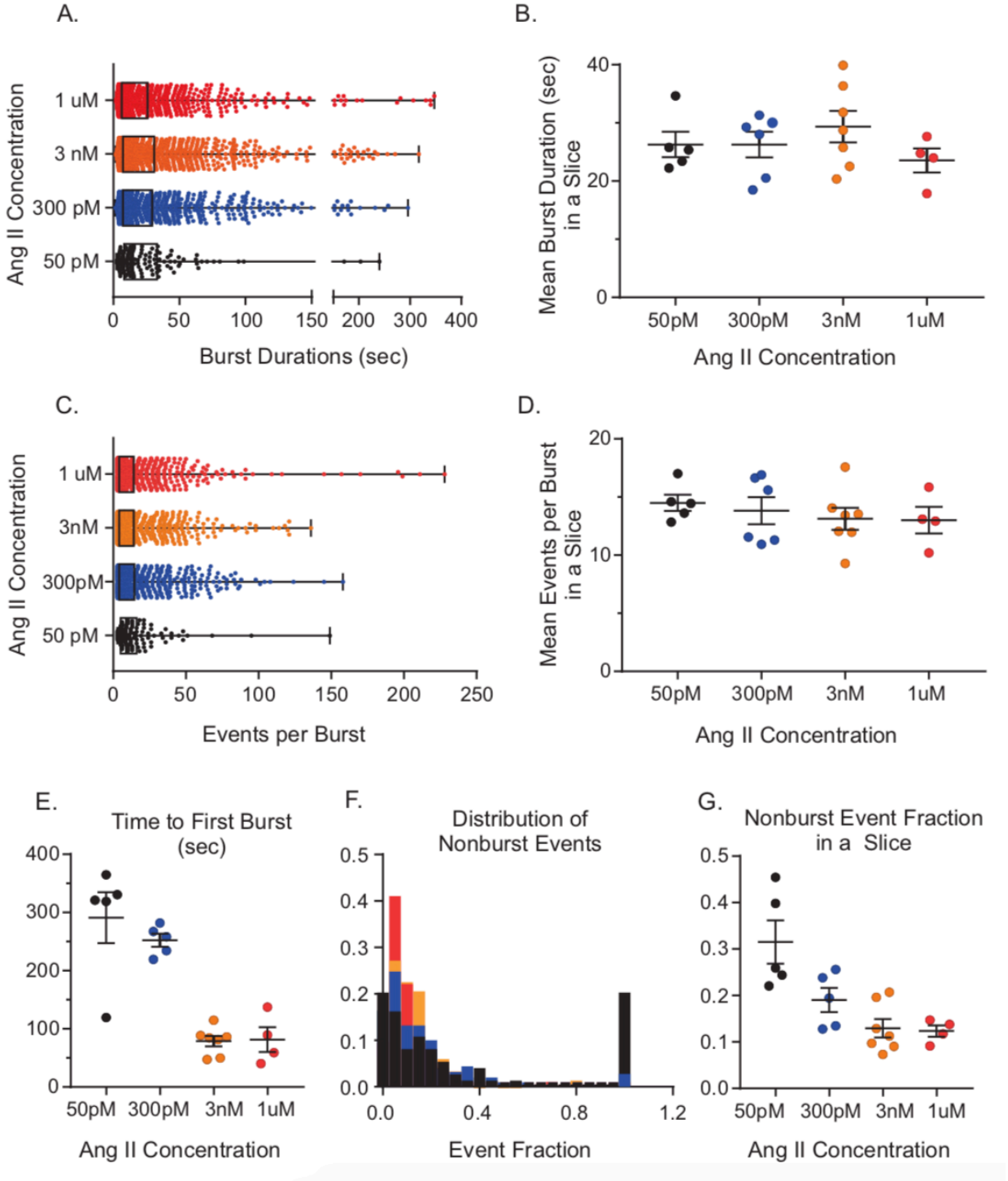

noteworthy that during exposure to lower Ang II concentrations, the epochs between successive zG cell bursts were not completely quiescent. Instead, these inter-burst periods were often punctuated with intermittent, aperiodic calcium spikes (i.e. *singlet* calcium spikes) that were most prevalent during 50pM Ang II application (**Figure S3.4G**). These data indicate that bursts evoked by Ang II are very stereotypic with a constant mean duration and a uniform mean number of events.

Extrinsic Factors Regulate zG Calcium Oscillations

The frequency of activity of a canonical intrinsic oscillator is voltage-dependent. In such cells, conductances that underlie oscillations enable slower oscillations at hyperpolarized membrane potentials and faster oscillations at more depolarized membrane potentials (within a restricted range)(21). Ang II is known to depolarize zG cells by constraining the activity of a variety of voltage-dependent potassium conductances in addition to inhibiting K2P potassium channels that support a hyperpolarized resting membrane potential (22). Because Ang II provides these well-characterized depolarizing stimuli to zG cells, we were surprised to find that Ang II did not evoke a dose-dependent increase in the frequency of recorded zG calcium oscillations within a burst (see **Figure S3.3C**). Thus, zG cells do not appear to be intrinsic oscillators as we had concluded previously (16). If not intrinsic oscillators, we next sought to understand if the rosette provides a platform for connection-based oscillations.

zG cells are thought to lack the most common molecular machineries necessary to support cellular communication. The zG layer is devoid of gap junctions as demonstrated by multiple independent assays [freeze fracture, transmission electron microscopy, live cell imaging, dye transfer, pharmacological blockade and mRNA assays (10, 11)]. In addition, within the layer there is scant evidence for direct modulation of zG cells by purinergic signals, in contrast to the

medullary zone where purinergic receptors (P2Xx- and P2Yx- subtypes) and secretory vesicles are abundant (23, 24). We therefore hypothesized that in the absence of these modalities the close proximity of zG cells situated within a rosette may provide a means for zG cell communication. Putatively, this could potentially occur via ephaptic transmission when the electrical fields of one cell influence closely apposed cells (25) or via mechanical transmission when membrane stress imposed on morphologically tethered cells is shared (26, 27). We therefore tested whether close proximity regulates zG calcium bursts.

Cadherins represent a family of transmembrane proteins mediating junctional connections that tether cells one to another (28). N-cadherins (NCADs) play well-established roles in cell-cell adhesion and are the major constituent of the adherens junctional complex (AJ). NCADs are expressed in many tissues, including brain, muscle and endothelium (29), and are notably abundant in rosette structures where they are required for rosette formation (6). Using immunohistochemical approaches, we localized NCADs to zG cell-containing adrenal rosettes. Consistent with previous observations of NCAD subcellular localization (30), we detected strong staining around the membrane surface of zG cells (**Figure S3.5A, left panel**). Filamentous actin (F-actin), an additional key component of AJs, was also evident at cell-cell contacts (**Figure S3.5A, middle panel**) and detected among larger, NCAD-positive aggregates found at the interface of multiple zG cells (**Figure S3.5A, right panel**). To test for a functional role for AJs in zG calcium activity, we evaluated the consequences of weakening NCAD-mediated cellular junctions.

AJs are dynamic structures and the transcellular ecto-domain (EC) interactions of NCAD proteins are calcium-dependent (31). Antibodies directed towards these ecto-domains have been used to disrupt cellular connections mediated by AJs following calcium sequestration (32).

Figure S3.5. Disruption of N-cadherin shortens burst duration without affecting other Ca^{2+} spike parameters. (A) Immunohistochemistry showing N-cadherin (red, left) and F-actin (green, middle) are abundant in the zG layer (right, merged image with nuclear stain DAPI [blue]). Scale bar: 10μM. (B) Model of Ca^{2+} switch assay: Disrupting adherins junctional complex by lowering extracellular Ca^{2+} in the presence of EGTA. Anti-N-cadherin antibody (ab) binds to the now exposed extracellular (EC) N-cadherin binding cites, inhibiting reformation of strong cell-cell adhesion after Ca^{2+} is restored. For controls, we substituted an antibody directed to the intracellular domain (IC) of the N-cadherin, or incubation media containing no antibody. (C-G) Adrenal slices were stimulated with 300pM Ang II after 1.5 mins of baseline recording. No ab: *n* = 8, EC ab: *n* = 8; IC ab: *n* = 4. (C) Mean events per 1 min bin over a 10 min period; EC-ab treated slices trended toward fewer events over time, but 2-way ANOVA showed no significant difference among groups (P = 0.31). (D) Mean burst duration/slice was significantly reduced after cell adhesion disruption; means±SE (seconds): no Ab: 32.92±2.6; EC ab: 22.97±1.6; IC ab: 3.13±1.9; Kruskal-Wallis test: P = 0.0065; Dunn's multiple comparison test: EC vs IC *P = 0.047; EC vs none *P = 0.034; IC vs none P > 0.99. Neither, number of bursts/cell/slice (E, means±SEM: no Ab: 2.64±0.2; EC ab: 2.94±0.4; IC ab: 3.13±0.7; Kruskal-Wallis test: P > 0.99), intraburst Frequency (F, means±SEM [Hz]: no Ab: 0.510±0.03; EC ab: 0.550±0.03; IC ab: 0.515±0.05; Kruskal-Wallis test: P = 0.58), nor time to first burst (G, means±SEM [sec]: no Ab: 303.1±11.23; EC ab: 338.0±18.8; IC ab: 297.8±21.8; Kruskal-Wallis test: P = 0.25) differed from control experiments. (C-G) Mean data from each mouse were represented as a single point in calculating N/experimental condition.

Figure S3.5 (continued)

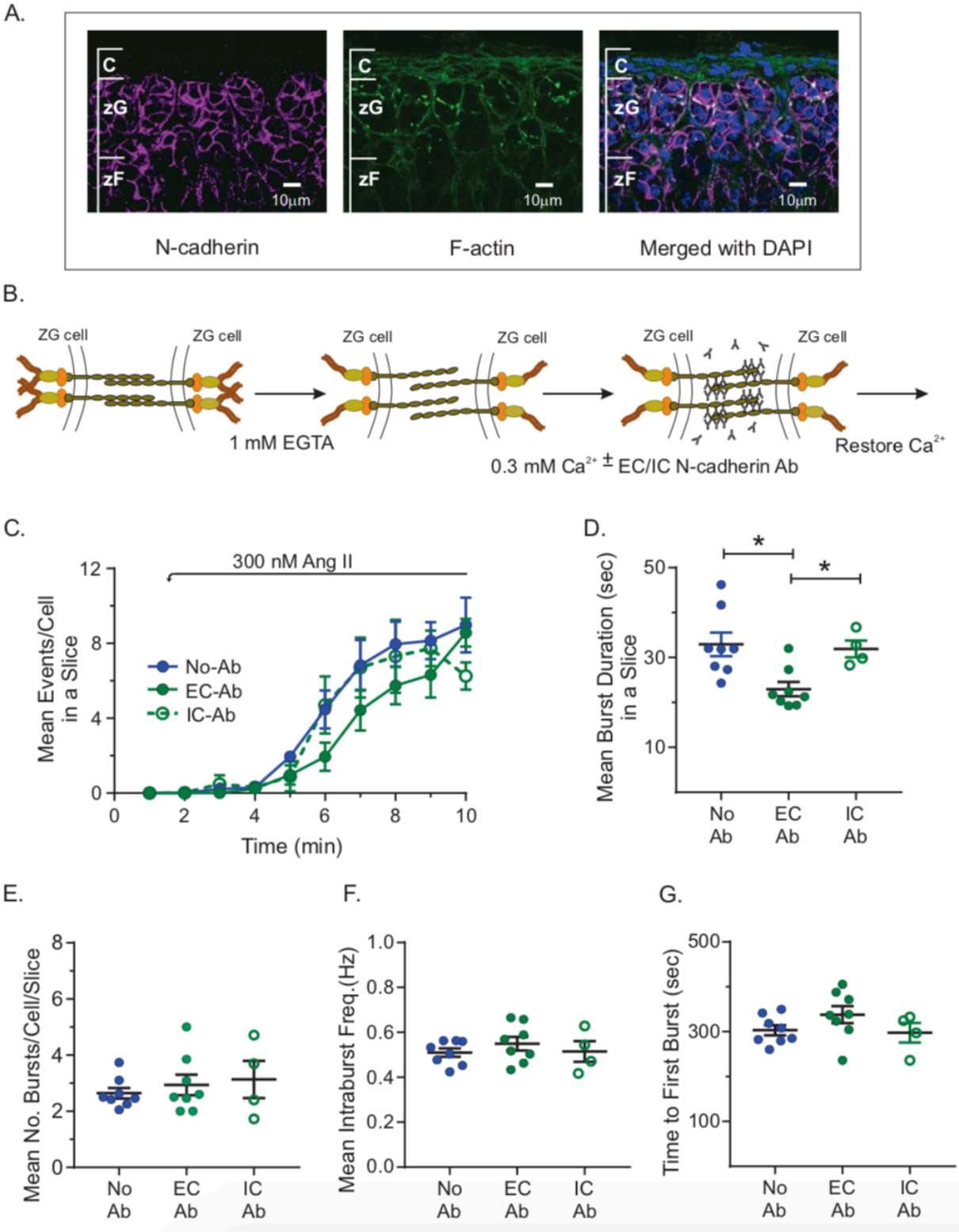

We employed this strategy (**Figure S3.5B**), termed the calcium switch assay, to evaluate the contribution of close cellular apposition to zG calcium oscillations. Specifically, we compared zG cell activity following a brief incubation with either an antibody directed towards the extracellular domain of NCAD (EC-ab), or an antibody directed towards the intracellular domain of NCAD (IC-ab). The latter served as a control for non-specific disruption as the inaccessibility of the IC-antigenic epitope would preclude IC-ab binding. In addition, we compared these experimental conditions to protocol-matched control conditions in which adrenal slices were not incubated with an antibody but exposed to equivalent sequential changes in extracellular calcium.

Adrenal slices incubated with the EC-ab reduced zG cell spiking activity. The mean number of spikes produced per minute by zG cells was lowest in adrenal slices incubated with the EC-ab, whereas activity with IC-ab incubation was equivalent to that of control solutions (**Figure S3.5C**). We found that reduced cellular activity elicited by EC-antibodies was primarily the result of shortening the burst duration; the average duration was ~30% briefer than burst durations occurring in IC and control incubations (**Figure S3.5D**). By contrast, across all conditions the number of bursts produced by zG cells remained unchanged (**Figure S3.5E**), as did the intra-burst spike frequency (**Figure S3.5F**) and the latency to activity following Ang II application (**Figure S3.5G**). Together, these data suggested that cell-cell interactions serve to prolong zG cell oscillatory activity.

Functional Clustering of zG cells Within Adrenal Rosettes

Because the preceding set of experiments indicated that zG cells functionally interact, we next explored the consequences of such interactions. We were intrigued by our cursory observation that the macroscopic calcium spiking behavior among zG cells in close proximity appeared similar. To objectively evaluate this possibility, we applied a functional clustering algorithm (33)

(FCA, see Methods) to identify zG cells with similar activity patterns. In brief, the FCA pairs cells that produce similar patterns of activity, and then evaluates the statistical significance of such pairing by comparing the observed, biological spike trains to numerous, randomly generated surrogate spike trains. Groups of similarly active cells are assigned to *functional clusters* and are represented as a uniformly colored branch on a dendrogram (**Figure S3.6A**). While we applied the FCA to zG cell activity recorded in slices across all Ang II concentrations, we present only those results derived from 3nM Ang II applications; the calcium spike singlets frequently observed at the lowest Ang II concentration (see **Figure S3.4G**) yielded inconsistent cell clusters following multiple FCA runs (unlike those derived from other Ang II experiments).

Applying the FCA to zG cell calcium spike trains recorded during 3nM Ang II consistently yielded clusters of cells with similar activity patterns. In **Figure S3.6**, we present a representative dendrogram in which zG cell clusters are color-coded (**Figure S3.6A**), and we show corresponding activity rasters for all zG cells comprising the dendrogram (**Figure S3.6B**). These color-coded activity rasters demonstrate that the activity patterns within a functional cluster of zG cells, as defined by the FCA, are similar. Next, we localized the anatomical location of each zG cell within the adrenal slice and discovered that functionally-paired cells appeared to be situated within the same rosette (**Figure S3.6C**).

Unambiguous, visual identification of a complete rosette can be challenging in some acute adrenal slices. We therefore sought objective criteria to evaluate the anatomical relationships among zG cells within a functional cluster (i.e. *clustered pairs*), and among zG cells assigned to different clusters by the FCA (i.e. *non-clustered pairs*). The centroid coordinates of each region of interest (ROI) used to measure the fluorescence intensity of individual zG cells correspond to the X-Y location of the center of each zG cell within the time-lapsed image. These coordinates

Figure S3.6. zG cells within rosettes functionally cluster with neighboring cells after stimulation with 3nM Ang II. (A-C) Representative data from an adrenal slice stimulated with 3nM Ang II. (A) Dendrogram output from the functional clustering algorithm for ROIs shown in C, indicating cell pairings based on Ca^{2+} spike synchrony. Cell pairings (X axis) are ranked by mean least temporal distance between Ca^{2+} spikes; those that pair best are ranked first and grouped together (Y axis), while pairs with more diverse temporal spike relationships have increasingly greater ranks. (A-C) Each color represents a group of cells that significantly paired with each other. (B)Raster plot of Ca^{2+} spikes across all cells marked, arranged by groupings. (D, E) The distance between cells that cluster together is markedly smaller than cells that do not pair (D, box plot of individual pairs, median value (25-75%) [μm]: clustered: 7.2 (5.7-10.8), n=226); non-clustered: 37.0 (21.8-56.4), n=1827). E, means±SEM (μm) per adrenal slice: clustered: 8.9±1.1; non-clustered: 37.7±5.0; Mann-Whitney test: *P = 0.0156. Mean data from each mouse were represented as a single point in calculating N/experimental condition.

Figure S3.6 (continued)

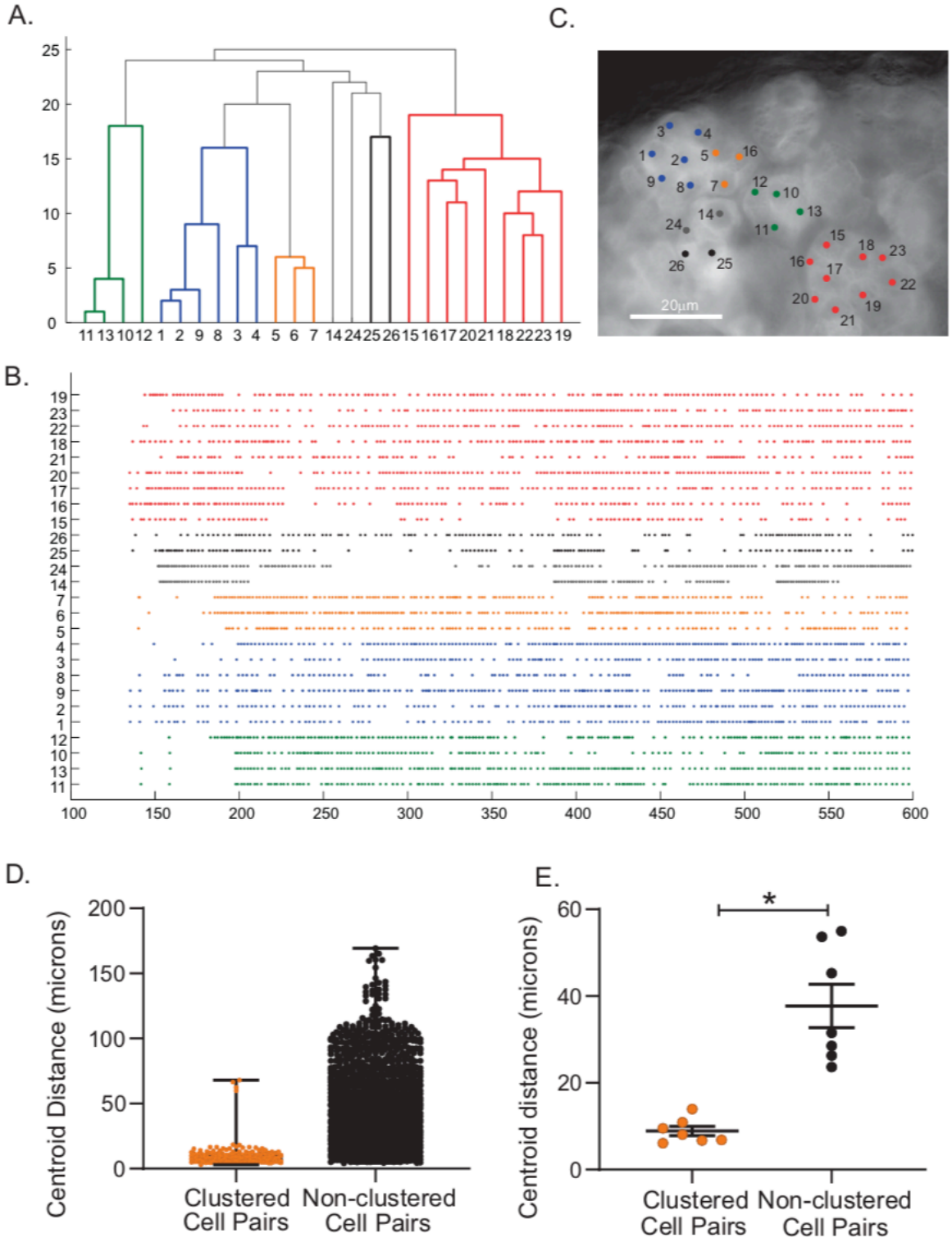

Figure S3.7. Calculations for determining a threshold value for defining inter-burst vs. intra- burst spikes. (A) Fitted parameters for a Gaussian-Exponential distribution fit to the inter-calcium spike interval distribution. This model assumes that bursts occur as a Poisson process (with inter-arrival times drawn from an exponential distribution with mean μ2) and that inter-spike intervals within bursts are drawn from a Gaussian distribution N(μ1, σ1). The two distributions are combined with a weight λ between 0 and 1. (B) Fitted parameters for a multi-Gaussian distribution fit to the inter-calcium spike interval distribution based on the sub-threshold oscillation model proposed by Bodova et al. This model assumes that a cell is in either a quiescent (Q) state or a spiking (S) state. The state transitions occur as a Markov process with transition probabilities pSQ and pQS and with the inter-arrival times for states S and Q drawn from a Gaussian distributions N(μ1, σ1) and N(μ2, σ2) respectively. (C) Thresholds (seconds) for the maximum intra-burst interval as calculated from the Gaussian-Exponential model or the multi-Gaussian model (Bodova) for each dose of Ang II. For the Gaussian-Exponential model, the intersection between the Gaussian and exponential component is used. For the Bodova model, the sum of the mean quiescent (Q) state period and the mean spiking (S) state period is used, as the minimum sequence for burst separation is SQS under this model.

Figure S3.7 (continued)

A

Gaussian-Exponential Intersection

$$y = \lambda \frac{1}{\sigma\sqrt{2\pi}} e^{\frac{-(x-\mu_1)^2}{2\sigma^2}} + (1-\lambda)\frac{1}{\mu_2} e^{\frac{-x}{\mu_2}}$$

	λ	μ_1	σ	μ_2
50pM	0.8555	2.034	0.7142	32.6169
300pM	0.8157	1.9884	0.7334	16.5089
3nM	0.7739	2.2944	0.8121	8.1901
1uM	0.8132	1.9924	0.6444	6.7698

B

Bodova

$$y = (1-pSQ)\frac{1}{\sigma_1\sqrt{2\pi}} e^{\frac{-(x-\mu_1)^2}{2\sigma_1^2}} + pSQ * pQS \frac{1}{\sqrt{\sigma_1^2+\sigma_2^2}\sqrt{2\pi}} e^{\frac{-(x-(\mu_1+\mu_2))^2}{2(\sigma_1^2+\sigma_2^2)}} + \cdots$$

$$pSQ * (1-pQS) * pQS \frac{1}{\sqrt{\sigma_1^2+2\sigma_2^2}\sqrt{2\pi}} e^{\frac{-(x-(\mu_1+2\mu_2))^2}{2(\sigma_1^2+2\sigma_2^2)}} + \cdots$$

$$pSQ * (1-pQS)^2 * pQS \frac{1}{\sqrt{\sigma_1^2+3\sigma_2^2}\sqrt{2\pi}} e^{\frac{-(x-(\mu_1+3\mu_2))^2}{2(\sigma_1^2+3\sigma_2^2)}} + \cdots$$

$$pSQ * (1-pQS)^3 * pQS \frac{1}{\sqrt{\sigma_1^2+4\sigma_2^2}\sqrt{2\pi}} e^{\frac{-(x-(\mu_1+4\mu_2))^2}{2(\sigma_1^2+4\sigma_2^2)}}$$

	pSQ	pQS	μ_1	σ_1	μ_2	σ_2
50pM	0.1161	0.8967	2.0995	0.7942	2.2367	60.7067
300pM	0.1313	0.7637	2.0734	0.8410	2.8692	23.3050
3nM	0.1211	0.8764	2.3865	0.9941	2.6421	13.0360
1uM	0.1273	0.9411	2.0196	0.6797	1.5021	7.5822

C

Thresholds

	Gaussian + Exponential	Bodova
50pM	4.2479	4.3361
300pM	4.0438	4.9425
3nM	4.3334	5.0286
1uM	3.6847	3.5216

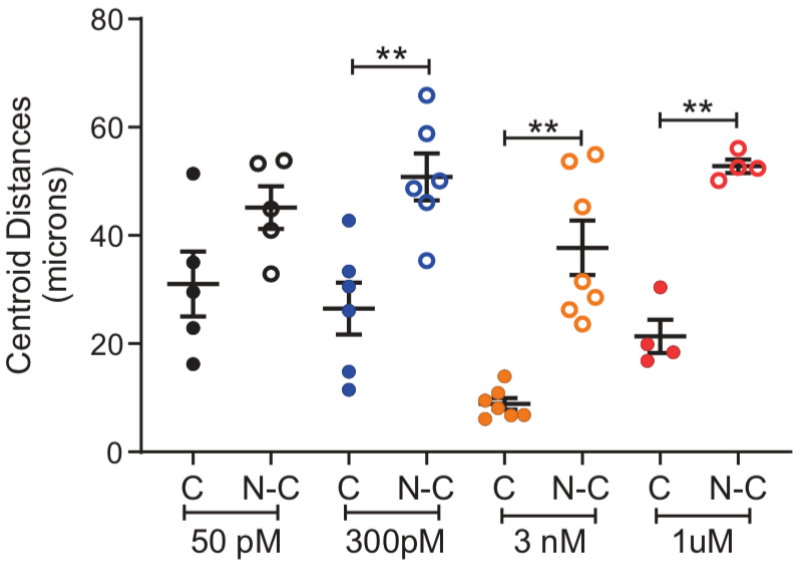

Figure S3.8. Quantitative analysis of centroid distances across Ang II doses: clustered vs non-clustered cells. Two zG cells identified as a clustered (C) pair by a functional clustering algorithm tend to be closer together than pairs that are non-clustered (N-C) across Ang II doses (mean±SE C/N-C: 50pM 31.0±6.0/45.2±3.9, 300pM 26.5±4.8/50.8±4.8, 3nM 8.9±1.1/37.7±5.0, 1μM 21.4±3.1/52.8±1.2; 1-way ANOVA: $P < 0.0001$, Bonferroni's multiple comparison test: 50pM $P = 0.119$, 300pM $^{**}P = 0.006$, 3nM $^{**}P<0.0001$, 1μM $^{**}P =0.0003$). Mean data from each mouse were represented as a single point in calculating N/experimental condition.

then were used to determine the Euclidian distances between all pairs of zG cells within the slice. The centroid distances were assigned to one of two groups: (1) distances between zG cells within a functional cluster, or (2) distances between zG cells in different functional clusters. All zG cell-zG cell distances measured across all 3nM Ang II experiments are shown in **Figure S3.6D**. The corresponding means for each group from each experiment are shown in **Figure S3.6E**. Clearly, functional zG cell clusters are composed of cells that are in close proximity, relative to non-clustered zG cell pairs. The mean Euclidian distance for clustered pairs was ~10μm, a value that roughly corresponds to the distance between the centers of two adjacent zG cells situated within a rosette. Centroid distances between non-clustered and clustered cell pairs were similarly significant at 1 μM Ang II and 300nM, with a trend at 50pM (**Figure S3.8**). Together, these data support a role for the rosette in the coordination of oscillatory calcium signals evoked by Ang II.

Discussion

In the experiments described above, we demonstrate that zG cells situated within their native rosette structure produce robust, sustained calcium oscillations in response to the primary regulator of aldosterone production, Ang II. We show that the intensity of Ang II-evoked calcium oscillations is strongly dose-dependent, and that such dependency does not involve a simple increase in oscillation frequency with increasing Ang II concentration. Instead, we find that the highly stereotyped, macroscopic pattern of zG cell calcium activity – the zG calcium burst – is the fundamental unit of zG cell activity that is evoked more frequently when increasing Ang II dose. We also show that cellular junctions between closely-apposed zG cells regulate zG calcium bursts, suggesting that the adrenal rosette provides an anatomical substrate for functional regulation of zG cell activity. Further support for this hypothesis is provided by our findings that calcium oscillations produced by zG cells within a rosette are highly coordinated.

Collectively, these outcomes motivate us to rethink the molecular and cellular processes that govern the zG cell calcium signal required for aldosterone production. Below, we provide context for our findings, beginning with our current understanding of the ionic basis of intrinsically-driven, cellular-level oscillations.

Many examples of intrinsic cellular oscillators exist (21, 34-36). Generally, such cells are endowed with the capacity to produce highly periodic ionic (and, therefore, voltage) fluctuations on their own. To achieve such rhythmogenesis, these cells must express the appropriate combination of voltage- and time-dependent conductances that operate in concert to sustain cellular oscillations without input from other cells. As the underlying conductances driving endogenous oscillators are voltage-dependent, such oscillations are only observed within a range of membrane potentials. For example, the hyperpolarized-activated cation current (I_h) and the low threshold, t-type calcium current (I_t), two voltage-dependent conductances, are sufficient to endow thalamocortical neurons with the capacity to produce 1-2 Hz voltage oscillations (34, 37). However, such oscillations are abolished when these neurons are sufficiently hyperpolarized or depolarized to membrane potentials that cause sustained I_h and/or I_t channel closure (34, 38). Thus, one feature of an endogenous oscillator is the production of self-sustained electrical oscillations, usually within a range of membrane potentials.
Another feature of endogenous biological oscillators is that the frequency at which oscillations are produced is voltage-dependent. For example, the periodicity of endogenous voltage oscillators studied in barnacle muscle fibers (21, 39), crustacean feeding circuits (40) and mammalian thalamic circuits (34, 38) increases with depolarization. This property generally results from shifting the voltage-dependent activation and inactivation gating kinetics (41) of the underlying conductances. Thus, one defining feature of an endogenous biological oscillator is the generation of voltage oscillations whose frequency is voltage-dependent.

Several observations indicate that zG cells of the adrenal gland are not strict endogenous oscillators. First and foremost, isolated zG cells do not produce robust, sustained voltage oscillations, even in the presence of Ang II (42, 43). While the agonist depolarizes isolated zG cells (44) and can evoke brief oscillatory bouts of activity in a small subset of isolated cells (45, 46), the conclusion from many studies of zG cells removed from their native adrenal environment is that isolated zG cells do not oscillate. In stark contrast to this conclusion is the finding that robust, highly stereotyped voltage and calcium oscillations produced by zG cells are readily observed *in situ* (16, 47, this study).

A second piece of evidence that indicates zG cells are not strict endogenous oscillators is inferred from our current observation that the frequency of calcium oscillations is dose-invariant; irrespective of Ang II concentration, the intra-burst interval of calcium spikes in zG cells was always ~2 seconds. If Ang II depolarizes zG cells, and the strength of this depolarization is dose-dependent as is observed (42, 43), then the frequency of calcium oscillations produced by an endogenously oscillating zG cell should also be dose-dependent. As we did not observe such dependency, we therefore conclude that either the sensitivity of our assay is insufficient to resolve voltage-dependent frequency changes in an endogenously oscillating zG cell, or the zG cell is not an endogenous oscillator. In aggregate, the evidence currently supports the latter hypothesis.

If zG cell oscillatory activity is defined by the presence or absence of factors normally found within the adrenal tissue, then one primary goal becomes the identification of such factors. Fully realizing this goal is complicated by multiple lines of evidence demonstrating that zG cells do not contain the standard molecular components that support extrinsically-driven voltage

oscillations. zG cells neither express gap junctions that can mediate electrical transmission between cells (10, 11), nor do they contain the morphological substrates associated with chemical transmission (i.e. vesicles) (23, 24). Indeed, from a molecular and morphological perspective, one would conclude that zG cells should exist as endogenous oscillators. However, from a functional perspective, they do not. What zG layer feature then, provides a platform for Ang II-evoked zG cell oscillations and their coordination?

Here we provide evidence that the adrenal rosette, with its abundant expression of NCADs, likely provides the scaffold necessary for the expression of robust voltage and calcium oscillations evoked by Ang II. Within the rosette, NCADs regulate cell-cell contact (48). Their *trans*-bond engagement produces adhesive tension and initiates the recruitment of the catenins (p120-catenin, 🚲-catenin, ✔-catenin) to the NCAD intracellular domain (49). NCAD clustering and the mechanosensitive recruitment of other actin binding proteins strengthens the anchoring of NCADs to the actin cytoskeleton (50). Thus, within a rosette NCADs serve to interconnect the cytoskeletons of constituent cellular members (51). In addition, the NCAD-elicited pull between adhesion tension and acto-myosin cortex tension largely governs interfacial tension (8, 51), a mechanical signal that can regulate the activity of ion channels and G-protein coupled receptors (GPCRs) that are tension sensitive (52). Ligand-independent activation of GPCRs is widely acknowledged (53). In the absence of ligand, mechanical stress activates Ang II AT1R (54) offering the intriguing possibility that the previously reported “intrinsic” oscillatory activity observed in patch-clamp recordings may have been evoked by membrane stress produced by tight-seal formation between the membrane and the patch pipette.

NCADs junctions are highly dynamic structures that possess the capacity to reorganize after disruption (30, 55). Calcium binding rigidifies the NCAD extracellular domains promoting both

trans and cis (dimerization) interactions that support adhesion (56). Conversely, lowering calcium disrupts binding and adhesion (30). Among the large CAD family, NCAD is the least calcium sensitive member with a K_D for calcium binding of ~0.65mM (31). This low affinity indicates that NCADs are ideally suited to respond to reductions in extracellular calcium predicted to occur in synaptic clefts during high frequency firing and/or high K^+-mediated depolarization (57), two stimuli that trigger extensive molecular reorganization and synapse remodeling. Therefore, it is noteworthy that interference with neuronal NCAD function using specific EC-domain antibodies is reported to prevent both the structural reassembly of N-cadherin puncta following synaptic stimulation (55) and reduce the functional induction of long-term potentiation (58). Using specific EC- but not IC-domain antibodies, we show here that NCADs may also have a functional role in the closely packed environment of the adrenal rosette. EC-domain antibodies specifically altered the structure of the burst by shortening its duration. Whether complete cessation of oscillatory activity could be achieved by a more efficient junctional disruption strategy remains unknown. Nonetheless, our findings indicate that NCADs localized within the adrenal rosette functionally regulate burst termination in contrast to Ang II whose singular function is to regulate burst initiation.

Within the adrenal rosette, our data show that 3nM Ang II reliably evokes oscillatory activity that is coordinated among rosette members. If activity coordination were based on event frequency, cluster analysis should have assigned all analyzed cells in a slice to one functional group, as intra-burst frequency was invariant. Rather, because multiple functional groups were identified that regularly mapped to structural rosettes, our data indicate that burst timing, both on- and off-set, is a major determinant of coordination. As such, both extrinsic (Ang II) and intrinsic factors (NCAD) then play key roles in adrenal activity coordination. Currently, our data cannot address the physiological significance of activity coordination because there is no single cell assay for

aldosterone. Nevertheless, one can speculate that coordination may serve to amplify aldosterone output by recruiting and then entraining the activity of less responsive zG cells, although admittedly other functional explanations remain possible.

Aldosterone associated hypertension is a more prevalent disease than originally acknowledged (59, 60). As a syndrome, it includes a spectrum of disorders characterized by variable degrees of hypersensitivity and autonomy to Ang II (59). Aldosterone associated hypertension carries higher cardiovascular risks than equivalent degrees of hypertension (61). Herein, we provide the first quantitative analysis of calcium activity in the zG layer. We define the fundamental unit of activity of the zG layer, the burst, and highlight a previously unrecognized signaling role for the rosette. This analysis can serve as a foundation for a molecular understanding of rosette-based mechanisms that underlie the control of burst firing in the zG layer, and thus may have broad impact to the treatment of Ang II-dependent and Ang II-independent aldosterone driven hypertension.

Methods

Mice: *AS* (aldosterone synthase)$^{+/Cre}$ mice, where Cre expression is under the control of the aldosterone synthase promoter (as described in (3)), were bred to B6;129S-*Gt(ROSA)26Sor*$^{tm38(CAG-GCaMP3)Hze}$/J (purchased from Jackson Laboratory, stock 014538) generating mice with zG specific GCaMP3 expression. Mice were group housed in a temperature and humidity controlled room on a 12:12 light:dark cycle.

Adrenal Slice Preparation: Male GCaMP3 mice between 40-100days of age were anesthetized with ketamine (15mg, i.p.), and adrenals dissected. Adrenals were sectioned (60-70μm) in ice-cold PIPES incubation buffer (in mM: 20 PIPES, 117 NaCl, 3 KCl, 1 $CaCl_2$, 1 MgCl,

25 D-Glucose, 5 $NaHCO_3$, pH 7.3). Sections were kept at 37°C for 30 min, then allowed to return to room temperature for the duration of the experiment. Sections used for CPA experiments were pretreated for 20 min with either 20μM CPA or vehicle (0.1% DMSO) in incubation buffer. Sections used for N-cadherin disruption experiments were returned to 37°C and incubated in a low calcium (0.3mM) Pipes buffer for 20 minutes, followed by low calcium buffer containing 1mM EGTA with anti-N-cadherin (1:25, Sigma Aldrich), anti-P-cadherin (1:25, Sigma Aldrich), or no antibody for 20 minutes. The final incubation solution contained no EGTA, 1mM calcium, and incubation antibody (1:25), if applicable.

Immunostaining of Adrenal Slices: After dissection, adrenals were trimmed of surrounding fat tissue, rinsed in PBS, cut in halves with a surgical blade, and fixed in 4% PFA at 4ºC for 1 hr. PFA-fixed adrenals were washed in PBS and embedded in 4% low-melting-temperature SeaPlaque Agarose (Lonza, 50100), and sectioned on a vibratome at a thickness of 100 μm. Slices were washed with 0.1% Tween-20 in PBS for 10 min for three times, and blocked in 5% Normal Goat Serum, 1% Bovine Serum Albumin, 0.1% Tween-20 in PBS for 1 hour at RT with gentle rocking. Slices were incubated with a polyclonal rabbit anti N-cadherin primary antibody (Novus Biologicals, NBP2-38856) diluted 1:100 in blocking solution at 4ºC overnight. After three 20 min washes with 0.1% Tween-20 in PBS, adrenal slices were incubated with an Alexa Fluor 488-conjugated goat anti rabbit IgG secondary antibody (Invitrogen, A-11034) diluted 1:100 in 0.1% Tween-20 in PBS for 2 hr at RT. For F-actin staining, Alexa Fluor 647-conjugated Phalloidin (Invitrogen, A22287) was added to the secondary antibody mix for the last 30 min at final concentration of 1:100. For nuclear staining, DAPI was added to secondary antibody mix for the last 5 min at final concentration of 1:500-1:1000. Slices were then washed with 0.1% Tween-20 in PBS for 20 min for three times and mounted on Superfrost Plus slides (Fisher Scientific, 12-550-15) with Prolong Gold (Life Technologies, P36930). Images were acquired

using a Zeiss LSM710 confocal microscope with a 63X/1.4 oil immersion Plan-Apochromat objective and adjusted for brightness and contrast using ImageJ.

Data Acquisition: Adrenal slices were imaged in a PIPES buffer (in mM: 20 PIPES, 122 NaCl, 3 KCl, 1 $CaCl_2$, 1 MgCl, 25 D-Glucose, pH 7.3) on a Zeiss Axio-Examiner microscope fitted with a xenon arc light source (Lamda DG4, Sutter Inst) with a custom-made stage configured for a perfusion system, and images acquired at 20 Hz with a sCMOS camera (Hamamatsu Orca-Flash 4.0) using HCImageLive software (Hamamatsu). Each experiment started with a 90s baseline acquisition before adding hormone/drug through the perfusion system. Experiments lasted between 10 and 15 minutes and were saved as high quality multipage tiffs for analysis. The following drugs were used: Angiotensin II (50pM-1μM, Fisher), TTA-P2 (10μM, Merck), Cyclopiazonic acid (CPA, 20μM, Cayman Chemicals).

Data Analysis:

Signal extraction. Fluorescence intensity is extracted from ROIs (regions of interest) using Caltracer software (Yuste lab, Columbia U.) to produce a time series of average ROI intensity. ROI placement is performed manually on identified cells in each slice using a stacked image (multipage tiff) from an initial segment of the optical time-series and registered to correct for movement artifacts when necessary. Image output levels were adjusted to include all information-containing pixels, and balance and contrast adjusted to reflect true rendering as much as possible for ROI placement (e.g., **Figure S3.1A**). Additional ROIs are placed as background controls.

Event detection. Calcium transient events in each time-series are identified using custom Matlab software combining an automated event detection algorithm with manual corrections for erroneous or missing events by an investigator.

Cell activity. Calcium activity is presented in raster plots and quantified to determine mean events/cell, mean frequency/cell, and bursting activity. Periodicity is determined by Fourier transform and by inter-event interval. To assess manipulation-dependent changes in cellular activity, Ca^{2+} events are binned into time segments (e.g.,1-min bins) and averaged across cells to establish slice behavior; each slice represents a sample size of one prepared from a single animal.

Burst detection. Events were grouped into bursts as follows: The inter-event interval distribution was fitted with a mixture of Gaussian and exponential distributions (see equation for **Figure S3.7A**). Our method was based on the assumption that (i) bursts occur infrequently but independently of each other at a constant rate and can be modelled as a stationary Poisson process (which yields exponentially distributed inter-arrival times) and (ii) events within bursts have periods drawn from a Gaussian distribution. The inter-event interval value at the intersection of the Gaussian and exponential component of the distribution was taken as the maximum inter-event interval within a burst.

A separate method for fitting the inter-event interval distribution with a series of Gaussian distributions based on Bodova et al 2015 was also implemented (see equation for **Figure S3.7B**). Bodova et al.'s method was based on the assumption that there is a subthreshold oscillation of two states (quiescent versus spiking) that transitions with fixed probability (as a Markov chain) and have periods drawn from two different Gaussian distributions. In this model,

the sum of the two fitted Gaussian distribution means were used as the maximum inter-event interval within a burst.

Events were then grouped as bursts if there were at least three consecutive events with inter-event intervals all greater than the threshold described above. The resulting burst detection were then plotted and visually inspected for verification of the algorithm.

Functional Clustering Algorithm: Within each slice experiment, a functional clustering algorithm was used to analyze event patterns among cells completely blind to a cells location, as described in (33). In brief, cells are sequentially paired according to the degree of similarity between event patterns. The relationship of each cell-pair is assessed by calculating the minimum duration between an event in one cell and the nearest event in a second cell. The mean minimum duration of all events in the pair defines activity similarity and is used to assign functional groups. Statistical significance of detected clusters is determined by comparisons to surrogate data sets. Finally, degree of similarity and cluster membership are depicted in a dendrogram. These analyses are computationally intensive and, therefore, run on UVA's Rivanna High Performance cluster.

Statistic: Data were presented as mean ± standard error or median followed by 25-75 percentile values. When comparing means, cells from a single slice were considered a single data point when calculating N for statistical analysis, and only one slice was used per animal for a given experimental condition. Prism 7 software (Graphpad) was used for all statistical analysis. Parametric ANOVAs (1- or 2-way) with Bonferroni (1-way) or Tukey's multiple comparison test (2-way) wer used to compare means if the data passed the Shapiro-Wilk

normality test, otherwise we used non-parametric Kruskal-Wallis test with Dunn's multiple comparison test. Difference were considered significant if $P < 0.05$ using a two-tailed test.

Study Approval. All experiments were performed in accordance with the National Institutes of Health Guide for the Care and Use of Laboratory Animals and approved by the University of Virginia Animal Care and Use Committee.

References

1. Xing Y, Lerario AM, Rainey W, and Hammer GD. Development of adrenal cortex zonation. Endocrinol Metab Clin North Am. 2015;44(2):243-74.

2. Vidal V, Sacco S, Rocha AS, da Silva F, Panzolini C, Dumontet T, Doan TMP, Shan J, Rak-Raszewska A, Bird T, et al. The adrenal capsule is a signaling center controlling cell renewal and zonation through Rspo3. Gene & Development. 2016;30(1-6.

3. Freedman BD, Kempna PB, Carlone DL, Shah M, Guagliardo NA, Barrett PQ, Gomez-Sanchez CE, Majzoub JA, and Breault DT. Adrenocortical zonation results from lineage conversion of differentiated zona glomerulosa cells. Dev Cell. 2013;26(6):666-73.

4. Mitani F. Functional zonation of the rat adrenal cortex: the development and maintenance. Proc Jpn Acad Ser B Phys Biol Sci. 2014;90(5):163-83.

5. Pihlajoki M, Dorner J, Cochran RS, Heikinheimo M, and Wilson DB. Adrenocortical zonation, renewal, and remodeling. Front Endocrinol (Lausanne). 2015;6(27.

6. Harding MJ, McGraw HF, and Nechiporuk A. The roles and regulation of multicellular rosette structures during morphogenesis. Development. 2014;141(13):2549-58.

7. Martin AC, and Goldstein B. Apical constriction: themes and variations on a cellular mechanism driving morphogenesis. Development. 2014;141(10):1987-98.

8. Lecuit T, and Lenne PF. Cell surface mechanics and the control of cell shape, tissue patterns and morphogenesis. Nat Rev Mol Cell Biol. 2007;8(8):633-44.

9. Walczak EM, and Hammer GD. Regulation of the adrenocortical stem cell niche: implications for disease. Nat Rev Endocrinol. 2015;11(1):14-28.

10. Davis KT, Prentice N, Gay VL, and Murray SA. Gap junction proteins and cell-cell communication in the three functional zones of the adrenal gland. J Endocrinol. 2002;173(1):13-21.

11. Bell CWaM, S.A. Adrenocortical Gap Junctions and Their Functions. Front Endocrinol(Lausanne). 2016;7(82):1-14.

12. Spat A, and Hunyady L. Control of aldosterone secretion: a model for convergence in cellular signaling pathways. Physiol Rev. 2004;84(2):489-539.

13. Quinn SJ, Williams GH, and Tillotson DL. Calcium oscillations in single adrenal glomerulosa cells stimulated by angiotensin II. Proc Natl Acad Sci U S A. 1988;85(15):5754-8.

14. Johnson EI, Capponi AM, and Vallotton MB. Cytosolic free calcium oscillates in single bovine adrenal glomerulosa cells in response to angiotensin II stimulation. J Endocrinol. 1989;122(1):391-402.

15. Rossig L, Zolyomi A, Catt KJ, and Balla T. Regulation of angiotensin II-stimulated Ca2+ oscillations by Ca2+ influx mechanisms in adrenal glomerulosa cells. J Biol Chem. 1996;271(36):22063-9.

16. Hu C, Rusin CG, Tan Z, Guagliardo NA, and Barrett PQ. Zona glomerulosa cells of the mouse adrenal cortex are intrinsic electrical oscillators. J Clin Invest. 2012;122(6):2046-53.

17. Natke E, Jr., and Kabela E. Electrical responses in cat adrenal cortex: possible relation to aldosterone secretion. Am J Physiol. 1979;237(2):E158-62.

18. Shipe WD, Barrow JC, Yang ZQ, Lindsley CW, Yang FV, Schlegel KA, Shu Y, Rittle KE, Bock MG, Hartman GD, et al. Design, synthesis, and evaluation of a novel 4-aminomethyl-4-fluoropiperidine as a T-type Ca2+ channel antagonist. J Med Chem. 2008;51(13):3692-5.

19. Moncoq K, Trieber CA, and Young HS. The molecular basis for cyclopiazonic acid inhibition of the sarcoplasmic reticulum calcium pump. J Biol Chem. 2007;282(13):9748-57.

20. Bodova K, Paydarfar D, and Forger DB. Characterizing spiking in noisy type II neurons. J Theor Biol. 2015;365(40-54.

21. Morris C, and Lecar H. Voltage oscillations in the barnacle giant muscle fiber. Biophys J. 1981;35(1):193-213.

22. Guagliardo NA, Yao J, Hu C, and Barrett PQ. Minireview: aldosterone biosynthesis: electrically gated for our protection. Endocrinology. 2012;153(8):3579-86.

23. Afework M, and Burnstock G. Distribution of P2X receptors in the rat adrenal gland. Cell Tissue Res. 1999;298(3):449-56.

24. Burnstock G. Purinergic signalling in endocrine organs. Purinergic Signal. 2014;10(1):189-231.

25. Anastassiou CA, Perin R, Markram H, and Koch C. Ephaptic coupling of cortical neurons. Nat Neurosci. 2011;14(2):217-23.

26. Ladoux B, Nelson WJ, Yan J, and Mege RM. The mechanotransduction machinery at work at adherens junctions. Integr Biol (Camb). 2015.

27. Stapleton SC, Chopra A, and Chen CS. Force measurement tools to explore cadherin mechanotransduction. Cell Commun Adhes. 2014;21(3):193-205.

28. Harris TJ, and Tepass U. Adherens junctions: from molecules to morphogenesis. Nat Rev Mol Cell Biol. 2010;11(7):502-14.

29. Gumbiner BM. Regulation of cadherin-mediated adhesion in morphogenesis. Nat Rev Mol Cell Biol. 2005;6(8):622-34.

30. Kim SA, Tai CY, Mok LP, Mosser EA, and Schuman EM. Calcium-dependent dynamics of cadherin interactions at cell-cell junctions. Proc Natl Acad Sci U S A. 2011;108(24):9857-62.

31. Baumgartner W, Golenhofen N, Grundhofer N, Wiegand J, and Drenckhahn D. Ca2+ dependency of N-cadherin function probed by laser tweezer and atomic force microscopy. J Neurosci. 2003;23(35):11008-14.

32. Corada M, Liao F, Lindgren M, Lampugnani MG, Breviario F, Frank R, Muller WA, Hicklin DJ, Bohlen P, and Dejana E. Monoclonal antibodies directed to different regions of vascular endothelial cadherin extracellular domain affect adhesion and clustering of the protein and modulate endothelial permeability. Blood. 2001;97(6):1679-84.

33. Feldt S, Waddell J, Hetrick VL, Berke JD, and Zochowski M. Functional clustering algorithm for the analysis of dynamic network data. Phys Rev E Stat Nonlin Soft Matter Phys. 2009;79(5 Pt 2):056104.

34. McCormick DA, and Pape HC. Properties of a hyperpolarization-activated cation current and its role in rhythmic oscillation in thalamic relay neurones. The Journal of Physiology. 1990;431(1):291-318.

35. Marder E, and Calabrese RL. Principles of rhythmic motor pattern generation. Physiological Reviews. 1996;76(3):687-717.

36. Nusbaum MP, and Beenhakker MP. A small-systems approach to motor pattern generation. Nature. 2002;417(6886):343-50.

37. Soltesz I, Lightowler S, Leresche N, Jassik-Gerschenfeld D, Pollard CE, and Crunelli V. Two inward currents and the transformation of low-frequency oscillations of rat and cat thalamocortical cells. The Journal of Physiology. 1991;441(1):175-97.

38. Leresche N, Lightowler S, Soltesz I, Jassik-Gerschenfeld D, and Crunelli V. Low-frequency oscillatory activities intrinsic to rat and cat thalamocortical cells. The Journal of Physiology. 1991;441(1):155-74.

39. Skinner FK, Turrigiano GG, and Marder E. Frequency and burst duration in oscillating neurons and two-cell networks. Biol Cybern. 1993;69(5-6):375-83.

40. Bal T, Nagy F, and Moulins MJ. The pyloric central pattern generator in Crustacea: a set of conditional neuronal oscillators. Journal of Comparative Physiology A. 1988;163(6):715-27.

41. Hodgkin AL, and Huxley AF. A quantitative description of membrane current and its application to conduction and excitation in nerve. The Journal of Physiology. 1952;117(4):500-44.

42. Lotshaw DP. Role of membrane depolarization and T-type Ca2+ channels in angiotensin II and K+ stimulated aldosterone secretion. Mol Cell Endocrinol. 2001;175(1-2):157-71.

43. Vassilev PM, Kanazirska MV, Quinn SJ, Tillotson DL, and Williams GH. K+ channels in adrenal zona glomerulosa cells. I. Characterization of distinct channel types. Am J Physiol. 1992;263(4 Pt 1):E752-9.

44. Brauneis U, Vassilev PM, Quinn SJ, Williams GH, and Tillotson DL. ANG II blocks potassium currents in zona glomerulosa cells from rat, bovine, and human adrenals. Am J Physiol. 1991;260(5 Pt 1):E772-9.

45. Quinn SJ, Cornwall MC, and Williams GH. Electrophysiological responses to angiotensin II of isolated rat adrenal glomerulosa cells. Endocrinology. 1987;120(4):1581-9.

46. Quinn SJ, Cornwall MC, and Williams GH. Electrical properties of isolated rat adrenal glomerulosa and fasciculata cells. Endocrinology. 1987;120(3):903-14.

47. Penton D, Bandulik S, Schweda F, Haubs S, Tauber P, Reichold M, Cong LD, El Wakil A, Budde T, Lesage F, et al. Task3 potassium channel gene invalidation causes low renin and salt-sensitive arterial hypertension. Endocrinology. 2012;153(10):4740-8.

48. Guillot C, and Lecuit T. Mechanics of epithelial tissue homeostasis and morphogenesis. Science. 2013;340(6137):1185-9.

49. Mege RM, and Ishiyama N. Integration of Cadherin Adhesion and Cytoskeleton at Adherens Junctions. Cold Spring Harb Perspect Biol. 2017;9(5).

50. Adams CL, Nelson WJ, and Smith SJ. Quantitative analysis of cadherin-catenin-actin reorganization during development of cell-cell adhesion. J Cell Biol. 1996;135(6 Pt 2):1899-911.

51. Maitre JL, and Heisenberg CP. Three functions of cadherins in cell adhesion. Curr Biol. 2013;23(14):R626-33.

52. Storch U, Mederos y Schnitzler M, and Gudermann T. G protein-mediated stretch reception. Am J Physiol Heart Circ Physiol. 2012;302(6):H1241-9.

53. Wang W, Qiao Y, and Li Z. New Insights into Modes of GPCR Activation. Trends in Pharmacological Sciences. 2018;39(4):367-86.

54. Zou Y, Akazawa H, Qin Y, Sano M, Takano H, Minamino T, Makita N, Iwanaga K, Zhu W, Kudoh S, et al. Mechanical stress activates angiotensin II type 1 receptor without the involvement of angiotensin II. Nat Cell Biol. 2004;6(6):499-506.

55. Tanaka H, Shan W, Phillips GR, Arndt K, Bozdagi O, Shapiro L, Huntley GW, Benson DL, and Colman DR. Molecular modification of N-cadherin in response to synaptic activity. Neuron. 2000;25(1):93-107.

56. Tai CY, Kim SA, and Schuman EM. Cadherins and synaptic plasticity. Curr Opin Cell Biol. 2008;20(5):567-75.

57. Egelman DM, and Montague PR. Calcium dynamics in the extracellular space of mammalian neural tissue. Biophys J. 1999;76(4):1856-67.

58. Tang L, Hung CP, and Schuman EM. A role for the cadherin family of cell adhesion molecules in hippocampal long-term potentiation. Neuron. 1998;20(6):1165-75.

59. Stowasser M, and Gordon RD. Primary Aldosteronism: Changing Definitions and New Concepts of Physiology and Pathophysiology Both Inside and Outside the Kidney. Physiol Rev. 2016;96(4):1327-84.

60. Baudrand R, Guarda FJ, Fardella C, Hundemer G, Brown J, Williams G, and Vaidya A. Continuum of Renin-Independent Aldosteronism in Normotension. Hypertension. 2017;69(5):950-6.

61. Monticone S, D'Ascenzo F, Moretti C, Williams TA, Veglio F, Gaita F, and Mulatero P. Cardiovascular events and target organ damage in primary aldosteronism compared with essential hypertension: a systematic review and meta-analysis. Lancet Diabetes Endocrinol. 2018;6(1):41-50.

Appendix IV:

Generation of AS-Cre^{ER} Mouse

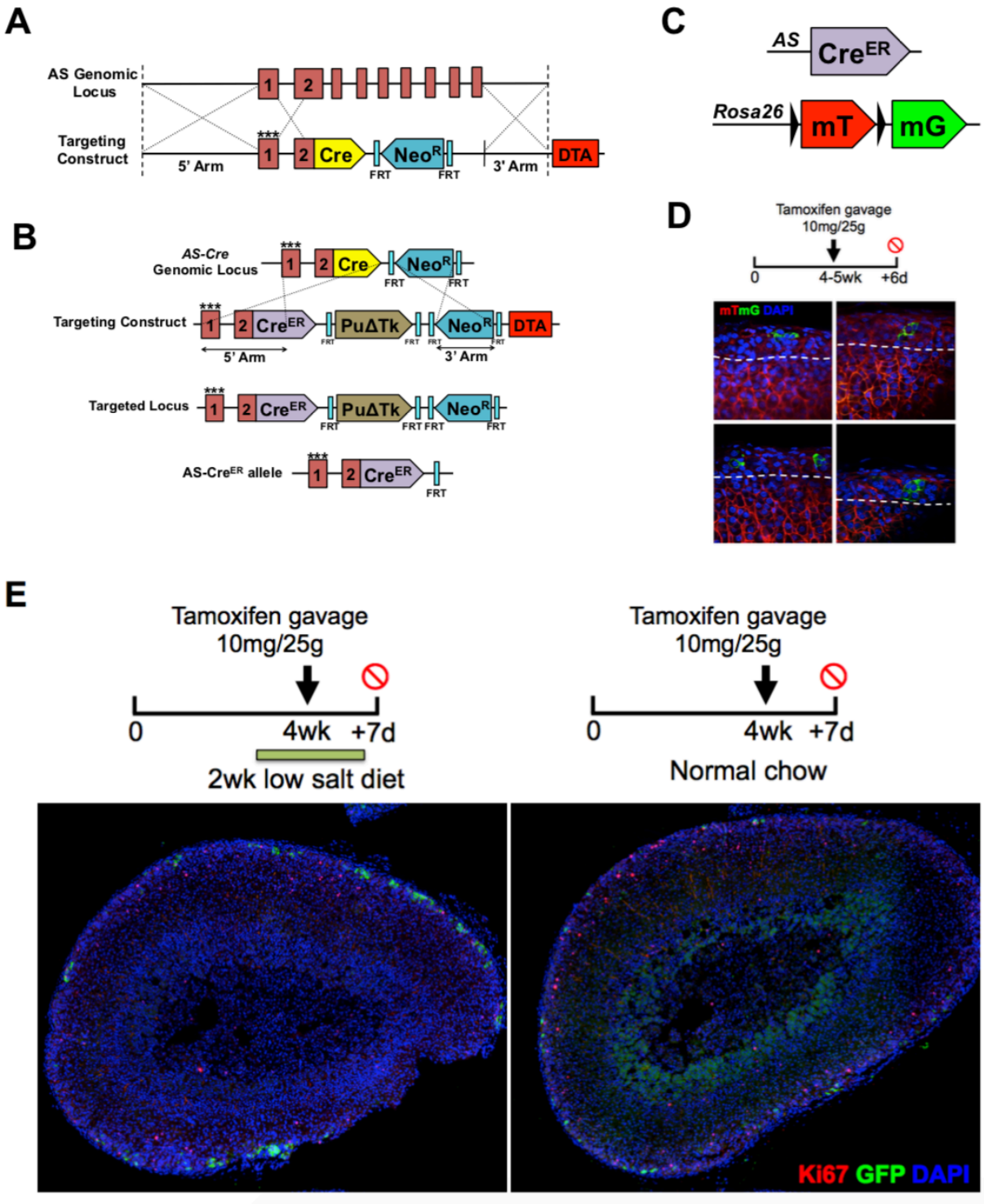

Figure S4.1. Generation of AS-Cre^{ER} mouse model. A, schematic showing the targeting strategy of the endogenous AS locus to generate AS-Cre mouse. B, schematic showing the re-targeting strategy of the AS-Cre locus. C, schematic of the AS-Cre^{ER}/+; R26R-mTmG mouse. D, zG specific GFP expression after one dose of Tamoxifen exposure. E, enhanced AS-CreER locus activity with 2 weeks of sodium restriction.

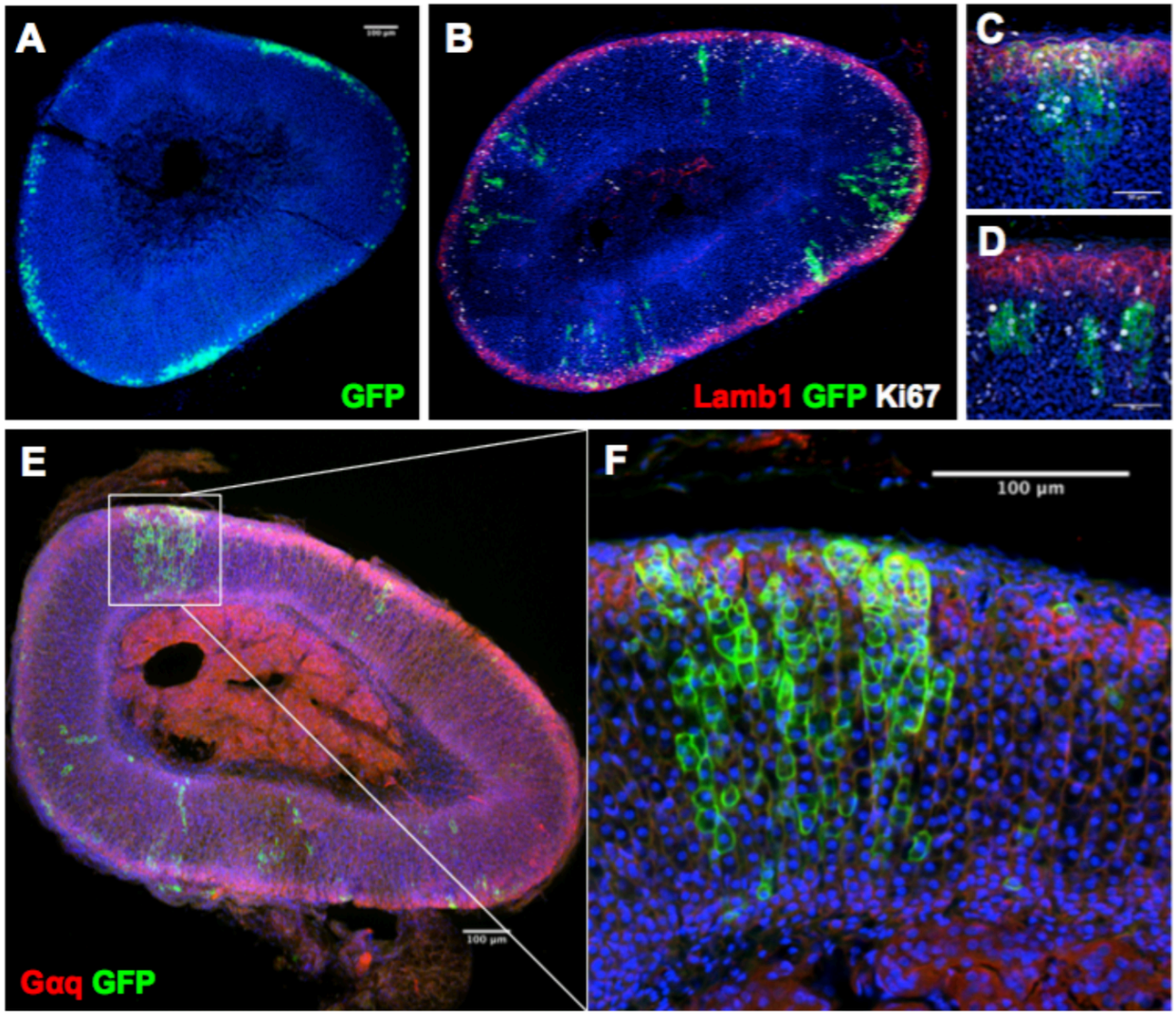

Figure S4.2. Lineage tracing analyses using the AS-Cre^{ER}/+; R26R-mTmG mouse. Adult mice were maintained on low sodium diet for one week, exposed to 2 doses of Tamoxifen by gavage, and chased for various time. A, 7-day chase. B-D, 80-day chase. E-F, 120-day chase

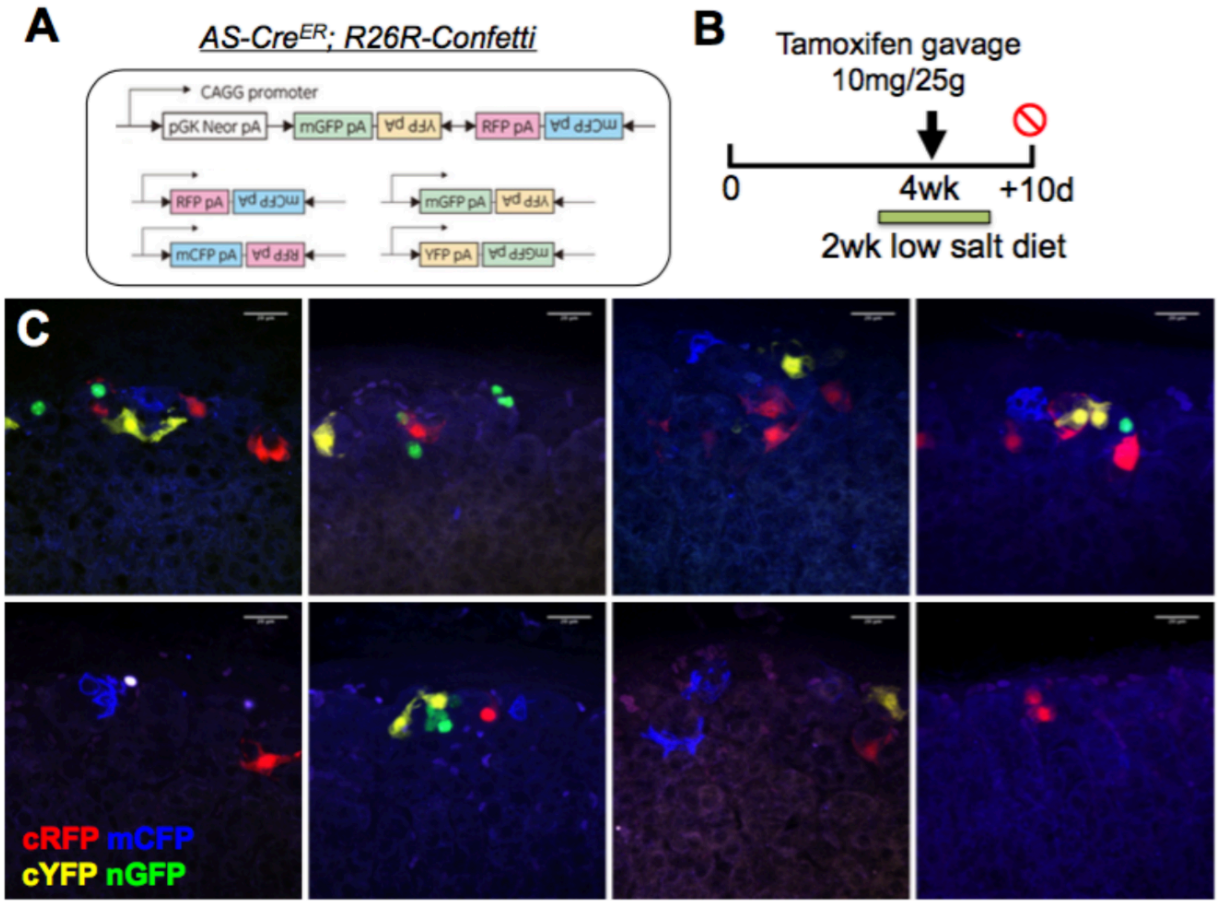

Figure S4.3. Analysis of clonal dynamic using AS-Cre^{ER}/+; R26R-Confetti mouse. A, schematic of the Confetti allele. B, schematic of Tamoxifen treatment. C, images of adrenal slices after 10-day chase. Bars, 20 μm.